UNIVERSITE D'AIX-MARSEILLE

ECOLE DOCTORALE DES SCIENCES DE L'ENVIRONNEMENT

OBSERVATOIRE DES SCIENCES DE L'UNIVERS - INSTITUT PYTHEAS

CENTRE EUROPEEN DE RECHERCHE ET D'ENSEIGNEMENT DES GEOSCIENCES DE L'ENVIRONNEMENT

THESE DE DOCTORAT

Discipline : Géosciences de l'environnement

Céline Roux

Etude des mécanismes de transfert des radionucléides en aval de la fosse T22 du Site expérimental de Tchernobyl

Soutenue le 18 octobre 2013

COMPOSITION DU JURY

Marc BENEDETTI	Rapporteur
Werner BALDERER	Rapporteur
Dmitri BUGAY	
Bruno HAMELIN	
Armand MASION	
Jean-Luc MICHELOT	
Caroline SIMONUCCI	
Nathalie VAN MEIR	
Corinne LE GAL LA SALLE	
Joël LANCELOT	

THESE

IRSN
INSTITUT
DE RADIOPROTECTION
ET DE SÛRETÉ NUCLÉAIRE

Faire avancer la sûreté nucléaire

Etude des mécanismes de transfert des radionucléides en aval de la fosse T22 du Site expérimental de Tchernobyl

Céline Roux

Thèse de doctorat

[PRP-DGE/SRTG/2013-xx]

cnrs
dépasser les frontières

GÉOSCIENCES DE L'ENVIRONNEMENT
CEREGE

Pôle radioprotection, environnement, déchets et crise

Service de recherche sur les transferts dans la géosphère

Aix*Marseille université

RESUME

De façon à réduire l'exposition aux radiations et éviter une resuspension atmosphérique des radionucléides relâchés lors de l'accident de Tchernobyl (avril 1986), la matière contaminée a été enfouie dans environ 800 tranchées creusées dans la zone d'exclusion. Depuis 1999, le Site Pilote de Tchernobyl (CPS) est voué à l'étude de la migration des radionucléides à partir de l'une de ces tranchées, la tranchée T22 dans l'Environnement (biosphère, zone non-saturée et zone saturée). L'objectif de cette étude est d'étudier les processus de migration des éléments dans la nappe phréatique sous-jacente.

D'abord, l'extension maximale du panache de contamination est étudiée à l'aide du traceur conservatif ^{36}Cl. Les rapports $^{36}Cl/Cl$ sont 1 à 4 ordres de grandeur supérieurs au rapport naturel théorique, ce qui signifie une importante contamination de la nappe par le ^{36}Cl, attribuée aux processus de migration depuis la tranchée. Ensuite, l'aspect réactif des migrations est considéré. Un modèle conceptuel des principaux processus géochimiques est proposé à partir de l'étude des concentrations en éléments majeurs ($[Cl^-]$, $[HCO_3^-]$, $[SO_4^{2-}]$, $[NO_3^-]$, $[Na^+]$, $[Ca^{2+}]$, $[K^+]$ $[Mg^2+]$, [Si]), en $[Fe^{2+}]$, en $[Mn^{2+}]$ et des rapports $\delta^{18}O$ et δ^2H. La recharge de la nappe est d'origine météorique. Certains éléments sont très influencés par la présence de la tranchée. Cependant, des processus géochimiques naturels ont aussi une influence sur géochimie des eaux : des processus d'altération/dissolution de minéraux, d'échanges cationiques ou de drainage sont supposés pour expliquer les variations de concentrations. Puis, la migration d'Uranium et du Strontium est étudiée à l'aide de la mesure des rapports isotopiques $^{238}U/^{235}U$, $^{86}Sr/^{88}Sr$ et $^{87}Sr/^{86}Sr$. En effet, la dissolution des particules de combustible enfouies dans la tranchée et le lessivage des radionucléides qui leur sont associés sont supposés avoir un impact significatif sur les rapports isotopiques dans la nappe. Cependant, malgré une augmentation des concentrations en $[^{238}U]$ en aval de la tranchée, les rapports $^{238}U/^{235}U$ mesurés dans la nappe sont dans la gamme naturelle. La procédure analyse des rapports $^{86}Sr/^{88}Sr$ et $^{87}Sr/^{86}Sr$ ne permet pas d'avoir une précision suffisante pour observer un changement de ces rapports en aval de la tranchée. Cependant, une diminution du rapport $^{87}Sr/^{86}Sr$ est clairement observée en profondeur.

ABSTRACT

To reduce radiation exposure rates at the site and prevent atmospheric resuspension of radionuclides released by the Chernobyl reactor 4 explosion (April 1986), about 800 trenches were dug on site to dispose contaminated material. Since 1999, the Chernobyl Pilot Site (CPS) was set up to study the migration of radionuclides from one of these trenches, the trench T22, in the Environment (biosphere, unsaturated zone, saturated zone). The aim of this study is to investigate migration processes in groundwater.

At first, the maximal extent of the contaminant plume is studied based on the understanding of the conservative tracer ^{36}Cl behavior. High contamination of groundwater by ^{36}Cl is shown, with $^{36}Cl/Cl$ ratios 1 to 4 orders of magnitude higher than the theoretical natural ratio. This contamination is attributed to migration from the trench. Then, a reactive approach is considered. A conceptual model of the main geochemical processes in groundwater is proposed based on the study of major elements concentrations ($[Cl^-]$, $[HCO_3^-]$, $[SO_4^{2-}]$, $[NO_3^-]$, $[Na^+]$, $[Ca^{2+}]$, $[K^+]$ $[Mg^2+]$, [Si]), $[Fe^{2+}]$ concentrations, $[Mn^{2+}]$ concentrations, $\delta^{18}O$ and δ^2H. Meteoric origin of groundwater is showed. Some element concentrations are mainly governed by migrations from the trench. However, natural geochemical processes are also assessed to have an influence on groundwater geochemistry: thus, weathering of minerals, cation exchanges and leakage are supposed. Next, uranium and strontium migrations are investigated based on measurements of $^{238}U/^{235}U$, $^{86}Sr/^{88}Sr$, $^{87}Sr/^{86}Sr$ ratios. Indeed, dissolution fuel particles buried in the trench and the release of associated radionuclides is supposed to have a significant impact on those ratios in groundwater. However, in spite of an increase of $[^{238}U]$ concentrations downgradient of the trench, measured $^{238}U/^{235}U$ ratios in groundwater are in the natural range. Analytical procedure for $^{86}Sr/^{88}Sr$ and $^{87}Sr/^{86}Sr$ ratio measurement does not allow observing some trend downgradient of the trench; however, $^{87}Sr/^{86}Sr$ ratios clearly decrease with the depth.

Tables of contents

Illustrations

Tables

I. INTRODUCTION

I.1 CHERNOBYL EXPLOSION AND CONTAMINATION MANAGEMENT

In the context of evaluating radiation exposure linked to major nuclear hazards, such as Chernobyl accident in 1986 and then Fukushima accident in 2011 or such as ancient mining sites management, improvements in the knowledge about radionuclide migration in the environment (atmosphere, geosphere, biosphere, hydrosphere) is required.

The explosion of unit 4 of the Chernobyl Nuclear Power Plant on April 26th 1986 released around $12x10^{18}$ Becquerel of radionuclides in the atmosphere (UNSCEAR, 2000), leading authorities to set up a 30 km exclusion zone. Since 1987, remediation actions were carried out to reduce radiation exposure and to prevent atmospheric resuspension of deposited radionuclides. These included burying dead vegetation, debris and contaminated top soil in trenches and mounds, which were then covered by the excavated topsoil (Figure I-1). However, the permeable sandy formation where the nuclear waste was deposited does not constitute an efficient barrier against the migration of radionuclides in the shallow aquifer (Dzhepo and Skal'skii, 2002). Moreover, the groundwater table is periodically high enough to flood trenches and the bottom of waste mounds, promoting radionuclide migration in soils and groundwater and groundwater contamination by strontium-90 was evidenced in the exclusion zone (Shestopalov, 2002).

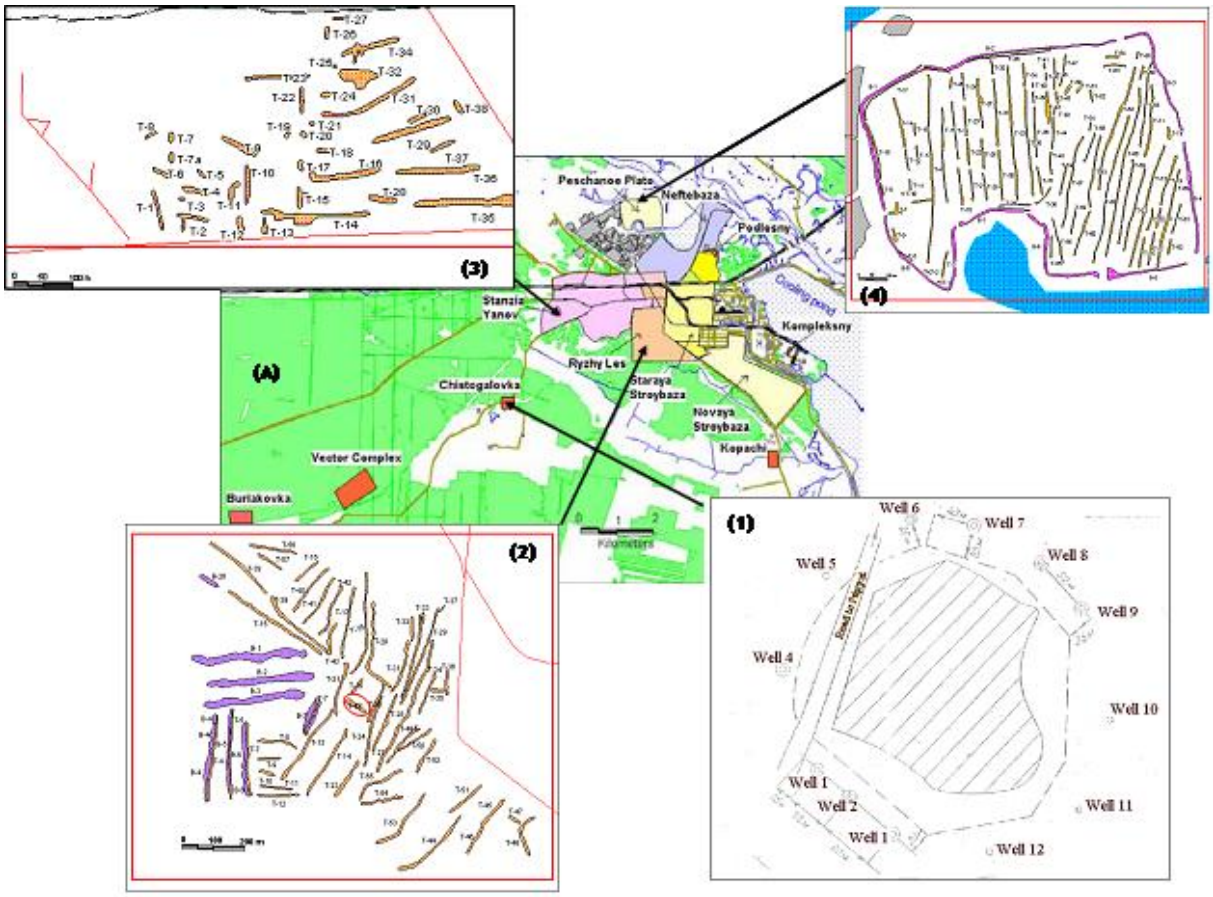

Figure I-1: Map of trenches and talus according to Antropov et al. (2001) (figure from Ferrand, 2011)

Since 1999, studies were carried out to understand radionuclide migration processes in the biosphere and subsoil from one of the nuclear waste disposals, trench T22. These studies were based on collaborations between the French Institute of Radioprotection and Nuclear Safety (IRSN), the Ukrainian Institute of Geological Sciences (IGS) and the Ukrainian Institute of Agricultural Science (UIAR-NuBiP), at the Chernobyl Pilot Site project (CPS), and then with the Experimental Plateform In Chernobyl (EPIC). Collaborations were hereafter reinforced in 2008 with the GNR-TRASSE project (National Research Groupment on Radionuclides Transfer in Soil, Subsoil and Ecosystems), involving the French National Centre for Scientific Research (CNRS). This thesis project is based on this last collaboration, co financed by CNRS and IRSN.

I.2 PROBLEM STATEMENT

A water quality survey of groundwater in the vicinity of trench T22 showed the presence of a strontium-90 plume with an extension of twenty meters or so downgradient of the trench (Dewière *et al.*, 2004). Released from the trench, strontium-90 migrates through the unsaturated zone to the groundwater. Strontium-90 migration in the unsaturated zone was the topic of two previous PhD theses (Szenknect, 2003; Mazet, 2008). In unsaturated conditions, among parameters governing ^{90}Sr retention, physical-chemical conditions and geochemical background, particularly $[Sr^{2+}]$ and $[Ca^{2+}]$, were shown to have an important influence (Szenknect, 2003; Mazet, 2008). In groundwater, strontium-90 migration velocity was shown to be 9% of the groundwater velocity (Dewière *et al.*, 2004). This retardation is supposed to be the result of retention processes, such as cation exchanges processes. However, discrepancies exist between coefficient of retention K_d measured *in situ*, in laboratory and used for simulations (Szenknect, 2003; Dewière *et al.*, 2004; Van Meir *et al.*, 2009; Bugai *et al.*, 2012b), underscoring a lack of understanding in the strontium-90 migration processes.

Processes that may influence radionuclide migration from the trench have to be characterized in order to better understand these migrations. The present study aims at identifying processes occurring in groundwater which may have an important impact on migration of radionuclides in groundwater.
Advective-dispersive transport is assumed to be a dominant migration process. Reactive processes would also have an important impact on radionuclide migration. For instance, some radionuclides are sensitive to redox conditions changes and may be more or less immobilized following their speciation. Consequently, the identification of processes influencing radionuclide migration in groundwater involves three main issues:

- Determining the extent of the contaminant plume considering only non reactive processes
- Identifying the reactive processes occurring in groundwater
- Assessing the impact of these processes on radionuclide migration

Chapter 2 gives an overview of the Chernobyl Pilot Site and of the studies which were carried out on radionuclide releases from the trench and radionuclide migration processes evidenced in groundwater until now.

Chapter 3 focuses on element migration avoiding a maximum of chemical reactions to investigate extent of the contaminant plume under non reactive conditions. The radioisotope chlorine-36 (^{36}Cl) is assumed to be potentially a good tracer to study such migration, considering that at short time scale, ^{36}Cl radioactive decay is negligible and because ^{36}Cl is a product of nuclear activity and has been most likely released during the Chernobyl accident (Chant *et al.*, 1986). The origins of ^{36}Cl in the Chernobyl Pilot Site groundwater are reviewed and implication for non reactive processes is studied through the comparison with chloride concentrations, ^{90}Sr concentrations and simulation of the transport in groundwater.

Next, reactive processes are considered in Chapter 4. First, the main reactive processes governing groundwater geochemistry has to be defined. The major species concentrations (Na^+, K^+, Ca^{2+}, Mg^{2+}, Cl^-, SO_4^{2-}, HCO^-, N-species, Si), water isotopes ($\delta^{18}O$, δ^2H), some trace elements (Fe, Mn, Sr) as well as pH and redox conditions are studied and an overall conceptual model is proposed.
Then, the investigation focuses on the impact of reactive processes on migration of element. Uranium and strontium are assumed to be released from the trench and their behavior in groundwater is studied based on isotopic approach. Uranium migration from the trench to groundwater should be shown through the study of $^{238}U/^{235}U$ ratio. Indeed, fuel particles buried in the trench are enriched in ^{235}U and are subjects to dissolution processes (Kashparov *et al.*, 2000; Kashparov *et al.*, 2004). The natural $^{238}U/^{235}U$ ratio is theoretically constant and could be impacted by migration of uranium released by fuel particle dissolution. Finally, $^{87}Sr/^{86}Sr$ and $^{86}Sr/^{88}Sr$ ratios are studied in groundwater to evidence strontium behavior in groundwater and more specifically if the competitivity of strontium isotopes on exchange sites, comparing them with [^{88}Sr] and [^{90}Sr]. Because of ^{87}Sr and ^{88}Sr are shown to be produced by fission of uranium, natural $^{87}Sr/^{86}Sr$ and $^{86}Sr/^{88}Sr$ ratios may be influenced by the migration of these isotopes from trench T22. $^{238}U/^{235}U$, $^{87}Sr/^{86}Sr$ and $^{86}Sr/^{88}Sr$ ratio analyses required analytical development on Thermal-

Ionization Mass Spectrometer. Both are analyzed by the total evaporation method using Re filaments and activators.

This manuscript is written in order to facilitate the valorization of this work under scientific articles hereafter. Then, each section is organized starting with a material and method part, and then results and discussion.

Next, the study focus on the identification of main geochemical processes based on the major element concentrations ($[Cl^-]$, $[HCO_3^-]$, $[SO_4^{2-}]$, $[NO_3^-]$, $[Na^+]$, $[Ca^{2+}]$, $[K^+]$ $[Mg^2+]$, [Si]), $[Fe^{2+}]$, $[Mn^{2+}]$, $\delta^{18}O$ and δ^2H, in order to define reactive processes which may hinder or promote radionuclide migration in groundwater. Then, in the light of these observations, uranium and strontium migration are investigated in groundwater. Indeed, they are both supposed to be released from the trench in isotopic proportions different than the natural environment. Thus, the impact of these releases is estimated based on the studies of uranium isotopic ratio $^{238}U/^{235}U$ and strontium isotopic ratios $^{86}Sr/^{88}Sr$ and $^{86}Sr/^{87}Sr$.

II. STUDY SITE

The explosion of the unit 4 of the Chernobyl Nuclear Power Plant in April 1986, the 26th released around 12 x10^{18} Becquerel of radionuclides in the atmosphere. The most abundant were xenon-133, tellure-132, iodine-131, iodine-133 and neptunium-239 (UNSCEAR, 2000) and because of the soil contamination by these radionuclides an exclusion area of 30 km around the Chernobyl Nuclear Power Plant was set up (Figure II-1). However, twenty five years later, the residual contamination of soils is mainly linked to the presence of cesium-137, strontium-90 and plutonium isotopes. Other radionuclides were dispersed in atmosphere, decayed (most have half-live under a year) or are in smaller amount (Figure II-2).

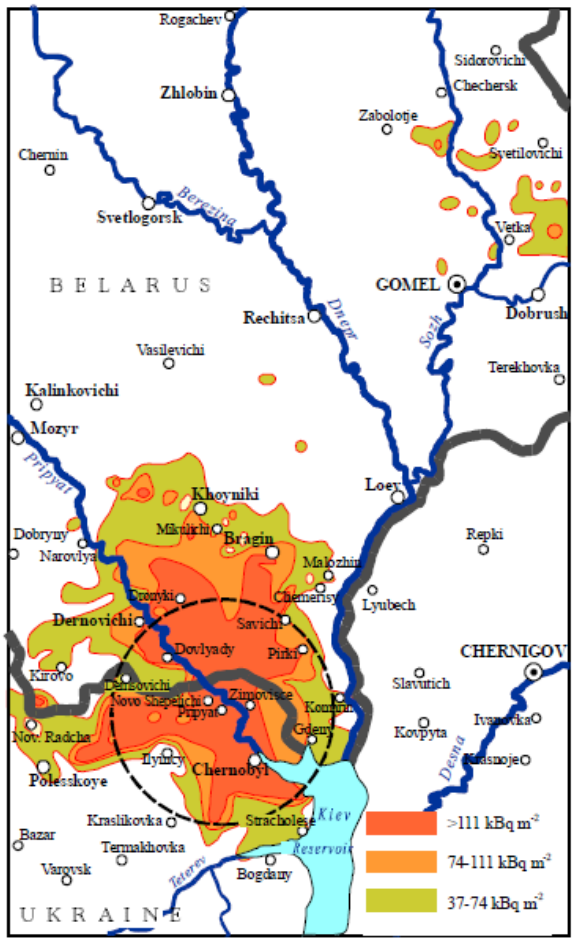

Figure II-1: Map of soil contamination by strontium-90 released in the Chernobyl accident (UNSCEAR, 2000)

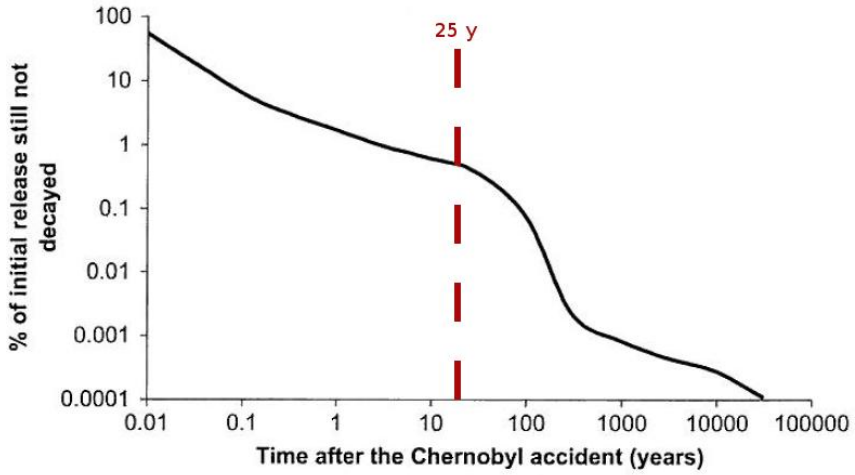

Figure II-2: Evolution of radionuclide content in time (according Smith and Beresford, 2005)

In order to reduce radiation exposure and hinder atmospheric resuspension of radionuclides released by the Chernobyl explosion, about 800 trenches and mounds were dug in the exclusion area to bury radioactive materials (Figure II-3). These radioactive materials were composed of contaminated topsoil and litters, dead plants and explosion fallout. Total buried volume was estimated to be 10^6 m^3 (Dzhepo and Skal'skii, 2002).

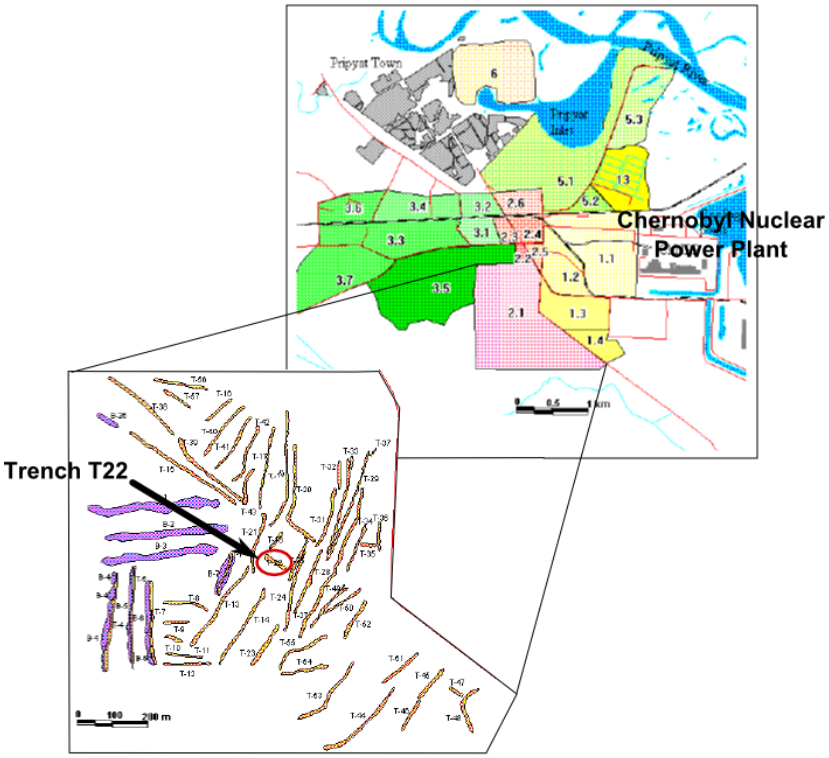

Figure II-3: Zones of buried waste in the Chernobyl exclusion zone (maps from Antropov et al., 2001)

The Chernobyl Pilot Site was set up on one of these trenches, Trench T22, located 2.5 km at the south-west of the Chernobyl Nuclear Power Plant (Figure II-3).
This part aims at describing the Chernobyl Pilot Site settings. At first, the geology is described (regional context, lithology). Then, the Pilot Site itself is described (studied elements, instrumentation) and the studies on radionuclides migrations from the trench are reviewed.

II.1 GEOLOGY AND HYDROGEOLOGY

II.1.1 LARGE SCALE SETTINGS

The Chernobyl Nuclear Power Plant (ChNPP) and the Chernobyl Pilot Site (CPS) are located on the Prypyat River's first alluvial terrace. (Figure II-4). Topography is almost flat and the elevation is between 110 m and 115 m above the sea level (m.a.s.l) (Dzhepo and Skal'skii, 2002).
This terrace constitutes the superficial layer of marine and continental sedimentary structure, which covers the North-west slope of the Ukrainian shield (Matoshko *et al.*, 2004). The thickness of those layers is 130 m to 190 m (Matoshko *et al.*, 2004). A geologic section is presented in Figure II-4.
Three main aquifers can be distinguished:

- Pliocene and Pleistocene-Holocene free aquifer (Q_{1-2}, Q_3 and Q_4 areas in Figure II-4). It is 30 m thick and the free groundwater is 1 to 10 m depth (Matoshko *et al.*, 2004; Dzhepo and Skal'skii, 2002).
- Eocene sand captive aquifer (P_2 area in Figure II-4). It is separated of the upper aquifer by a silty and marly layer, called Kiev suite of Eocene (P_2kv area, Figure II-4) (Matoshko *et al.*, 2004; Dzhepo and Skal'skii, 2002). Other sedimentary formations are 50 meters thick, composed mainly of quartz and glauconite (Dzhepo and Skal'skii, 2002). The artesian groundwater in this aquifer is exploited as drinking water (Dzhepo and Skal'skii, 2002).
- Jurassic and Cretaceous captive aquifer. It is separated by the upper layer by 100-m-thick marly chalk (Dzhepo and Skal'skii, 2002). This system of artesian groundwater is composed by sand, micro-sandstone, clay, marl, limestone, fissured sandstone and marly chalk (Dzhepo and Skal'skii, 2002).

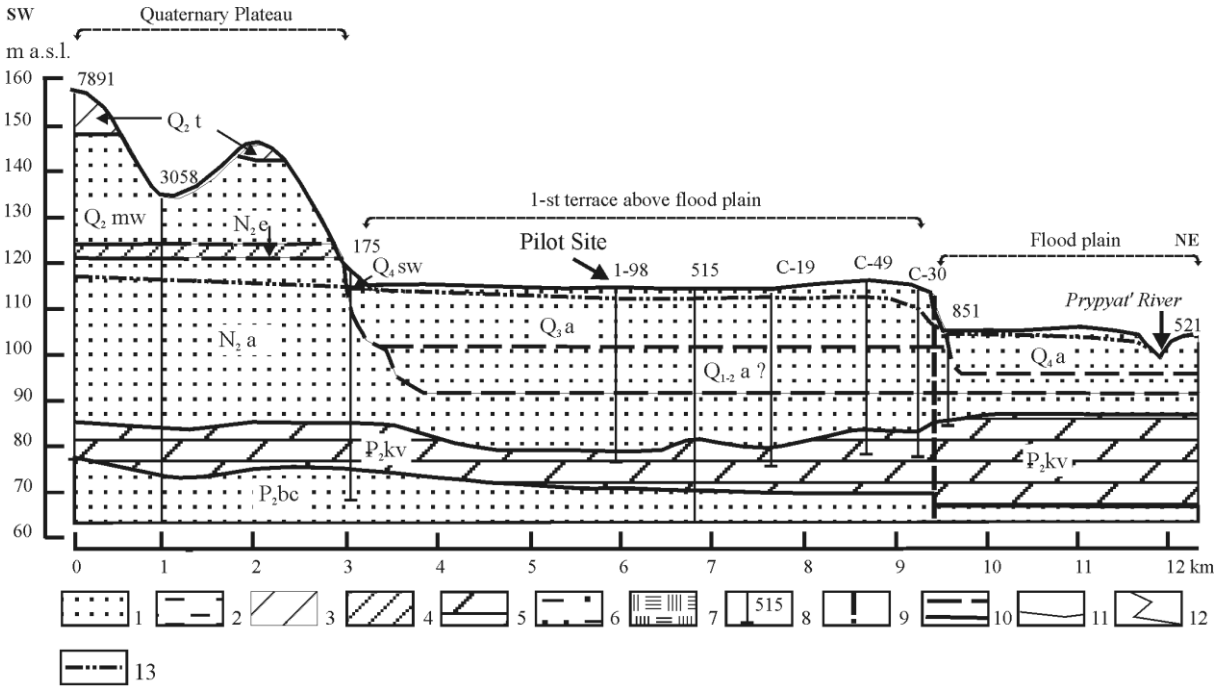

Legend: 1 – sands, 2- silts, 3 – basal till, 4 – clay, 5 – marl, 6 – inter-bedding of sands and silts, 7 – peat and peaty sand, 8 – boreholes (numbered), 9 – inferred fault, 10 – boundaries between suites: supposed (upper) and established (lower), 11 - boundaries between depositional facies, 12 – facial replacement, 13 – groundwater level (generalized).
Indices: Q4 - Holocene, Q3-4 - Upper Pleistocene - Holocene unstratified, Q3 - Upper Pleistocene, Q1-2 - Lower Pleistocene - Middle Pleistocene unstratified, N2 - Pliocene, P2 – Eocene; kv - Kyiv, bc – Buchack.

Genetic types of deposits: a - alluvial, mw – melt-water, eol - eolian, e - presumably waste mantle, sw – slopewash.
Facies: ob – overbank, ch – channel, a-ch – abandoned channel.

Figure II-4: Lithological cross-section of the upper suites (from Matoshko et al., 2004)

Free groundwater is vulnerable to pollution because of the low depth of the water table in almost the whole exclusion zone: contamination of groundwater by ^{137}Cs, ^{134}Cs, ^{106}Ru et ^{90}Sr was evidenced since 1987 (Dzhepo and Skal'skii, 2002). However, no contamination of the underlying captive groundwater was shown (Dzhepo and Skal'skii, 2002). Consequently, studies focus only on the free groundwater (Figure II-4).

II.1.2 MINERALOGY OF THE FREE AQUIFER

The mineralogical study of the free aquifer was carried out from samples collected in a non contaminated site, "Prypyat Zaton Site", assumed to be similar to the Chernobyl Pilot Site. Two main layers were distinguished:

- The upper layer is composed of aeolian sands. The most represented mineral phase is quartz (98-99%) with feldspars, micas, chlorite and some traces of illite, kaolinite and carbonates (Szenknect, 2003). Its thickness varies from 3.5 to 5 m at the CPS. Trenches were dug in this permeable formation (Table II-1) and excavated sand was used to cover buried materials and it constitutes a layer of 0.3 to 0.5 m (Bugai *et al.*, 2012a).
- The underlying layer is composed by alluvial sediments. This formation is more heterogeneous, with channel, over-bank or abandoned-channel facies. Presence of inter-bedded lenses was also reported (Table II-1) (Matoshko *et al.*, 2004). Quartz is the main mineral phase, associated with sodic and potassic feldspars (5-9%) and some heavy metals (<0.5%). Moreover, quartz, phyllosilicates (montmorillonites, hydromicas), fine-dispersed calcite and amorpheous iron oxides are represented in the fine fraction (<0,01mm) (Matoshko *et al.*, 2004).
- Some cryogenic veins were also identified between those two layers at the « Prypiat Zaton Site ». They are composed by iron oxides (Matoshko *et al.*, 2004).

Hydrogeologic and granulometric characteristics as well as cation exchange capacities of the two main layers are synthetized in Table II-1 and Figure II-5.

Table II-1: Description of Pliocène et Pléistocène-Holocène aquifer (Matoshko et al., 2004; Dzhepo and Skal'skii, 2002)

	Porosity (%)	Permeability ($m.s^{-1}$)	Mineralogical composition of the fraction >0.01 mm
Aeolian layer	34-36	From 4.10^{-5} to 6.10^{-5}	Quartz (98-99%) Heavy minerals (1-2%)
Alluvial layer - over-bank and abandoned-channel facies	35	Horizontaly : 1.10^{-5} Verticaly : 1.10^{-7}	Quartz Feldspars Na-K Heavy minerals
Alluvial layer – river bed facies	37	From 6.10^{-5} to 2.10^{-4}	
Kiev suite of Eocene	-	from 2.10^{-7} to 2.10^{-9}	Marine carbonates

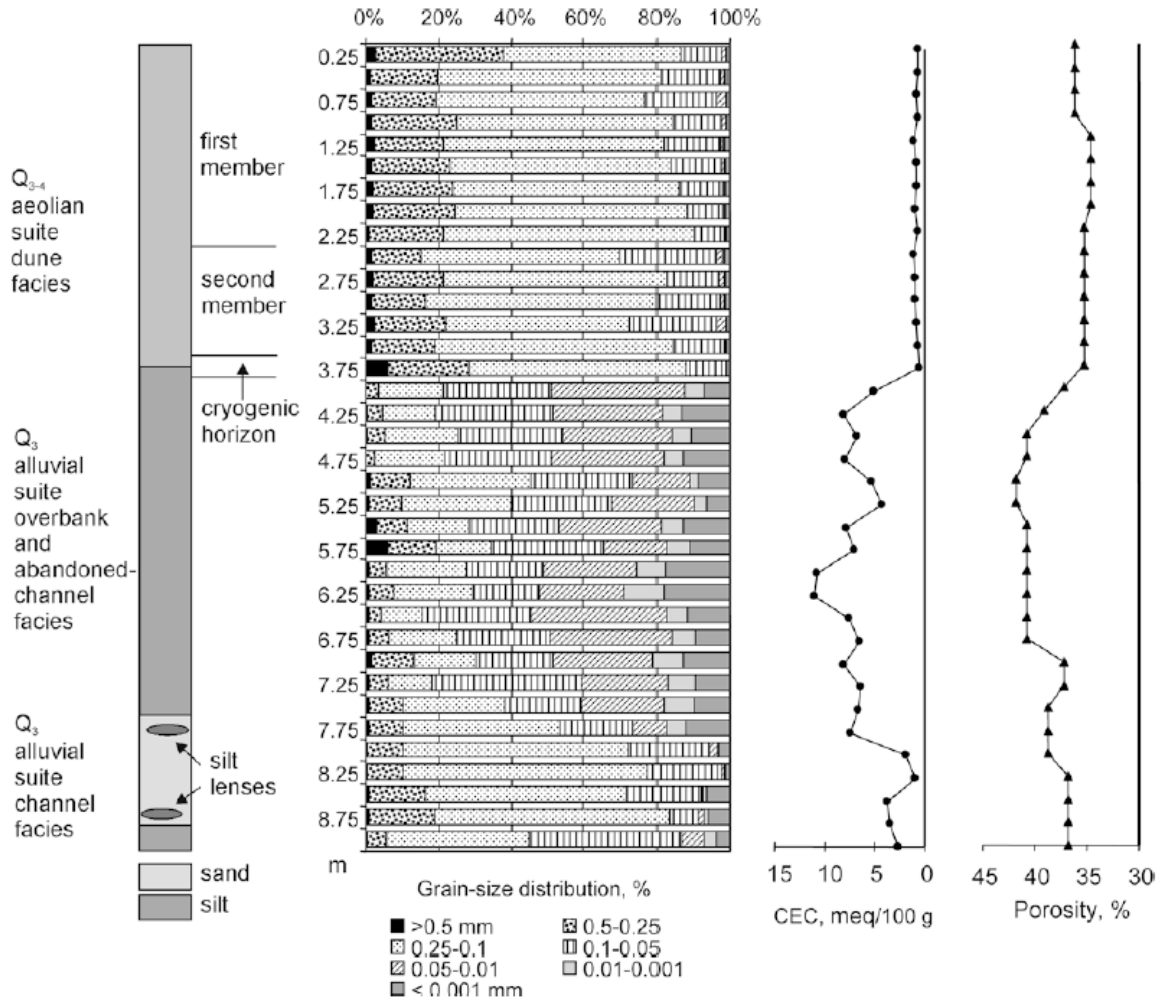

Figure II-5: Granulometry, Cation Exchange Capacity and Porosity of the aeolian and alluvial layers (from Matoshko et al., 2004)

II.1.3 PHREACTIC GROUNDWATER

Mean precipitations are 600 mm.y^{-1} (Dzhepo and Skal'skii, 2002; Bugai *et al.*, 2012b). Recharge of groundwater by infiltration was studied between 2000 and 2004 at the CPS, and infiltrated water was shown to represent between 30% to 50% of the yearly precipitation, meaning between 180 and 300 mm.y^{-1} (Bugai *et al.*, 2012b).

Water table is located between 1 and 4 meters depth (Bugai *et al.*, 2012a) with seasonal variations of 1 m. (observation on the period 2000-2004 – Bugai *et al.*, 2012b). Spring is the main recharge period when snow melt and rainwater are

infiltrated. A significant contribution of intense rainfall in summer-autumn was also shown (Bugai *et al.*, 2012b).

Regional groundwater hydraulic gradient varies between 0.001 and 0.003 (Dzhepo and Skal'skii, 2002). Wetland and temporary surface water presence were supposed to have an influence on this gradient (Bugai and Dewière, 2004). Groundwater flows until Prypyat River, sometimes through Rodvinon and Borschii Rivers or draining channel and the cooling pond of the Chernobyl Nuclear Power Plant (Figure II-6) (Bugai and Dewière, 2004).

At the CPS, groundwater in the aeolian layer flows along the direction of North-North-East with a variation of the direction ±10-15° and with a hydraulic gradient of 0.0015 (Bugai *et al.*, 2012a). In the upper alluvial part, hydraulic gradient is almost vertical and equals to 0.02 – 0.04 (Bugai *et al.*, 2012a). A pore velocity (Dacy velocity) in the aeolian layer of 11 $m.y^{-1}$ was measured by infiltration and tracing tests (^{36}Cl) (Bugai *et al.*, 2012b).

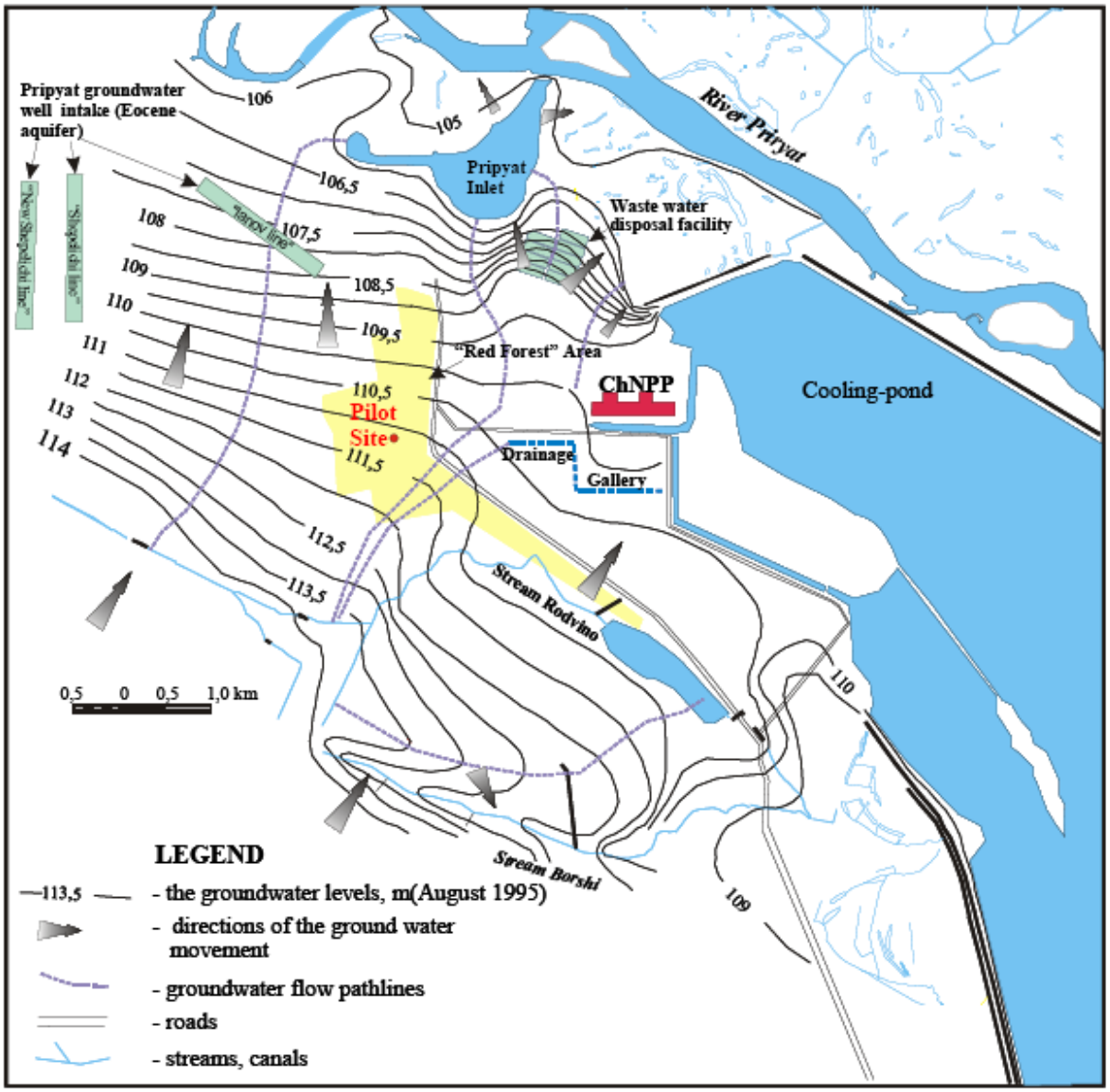

Figure II-6: Groundwater flow (from Bugai and Dewière, 2004)

II.2 CHERNOBYL PILOT SITE

II.2.1 DESCRIPTION

CPS is located in the Red Forest, where groundwater contamination by ^{90}Sr is particularly high: ^{90}Sr volumetric activity was between 100 and 20500 $Bq.L^{-1}$ between 1993 and 1995 (Dzhepo and Skal'skii, 2002).

Trench T22 is 70-meters-long, 8 to 10-meters length and 2 to 2.5-meters depth. Its direction is North-west/South-east, perpendicularly to the main groundwater flow direction (Figure II-7) (Bugai *et al.*, 2005).

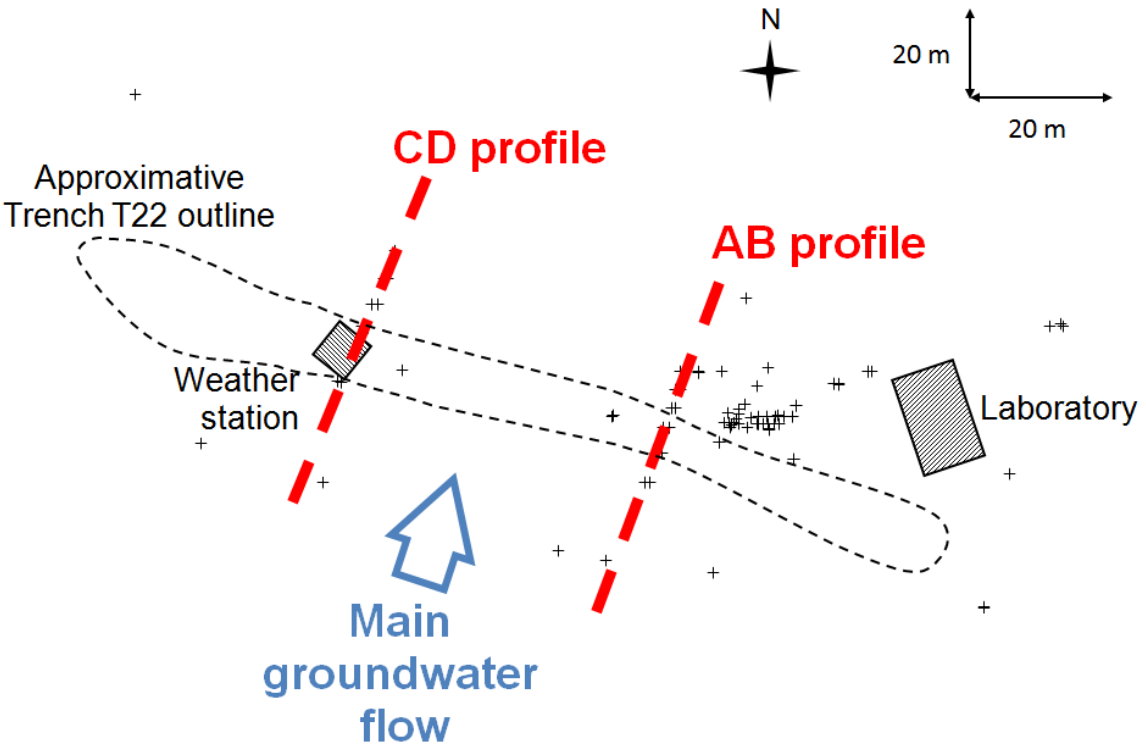

Figure II-7: Map of the Chernobyl Pilot Site

Around 100 piezometers were installed in the vicinity of the trench in order to follow radionuclides migration (Figure II-7). Most of them were organized along two lines, called hereafter AB-profile (or AA' profile or "Laboratory" profile) and CD-profile (or "Weather Station" profile) (Figure II-8 and Figure II-9). Some piezometers were equipped with TD-diver sensors to record groundwater table variations. Porous cup were planted in the trench to study soil solution. A weather station was also set up to collect precipitations data, wind direction… A "field laboratory" was set up for sample filtration, *in situ* measurements (alkalinity, sulfur…) and material storage. The map of the Chernobyl Pilot Site and profiles of piezometers are reported in Annexes 1 and 2.

Most of piezometers are made of PVC tubes with a diameter of 2.5 cm, a 20 cm long stainless steel mesh screens and isolated by a 20 cm thick bentonite layer, in order to avoid cross-contamination between piezometers (Dewière *et al.*, 2004).

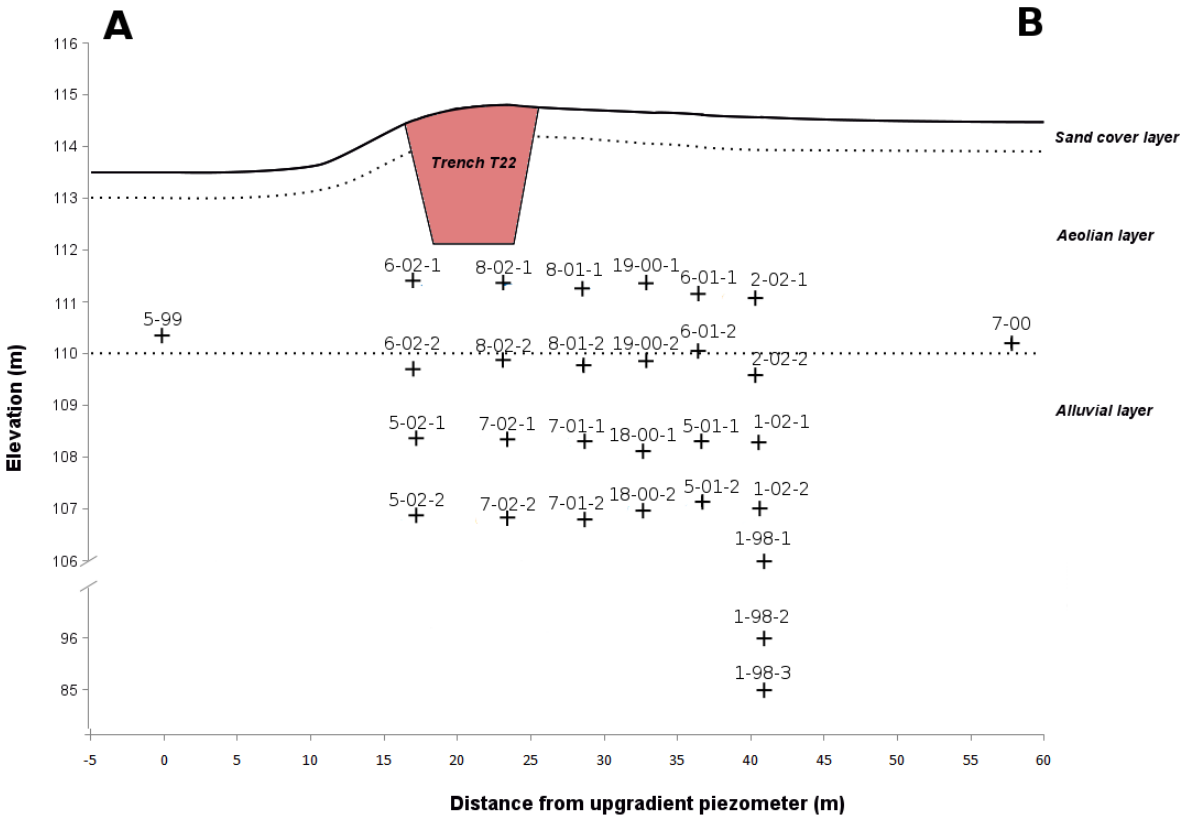

Figure II-8: Piezometers on AB profile

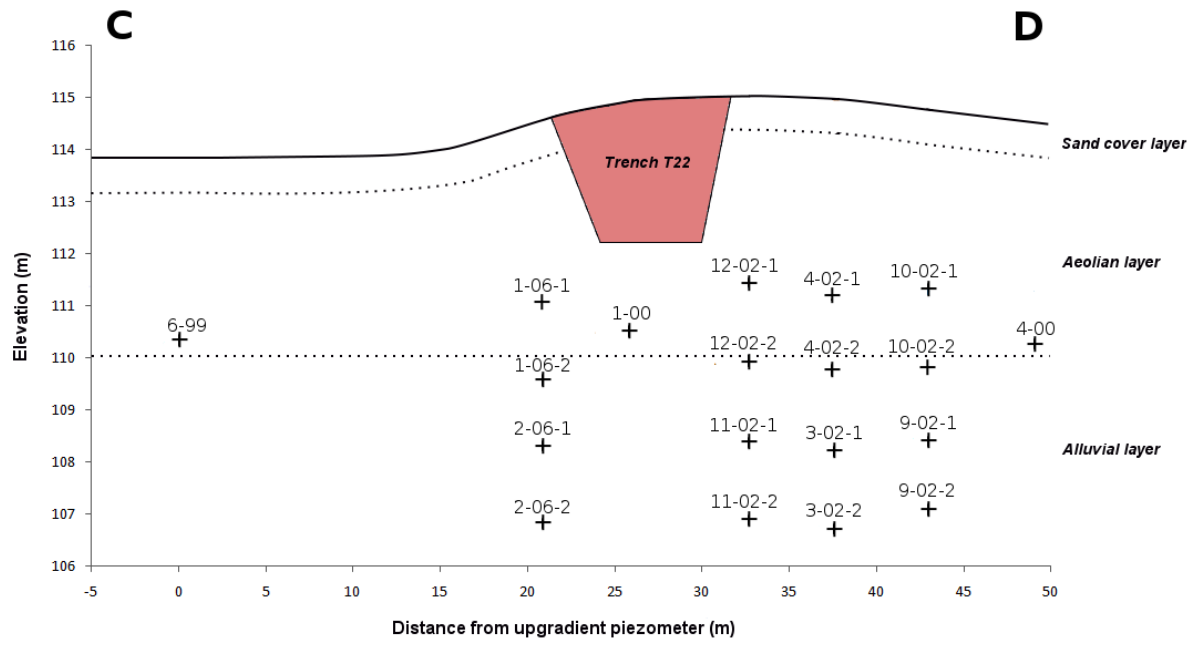

Figure II-9: Piezometers on CD profile

Almost all piezometers are organized to sample groundwater at the same place at four different depths: the screen of the first piezometer is located at 4-meters-depth in the aeolian layer, the screen of the second at the interface between the aeolian and alluvial layers (around 5-meters-depth), and the screens of the last two piezometers are in the alluvial layer, at 6 and 8 meters depth respectively. On the AB-profile, three piezometers (1-98-1, 1-98-2 and 1-98-3) were installed to sample groundwater at greater depth, respectively at 10, 20 and 30 meters-depth. These last piezometers were not isolated by a bentonite layer.

Spatial scattering of those piezometers allow a good identification of the ^{90}Sr contaminant plume as shown in Figure II-10.

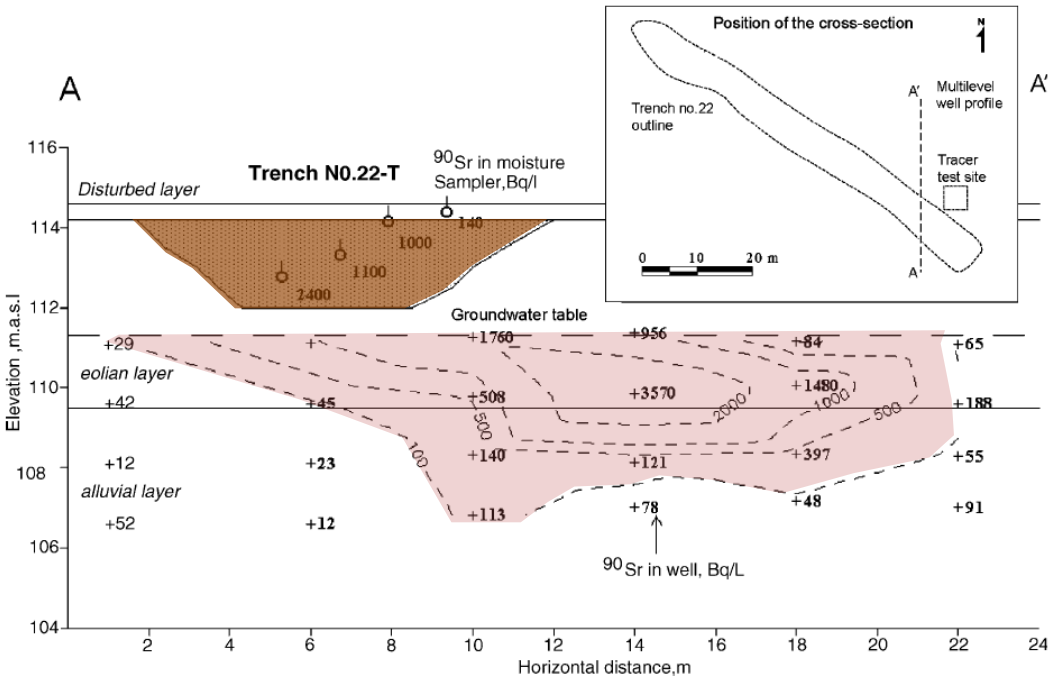

Figure II-10: ^{90}Sr plume downgradient of the trench T22 (from Dewière et al., 2004)

II.2.2 MIGRATIONS FROM THE TRENCH T22

II.2.2.1 Alteration of buried fuel particles and associated radionuclides

Particles from the Chernobyl unit 4 explosion were identified far away from the Power Plant (Pöllänen *et al.*, 1997; Kuriny *et al.*, 1993). Different kinds of fuel particles were formed following the explosion. The inventory of the particles showed two kinds of particles (Ahamdach and Stammose, 2000; Kashparov *et al.*, 2009; Van Meir *et al.*, 2009; Kashparov *et al.*, 2012):

- particles with a Zr-U-O matrix, chemically stable. They are linked to the melt of combustible sheath and were formed during the early stage of the accident. Their dissolution is very slow.
- non oxided UO_2 and oxided particles UO_{2+x}. The first are almost chemically stable. Dispersion of those particles results from the reactor destruction and not from the burning. The second particles are the less chemically stable: dissolution figures were observed on surface. They were formed following the burning of the core by oxidation of the fuel.

Among those particles, uranium oxides were identified and show isotopic signature close to the enriched fuel at 2-2.4% in ^{235}U of the unit 4 core: In soils of the exclusion zone, $^{238}U/^{235}U$ ratio were measured after the accident and showed ratios between 39.18 and 124.67 (leaching by HCl, Sobotovitch and Bondarenko, 2001). In the Red Forest area, $^{238}U/^{235}U$ ratio in soil was 57.07 (Sobotovitch and Bondarenko, 2001), suggesting the presence of fuel particles.

The dissolution of fuel particles results in the release of uranium and radionuclides associated to the fuel particles matrix (Kashparov *et al.*, 2000; Kashparov *et al.*, 2004). This dissolution was shown to depend on the type, the oxidation state of the particles and the solution p*H* (Kashparov *et al.*, 2000). Globally, at neutral p*H* (natural water), dissolution rate is low while it increases at lower and higher p*H* (Figure II-11) (Kashparov *et al.*, 2000; Van Meir *et al.*, 2009).

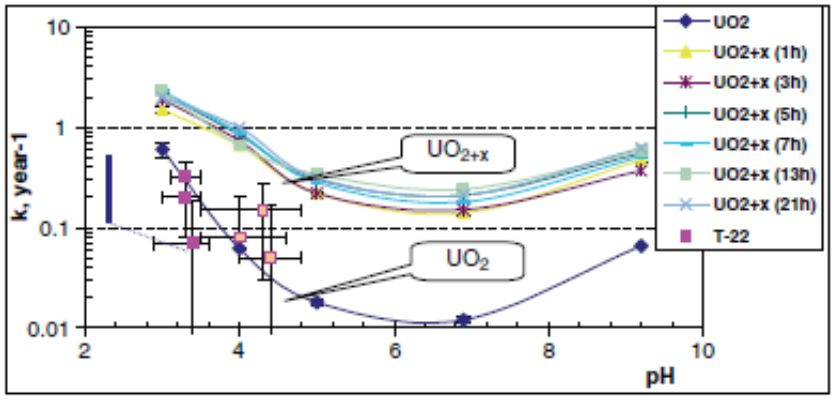

Figure II-11: Kinectics of dissolution of more or less annealed fuel particles following pH (from Van Meir et al., 2009)

In 2000, inventory of radionuclides buried in the trench T22 was calculated from the ^{137}Cs specific activity and from the 600 ± 240 GBq of ^{137}Cs, it was deduced 4 ±

1.6 GBq of ^{154}Eu and 290 ± 140 GBq of ^{90}Sr (Kashparov *et al.*, 2012). 10-30% of this inventory should be associated to stable fuel particles Zr-U-O (Dewière *et al.*, 2004). Among this ^{90}Sr total activity (Dewière *et al.*, 2004):

- between 30 and 60% should be associated to quite stable UO_2 particles;
- 36% of this activity is not associated to fuel particles and are potentially under a mobile form. Between 1987 and 2000, ^{90}Sr fraction which could have migrated was estimated to 7 ± 5% of the total initial activity (Kashparov *et al.*, 2012). This quantity is in agreement with the estimation of the ^{90}Sr in groundwater (Dewière *et al.*, 2004).

II.2.2.2 Other processes in the trench

Other processes occurring in the trench are supposed to have important impacts on groundwater geochemistry and radionuclide migration, such as biogeochemical processes. Indeed, organic matter is supposed to be less than 17% of the buried material and the presence of this organic matter can have an impact on microbial activity and plant uptake (Bugai *et al.*, 2012a). Trench T22 is favorable to organic matter decomposition (litter quality, O_2 access, water saturation…) and processes of CO_2 production (and consequently acidification of water) and nitrification are assumed (Bugai *et al.*, 2012a; Martin-Garin *et al.*, 2012).

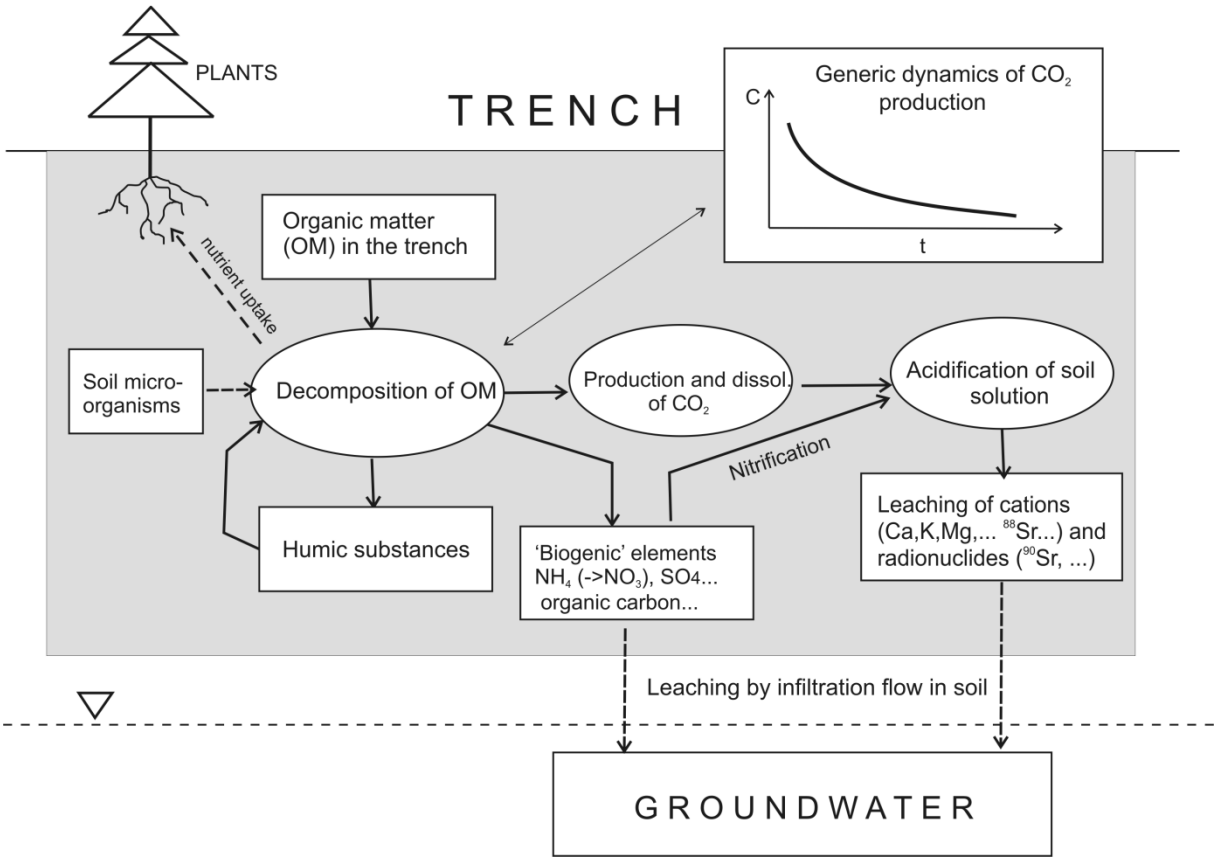

Figure II-12: Biogeochemical processes in trench T22 according to Martin-Garin et al., 2012

^{90}Sr was also assessed to be uptaken by vegetation (Bugai *et al.*, 2012a).

These biogeochemical processes result in increase of concentrations (Ca^{2+}, K^{+}, H^{+}, NO_3^{-}, SO_4^{2-}) in groundwater compared with "background" groundwater, even if this is less observed since few years (Bugai *et al.*, 2012a).

II.2.2.3 Strontium-90 migration from the trench in the aquifer

^{90}Sr plume in groundwater was shown from the trench along the main flow direction (Dewière *et al.*, 2004) (Figure II-10). In 2001, ^{90}Sr volumetric activities of 1000-2000 $Bq.L^{-1}$ were measured until 10 m downgradient of the trench (Dewière *et al.*, 2004). This migration would be the result of ^{90}Sr leaching from the trench by meteoric water infiltration, which would then cross the unsaturated area to join the groundwater where it would be easily transported horizontally promoted by the aeolian layer permeability (Dewière *et al.*, 2004) (Table II-1). In groundwater, ^{90}Sr velocity was shown to be 9% of the groundwater flow velocity (Dewière *et al.*, 2004).

Sorption processes in the aquifer were studied to explain this retardation, more specifically in the unsaturated aeolian layer (Szenknect, 2003; Mazet, 2008). Szenknect (2003) showed that ^{90}Sr migration was influenced by the number of exchange sites, physic-chemical conditions, exchanger composition and the presence of competitive ions (Ca^{2+}, Sr^{2+}). Water saturation was shown to influence the dispersivity of the plume (Szenknect, 2003). In transient state, Mazet (2008) showed that diffusion of ^{85}Sr to the immobile water can be negligible when exchange time is low compared to residence time.

Consequently, ^{90}Sr migration can be described directly by advective-dispersive equation using coefficient of retention K_d (Szenknect, 2003). Laboratory experiments (Szenknect, 2003; Mazet, 2008), *in situ* measurements (Bugai *et al.*, 2012a) were carried out in order to determine K_d:

- In the aeolian layer, K_d were estimated to be 1 to 3 $mL.g^{-1}$ in batch reactor experiments (Bugai *et al.*, 2012b) and between 0.2 to 5 $mL.g^{-1}$ by *in situ* and laboratory measurements (Bugai *et al.*, 2012b).
- Laboratory tests showed alluvial layer K_d of 20-50 $mL.g^{-1}$ in silty facies, 6°$mL.g^{-1}$ in interbed facies, and estimated to be 0.5 to 4 $meq.g^{-1}$ in dead channel facies from [Ca^{2+}] concentrations (Matoshko *et al.*, 2004). Other laboratory measurements showed K_d between 25 and 43 $mL.g^{-1}$ (Van Meir *et al.*, 2009).

In unsaturated conditions, ^{90}Sr migration simulations fit well with data using coefficients of 0.5 $mL.g^{-1}$ in the aeolian layer and 1-4 $mL.g^{-1}$ in the alluvial layer (Van Meir *et al.*, 2009). These K_d are quite different from values determined in laboratory. This can be explained by higher exchange site access in laboratory experiments (particularly in static experiments), quite different physic-chemical conditions and influence of competitive cation, such as Ca^{2+} and stable Sr^{2+} (Szenknect, 2003). Based on the hydrological knowledge, ^{90}Sr migration was simulated in groundwater and modeling predictions were carried out (Figure II-10) (Van Meir *et al.*, 2009; Bugai *et al.*, 2012b).

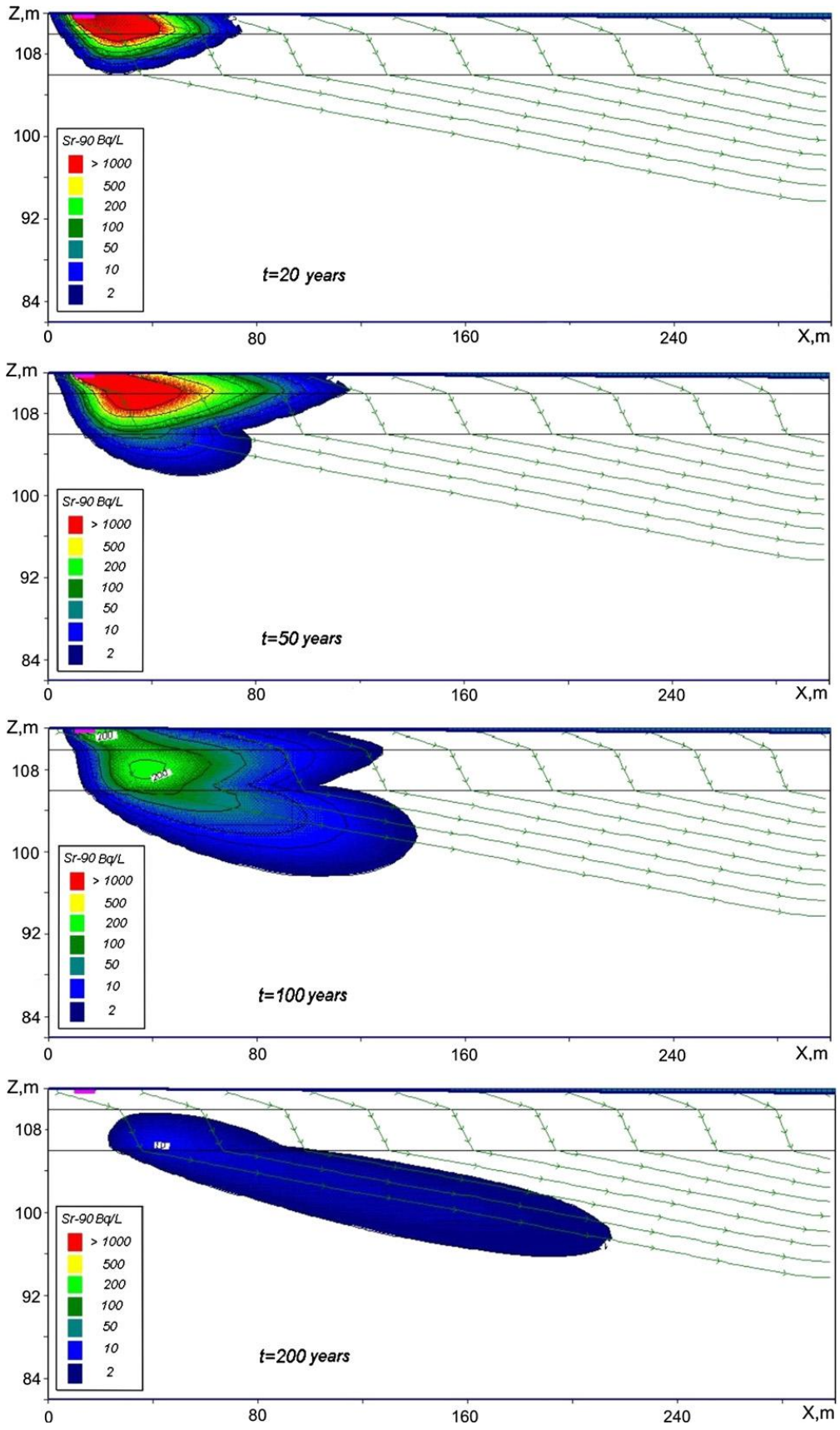

Figure II-13: Modelling predictions of ^{90}Sr migration in groundwater (from Bugai et al., 2012b)

III. NON-REACTIVE TRANSPORT

III.1 INTRODUCTION

In order to predict radionuclide migration from trench T22 in groundwater, the maximal extent of contaminant plume has to be determined. This extent corresponds to the distance travelled by radionuclides from the trench following the fastest transport process.

Strontium-90 is the main contaminant of the aquifer and the migration of this radionuclide was largely investigated (Szenknect, 2003; Dewière *et al.*, 2004; Mazet, 2008; Bugai *et al.*, 2012b; Bugai *et al.*, 2012a; Van Meir *et al.*, 2009). Thus, after 15 years since waste burial, a 20-meters plume was shown in groundwater downgradient of trench T22 (Dewière *et al.*, 2004).

However, strontium is a reactive element and was shown to be retarded relatively to the groundwater flow by retention processes (Dewière *et al.*, 2004). Consequently, the strontium-90's plume does not show the maximal extent of the contamination because less reactive elements, less constrained by such processes, should have migrated further. Migration of elements following non reactive process has to be investigated to determine the maximal extent of the contaminant plume.

III.1.1 NON-REACTIVE TRANSPORT PROCESSES

Considering that reactions such as sorption or precipitations are mostly slowing down element migrations in groundwater, the study has to focus only on non-reactive processes. In non-reactive transport, two main processes are considered: transport by advection and transport by concentration gradient (Fetter, 2008).

Transport by advection is the migration of a solute with the groundwater flow. This flow can be described by Darcy's law (Appelo and Postma, 2005). Consequently, the mass flux of solute by advection depends on this law and can be obtained by multiplying the water velocity by the concentration (Appelo and Postma, 2005; Fetter, 2008):

Equation III-1

$$F = \frac{-K}{n_{eff}} \times \frac{dh}{dl} \times C$$

where F is the mass flux of solute ($m^2.s^{-1}$), K is the hydraulic conductivity ($m.s^{-1}$), n_{eff} is the effective porosity, dh/dl is the gradient of hydraulic head ($m.m^{-1}$) and C is the concentration of solute ($mol.m^{-3}$).

Transport by concentration gradient, also called diffusion, can be defined as the migration of a solute from a concentrated area to a less concentrated area. It is described by Fick's laws (Fetter, 2008).

Equation III-2

$$F = -D_d\left(\frac{dC}{dx}\right)$$

where, F is the flux ($m^2.s^{-1}$), D_d is the diffusion coefficient ($m^2.s^{-1}$), C is the concentration ($mol.m^{-3}$) and x is the distance (m).

In groundwater, diffusion processes cannot be mathematically dissociated from mechanical dispersion processes, which can be also described by Fick's laws (Appelo and Postma, 2005). The dispersion process is described as the difference between a solute velocity and the average groundwater velocity; it depends on pore size, path length and friction in pores (Fetter, 2008). Diffusion and dispersion are defined by a common parameter called the hydrodynamic dispersion coefficient.

At the Chernobyl Pilot Site, transport by advection-dispersion was largely investigated and most of the related hydrodynamic parameters were determined (Dewière *et al.*, 2004; Matoshko *et al.*, 2004; Bugai *et al.*, 2012b) (See Chapter II Study Site).

III.1.2 CONSERVATIVE TRACER

In groundwater, strictly non-reactive elements do not exist however, in natural water, some elements may be considered as non-reactive. Here, a conservative tracer is defined as any element that has negligible interaction with the porous medium in which it travels and is solely influenced by the groundwater movement.

In groundwater, chlorine is a well-known conservative tracer (Bentley *et al.*, 1986; Phillips, 2000); the chloride ion, Cl^-, is transported at water velocity, as a consequence of the high stability of Cl^- in the aquatic environment and the negative charge limiting adsorption onto silicates surfaces, mostly charged

negatively (Phillips, 2000). It is transported by advection at the groundwater flow velocity and, in some instances, it may move at a slightly higher velocity than the mean velocity of the groundwater because of the anionic exclusion effect, repulsing negative charges (Phillips, 2000). Moreover, [Cl-] concentrations are less influenced by geochemical processes in groundwater, excepted evapotranspiration processes, NaCl and KCl dissolutions and anthropogenic pollutions.

The radioisotope chlorine-36 (^{36}Cl), which is a product of nuclear activity and which has been most likely released during the Chernobyl accident (Chant *et al.*, 1986), is of interest at such short time scale (half-life: $3.01\times10^5 \pm 0.04\times10^5$ years; Endt and Van der Leun, 1973). This tracer is commonly used as a tool for dating groundwater (determination of residence time, reconstitution of paleoclimatic variations), to study transport processes (mixing processes, determination of hydrodynamic parameters, groundwater velocity calculation), in the determination of the origin of salinity and subsurface concentration processes… (Bentley *et al.*, 1986 ; Phillips, 2000). ^{36}Cl is also known to be produced by nuclear activity, mostly by neutron activation of ^{35}Cl (Phillips, 2000). For example, an important amount of ^{36}Cl was produced during thermonuclear tests performed in the 1950's. The signature of this release was found in rainwater, groundwater and soils and recorded in glaciers all over the world (Elmore *et al.*, 1982; Bentley *et al.*, 1982; Schaeffer *et al.*, 1960; Finkel *et al.*, 1980; Green *et al.*, 2000; Green *et al.*, 2004 ; Scanlon *et al.*, 1990). Furthermore, this bomb-pulse may be used as a specific tracer in groundwater studies: identification of saline sources, studies of soil water movement (usually compared with ^{3}H content), determination of groundwater velocity or dispersivity and recharge characterization (Bentley *et al.*, 1986 ; Phillips, 2000)…

III.1.3 PROBLEM STATEMENT

In order to determine the maximal extent of the contaminant plume from trench T22 and study the influence of non-reactive transport processes, migration of low reactive elements needs to be investigated. ^{36}Cl should be a good tracer in such investigation because of its conservative properties and because of its potential nuclear release during the Chernobyl accident.

First, the ^{36}Cl content is characterized in groundwater and the potential origins in the Chernobyl Pilot Site groundwater are discussed. Then, processes involved in ^{36}Cl migration in groundwater are investigated based on the comparison with [Cl^-]

concentrations and ^{90}Sr volumetric activities, focusing more specifically on potential mixing processes. Finally, ^{36}Cl migration from trench T22 is simulated according to the present hydrogeological knowledge of the system and the results are compared to the observed data.

III.2 SAMPLES AND ANALYSES

III.2.1 SAMPLING

In order to investigate ^{36}Cl content in the Chernobyl Pilot Site groundwater, three sampling campaigns were carried out: two when the water table was low (October 2008 and October 2009) and one when the water table was high (May 2011).

III.2.1.1 Strategy of sampling

In the early 2000's, tracer tests were performed at the Chernobyl Pilot Site, injecting ^{36}Cl downgradient of the trench, in the vicinity of the AB-profile (Annex 1). The tests aimed at determining groundwater velocity (1999-2001, Bugai *et al.*, 2012b). Hence, in order to avoid any ^{36}Cl contamination, most groundwater samples were collected along the CD profile (Annex 1).

Indeed, because of the North-north-east groundwater flow direction, the injected ^{36}Cl cannot reach the CD profile. Furthermore, considering a pure advective transport with a flow velocity of 3.5×10^{-7} $m.s^{-1}$ (≈3 $cm.day^{-1}$; Bugai *et al.*, 2012b), after 7 years (*i.e.* 2008), the injected ^{36}Cl would move 77.3 m in the aeolian layer. That is twice as far than the distance between the injection points and the furthest piezometer on the CD profile (40-45 m).

As seen earlier (§III.2.1.1), deeper groundwater are sampled in several points. Three particularly interesting deep piezometers (1-98-1, 1-98-2, 1-98-3 piezometers) are located on the AB profile (Annex 1), reaching a depth of 10, 20 and 30 meters, respectively. The absence of contamination tracer test of groundwater sampled in these piezometers is assumed, based on the apparent ages of groundwater of the two deeper piezometers (older than 33 years, Le Gal La Salle *et al.*, 2012) corroborated by the distance travelled by the tracing test in 7 years, and another groundwater sample collected at 10-meters-depth far from the injection point contamination.

III.2.1.2 Sampling

First investigations were carried out during the sampling campaigns of October 2008 and October 2009 and groundwater was sampled in a total of 10 piezometers. In order to obtain a complete dataset on the CD-profile of the ^{36}Cl content in the groundwater and to compare low water table period with high water table period, a last sampling campaign was performed in May 2011 when 21 groundwater samples were collected at the Chernobyl Pilot Site. In addition, to better identify ^{36}Cl origins, samples from leaves (birch) were collected and a soil water sample from a porous ceramic cup located at 1.25 meters depth into the trench on the CD profile was analyzed. A groundwater sample outside the Chernobyl Pilot Site, located upgradient and in the vicinity of waste mounds and the water of the Borshchii River were collected for comparison.

Groundwater was sampled using a peristaltic pump. A volume between 3 to 5 L of water was firstly pumped to purge piezometers and to clean the pumping device, then sampling was carried out. 1.5-2 L of water were pumped and filtered. 200 mL of this volume were conditioned in two 125 mL polyethylene bottles for anion analysis (including chloride) and for cation analysis (including ^{90}Sr). Bottles for cation analysis were acidified at a pH lower than 2.5 with concentrated HNO_3. For $^{36}Cl/Cl$ ratio analyses, between 1 and 8 L were pumped and conditioned in polyethylene bottles. During the 2008 campaign, samples for $^{36}Cl/Cl$ ratio analyses were preconcentrated on site by a factor 6 to reduce sample volume. In May 2011, in regard to the high ^{36}Cl content measured, the volume of sample was reduced to 250 mL of sample (see below for the applied protocol of sample preparation for ^{36}Cl analyses §III.2.2.3).

The soil water was sampled from a porous cup using a manual vacuum pump. As the volume of sample in the porous cup is commonly very limited, the cleaning volume was reduced. Water was filtered and conditioned in two 125 mL polyethylene bottles for anion and cation analysis. As before, the cation bottle was also acidified at pH below 2.5. $^{36}Cl/Cl$ ratios were analyzed from the bottle reserved for anion analysis.

Birch leaves samples were taken on the edge of the CD profile above trench T22. A dose rate of 15 $\mu Sv.h^{-1}$ was measured on contact, showing that these trees have taken up radioactive water from the soil. Two different extracting protocols were

tested. In the first, approximately 350 leaves (about 28g) were crushed and leached with distillated water. In the second, about 90 g of leaves were burnt in an oven at 400°C until reduction to ashes. Ashes were then leached with distillated water. Then, both solutions were acidified at pH 4. In order to remove any radioactive cation from the solution, the leachate was filtered through DOWEX resin (DOW inc.). The same resin was used for both leachates: crushed leaf leachate was filtered first, then the resin was cleaned with HCl and finally, the ashed leaf leachate was filtered. Leachates were then conditioned in 250mL bottles. Hereafter, the sample from crushing is named TCV 1 and sample from the burning is named TCV 2 (for TChernobyl Vegetation 1 and 2).

The groundwater sampled outside the Chernobyl Pilot Site (IGS33 piezometer) was collected using the manual peristaltic pump and after a purge of the piezometer. The sample was then filtered and conditioned in two 125 mL polyethylene bottles for anion and cation analysis. The cation bottle was acidified at p*H* lower than 2.5 too. For $^{36}Cl/Cl$ ratio analysis, 250 mL of sample were conditioned separately.

Borshchii river water was sampled close to the outlet, filtered and conditioned in two 125 mL polyethylene bottles for anion and cation analysis. Again, the cation bottle was acidified at p*H* lower than 2.5. For $^{36}Cl/Cl$ ratio analysis, a volume of 6 mL was taken from the 125mL bottle reserved for anion analysis.

III.2.2 ANALYSES

III.2.2.1 Strontium-90 analyses

^{90}Sr volumetric activities were measured at the Analysis and Experimental facilities Laboratory (IRSN/LAME) by liquid scintillation: 10 mL of samples were mixed with 10 mL of Ultimagold AB and were then analyzed on Liquid Scintillation Analyzer TRI-CARB 3170 TR/SL (Packard inc., Bassot *et al.*, 2010).

Then, those activities are reported in $[^{90}Sr]$, in $mmol.L^{-1}$, using the equation:

Equation III-3

$$\left[^{90}Sr\right] = \frac{A_{^{90}Sr} * 1000 * 365.25 * 24 * 3600}{\lambda_{^{90}Sr} * N_A}$$

where A_{90Sr} is the ^{90}Sr volumetric activity ($Bq.L^{-1}$), λ_{90Sr} the constant of ^{90}Sr radioactive decay, equal to 0.024 y^{-1}, and N_A the Avrogadro number.

III.2.2.2 Chloride analyses

Chloride concentrations were measured by ion chromatography at the Analysis and Experimental facilities Laboratory (IRSN/LAME) on a Compact IC 861 Metrohm Ion Chromatograph (Metrohm inc.; Bassot *et al.*, 2010[1]). Three measurements were performed to assess repeatability. Resulting analytical uncertainties range between 0.0002 and 0.04 mmol.L^{-1}. Results are reported in Annex 5.

III.2.2.3 Chlorine-36 analyses

III.2.2.3.1 Australian National University measurements

The October 2008 and October 2009 samples were analyzed by accelerator mass spectrometry (AMS) at the Department of Nuclear Physics at the Australian National University (ANU). The protocol followed for sample preparation was adapted from Conard *et al*. (1986).

Before sample preparation, all laboratory ware (tubes, beakers) was cleaned in a bath of HNO_3 65% solution diluted with tri-distilled water. Between 1 to 6 L of each sample was evaporated in 1 L glass beakers to 300 mL approximately. Two blanks of Weeks Island halite were prepared in parallel. Chlorine was precipitated as AgCl by adding an excess of $AgNO_3$ (relative to chloride concentration). The precipitate was left to settle overnight and most of the liquid phase was removed. The precipitate was then dissolved by adding few milliliters of ammonia solution at 25%. A few milliliters of a saturated solution of $BaNO_{3\ aq}$ were added to precipitate any sulfate as barium sulfate. The solution was filtered to remove the barium sulfate to minimize the ^{36}S content of the sample. The filtrate was poured into a centrifuge tube and AgCl reprecipitated by adding few milliliters of HNO_3 at 65%.The tube was then centrifuged, the supernatant poured off, and the precipitate rinsed twice with tri-distilled water. Finally, the precipitate was dried at 50-60°C, with the tube wrapped in an aluminum foil to protect the precipitate from direct light.

^{90}Sr volumetric activities were measured in each removed supernatant of the most contaminated sample (4-00) in order to verify that most of the ^{90}Sr was removed from the AgCl precipitate.

[1] Detection limit: close to 0.001 mmol.L^{-1}

As these first measurements revealed unexpectedly high $^{36}Cl/Cl$ ratios, approaching 10^{-8} at.at^{-1} for the most ^{36}Cl-concentrated sample, counting times were reduced to prevent contamination of the AMS ion source. Large uncertainties resulted from very short counting times used. The two blanks of Weeks Island halite were analyzed after the high-level samples, and gave $^{36}Cl/Cl$ ratios of 1.4×10^{-13} and 1.8×10^{-13} at.at^{-1}. These high values are two orders of magnitude higher than typical blanks, and result from cross-contamination of the high-level samples in the ion source.

III.2.2.3.2 ASTER measurements

To confirm the measurements and reduce these uncertainties, isotopic dilution was carried out on two samples from the October 2008 field campaign, samples chosen are those showing the lowest and the highest $^{36}Cl/Cl$ ratios, respectively groundwater sampled in piezometers 1-98-2 and 4-00, both diluted with halite solutions of known chloride concentration (measured by ionic chromatography in the hydrogeology laboratory of Avignon University, LHA) and analyzed on the French AMS national facility, ASTER, located at CEREGE. $^{36}Cl/Cl$ ratios are calculated from measured $^{36}Cl/^{35}Cl$ ratio and considering the average natural $^{35}Cl/Cl$ ratio of 0.7575 (Rosman and Taylor, 1998). Calculated uncertainties on $^{36}Cl/Cl$ ratios take into account the measurement uncertainty as well as the natural variation of the $^{37}Cl/^{35}Cl$ ratio[2] (Rosman and Taylor, 1998). The $^{36}Cl/Cl$ ratio of the original sample is derived from the following equation:

Equation III-4

$$\left(\frac{^{36}Cl}{Cl}\right)_{measured} = \frac{^{36}Cl_{sample} + ^{36}Cl_{halite}}{Cl_{sample} + Cl_{halite}}$$

where $^{36}Cl_{\ sample}$ and $^{36}Cl_{\ halite}$ are the amount in atoms of ^{36}Cl in the sample and in the halite solution respectively and $Cl_{\ sample}$ and $Cl_{\ halite}$ are the amount in atoms of Cl in the sample and in the halite solution respectively.

The sample $^{36}Cl/Cl$ ratio can be written as follows:

[2] In the environment, chlorine has two natural isotopes, ^{35}Cl (75.64 to 75.86% of total chlorine) and ^{37}Cl (24.36 to 24.14% % of total chlorine) (Rosman and Taylor, 1998)

Equation III-5

$$\left(\frac{^{36}Cl}{Cl}\right)_{sample} = \left(\frac{^{36}Cl}{Cl}\right)_{measured} * \frac{Cl_{sample} + Cl_{halite}}{Cl_{sample}} - \left(\frac{^{36}Cl}{Cl}\right)_{halite} * \frac{Cl_{halite}}{Cl_{sample}}$$

The $^{36}Cl/Cl$ ratio of halite solutions were analyzed and showed as expected very low $^{36}Cl/Cl$ ratios of $5.4\times10^{-16} \pm 1\times10^{-16}$ and $2.1\times10^{-15} \pm 0.7\times10^{-15}$ at.at^{-1} (Annex 3).

The duplicates analyzed both at ANU and on ASTER lead to coherent values (in Annex 5). Reassured by these results, the samples from May 2011 were handled in a similar way: three isotopic dilutions were carried out for each sample collected during the May 2011 sampling campaign and analyzed on ASTER. Dilutions were performed with two solutions with different concentration in halite standard (NIST SRM 999b), of which [Cl^-] concentrations were analyzed at the Analysis and Experimental facilities Laboratory (IRSN/LAME) and prepared as blanks for ASTER analyses. Results of these analyses, calculated values and [Cl^-] concentrations are given in Annex 4.

[^{36}Cl] concentrations are calculated from inferred groundwater $^{36}Cl/Cl$ ratio and measured [Cl^-] concentrations, in mmol.L^{-1}, using the equation:

Equation III-6

$$[^{36}Cl] = \left(\frac{^{36}Cl}{Cl}\right)_{calculated} * [Cl^-]$$

III.3 RESULTS

$^{36}Cl/Cl$ ratios, [^{36}Cl] concentrations, [Cl^-] concentrations and [^{90}Sr] concentrations are presented in four different tables, according to the type and time of sampling and location. These tables are reported in Annex 5.

The first table shows sampled piezometers, piezometer screen elevation, chloride concentrations, [^{90}Sr] concentrations, measured $^{36}Cl/Cl$ ratios and calculated [^{36}Cl] concentrations for samples collected in October 2008 and October 2009.

Results of sample analyses, from May 2011 campaign, are shown in the three following tables. These tables present all calculated $^{36}Cl/Cl$ ratios, according to the considered dilution. Corresponding measured $^{36}Cl/Cl$ ratios are given in Annexes 3 and 4. [Cl^-] concentrations, calculated $^{36}Cl/Cl$ ratios and calculated [^{36}Cl] concentrations for samples collected outside the Chernobyl Pilot Site are shown in

the second table of Annex 5. Calculated $^{36}Cl/Cl$ ratios in the two leaf leachates are given in the third (Annex 5). Finally, the fourth table (Annex 5) presents samples name, piezometer screen elevation, chloride concentrations, [^{90}Sr] concentrations, $^{36}Cl/Cl$ ratios and calculated [^{36}Cl] concentrations of soil and groundwater samples collected at the Chernobyl Pilot Site.

^{90}Sr concentrations range between below the detection limit (around 10^{-12} mmol.L^{-1}) and 4×10^{-8} mmol.L^{-1}. The highest value is measured in the soil water sampled in May 2011. In groundwater, the highest values are measured downgradient of trench T22 but groundwater sampled in the most upgradient piezometer (6-99) shows also some contamination with [^{90}Sr] concentrations up to 10^{-10} mmol.L^{-1} (for October 2008 and May 2011 sampling campaigns). The [^{90}Sr] concentrations are lower in deeper groundwater (alluvial layer) and in groundwater just upgradient of the trench (1-06-1, 1-06-2 piezometers). Most of the deepest groundwater [^{90}Sr] concentrations are below the detection limit (1-98-2, 1-98-3 piezometers) while sample collected in the 1-98-1 piezometer show [^{90}Sr] concentrations 5×10^{-12} mmol.L^{-1}.

At the Chernobyl Pilot Site, [Cl^-] concentrations range between 0.008 and 0.35 mmol.L^{-1} and are similar for the three field campaigns. May 2011 [Cl^-] are reported along the CD profile in (Figure III-1). The highest concentration is measured in the soil water sample collected in May 2011 on the CD profile. In shallow groundwater of the site, [Cl^-] concentrations are one order of magnitude lower, ranging from 0.008 to 0.035 mmol.L^{-1}: the highest [Cl^-] concentrations are close to 0.03 mmol.L^{-1} and are observed in groundwater sampled downgradient of trench T22 or in groundwater sampled in the more upgradient piezometer (6-99). Otherwise, [Cl^-] concentrations of groundwater at the Chernobyl Pilot Site are mostly between 0.01 and 0.02 mmol.L^{-1} as for groundwater sampled outside the Chernobyl Pilot Site. Deep groundwater (AB profile and 1-01 piezometers) shows higher [Cl^-] concentrations, of up to 0.024 mmol.L^{-1}. More specifically, the deep 1-98-2 piezometer shows the highest concentrations in groundwater, close to 0.05 mmol.L^{-1}, for both October 2008 and May 2011 field campaigns. [Cl^-] concentration at the outlet of the Borshchii river is close to this concentration, around 0.04 mmol.L^{-1}, which still remains in the meteoric water range (0.006 to 0.07 mmol.L^{-1}).

Calculated $^{36}Cl/Cl$ ratios and [^{36}Cl] concentrations range from 2 $\times10^{-12}$ to 1×10^{-8} at.at^{-1} and 6 $\times10^{-14}$ to 4 $\times10^{-9}$ mmol.L^{-1} respectively. $^{36}Cl/Cl$ ratios are reported in $\times10^{-10}$ at.at^{-1} along profiles in Figure III-2 and Figure III-3. Figure III-2 presents $^{36}Cl/Cl$ ratios for samples collected in October 2008 and October 2009 while Figure III-3 presents those for samples collected in May 2011. The highest $^{36}Cl/Cl$ ratio and [^{36}Cl] concentrations are observed in the soil water in the trench (Annex 5) and $^{36}Cl/Cl$ ratios in leaf leachates are in the same order of magnitude. Groundwater samples at the Chernobyl Pilot Site show $^{36}Cl/Cl$ ratios and [^{36}Cl] concentrations 1 to 4 orders of magnitude higher than the theoretical ratio in natural rainwater: highest $^{36}Cl/Cl$ ratios in groundwater are slightly up to 1×10^{-9} at.at^{-1} while highest [^{36}Cl] concentrations reaches 1×10^{-10} mmol.L^{-1}, those values are measured in groundwater downgradient of the trench. In shallow groundwater of the Chernobyl Pilot Site, other $^{36}Cl/Cl$ ratios and [^{36}Cl] concentrations are above 10^{-10} at.at^{-1} and 8 $\times10^{-12}$ mmol.L^{-1} respectively. The two deepest groundwater samples show the lowest $^{36}Cl/Cl$ ratio: at 20-meter-depth (1-98-2 piezometer), $^{36}Cl/Cl$ is close to 10^{-11} at.at^{-1} with a [^{36}Cl] concentrations of 1 $\times10^{-12}$ mmol.L^{-1} and decrease by one order of magnitude lower at 30-meters-depth (1-98-3 piezometer), where [^{36}Cl] concentration is 6×10^{-14} mmol.L^{-1}.

Groundwater sampled in the IGS-33 piezometer (outside the CPS) and in the Borschi river show $^{36}Cl/Cl$ ratios close to 10^{-11} at.at^{-1}. Borschi river shows [^{36}Cl] close to 1×10^{-12} mmol.L^{-1} whereas [^{36}Cl] in groundwater sampled in IGS33 piezometer is two orders of magnitude lower (3×10^{-13} mmol.L^{-1}).

In summary, three observations can be made. Firstly, both [^{90}Sr], [Cl^-] and $^{36}Cl/Cl$ ratios increase downgradient of the trench. Secondly, the most upgradient groundwater in the aeolian layer shows also high [^{90}Sr] and [^{36}Cl] too. Finally, [^{90}Sr] and [^{36}Cl] decrease with increasing depth, whereas [Cl^-] seem to slightly increase.

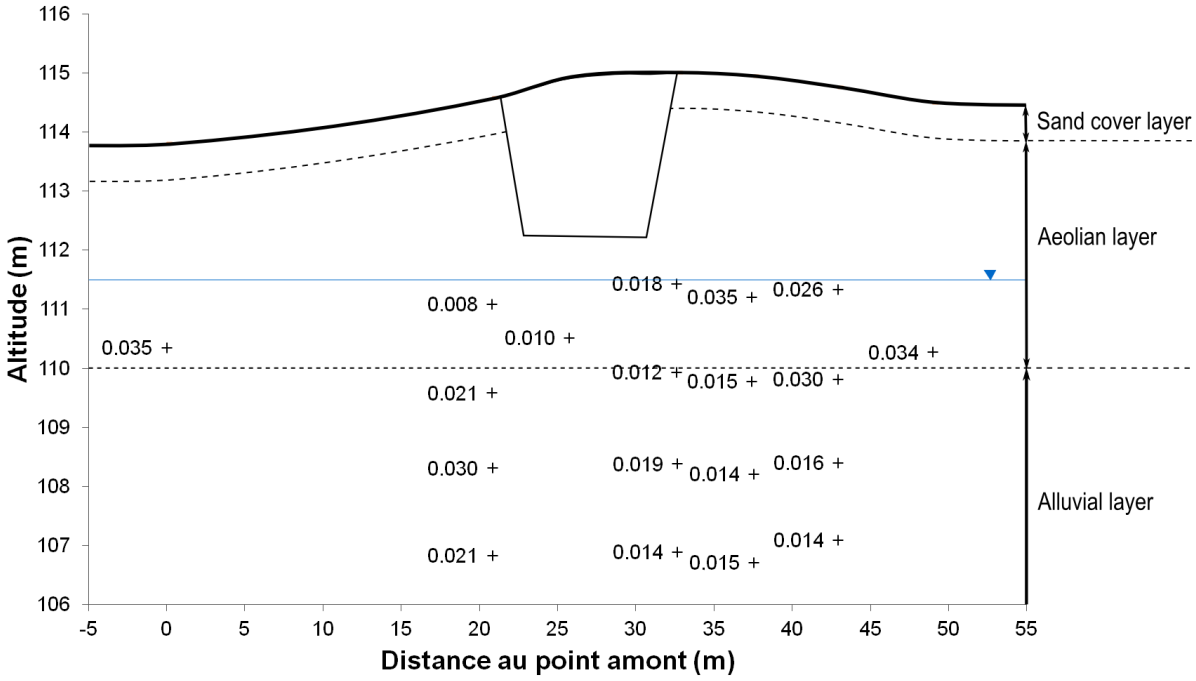

Figure III-1: Cl^- concentrations along the CD profile in May 2011 (in $mmol.L^{-1}$). Note that the y-scale is oversized in comparison with x-scale by approximately a factor 3.

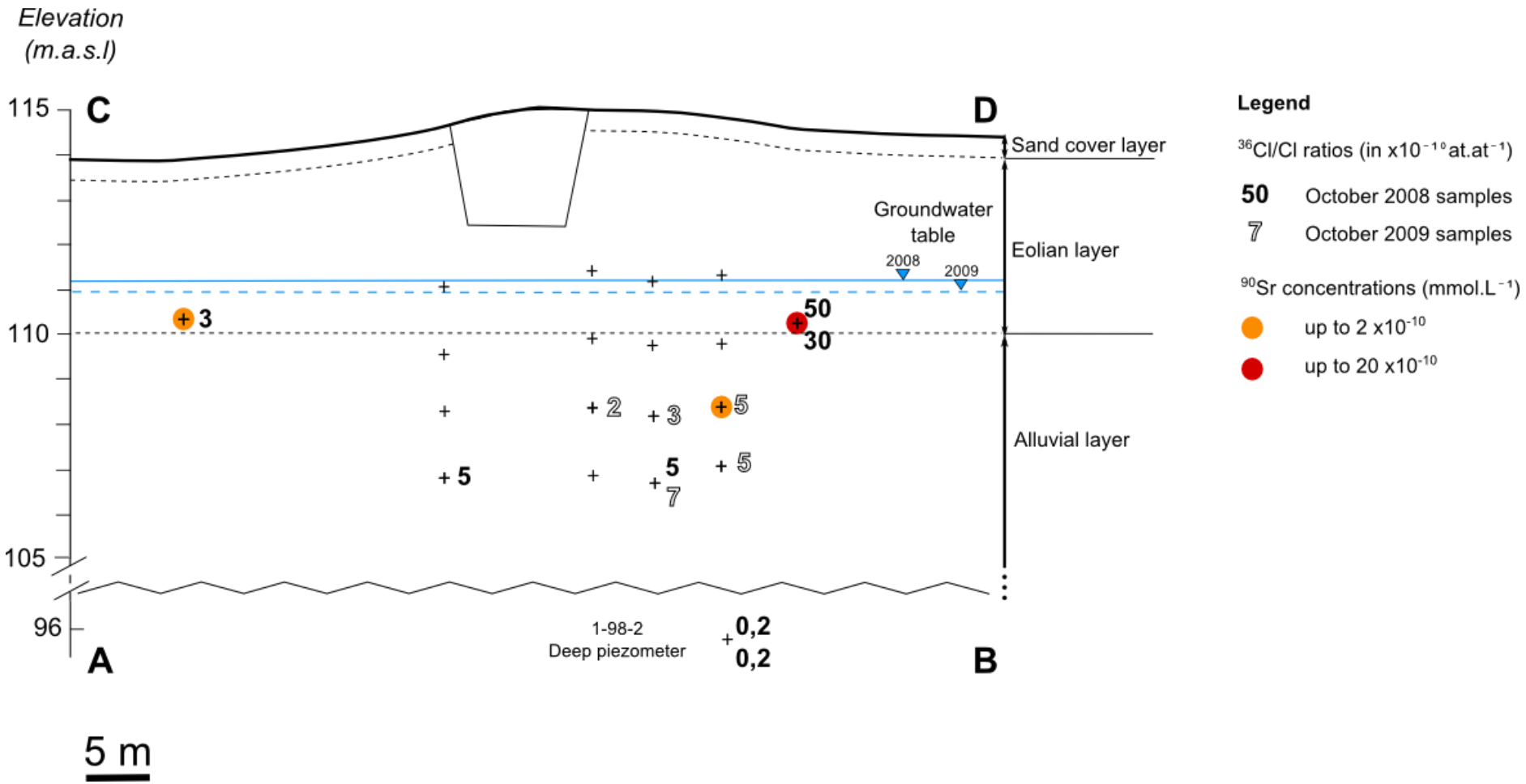

Figure III-2: $^{36}Cl/Cl$ ratios in groundwater along the CD profile in October 2008 and October 2009 (in $\times 10^{-10}$ at.at^{-1}). For the comparison, ^{90}Sr concentrations up to 2×10^{-10} are symbolized by colored circles. Note that the y-scale is oversized in comparison with x-scale by approximately a factor 3.

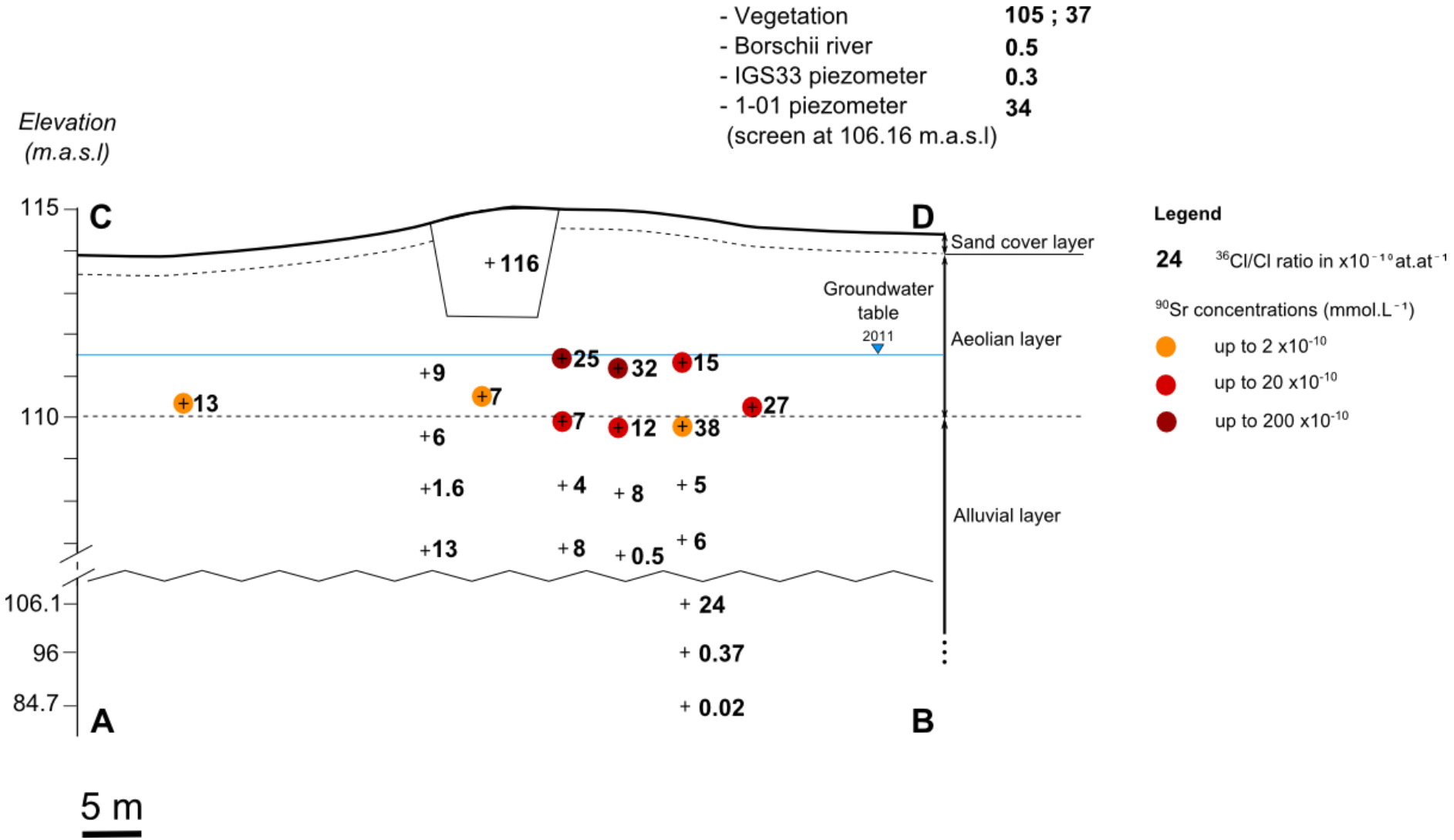

Figure III-3: $^{36}Cl/Cl$ ratios in groundwater along the CD profile in May 2011 (in $\times 10^{-10}$ at.at^{-1}). For the comparison, ^{90}Sr concentrations up to 2×10^{-10} are symbolized by colored circles. Note that the y-scale is oversized in comparison with x-scale by approximately a factor 3.

III.4 ^{36}Cl ORIGINS IN CHERNOBYL PILOT SITE GROUNDWATER

The increase of ^{90}Sr activities, [Cl^-] concentrations and ^{36}Cl/Cl ratios downgradient of trench T22 strongly suggests a migration of elements from the trench in the groundwater. In order to better understand radionuclide migration in groundwater, the source term has to be characterized.

Processes of release and ^{90}Sr migration from the trench were already discussed by Dewière *et al.* (2004) and Bugai *et al.* (2012a): the alteration of the fuel particles - in which ^{90}Sr is associated- leads to the release of ^{90}Sr through the unsaturated zone to the groundwater. However, ^{90}Sr interacts with the porous medium and is consequently not moving at groundwater velocity. Part of the ^{90}Sr released is also taken up by trees (Thiry *et al.*, 2009). According to Dewière *et al.* (2004), ^{90}Sr velocity was shown to be retarded at about 9% of the groundwater velocity.

However, identification of the ^{36}Cl sources is more complicated. Indeed, contrary to ^{90}Sr which is only from nuclear origin, ^{36}Cl is present in natural environments. In groundwater, ^{36}Cl has two origins: it can be produced *in situ* or it can result from the migration of ^{36}Cl produced elsewhere (Phillips, 2000). Moreover, in addition to natural sources, an anthropogenic production linked to nuclear activity has to be considered. All these potential origins of ^{36}Cl in Chernobyl Pilot Site groundwater are therefore reviewed.

III.4.1 NATURAL BACKGROUND

III.4.1.1 Cosmogenic production

Commonly, occurrence of ^{36}Cl in infiltrated meteoric water results from the leaching of ^{36}Cl deposited at the surface, originating from atmospheric production by cosmic ray spallation of ^{40}Ar, ^{40}Ar (n,p4n) ^{36}Cl, or by ^{36}Ar neutron capture, ^{36}Ar(n,p)^{36}Cl (Bentley *et al.*, 1986; Phillips, 2000). According to the deposition model proposed by Phillips (2000), the cosmogenic production can be estimated at Chernobyl latitude to be around 45 at.m^2.s^{-1}. The theoretical natural ^{36}Cl/Cl ratio in rainwater is estimated at 1.8×10^{-13} at.at^{-1}, considering a mean chloride concentration in meteoric water of 0.0209 mmol.L^{-1} and an average precipitation rate of 625 mm.y^{-1} (according to infiltration rate published by Bugai *et al.*, 2012b).

At the Chernobyl Pilot Site, groundwater recharge is mainly due to infiltration of meteoric water (Bugai *et al.*, 2012a ; Le Gal La Salle *et al.*, 2012). Consequently, a

cosmogenic origin of ^{36}Cl should lead to a $^{36}Cl/Cl$ of 1.8×10^{-13} at.at^{-1}. Evapotranspiration processes were suggested by Bugai *et al.* (2012a) at the Chernobyl Pilot Site with an enrichment factor of 2.5 but even if some fractionation process was possible, a multiplication by 2.5 of the ^{36}Cl cannot explain measured $^{36}Cl/Cl$ ratios in groundwater, which are up to 5 orders of magnitude higher.

III.4.1.2 Lithogenic production

In groundwater, additional natural reactions can produce ^{36}Cl in the upper section of the lithosphere. The main reaction is neutron activation of ^{35}Cl. The neutron flux production mainly comes from U and Th decay chain in rocks. Some spontaneous fission of Uranium may also occur, producing neutrons. A few lithogenic ^{36}Cl is also attributed to spallation reactions of ^{35}Cl but also of Ca, K, Ar (Fontes, 1984). The lithogenic production may become predominant in old groundwater where much of the atmospherically-derived ^{36}Cl has decayed away (Bentley *et al.*, 1986; Phillips, 2000). In groundwater when this lithogenic production equal the ^{36}Cl decay, (secular equilibrium), $^{36}Cl/Cl$ ratios are between 5 and 30×10^{-15} at.at^{-1} (according to Fontes, 1984). In groundwater at the vicinity of uranium ores, the highest $^{36}Cl/Cl$ ratios reported from the literature data are close to 10^{-11} at.at^{-1}, depending on ^{35}Cl concentration, the neutron flux produced by the U and Th content in the ore and the velocity of the groundwater [*e.g.* Fontes, 1984; Songsheng *et al.*, 1994; Cornett *et al.*, 1996). The highest $^{36}Cl/Cl$ ratios in CPS groundwater reach 10^{-9} at.at^{-1}.

$^{36}Cl/Cl$ ratios in Chernobyl groundwater are clearly higher compared to expected cosmogenic and lithogenic ratios, particularly in shallow groundwater reaching 10^{-9} at.at^{-1}. Therefore, at the Chernobyl Pilot Site, other sources of ^{36}Cl have to be considered.

III.4.2 Groundwater contamination by Anthropogenic Chlorine-36

Anthropogenic contamination can explain the high $^{36}Cl/Cl$ ratios measured in groundwater at the Chernobyl Pilot Site.

Nuclear activity may give ^{36}Cl by neutron activation of ^{35}Cl (^{35}Cl (n,γ) ^{36}Cl) or ^{36}Ar (^{36}Ar (n,p) ^{36}Cl) and in nuclear facilities, high contents were measured in reactors, concrete shielding, graphite rings, etc. (Bentley *et al.*, 1986; Milton *et al.*, 1994; Phillips, 2000; Bessho *et al.*, 2007; Hou *et al.*, 2007; Bondar'kov *et al.*, 2009). More

specifically for the Chernobyl Nuclear Power Plant, a mean ^{36}Cl activity of 1080 Bq/g was measured in graphite rings (used as moderators in RBMK reactors) of the unit 2 at the ChNPP after 11 years of storage in cooling pond (Bondar'kov *et al.*, 2009).

The explosion of Chernobyl unit 4 is most likely to have released ^{36}Cl, since high $^{36}Cl/Cl$ ratios (10^{-10} to 10^{-12} at.at^{-1}) were reported in lichens in Ukraine, Belarus and the Russian Federation after 1986 (Chant *et al.*, 1996). Another example are the $^{36}Cl/Cl$ ratios measured in groundwater downgradient from the low-level radioactive waste repository in the Snake river plain (USA) with values in the same order of magnitude as at the CPS (Beasley *et al.*, 1993).

Apparent ages of shallow groundwater measured on the AB profile in October 2008, (Le Gal La Salle *et al.*, 2012) are coherent with this assumption of groundwater contamination linked to the reactor explosion: those ages range from a few years to 20-25 years, which implies an infiltration of the contaminated rainwater after 1986. Assuming that shallow groundwater at similar depth on the CD profile infiltrated during the same period, ^{36}Cl contamination of groundwater occurred after the Chernobyl explosion. The timing is also coherent with the trench set up in 1987-1988.

III.4.2.1 Migration from trenches and ^{36}Cl contamination of recent groundwater

In groundwater sampled in the aeolian layer, $^{36}Cl/Cl$ ratios increase at least by a factor of two from upgradient to downgradient of the trench (Figure III-2; Figure III-3). Consequently, it can be assumed that trench T22 is releasing ^{36}Cl. As for the actual ^{90}Sr contamination, potential processes at the origin of the ^{36}Cl release from the trench are alteration of buried material with which ^{36}Cl is associated. Another potential source of ^{36}Cl can be supposed in the trench: some residual neutron flux (originating from buried fuel particles) could interact with ^{35}Cl and provide some ^{36}Cl. According to equations published by Songsheng *et al.* (1994), the neutron flux needed to produce such quantity can be estimated to be:

Equation III-7

$$\Phi n = \frac{^{36}Cl}{Cl} \times \frac{\lambda_{36}}{\sigma_{35}} \times \frac{N_{Cl}}{N_{35}}$$

where $^{36}Cl/Cl$ is the measured ratio, λ_{36} is the decay constant of ^{36}Cl (2.3×10^{-6} y^{-1}; Songsheng *et al.*, 1994), σ_{35} the thermal neutron capture cross section of ^{35}Cl

(44×10^{-24} cm²; Songsheng *et al.*, 1994) and N_{35}/NCl the proportion of ^{35}Cl in total Cl (0.7577; Rosman and Taylor, 1998)

At the Chernobyl Pilot Site, a neutron flux of 4×10^{8} n/cm² is needed to produce alone the highest $^{36}Cl/Cl$ ratio of 10^{-8} at.at^{-1} (order of magnitude of trench soil water). This highest neutron flux estimated by Songsheng *et al.*, 1994 in the vicinity of Lianshanguan uranium deposit is 2.6×10^{7} n/cm² and correspond to a uranium content of 98940 ppm.

The ^{36}Cl contamination of groundwater seems to persist until now as high ^{36}Cl content is still observed in shallow groundwater, apparently recharged over the last 10 years (aeolian groundwater).

The hypothesis of ^{36}Cl retention in soils and biosphere is supported by $^{36}Cl/Cl$ ratio measured in the trench soil water sample and leaf leachates collected on the top of the trench, which are at least one order of magnitude higher than $^{36}Cl/Cl$ ratios in groundwater. Several studies suggest the importance of the biogeochemical cycle of Cl to explain some delay of ^{36}Cl bomb-pulse migration in groundwater, particularly relatively to ^{3}H (Cornett *et al.*, 1997; Milton *et al.*, 2003). Processes involved in this retention are atmosphere recycling, adsorption on soil, vegetation uptake and emission under organochloride forms (Milton *et al.*, 2003). For instance, Cornett *et al.* (1997) estimated a residence time of at least 25 years for Cl in the terrestrial biosphere of the Eastern Ontario (Canada), increasing with the increasing biota. Studies of ^{36}Cl transfer in the soil-plant system, carried out in the Chernobyl exclusion zone, have shown retention of ^{36}Cl by live biota and exchanges characterized by quick transfers from the soil solution to plants and from dry vegetation to soil solution (Kashparov *et al.*, 2005; Kashparov *et al.*, 2007). The biotic cycle could explain the ^{36}Cl contamination observed in recent groundwater.

The high ^{36}Cl content observed upgradient from the trench could be explained by ^{36}Cl migration from upstream trenches in groundwater. The closest upgradient trench is less than 100 meters away (Antropov *et al.*, 2001). It can be noted that the groundwater from the IGS33 piezometer, sampled outside the Chernobyl Pilot Site, in a zone of a waste mounds, shows a lower ^{36}Cl contamination, with a $^{36}Cl/Cl$ ratio around 10^{-11} at.at^{-1} which is still two orders of magnitude higher than the theoretical natural ratio. The upgradient contamination of groundwater by ^{36}Cl may also be explained by potential residual soil contamination leaching or deferred

release by the biosphere. The duration of these releases may have been extended due to potential recycling of chlorine in soil and/or biosphere too (Cornett *et al.*, 1997). The involved retention processes need to be investigated.

III.4.2.2 Deep contamination issue

The deeper piezometers (1-98-1, 1-01, 1-98-2 and 1-98-3 piezometers) show contamination by ^{36}Cl while groundwater apparent recharge in 1-98-2 and 1-98-3 piezometers seem to occur before the accident (Le Gal La Salle *et al.*, 2012).

Contamination by the tracer test done between 1999 and 2001 with ^{36}Cl is discarded in spite of their location on the AB-profile, close to the theoretical tracer test plume (Dewière *et al.*, 2004; Bugai *et al.*, 2012b). As said at the beginning of the section, the absence of such ^{36}Cl contamination can reasonably be assumed in 1-98-2 and 1-98-3 piezometers for several reasons. At first, groundwater apparent ages, obtained from both $^{3}H/^{3}He$ and CFC dating methods, which provides groundwater recharge dates older than 33 years (Le Gal La Salle *et al.*, 2012). However, groundwater in these piezometers is supposed to be impacted by mixing processes; meaning apparent ages could be the result of the mixing of a groundwater older than infiltrated rainwater with an older groundwater. Then, in the aeolian layer, the tracer plume is calculated to have travelled 77 m since thte injection time, meaning it can be reasonably considered to have left the profile.

Moreover, in the case of the 1-98-1 piezometer, a comparison will be made with the ^{36}Cl content in groundwater sampled in the 1-01 piezometer, located approximately at the same depth but not downgradient of the tracer test (1-01 is located at the North-east of the laboratory in Annex 1). This piezometer shows a ^{36}Cl content in the same order of magnitude, therefore discarding that some ^{36}Cl comes from the tracer tests.

In these piezometers, looking at the apparent ages, the ^{36}Cl contamination should result either from the Chernobyl Nuclear Power Plant before the explosion (its operation started in 1977 (Shestopalov, 2002), ^{36}Cl contamination was reported in the environment around nuclear facilities (Milton *et al.*, 1994; Seki *et al.*, 2007) or from the ^{36}Cl 'bomb-pulse' generated by nuclear tests between 1952 and 1971 (Elmore *et al.*, 1982; Finkel *et al.*, 1980; Bentley *et al.*, 1982). However, considering the potential mixing processes supposed in these deep piezometers (Le Gal La Salle *et al.*, 2012), the Chernobyl explosion and trench T22 cannot be

discarded. Moreover, cautions should be taken when interpreting 1-98-1, 1-98-2 and 1-98-3 piezometers data because unlike the other piezometers, screens are not isolated by a layer of bentonite, used to avoid cross-contamination of groundwater.

III.4.3 SYNTHESIS

In all collected samples, ^{36}Cl content is too high to have a natural origin. In the groundwater of the Chernobyl Pilot Site, $^{36}Cl/Cl$ ratios are 1 to 4 orders of magnitude higher than the natural theoretical ratio (Figure III-4).

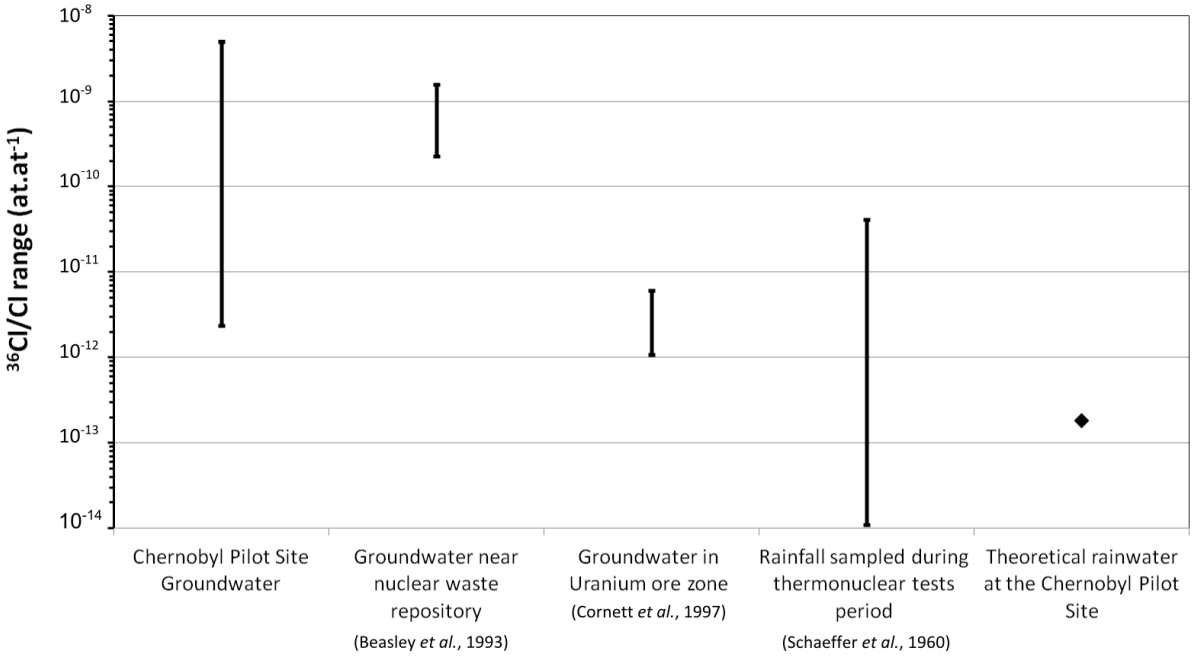

Figure III-4: $^{36}Cl/Cl$ ratios measured at the Chernobyl Pilot Site compared with the highest $^{36}Cl/Cl$ ratio found in the literature

Because of the groundwater recent apparent age spectrum, this high contamination of the groundwater occurred after the Chernobyl explosion.

Trench T22 acts as a point source of ^{36}Cl: soil water sampled in the trench body shows $^{36}Cl/Cl$ ratio five orders of magnitude higher than the natural theoretical ratio, one order of magnitude higher than the upgradient $^{36}Cl/Cl$ ratio and the most contaminated groundwater is located just downgradient of the trench. Further processes may increase this release: alteration of debris or organic matter containing ^{36}Cl, biosphere uptake and release, or even *in situ* production if some residual neutron flux remains.

Other sources of ^{36}Cl can be considered to explain the ^{36}Cl contamination of groundwater. Groundwater sampled in piezometers outside the site and at the outlet of the Borshchii River show also a contamination in ^{36}Cl, supporting the hypothesis of a global contamination over the whole area. Residual ^{36}Cl in soil and vegetation are shown, meaning that release by biogeochemical processes need to be considered to explain the actual ^{36}Cl contamination of shallow recent groundwater. Release of ^{36}Cl from upgradient trenches is a potential origin and can explain the contamination of the upgradient groundwater. The deep contamination of groundwater may have two origins. In regards of the apparent recharge before 1986, the ^{36}Cl contamination could be explained by the nuclear activity at the Power Plant before the accident, by thermonuclear tests or by hydraulic short circuiting due to piezometer design. However, the Chernobyl accident and quick migration from trench T22 are possible. All these potential origins of ^{36}Cl are summarized in Figure III-5.

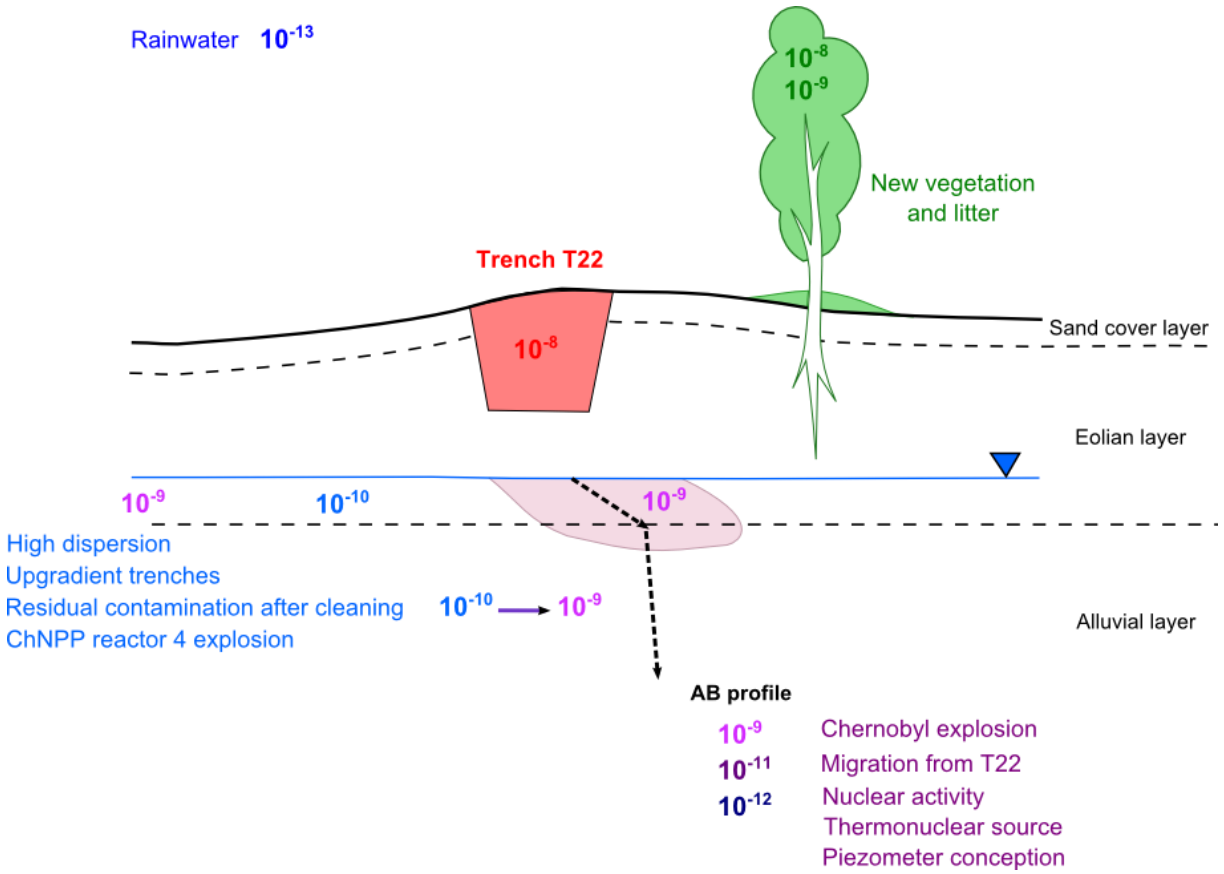

Figure III-5: Potential sources explaining ^{36}Cl contamination of Chernobyl Pilot Site groundwater

The high contamination by ^{36}Cl makes this isotope a good tracer for the investigation of the contaminant plume extent in groundwater. However, plume

extent of ^{36}Cl migrating from the trench is not obviously observable because of all the additional potential origins of ^{36}Cl in groundwater.

III.5 TRANSPORT PROCESSES

Advective transport is assessed to be the main transport process in CPS groundwater however, the influence of potential mixing processes has to be investigated to better constraint contaminant plume maximal extent.

Particularly, in mixing process, $^{36}Cl/Cl$ ratios can be studied by the comparison with $[Cl^-]$ concentrations. Then, ^{36}Cl concentrations are compared with ^{90}Sr concentrations in order to study the migration of those two elements released by the trench.

III.5.1 CHLORINE-36 AND MIXING PROCESSES

Firstly, ^{36}Cl content is compared with the total Cl content. As Cl is assessed to be conservative, only non-reactive processes influence ^{36}Cl and Cl behavior. The aim is to investigate potential mixing processes between end-members with different ^{36}Cl and Cl contents. Such studies are made to identify salt sources, as for example, in the "Drought Polygon" (Brasil, Bentley *et al.*, 1986). Mixing lines are calculated with several end-members and compared with measured $^{36}Cl/Cl$ ratios.

Figure III-6 and Figure III-7 present $^{36}Cl/Cl$ ratios and $[^{36}Cl]$ versus the inverse of $[Cl^-]$ measured in groundwater, trench soil water, river and leaf leachates in October 2008, October 2009 and May 2011. $^{36}Cl/Cl$ ratios measured in leaf leachate solutions are placed on the y-axis because $[Cl^-]$ initially in the leaves is not known. Because consequently their $[^{36}Cl]$ is not known too, they are not shown on the $[^{36}Cl]$ versus the inverse of $[Cl^-]$ concentrations diagram.

Same symbols are used in both diagrams. Samples are represented differently according to the year of sampling, their nature and the depth of sampling. October 2008 groundwater samples are always represented with full symbols, October 2009 groundwater samples with full symbols and a dark outline and May 2011 samples with empty symbols and a colored outline. Piezometer names are given near each symbol. Regarding groundwater samples, aeolian samples symbols are always red and squared, symbols for groundwater sampled at the aeolian/alluvial interface are purple and triangle. For alluvial groundwater samples, symbols are diamonds or circles, with a blue being darker with increasing of sampling depth. May 2011 leaf

leachate solutions are represented by empty triangles with green outline, May 2011 soil water sample by an empty square with brown outline and May 2011 outside samples (river and groundwater from IGS 33 piezometer) by orange symbols (empty square and empty circle respectively).

For the comparison, theoretical natural rainwater range is represented by three blue circles linked by a dark line, each circle representing minimal, mean and maximum measured [Cl^-] concentrations in rainwater (on 30 samples collected during the 2005-2006 period, Bugai *et al.*, 2012a). The calculated $^{36}Cl/Cl$ corresponds to the one calculated earlier (§III.4.1.1) and is supposed constant for different [Cl^-] concentrations. [^{36}Cl] is calculated from this theoretical constant ratio for the minimal, mean and maximum measured [Cl^-] concentrations.

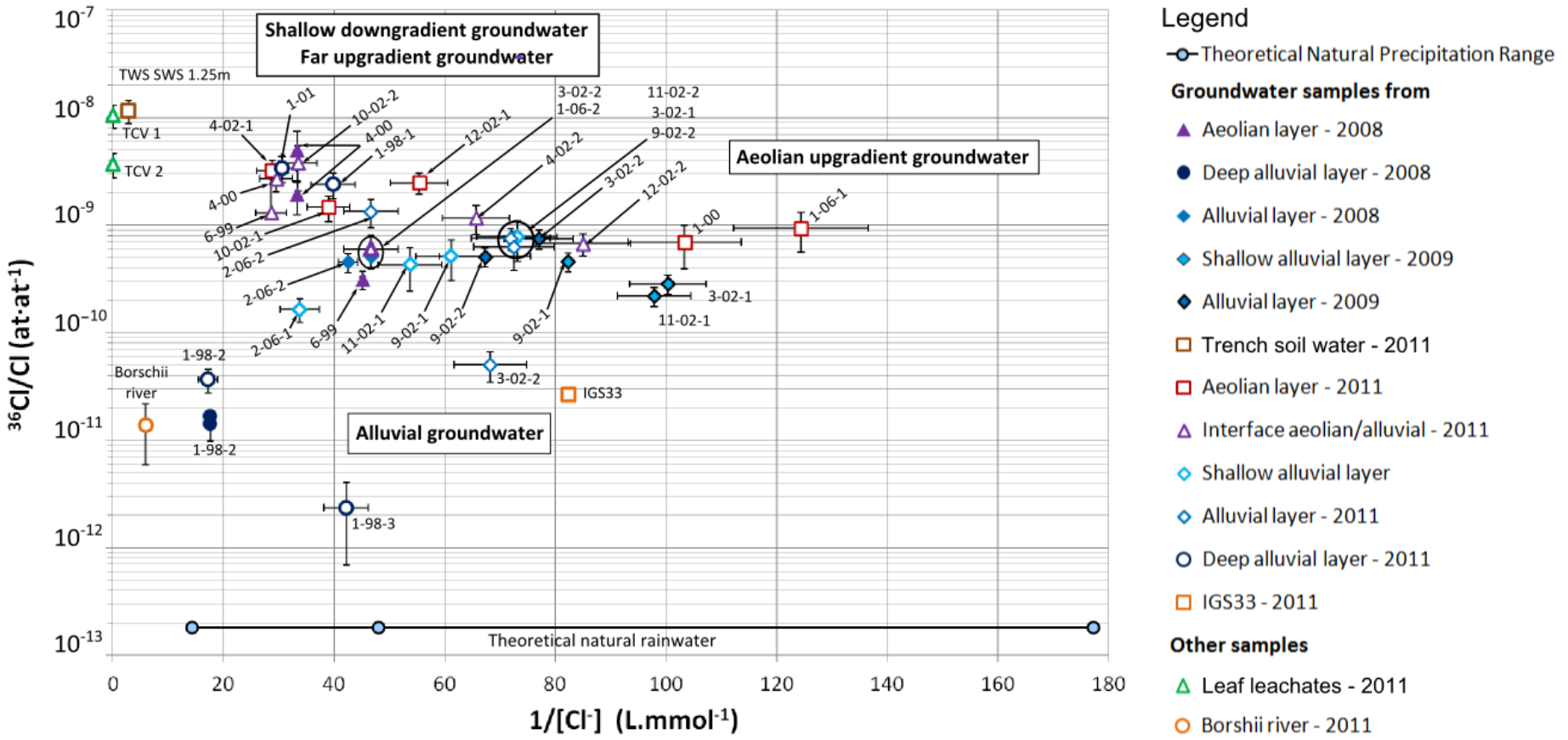

Figure III-6: $^{36}Cl/Cl$ ratios versus 1/[Cl$^-$]

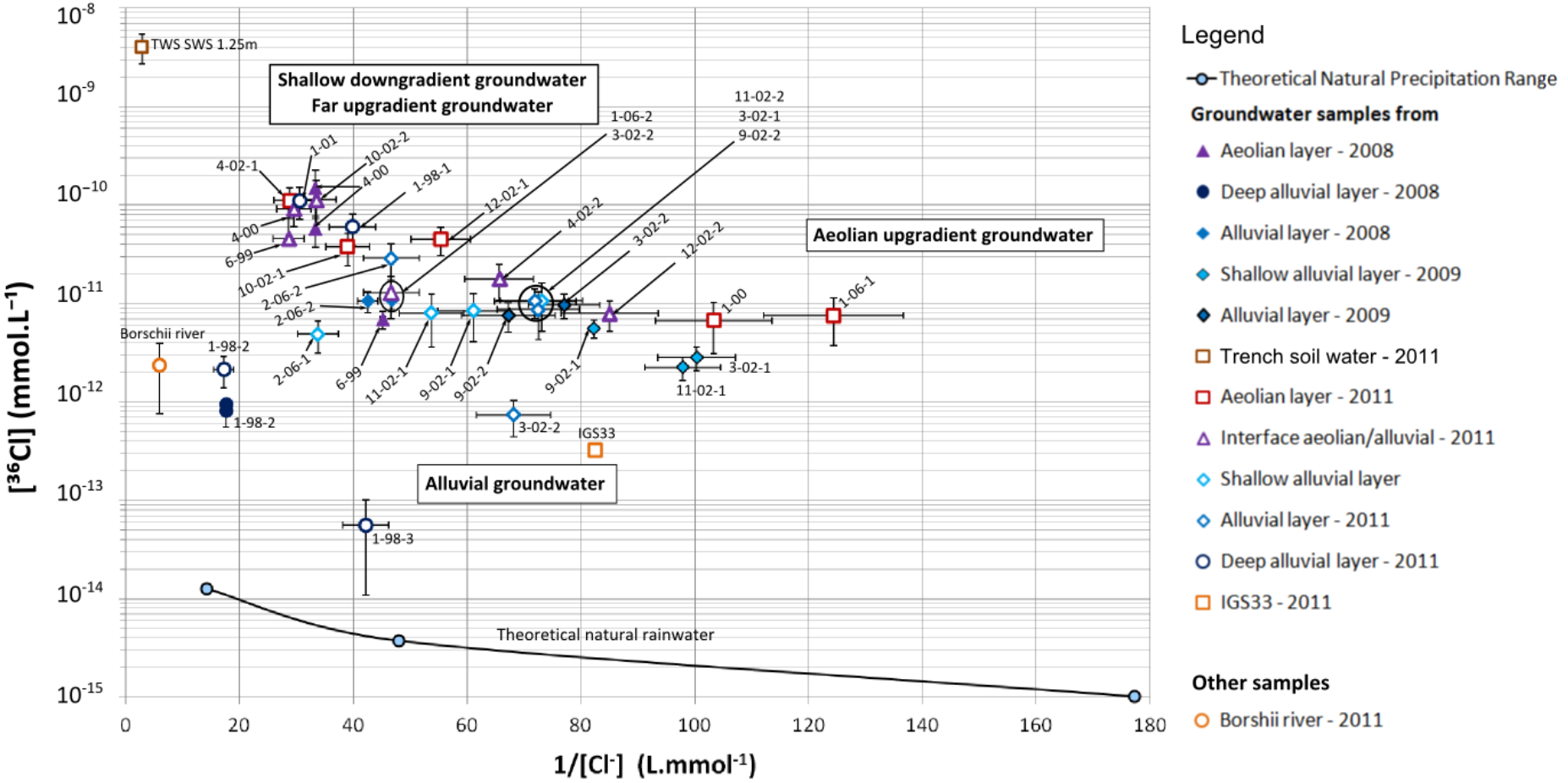

Figure III-7: [^{36}Cl] versus 1/[Cl^-]

III.5.1.1 Main trends

As noticed before (*c.f.* paragraph III.3), the most contaminated samples in ^{36}Cl are trench soil water and leaf leachates with $^{36}Cl/Cl$ ratios reaching 10^{-8} at.at^{-1}. Trench soil water sample also shows a high [Cl^-]. Groundwater samples of the Chernobyl Pilot Site are less concentrated in [^{36}Cl] and [Cl^-] than the trench soil water sample and their [Cl^-] remain within the rainwater concentrations range. On both diagrams, $^{36}Cl/Cl$ ratios and [^{36}Cl] decrease from the trench soil water sample to deep groundwater samples. This decrease seems to be linked to the increasing depth: one order of magnitude in $^{36}Cl/Cl$ ratio as well as in [^{36}Cl] is commonly found between aeolian and alluvial groundwater (except for deep groundwater sampled in 1-98-2 and 1-98-3 piezometers). Two different trends can be distinguished depending on the layer where the groundwater is collected.

In shallow groundwater (aeolian samples and samples collected at the interface aeolian/alluvial), $^{36}Cl/Cl$ ratios [^{36}Cl] and [Cl^-] are highly scattered .$^{36}Cl/Cl$ ratios, [^{36}Cl] and [Cl^-] decrease from groundwater sampled just downgradient of the trench to groundwater sampled just upgradient of the trench (4-02-1 and 1-06-1 piezometers, respectively).$^{36}Cl/Cl$ ratios and [^{36}Cl] of these two extreme samples vary by roughly one order of magnitude and their corresponding [Cl^-] change by a factor 4. Groundwater sampled far upgradient of the trench (6-99 piezometer) and in the 10-meter-deep piezometers (1-01 and 1-98-1) fall on this trend.

In groundwater sampled in the alluvial layer, [Cl^-] fall within the same range as shallow groundwater, while $^{36}Cl/Cl$ ratios and [^{36}Cl] seem to be less variable, mostly between 10^{-10} and 10^{-9} at.at^{-1} and 10^{-12} and 10^{-11} mmol.L^{-1}, respectively.

^{36}Cl contaminations in groundwater sampled in the deepest alluvial layer (1-98-2, 1-98-3 piezometers) are different from other Chernobyl Pilot Site groundwater samples. Groundwater sampled at 20-meter-depth (1-98-2 piezometer) shows $^{36}Cl/Cl$ ratios and [^{36}Cl] two orders of magnitude lower than in the other piezometers while [Cl^-] are one of the highest (still in the rainwater range). Groundwater 1-98-3 is the less ^{36}Cl contaminated with a $^{36}Cl/Cl$ ratio of 2×10^{-12} at.at^{-1}, a [^{36}Cl] concentration of 6×10^{-14} at.L^{-1} and a [Cl^-] concentration close to the mean rainwater concentration.

Water sampled outside the site (groundwater from the IGS33 piezometer and water from the Borschii river) show $^{36}Cl/Cl$ ratios and [^{36}Cl] close to groundwater sampled

in the 1-98-2 piezometer. However, groundwater sampled in IGS33 piezometer show a [Cl^-] with the rainwater range and a [^{36}Cl] in the same order of magnitude than alluvial sample on the CD profile at the Chernobyl Pilot Site.

III.5.1.2 Mixing processes

Subsequent to these observations, several end-members are envisaged to discuss potential mixing processes in Chernobyl Pilot Site groundwater:

- the soil solution sampled into the trench;
- rainwater end-members, with a constant $^{36}Cl/Cl$ but varying in [Cl^-] concentrations according to the recharge processes;
- deep groundwater end-member: the deepest piezometer 1-98-3 is considered here as end-member;
- shallow groundwater end-member, symbolized by two samples: the most contaminated shallow groundwater sampled in the 4-02-1 piezometer (downgradient of trench T22) and the less contaminated shallow groundwater sampled in the 1-06-1 piezometer.

Mixing lines are drawn using concentrations and ratios calculated with the following equations:

- for [Cl^-] concentrations:

Equation III-8

$$\left[Cl^-\right]_{mix} = x * \left[Cl^-\right]_{End-member1} + (1-x) * \left[Cl^-\right]_{End-member2}$$

- for [^{36}Cl] concentrations:

Equation III-9

$$\left[^{36}Cl\right]_{mix} = x * \left[^{36}Cl\right]_{End-member1} + (1-x) * \left[^{36}Cl\right]_{End-member2}$$

- for $^{36}Cl/Cl$ ratios:

Equation III-10

$$\left(\frac{^{36}Cl}{Cl}\right)_{mix} = \frac{[^{36}Cl]_{mix}}{[Cl^-]_{mix}}$$

where ***x*** varies between 0 and 1, ***mix*** is the solution resulting solution from the mixing process and *End-member1* and *End-member2* are the solutions considered for the mixing.

Data points and mixing lines are reported on Figure III-8 and Figure III-9. These figures present $^{36}Cl/Cl$ ratios and [^{36}Cl] versus the inverse of [Cl^-].

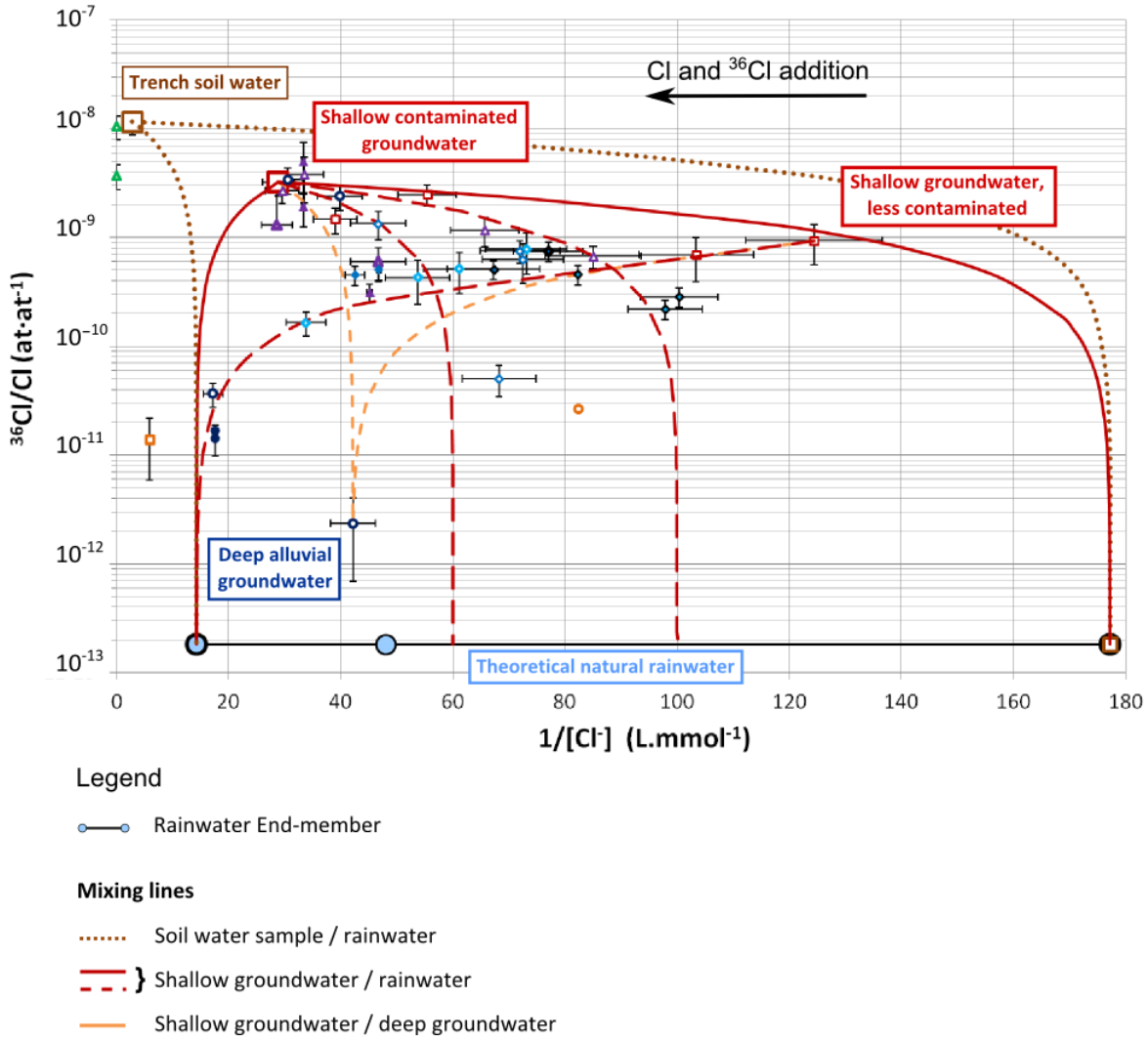

Figure III-8: $^{36}Cl/Cl$ ratios versus $1/[Cl^-]$ and mixing processes

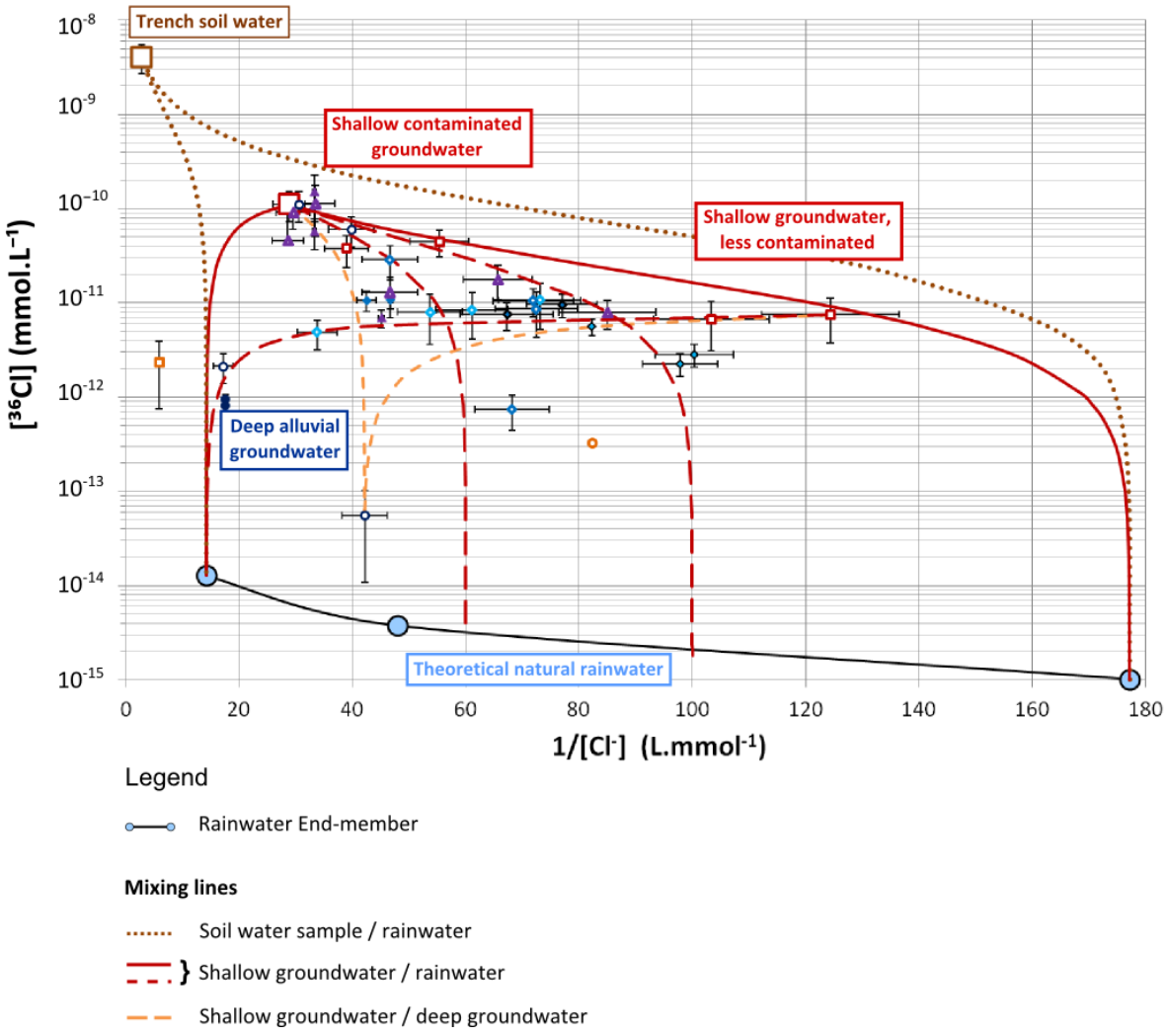

Figure III-9: [^{36}Cl] versus 1/[Cl^-] and mixing processes

The first considered mixing process is the dilution of trench soil water by rainwater. It is symbolized by two brown doted lines, one ending at the most [Cl^-] concentrated rainwater and the other ending at the less [Cl^-] concentrated rainwater. Considering the [Cl^-] variation of recharge, any point between the two lines and the rainwater range can be considered as a result of such mixing process, which is the case for all groundwater sampled at the Chernobyl Pilot Site.

The second considered mixing process is the dilution of the shallow groundwater (4-02-1 and 1-06-1 piezometers) in rainwater, shown by red line. Four red lines correspond to the mixing of the most ^{36}Cl contaminated sample (4-02-1 piezometer) with rainwater end-members. The two empty lines end at the two extreme rainwater end-members. Here again, considering the [Cl^-] concentration variation of the recharge, all groundwater samples on the Chernobyl Pilot Site fall between the mixing lines and the rainwater range and can be considered to result

of such processes. Two dashed lines end at two adjusted rainwater end-member to better fit with the dataset scattering. The last dashed red line shows the mixing of a less contaminated shallow groundwater (1-06-1 piezometer) with the highly-concentrated rainwater end-member.

The third considered mixing process involves the mixing of shallow groundwater (4-02-1 and 1-06-1 piezometers) with a deeper groundwater end-member (1-98-3 piezometer). It is presented by orange intermittent lines.

As suggested above, the mixing process between the soil water end-member and the rainwater end-members can by itself explain the whole dataset, considering the possible variation of [Cl^-] concentrations in rainwater end-members. Moreover, the mixing could be more or less pronounced depending on the recharge rate. However, the scattering of the dataset can be better constrained considering the mixing shallow groundwater with rainwater. The less convincing case is the dilution of shallow groundwater with deep groundwater, particularly because the deep groundwater sampled in 1-98-2 piezometer is not between the corresponding mixing lines. The most convincing cases are shown in simplified versions of the previous figures (Figure III-10 and Figure III-10). The dilution of the shallow groundwater in rainwater is reduced to three lines. ^{36}Cl contamination of shallow groundwater can be explained by dilution of the most contaminated groundwater (4-02-1 piezometer) by rainwater: they range between a line ending at an adjusted rainwater end-member and the line ending at the less Cl^- concentrated rainwater end-member. In groundwater sampled in the alluvial layer, only one mixing process can explain most of the scattering of the samples, involving the less contaminated shallow groundwater end-member and the most concentrated rainwater end-member.

Borschii river water is not on these mixing trends, suggesting other processes at the scale of the area.

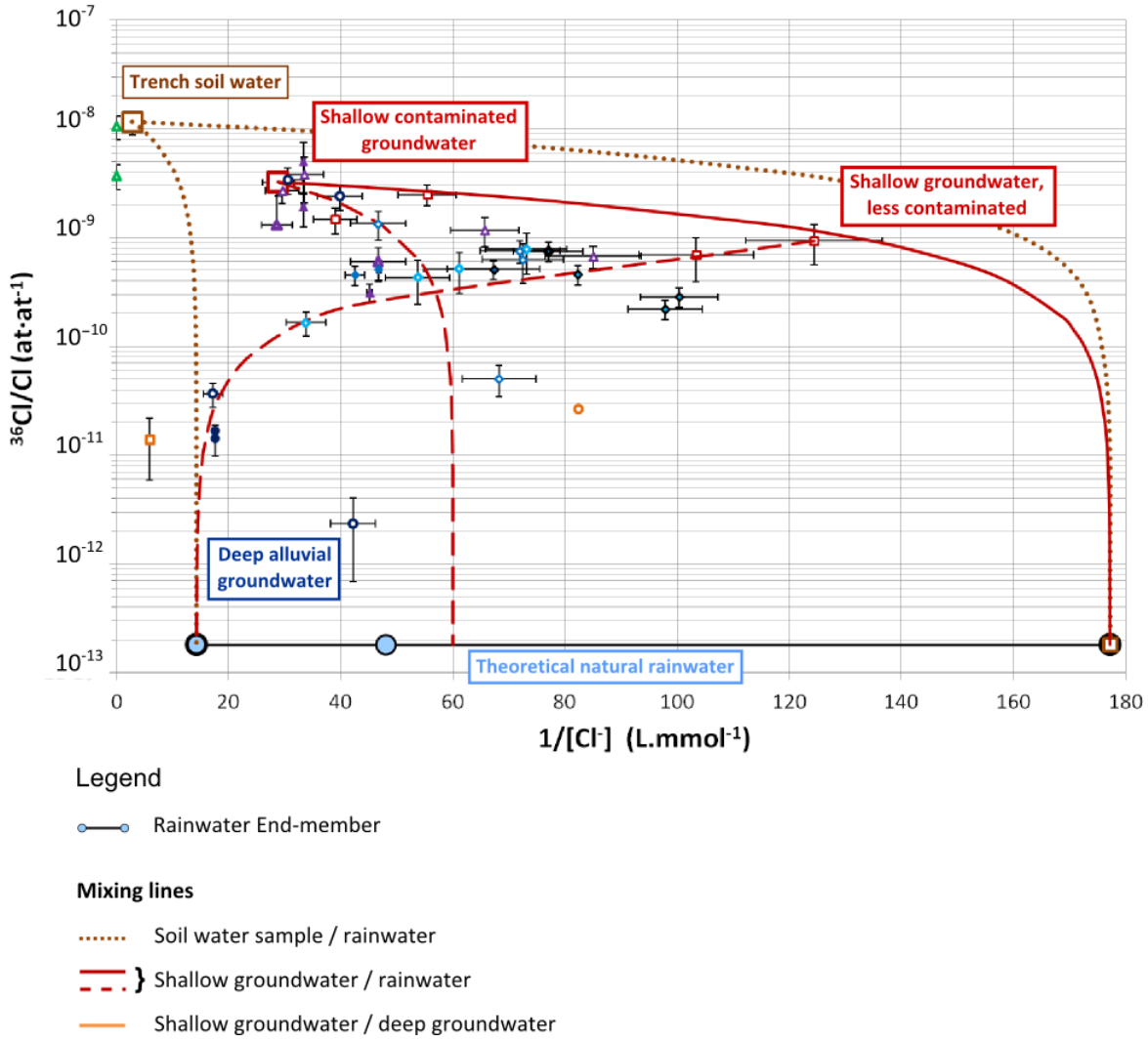

Figure III-10: $^{36}Cl/Cl$ ratios versus 1/[Cl$^-$] and most convicing mixing processes

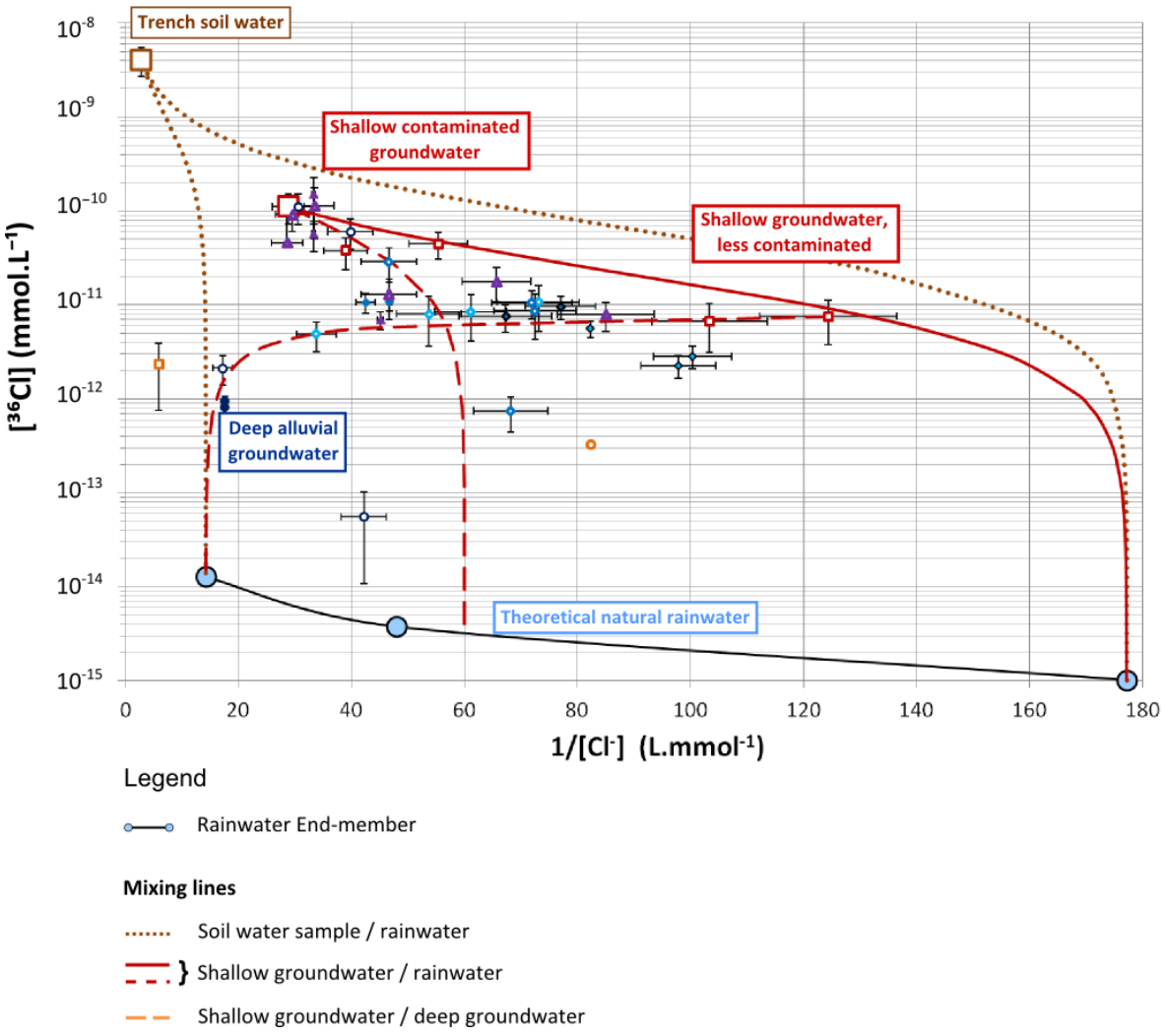

Figure III-11: [^{36}Cl] versus 1/[Cl^-] and mixing processes

Consequently, the ^{36}Cl contamination of shallow groundwater and deep groundwater can result from two different processes. In the case of the shallow groundwater, the ^{36}Cl contamination seems to be higher dependant of [Cl^-] variation in rainwater. The location of the sampled groundwater has also an impact on the [^{36}Cl] content. It can be interpreted as the dilution of a [Cl] concentrated source term by more-or-less concentrated rainwater. Taking into account the dataset scattering, some dispersive mixing may also occur. Then, considering the mixing processes may occur in deeper groundwater, ^{36}Cl contamination can be interpreted as dispersive-mixing. If mixing processes are not considered, a diffuse contamination, at the time of the Chernobyl explosion, can be envisaged. Such diffuse contamination at the scale of the area can also explain contamination of the Borschii river.

III.5.2 CHLORINE-36 BEHAVIOR RELATIVELY TO STRONTIUM-90 RADIONUCLIDE BEHAVIOR

The comparison of ^{36}Cl and ^{90}Sr behaviors can help to characterize processes involved in element migration through the comparison of two radioelements with a different reactivity and supposed to be migrating from the trench.

Figure III-12 presents [^{36}Cl] concentrations measured in the samples versus the [^{90}Sr] concentrations. [^{90}Sr] concentrations are calculated from ^{90}Sr activities and corrected by radioactive decay following Equation III-3.

Used symbols are the same as in the previous diagrams. Samples showing [^{90}Sr] activities under the detection limit are represented on the left outline of the diagram: this representation gives [^{36}Cl] concentration in the sample even if the [^{90}Sr] concentration is not known. May 2011 leaf leachates are not presented because even if their $^{36}Cl/Cl$ ratios were measured, their [^{36}Cl] concentrations and [^{90}Sr] concentrations are not known.

III.5.2.1 Main trends

The trench soil water sample is the most contaminated sample both, in ^{36}Cl as in ^{90}Sr.

The main trend shown by the overall dataset is a decrease of [^{36}Cl] and [^{90}Sr] from the trench soil water to shallow alluvial groundwater, followed by a decrease in [^{90}Sr] while [^{36}Cl] remain almost constant in the alluvial layer. The deepest groundwater samples show the lowest [^{36}Cl] decrease while [^{90}Sr] are under the detection limit. Different trends can be distinguished following the depth where the groundwater is sampled.

All shallow groundwater[3] samples located downgradient of trench T22 show decreasing [^{36}Cl] and [^{90}Sr] from the trench soil water sample to groundwater from the shallow alluvial layer located downgradient of the trench (9-02-1 piezometer). The most contaminated groundwater, aeolian groundwater located downgradient of trench T22 (4-02-1 and 12-02-1 piezometers), shows [^{36}Cl] are almost two orders of magnitude lower while [^{90}Sr] in the same order of magnitude lower than the trench soil water sample.

Then, in the alluvial layer, [^{90}Sr] decrease with depth and other upgradient samples (1-00, 1-06-1, 1-06-2, 2-06-1 and 2-06-2 piezometers), mostly collected in the alluvial layer, show lower [^{90}Sr] and deeper groundwater samples (11-02-1, 11-02-2,

[3] Shallow groundwater : groundwater sampled in the aeolian layer and at the interface aeolian/alluvial

2-06-2, 1-01 piezometers) show [^{90}Sr] under the detection limit. These low-contaminated samples show a quite constant [^{36}Cl], around 1×10^{-11} mmol.L^{-1}, except deep alluvial groundwater (1-98-2 and 1-98-3 piezometers), showing [^{36}Cl] one to two orders of magnitude lower and 1-01 and 1-98-1 piezometers showing [^{36}Cl] one order of magnitude higher.

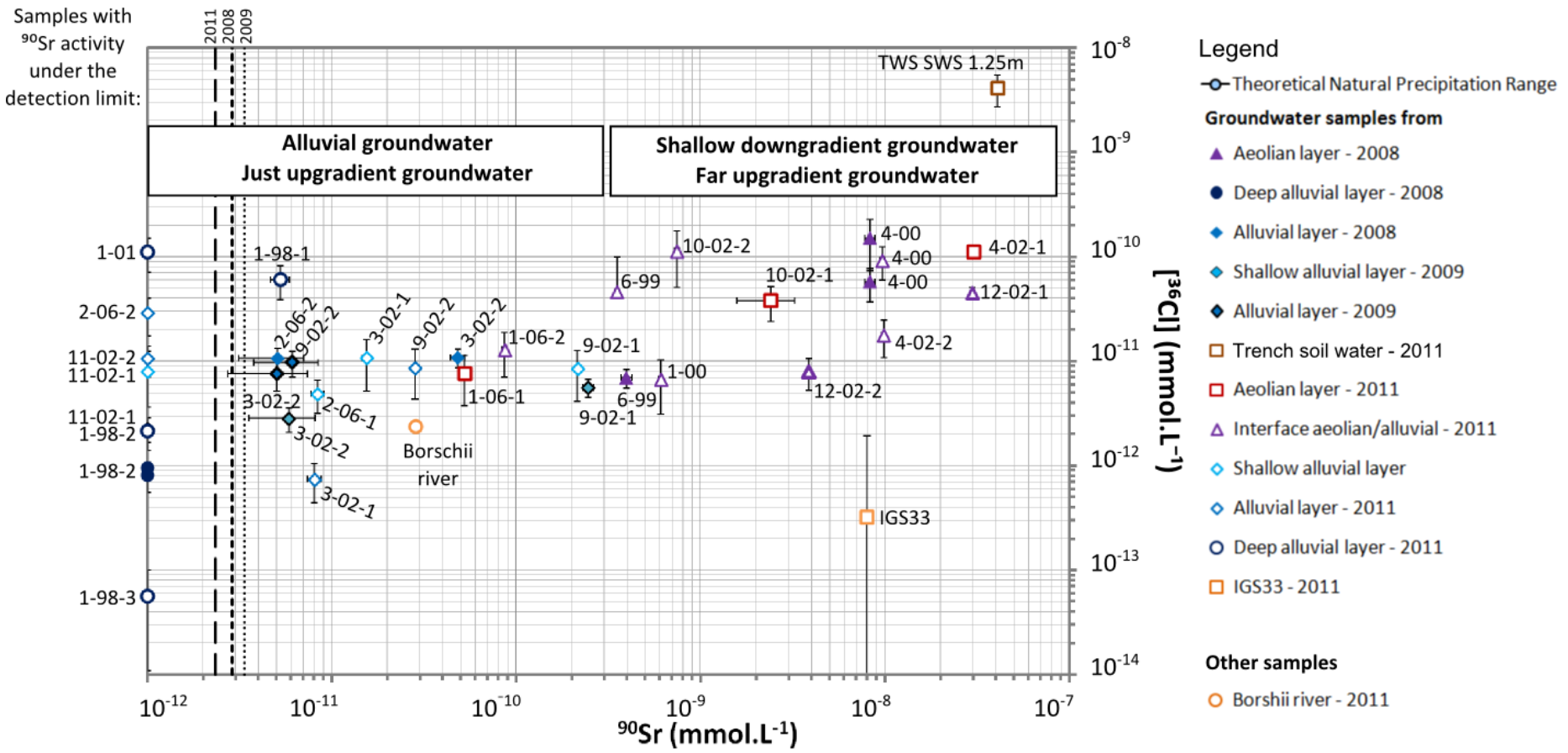

Figure III-12: [^{36}Cl] concentrations versus [^{90}Sr] concentrations

III.5.2.2 Mixing processes

As seen earlier, mixing processes can be involved in the contamination of groundwater by ^{36}Cl (*c.f.* section III.5.1). Same mixing processes are considered with the following end-members:

- Rainwater: an average [^{36}Cl] concentration is considered, calculated from the theoretical $^{36}Cl/Cl$ deposit (*c.f.* section III.4.1.1) and average [Cl^-] measured in rainwater (Bugai *et al.*, 2012a). Regarding [^{90}Sr] concentration, as ^{90}Sr is not supposed to exist in natural environment but as the diagram is presented in log, the value chosen is 1 at.L^{-1}, that to say about 1.7×10^{-21} mmol.L^{-1}.
- The trench soil water sample
- The most contaminated shallow groundwater, represented by the groundwater sampled in the 4-02-1 piezometer.
- An additional end-member is used, corresponding to a sample with low contamination in ^{90}Sr, with a ^{90}Sr above the detection limit, and showing some ^{36}Cl contamination, *i.e.* groundwater sampled in the 3-02-2 piezometer in October 2009.

To represent the mixing line, [^{90}Sr] concentrations are calculated following the equation:

Equation III-11

$$\left[^{90}Sr\right]_{mix} = x * \left[^{90}Sr\right]_{End-member1} + (1-x) * \left[^{90}Sr\right]_{End-member2}$$

Several mixing processes are reported in Figure III-13. Mixing of soil water with rainwater is shown by a brown line, mixing of the most contaminated sample (4-02-1) with rainwater by a red line and the mixing between low-contaminated groundwater (3-02-2) with rainwater by a dotted red line.

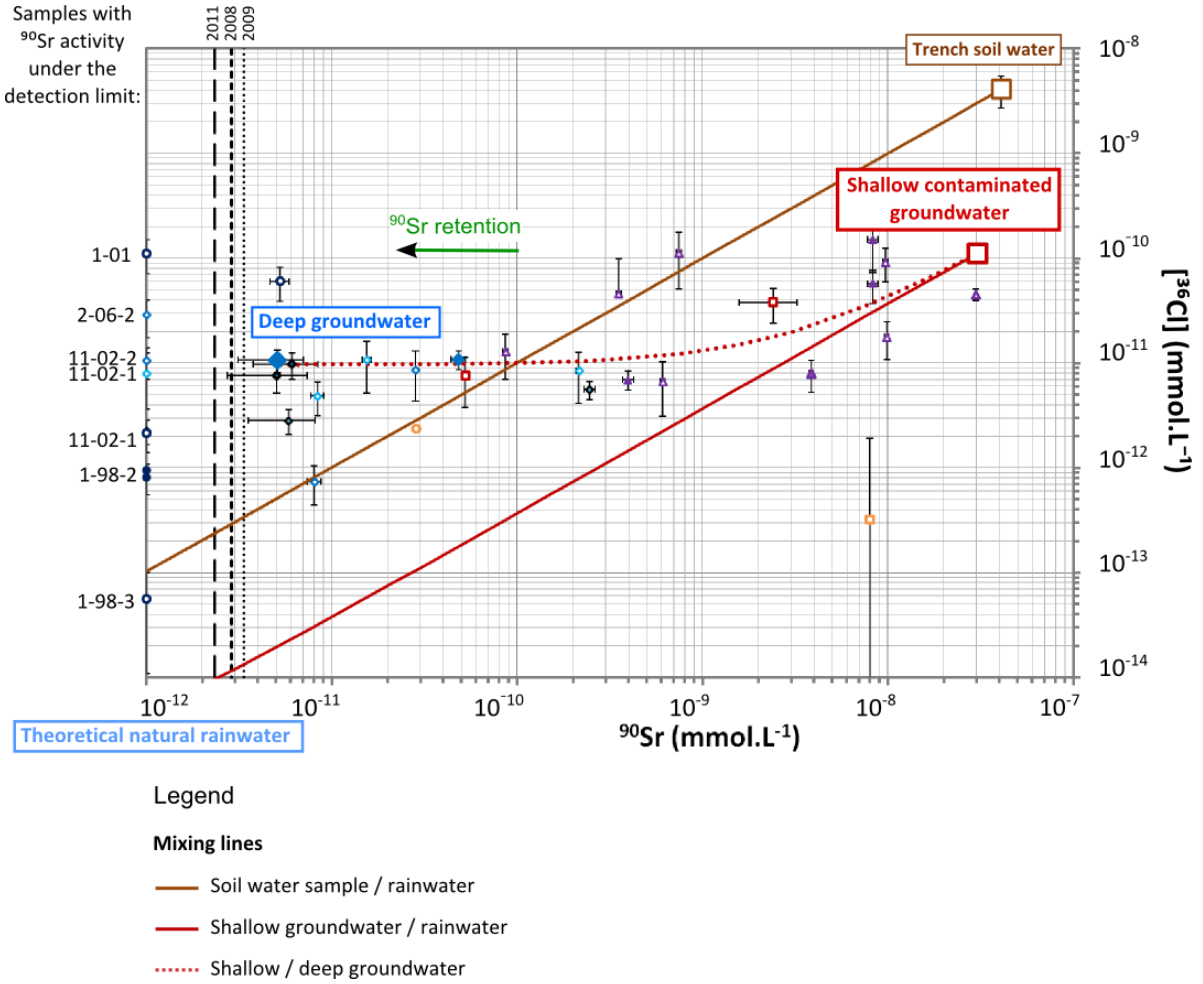

Figure III-13: [^{36}Cl] concentrations, [^{90}Sr] concentrations and mixing processes

Concentrations in groundwater sampled in the 4-02-1 piezometer seem not to be the result of the mixing of soil water sample with rainwater (brown line): while [^{90}Sr] concentrations of 4-02-1 piezometer and soil water sample are similar, [^{36}Cl] concentrations between the trench soil water and groundwater sampled in this piezometer are separated by almost two orders of magnitude. That is why a mixing line between such groundwater end-member and rainwater is considered (red line). It can be noted that groundwater sampled in the upgradient 6-99 piezometer could result of the mixing process between the soil water and rainwater. Most of the shallow groundwater and Borschii River water fall between the two mixing lines (brown and red lines).

Groundwater sampled in the alluvial layer do not follow the same trend: they show an excess in ^{36}Cl or concentrated deficit in ^{90}Sr. Mixing of groundwater from the 4-02-1 piezometer with a sample contaminated in ^{36}Cl with low [^{90}Sr] concentration, as groundwater from the 3-02-2 piezometer, seems to fit better with the alluvial sample trend. Two processes can explain the trend of the samples from the alluvial layer: mixing with water only contaminated in ^{36}Cl (case of a diffuse contamination) or loss (retention, decay) of ^{90}Sr. Considering that retention processes of Sr were shown in aeolian layer (Szenknect, 2003), that cation exchange capacity increases in the alluvial layer, and the radioactive decay of the ^{90}Sr, the second option is the most probable.

Regarding the deepest alluvial piezometers (1-01, 1-98-1, 1-98-2 and 1-98-3 piezometers), [^{90}Sr] is below the detection limit for most samples, consequently processes are not observable. Only groundwater sampled in 1-98-1 piezometer shows [^{90}Sr] above the detection limit, with a high [^{36}Cl], close to 10^{-10} mmol.L^{-1} and is not on the considered mixing processes. It can be the result of an additional source of ^{36}Cl or linked to special heterogeneity in the trench, as it is shown for ^{90}Sr release (Bugai *et al.*, 2012a).

In summary, mixing processes fit well with the dataset scattering, emphasizing again a difference in processes between shallow groundwater and alluvial groundwater: [^{36}Cl] and [^{90}Sr] can be explained as the result of dilution of a highly contaminated end-member with uncontaminated rainwater, particularly in shallow groundwater. However, the contaminated end-member could vary, specifically in ^{36}Cl, depending on preferential retention processes by soil and biosphere for example. Then, in the alluvial layer, ^{90}Sr is most likely lost by retention processes and radioactive decay while ^{36}Cl remains in solution.

III.5.3 SYNTHESIS

In the investigation of processes governing ^{36}Cl migration in groundwater, ^{36}Cl behavior was compared to two other element behaviors, Cl and ^{90}Sr. The first comparison aimed at studying potential mixing processes and the second to compare ^{36}Cl migration of two radioelements migrating from the trench.

Mixing processes seem to be involved in the groundwater contamination comparing ^{36}Cl content with both Cl^- and ^{90}Sr contents. These mixing processes can be summarized to the dilution of the trench soil water by rainwater: trench T22 may

be assumed as the main source of ^{36}Cl contamination of the Chernobyl Pilot Site groundwater. However, different processes seem to occur in groundwater in aeolian and alluvial layers. In the aeolian layer, ^{36}Cl contamination of groundwater should be very sensitive to the rainwater composition. The highly-contaminated downgradient groundwater seems not to be the direct dilution of trench soil water in rainwater: while [^{90}Sr] are close, [^{36}Cl] is one order of magnitude less, meaning that ^{36}Cl could be preferentially retained by biogeochemical processes for instance, as high $^{36}Cl/Cl$ ratios are shown in leaf leachates. The groundwater sampled in the alluvial layer shows a more-or-less constant ^{36}Cl, attributed to dispersive mixing. In this layer, ^{90}Sr contamination decreases with depth: ^{90}Sr could have been lost by retention processes or radioactive decay.

If these studies suggest that trench T22 (and other trenches) could be the main sources of ^{36}Cl in the Chernobyl Pilot Site groundwater, other sources of contamination, such as diffuse source of contamination at the time of the Chernobyl explosion, cannot be discarded, as suggested by the ^{36}Cl contamination of the Borschii river.

III.6 SIMULATION OF CL AND CL-36 MIGRATION AT THE CHERNOBYL PILOT SITE

In order to investigate the contaminant plume's maximal extent in groundwater, Cl and ^{36}Cl migrations are simulated in groundwater. This simulation is based on a simple conceptual model of constant release from trench T22, according to the modern contamination of groundwater downgradient of the trench, and using the current knowledge of CPS hydrological parameters on the unsaturated and saturated zones (Bugai *et al.*, 2012b; Mazet, 2008; Van Meir *et al.*, 2012).

For this simulation, the numerical flow and transport code Hytec is used (Hytec 3.6, Van der Lee *et al.*, 2003). Hytec couples the reactive module CHESS, with a transport module, R2D2; it is a finite-volume model that allows saturated and unsaturated flow in one, two or three dimensions, but assumes isotropic hydraulic conditions. More detailed information on the set-up and specificities of the model are described below. The results of non-reactive transport simulations are compared to estimations of groundwater velocity (Bugai *et al.*, 2012b) and measured [Cl^-] to validate the simulation.

First, model set-up is described: what grid and number of nodes, choice of hydrodynamic parameters and the considered source term. Results of non-reactive transport simulation are compared with measured data. Next, sensitivity analyses are run for different parameters to identify the governing parameter and an improved simulation is proposed based on these sensitivity analyses. Finally, perspectives for the numerical investigations are proposed in order to better constrain the model for Cl and ^{36}Cl migrations in the Chernobyl Pilot Site groundwater.

Mean velocities and directions, based on the direct Hype output (Hytec image output), are given in Annex 6. The simulated [Cl^-] and [^{36}Cl] are interpolated using kriging with Surfer 8.0 for representation on the figures.

III.6.1 SIMULATION PARAMETERS

III.6.1.1 Profile description

Cl and ^{36}Cl migrations are simulated from the trench through the soils and in groundwater on a cross-section of 9 meters thick and 55 meters long, corresponding to the CD profile and the piezometers location (Figure III-14).

The HYTEC script is given in Annex 6.

The mesh is built with 3000 nodes, with grid density properties depending on the considered layer. The simulation runs over 25 years during which 50 observation times are written to the output.

As a first approximation, two strong hypotheses are made: the source term is constant and the flow is considered at steady state.

The model discretization is given next (Figure III-14). There are five zones with different hydraulic characteristics depending on the lithologic composition and/or the fact that the zone is in the unsaturated or saturated zone. The different lithologic layers are defined by specific coefficients of diffusion, dispersivities, permeabilities and porosities. Because the model uses both unsaturated and saturated layers, Hytec runs in “unsaturated mode”, hence, for every zone the van Genuchten parameters (van Genuchten 1980) as well as the saturated and residual water content and an initial estimation of the average water content of the zone need to be given. To summarize, five zones are considered (Figure III-14): the trench, a few centimeter soil layer at the top of the profile, the unsaturated aeolian layer (from the bottom of the soil layer to 1 meter lower than the trench

bottom), the saturated aeolian layer which top is located at 111 m.a.s.l (approximately the water level during October 2008 and 2009 field campaigns) and a saturated alluvial layer at the bottom.

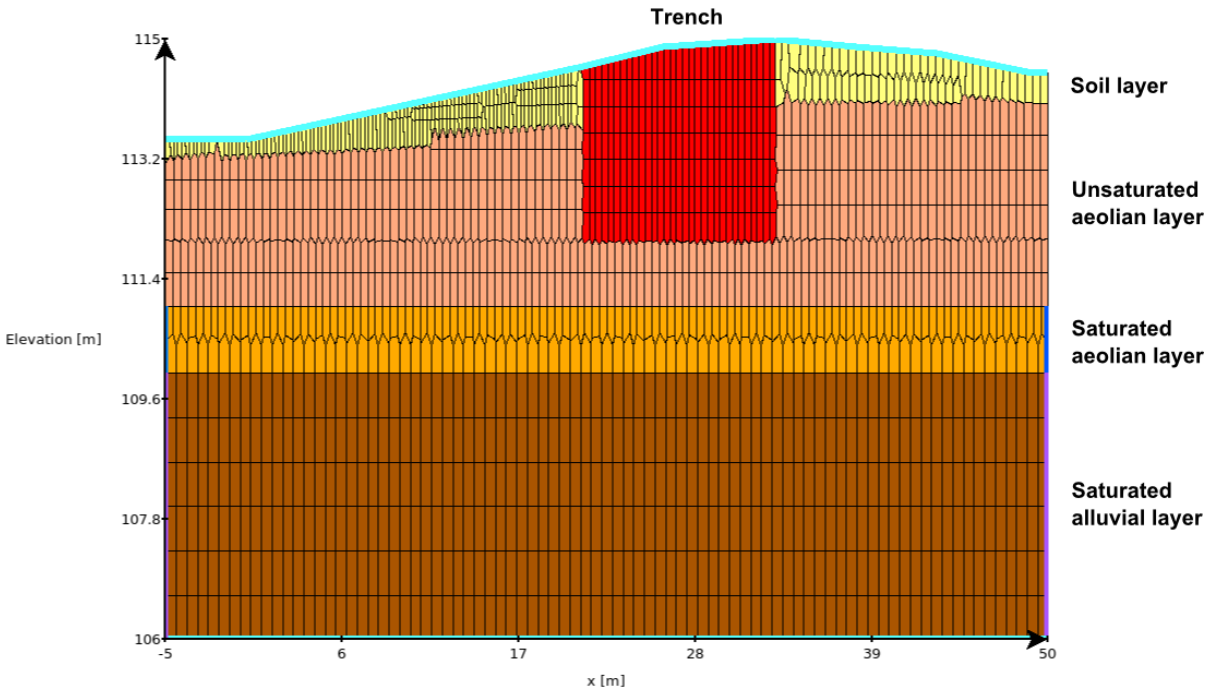

Figure III-14: Simulation grid

III.6.1.2 Hydraulic parameters

For each layer, hydraulic parameters are derived from values measured or calculated in previous studies (Van Meir *et al.*, 2012; Mazet, 2008; Bugai *et al.*, 2012b).

In the unsaturated areas, porosities, permeabilities and van Genuchten parameters are based on studies by Van Meir *et al.* (2012) and Mazet (2008) studies (Table III-1).

In saturated aeolian layer, the considered permeability is the value published by Bugai *et al.*, 2012b. However, HYTEC cannot take into account the anisotropy, thus, an intermediate permeability value is chosen in the alluvial layer (2×10^{-6} $m.s^{-1}$).The lower boundary is adjusted (see below) to reproduce the flow direction in the alluvial layer according to Bugai *et al.*, 2012b. The porosities of the saturated areas are based on Mazet's PhD thesis (2008): water content in the

aeolian sand column in laboratory was determined between 0.24 and 0.28 for a total porosity of 0.3.

Dispersivity coefficients are selected from tracer test studies performed by Bugai *et al.* (2012b), where values between 0.02 and 0.09 m were determined: an intermediate value of 0.05 is chosen for all the layers, except for the trench for which a lower value of 0.01 is considered. The same diffusion coefficient of 1×10^{-10} $m^2.s^{-1}$ is chosen for all layers.

All the used parameters are summarized in Table III-1.

Table III-1: hydraulic parameters used for the initial simulation

Layer	Effective porosity	Permeability ($m.s^{-1}$)	Dispersivity (m)	Diffusion coefficient (m^2/s)	Porosity	Van Genuchten parameters	
						α	n
Trench	0.28	2.0×10^{-5}	0.01	1×10^{-10}	0.28	3	2
Soil	0.3	4.5×10^{-5}	0.05	1×10^{-10}	0.30	7.5	2.5
Aeolian	0.28	4.17×10^{-5}	0.05	1×10^{-10}	0.28	6.5	1.8
Alluvial	0.24	2×10^{-6}	0.05	1×10^{-10}	0.24	20	2

III.6.1.3 Boundary conditions

The top boundary is a constant infiltration rate equal to 250 $mm.y^{-1}$, corresponding approximately to the mean infiltration rate at the Chernobyl Pilot Site, *i.e.* 30 to 50% of the yearly precipitations (Bugai *et al.*, 2012a). This infiltration is equilibrated by a constant outflow of 250 $mm.y^{-1}$ at the bottom of the cross-section.

In the aeolian zone, the left and right boundaries are defined by constant heads of 111.0825 m and 111 m, respectively. This aims at reproducing the observed hydraulic gradient of 0.0015. Indeed, the water table is considered to be constant at a level of 111 m.a.s.l. In the alluvial layer, a constant inflow/outflow equal to 270 $mm.y^{-1}$ is imposed to obtain a flow defined by Bugai *et al.*, 2012b.

III.6.1.4 Cl and ^{36}Cl

The Cl and ^{36}Cl migration in groundwater is simulated according to the following hypotheses on [Cl^-] and [^{36}Cl]:

- in background groundwater and in rainwater, a [Cl^-] of 0.02 mmol.L^{-1} is considered: this value corresponds to the mean concentration in meteoric water in the period 2005-2006 (Bugai *et al.*, 2012a) and approximately to the concentration measured in upgradient groundwater. Considered background [^{36}Cl] is 2×10^{-15} mmol.L^{-1}, corresponding to the natural theoretical value in rainwater (see section III.4.1.1.)
- in the trench, the source term concentrations are supposed to correspond to concentrations measured in the trench soil water sample in May 2011. The [^{36}Cl] of this sample is chosen as ^{36}Cl term source (4×10^{-9} mmol.L^{-1}). However, considering the difference of [Cl^-] between the trench soil water and the most concentrated groundwater, the [Cl^-] in the trench soil water appeared too high (0.35 mmol.L^{-1}), consequently, [Cl^-] in the source term is arbitrary adjusted to 0.1 mmol.L^{-1}. As said above, in this first approximation, the source term from the trench is considered constant.

III.6.2 RESULTS AND DISCUSSION

III.6.2.1 Results of the simulation

Simulated velocities and flow direction are presented in Figure III-15 and [Cl^-] and [^{36}Cl] are shown in Figure III-16 and Figure III-17.

In Figure III-15, the left side is the direct output of the simulation, showing for each node the flow direction colored following the value of the velocity. The right side is a simplified version, showing the global flow directions in saturated layers with the average simulated velocity in each saturated layer. In the aeolian layer, the average simulated velocity is 5.7×10^{-8} m.s^{-1} whereas a velocity of 3.5×10^{-7} m.s^{-1} was estimated by tracer test (Bugai *et al.*, 2012b). In the alluvial layer, no measurement are available but considering our hypothesis and a hydraulic head of 0.03 (Bugai *et al.*, 2012b), and according to the following calculation of average linear velocity:

Equation III-12

$$v_D = \frac{K}{\eta_{eff}} \times \frac{dh}{dl}$$

where v_D is the flow velocity in the vertical direction because groundwater flow in this layer is mainly vertical, K is the vertical hydraulic conductivity, η_{eff} is the effective porosityand dh/dl is the gradient of hydraulic head. A velocity of 6×10^{-8} $m.s^{-1}$ is expected. With the considered parameters, the simulation leads to an average alluvial groundwater velocity of 8.7×10^{-9} $m.s^{-1}$ $m.s^{-1}$, two orders of magnitude lower than theoretical values. If the direction flows are well reproduced according to the one published by Bugai *et al.*, 2012b, average velocities are really underestimated by almost one order of magnitude in both layers.

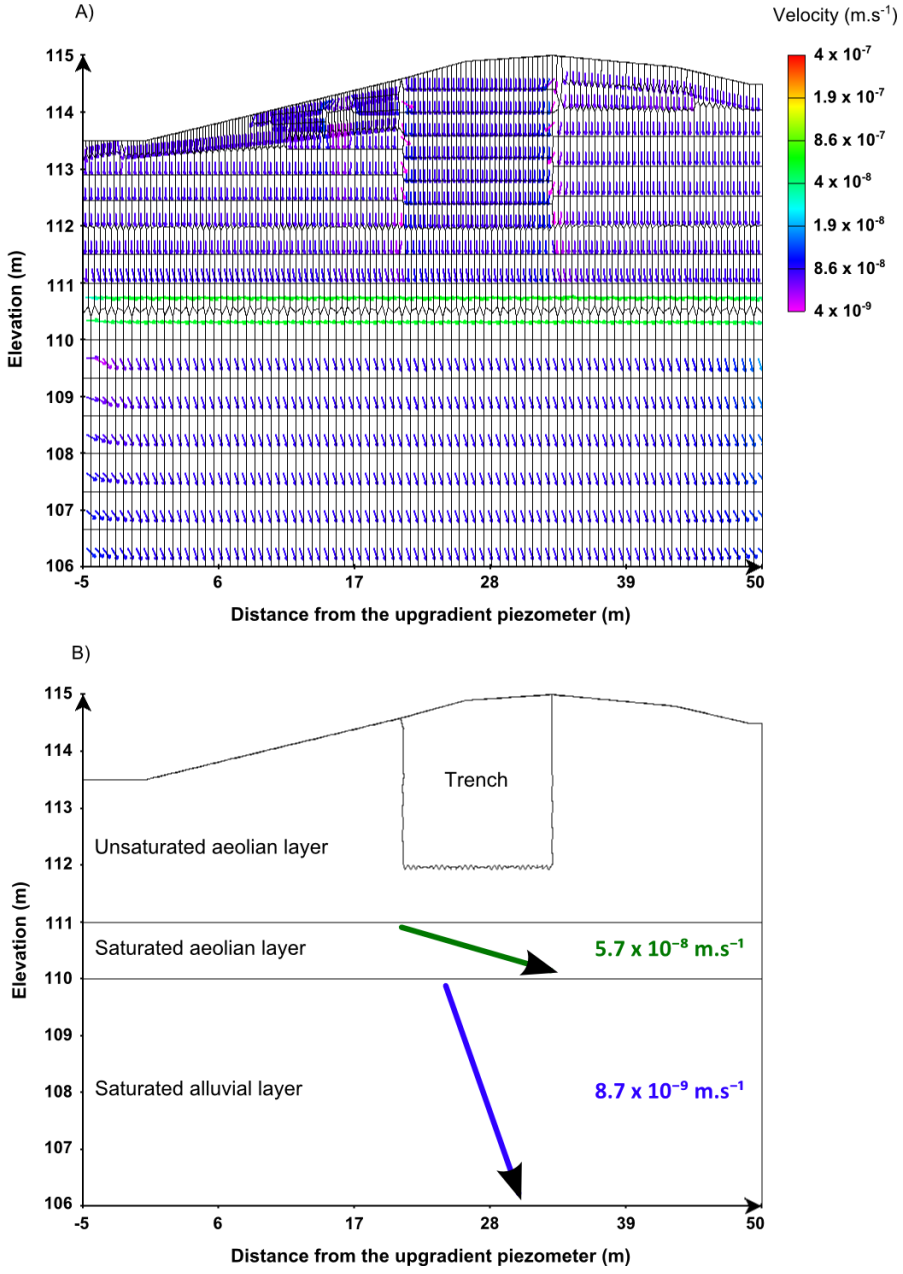

Figure III-15: Initial simulation velocities after 25y

Simulated [Cl^-] and [^{36}C] are presented after 25 years in Figure III-16 and Figure III-17, respectively, and are compared with the measured concentrations for each field campaign (from the top to the bottom: October 2008, October 2009 and May 2011). An equilibrium of Cl^- and ^{36}Cl plumes is reached after about 10 years of simulation: no change in plumes geometry is observed after this, at the scale of the simulation. At this time, the entire ^{36}Cl contamination of the groundwater downgradient of the trench shown.

[Cl^-] is initially imposed at 0.1 mmol.L^{-1}, as a constant source term in the trench. The simulated 0.03 mmol.L^{-1} concentration isoline is considered as the limit of trench plume maximal extent in groundwater, based on the mean [Cl^-] in rainwater which is 0.02 mmol.L^{-1} (Bugai *et al.*, 2012a). Downgradient part of the trench, the 0.03 mmol.L^{-1} concentration isoline is located just near the furthest piezometer, where [Cl^-] of 0.03-0.04 mmol.L^{-1} are measured in groundwater. Upgradient part of the trench, 0.03 mmol.L^{-1} concentration isoline is located near piezometers just upgradient of the trench, where most of measured [Cl^-] are of 0.01-0.02 mmol.L^{-1} with a maximum value of 0.03 mmol.L^{-1}. Consequently, the simulated [Cl^-] horizontal extent of the plume seems to fit quite well with the measured [Cl^-] concentrations. However, simulated [Cl^-] concentrations in groundwater of the alluvial layer are above 0.03 mmol.L^{-1} downgradient of the trench while measured [Cl^-] do not exceed this value. Hence, the deep extension of the simulated [Cl^-] is too deep considering the measured values. Also, in the Cl^- plume in groundwater downgradient of the trench, the maximum measured [Cl^-] is 0.06 mmol.L^{-1} (October 2008) while the simulated [Cl^-] can reach up to 0.08 mmol.L^{-1} in the simulation. Furthermore, in the center of the simulated plume, simulated [Cl^-] are 4 fold higher than values measured at the same location, while the plume in [Cl-] is identified 10 meters downgradient this simulated plume. Consequently, the simulated plume is too concentrated and located too much upgradient in comparison with the observed plume.

The comparison of the simulated and measured [^{36}Cl] in October 2008, October 2009 and May 2011 field campaigns leads to similar observations (Figure III-17). [^{36}Cl] imposed initially as source term in the trench is 4×10^{-9} mmol.L^{-1}. Overall, while maximum [^{36}Cl] measured in groundwater is around 10^{-10}-10^{-9} mmol.L^{-1} (October 2008, May 2011), simulated [^{36}Cl] are at least four times higher.

Moreover, the highest concentrations in the simulated plume are shifted to an upgradient location compared to measured [^{36}Cl] in groundwater. Deeper, simulated [^{36}Cl] are again overestimated in the alluvial layer. The [^{36}Cl] contrast between the alluvial and aeolian layer is not reproduced by the simulation. It can be noted that the 1.7×10^{-11} mmol.L^{-1} isoline reaches piezometers just upgradient of the trench, this increase of [^{36}Cl] in upgradient groundwater is not observed in measured [^{36}Cl] concentrations in these piezometers are below this value.

In summarize, this simulation cannot be accepted entirely because of the too low simulated velocities, the too deep extension and the shift of the plume with regard to measured concentration. However, this simulation can be improved by taking a closer look at the choice of parameter values and hypotheses on the initial concentration values in the source term.

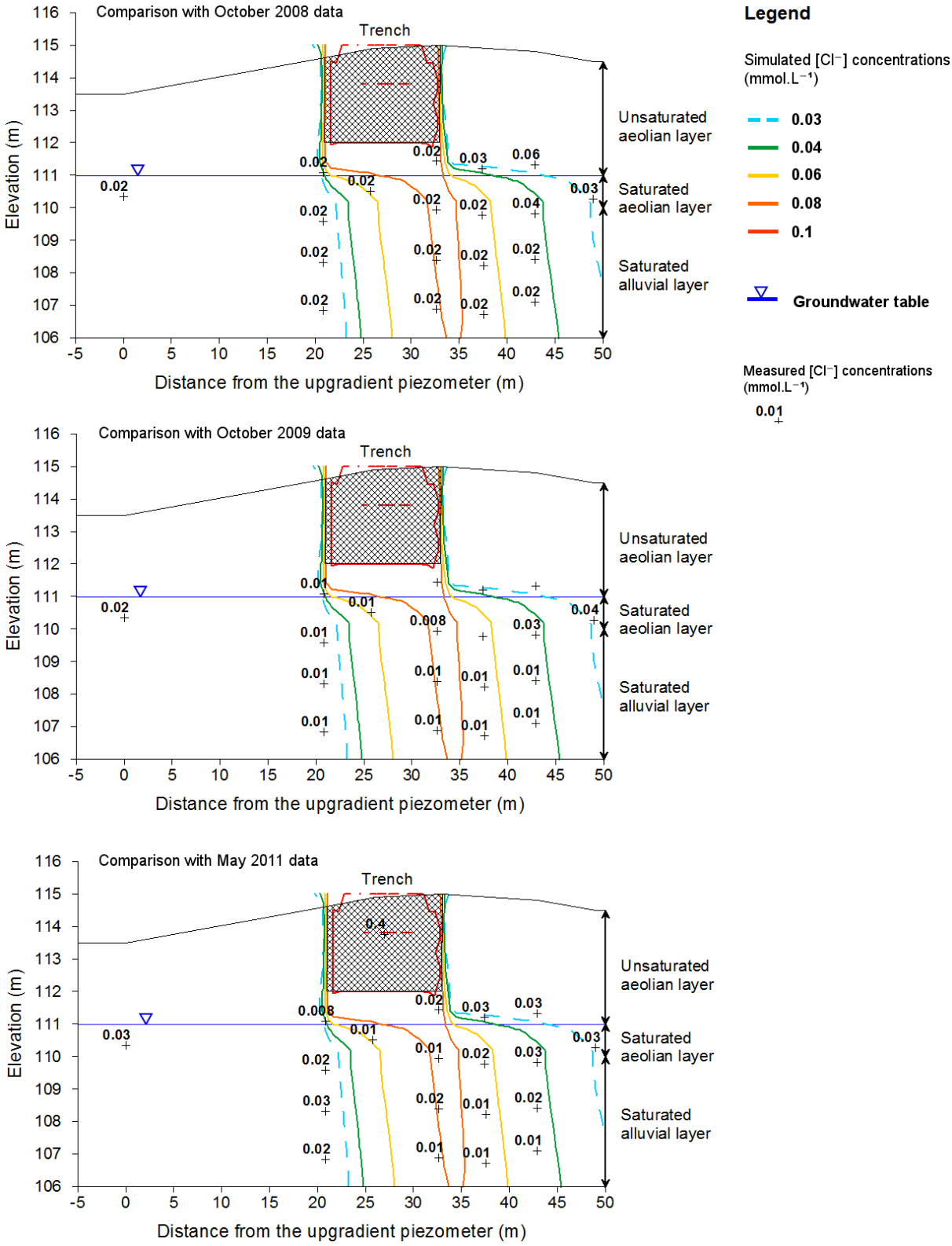

Figure III-16: Simulated [Cl^-] concentrations in the initial simulation after 25y and measured data

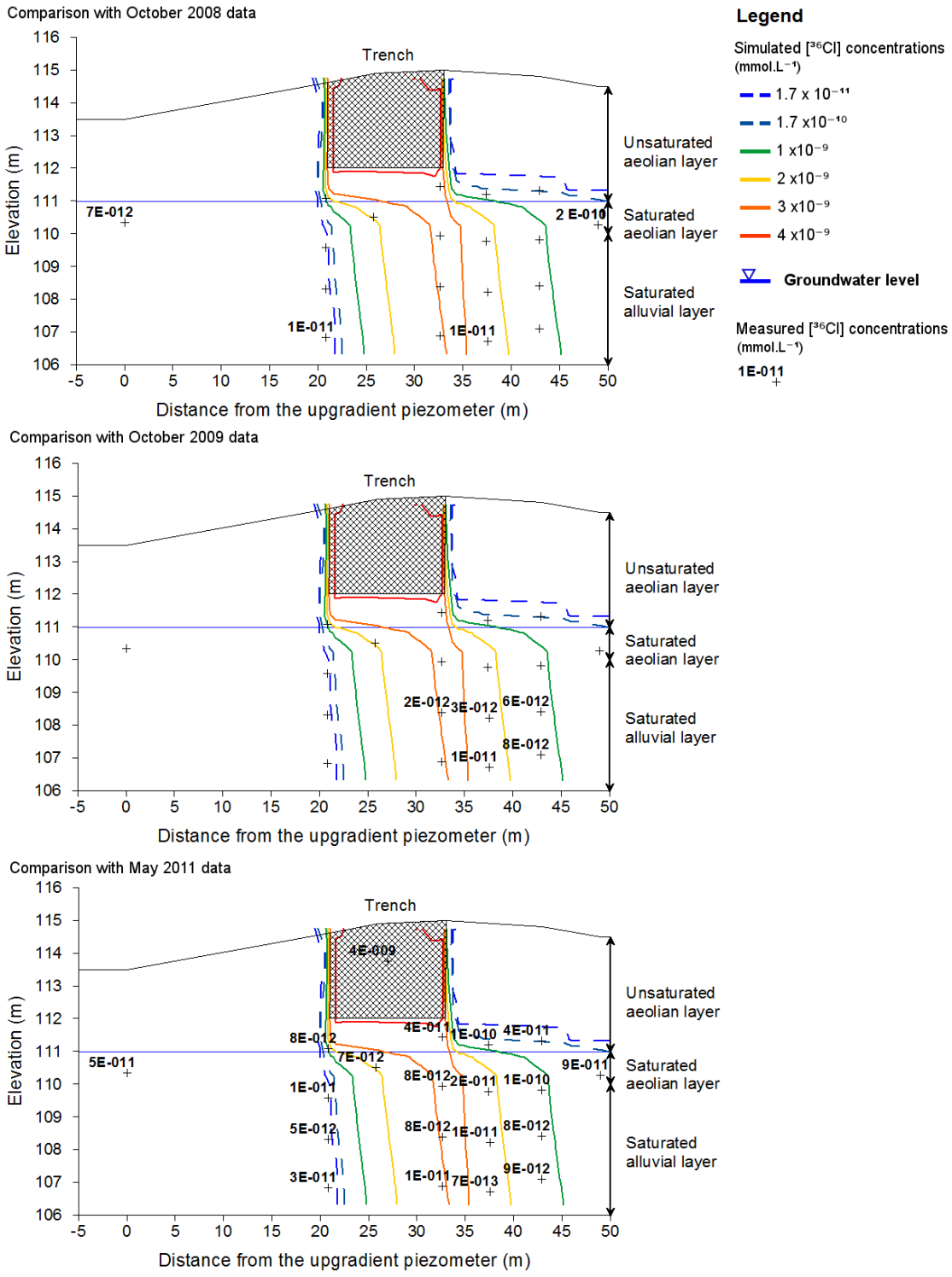

Figure III-17: Simulated [$^{36}Cl^-$] concentrations in the initial simulation after 25y and measured data

III.6.2.2 Simulation sensitivity

The discrepancies between the simulated and measured values may be explained by the choice of the parameter values used for the simulation. A sensitivity analysis is carried out on the source term and the flow parameters in the saturated zones. Firstly, sensitivity on the source term is investigated, as it is the least constrained

of all parameters. Then, hydraulic parameters can be optimized following parameters variations shown at the Chernobyl Pilot Site. The extreme observed values of parameters are used in the analysis of sensitivity. If a range of variation is not available, parameters are changed by multiplying or dividing them by a factor 2.

This sensitivity analysis usually aims at indentifying parameters having the most influence on the simulation results, in this case the migration of Cl and ^{36}Cl. The impact on flow velocities and directions are also studied.

III.6.2.2.1 Source term sensitivity

The parameter supposed to have the greatest influence on [Cl^-] and [^{36}Cl] in groundwater is the source term. In the initial simulation, the source term is defined with a [Cl^-] of 0.1 mmol.L^{-1} and a [^{36}Cl] of 4×10^{-9} mmol.L^{-1} and assessed to correspond approximately to values measured in the trench soil water sample in May 2011. In order to investigate the source term influence, [Cl^-] and [^{36}Cl] are simulated in groundwater, at first dividing and then multiplying the initial source term concentration by 2.

Simulated [Cl^-] and [^{36}Cl] are presented in Figure III-18 and Figure III-19 after 25 y of simulation. On both figures, the upper and lower profiles correspond to the less-concentrated and the most concentrated source term. Colors become darker with the increasing concentrations.

Concentrations in groundwater are obviously higher when the source term concentration is higher: simulated [Cl^-] in the center of the plume are close to 0.04 to 0.16 mmol.L^{-1} for source terms of 0.05 and 0.2 mmol.L^{-1}, respectively. The horizontal extension of the plume is also modified: it is widen when the source term is higher. For instance, it is evidenced by 0.03 mmol.L^{-1} isoline (dashed light blue line) in the [Cl^-] representations.

Simulated [^{36}Cl] show similar trends with concentrations reaching 1×10^{-9} and 6×10^{-9} mmol.L^{-1} in the case of a low and a high source term, respectively. The influence on plume extent can be observed with the 1×10^{-9} mmol.L^{-1} isoline for instance.

The variation of the source term is confirmed to have a high influence on concentrations in groundwater. In order to better fit simulated [Cl^-] in groundwater with measured data, the initial term source concentrations should be decreased down to at least 0.05 mmol.L^{-1}, considering that the highest [Cl^-] in the plume

measured downgradient of the trench are of 0.04 $mmol.L^{-1}$ or of 0.06 $mmol.L^{-1}$ following the year of sampling. This value is much lower than the [Cl^-] measured in the trench soil water, which implies that processes of Cl- migration in groundwater are more complexes than a simple dilution of this water in rainwater. In the case of the [^{36}Cl], even in the lowest considered term sources, [^{36}Cl] still remain at least one order of magnitude higher than the observed concentrations (Figure III-19).

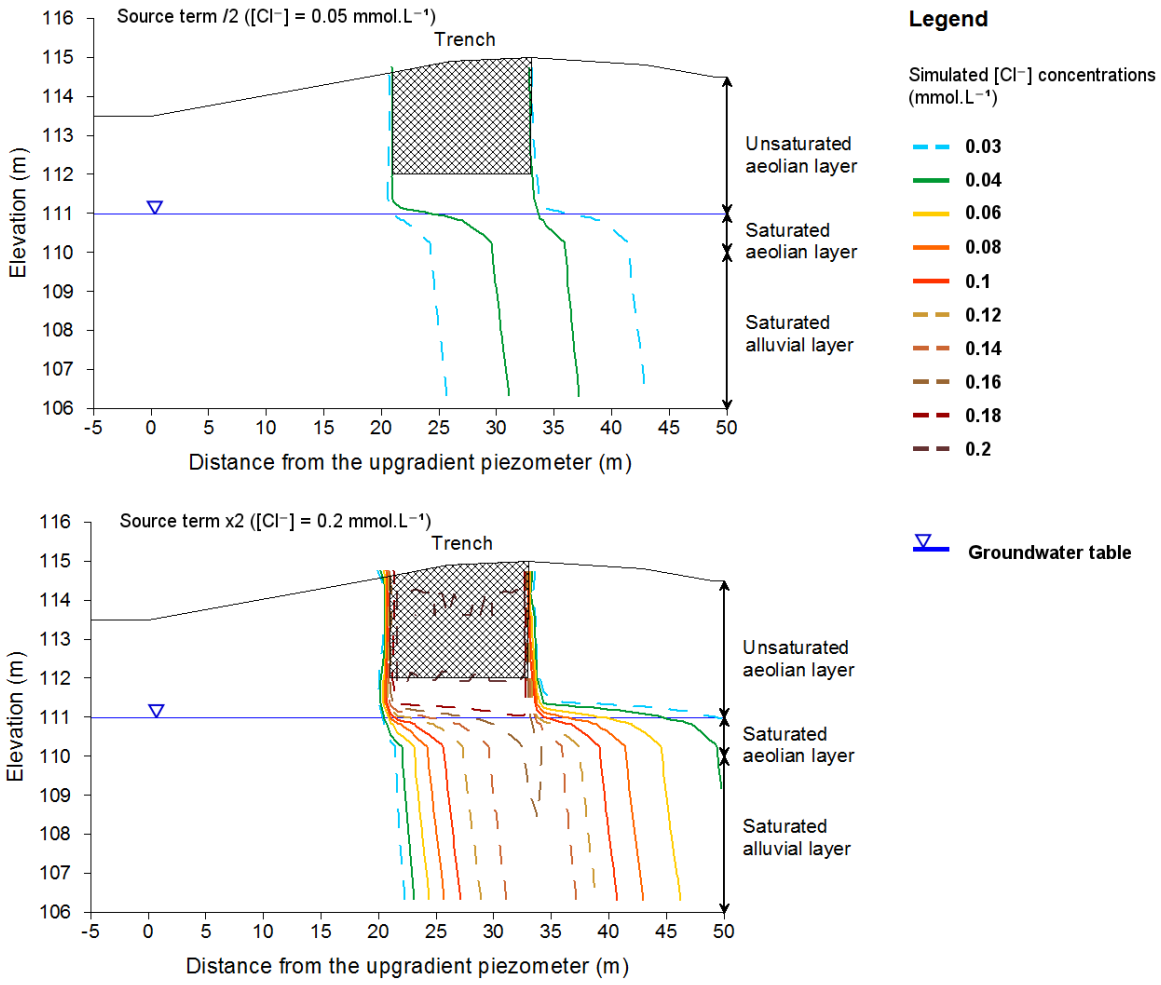

Figure III-18: Sensitivity analysis about Cl term source

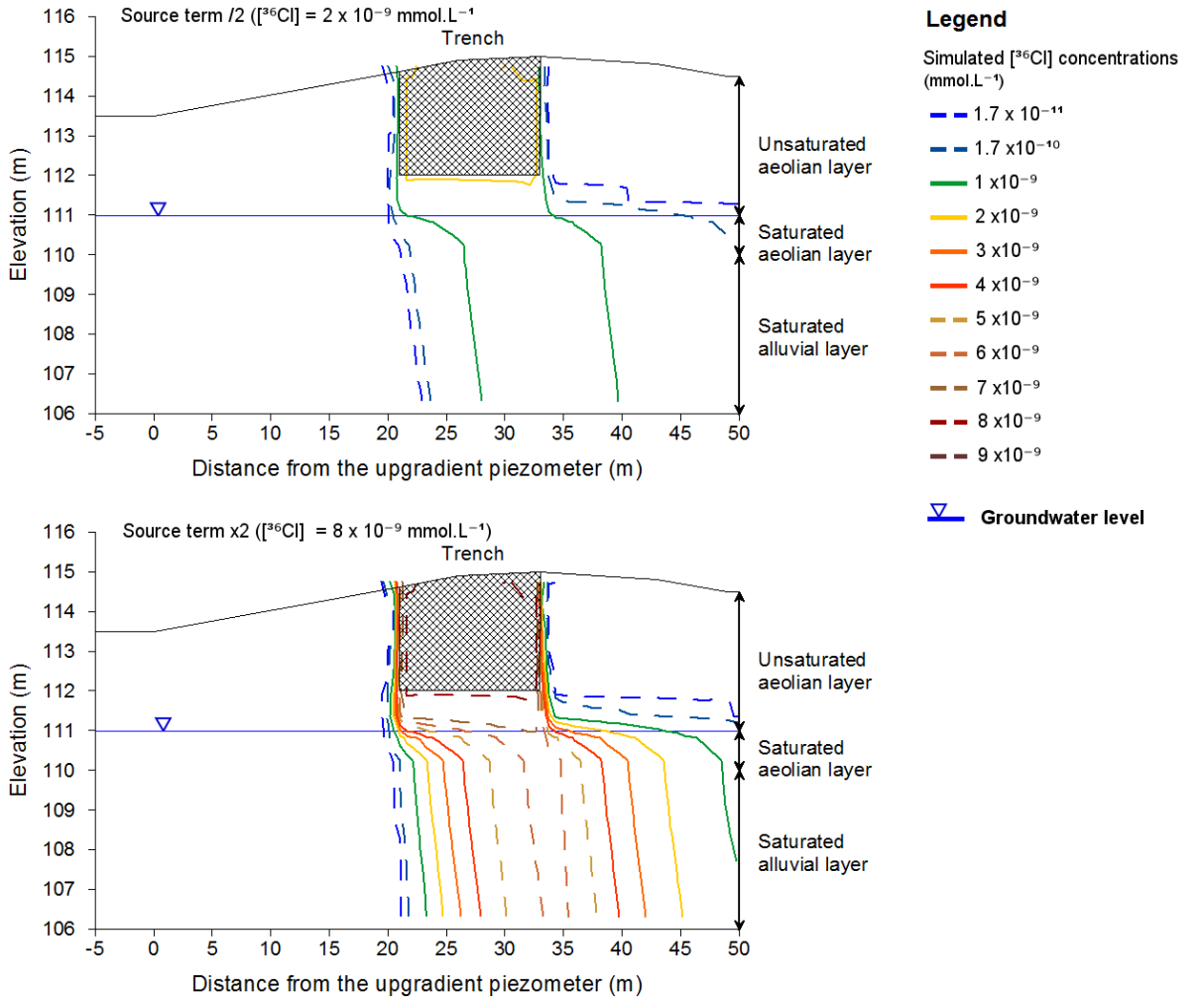

Figure III-19: Sensitivity analysis about ^{36}Cl term source

III.6.2.2.2 Flow parameters sensitivity

The second important issue of the initial simulation is that simulated velocities are too low.

In order to improve the model, parameters involved in advective transport in groundwater (Equation III-12) can be adjusted to better fit with theoretical velocities. The impact of dispersivity coefficient variation, a parameter defining dispersive transport, is also studied. The initial [Cl^-] source term of 0.1 mmol.L^{-1} is used again. Parameters are tested following their available range of variations or by dividing and multiplying them by a factor 2. Tested values are given in Table III-2.

- As the only value available is the one used in the initial simulation, changes of aeolian permeability parameter is investigated at first dividing and then multiplying it by a factor 2.

- Alluvial layer was shown to be anisotropic and the vertical permeability and the horizontal permeability are separated by one order of magnitude (Bugai *et al.*, 2012b). As mentioned above, one of the limitations of the HYTEC code is its inability to take into account anisotropy. Consequently, two simulations are carried out, firstly with values close to the vertical permeability and then with values close to the horizontal permeability, as they were defined by Bugai *et al.* (2012b).
- The simulation is tested with lower hydraulic head of 0.001. This value corresponds to the lowest value of the theoretical hydraulic head range. The highest value is used in the initial simulation (0.0015) (Bugai *et al.*, 2012b).
- Effective porosity (0.28) is perhaps overestimated in the initial simulation because the used value came from laboratory water content in column of aeolian sand, supposed to be close to field conditions (Mazet, 2008). Based on tracer tests performed in the early 2000's showed groundwater velocities in this layer around 3.5×10^{-7} m.s^{-1} and considering an aeolian permeability of 4.5×10^{-5} m.s^{-1} (Bugai *et al.*, 2012b), according to the calculation for the velocity (Equation III-12), an effective porosity of 0.19 is obtained. This value is rounded to 0.2.
- Bugai *et al.* (2012b) determined dispersivity coefficient values with tracer test: the values range from 0.02 to 0.09 m. These values are rounded to 0.01 and to 0.1.

Table III-2: Tested values in the sensitivity analysis

	Initial value	Minimum value tested	Maximum value tested
Aeolian permeability (m.s^{-1})	4.5×10^{-5}	2.25×10^{-5}	8.34×10^{-5}
Alluvial permeability (m.s^{-1})	2×10^{-6}	3×10^{-7}	5.8×10^{-6}
Effective porosity	0.28	0.2	0.28
Gradient of hydraulic head	0.0015	0.001	0.0015
Dispersivity (m)	0.05	0.01	0.1

Their impact on [Cl^-], flow velocities and directions are discussed. All the figures associated with this analysis are given in Annex 7, after 25 years of simulation.

- Simulated velocities in the aeolian layer can be increased by increasing aeolian permeability. Consequences are mainly shown in the aeolian layer flow: the flow direction becomes more horizontal with an increase of the mean velocity up to 1.1×10^{-7} m.s^{-1} for a permeability of 8.34×10^{-5} m.s^{-1}. Consequently, [Cl^-] are lower reaching 0.06 mmol.L^{-1} and plume horizontal extension is higher.
- Lowering the permeability in the alluvial layer (3×10^{-7} m.s^{-1}) leads to a more vertical direction flow (the bottom outflow remains constant) and its increasing (5.8×10^{-6} m.s^{-1}) gives a more horizontal flow. With such increase of permeability, the [Cl^-] plume is less deep.
- No significant changes are observable between a porosity of 0.28 and a porosity of 0.2, neither in flow direction, in mean velocity, in plume extent or in [Cl^-]. This parameter is not a major parameter to better constrain Cl and ^{36}Cl migration by simulation.
- The application of a lower hydraulic head gradient in the aeolian layer results in lower velocities than these observed in the initial simulation with a more vertical flow direction. Consequently, the [Cl^-] plume is less concentrated and less horizontally dispersed. And yet, even if the simulated [Cl^-] plume seems to better correspond to observed plume, the simulated velocities (3.8×10^{-8} m.s^{-1}) are still very low in comparison with measurement of solute velocity by tracer tests (3.5×10^{-7} m.s^{-1}) (Bugai *et al.*, 2012b). Since the tracer test is a direct measurement, lowering the gradient in the alluvial is not seen as a good optimization of the simulation.
- No major changes are observed with dispersivity changes, except eventually a slight decrease of the 0.08 mmol.L^{-1} isoline extension with depth with the increase of dispersivity. But this observation is most likely an artifact of the kriging method used for the interpolation of simulated concentrations.

III.6.2.3 Optimal simulation

As seen previously, the problem of our initial simulation was that the simulated [Cl] plume was too extended and not shifted far enough horizontally.

Based on the sensitivity analysis, an optimized simulation is proposed by increasing aeolian and alluvial permeabilities and decreasing the source term concentrations, using the extreme values used in the sensitivity analysis (Table III-3).

Table III-3: parameters tested in the simulations

	Initial value	Minimum tested value	Maximum tested value	"Optimal" simulation value
Aeolian permeability ($m.s^{-1}$)	4.17×10^{-5}	2.25×0^{-5}	8.34×10^{-5}	8.34×10^{-5}
Alluvial permeability ($m.s^{-1}$)	2×10^{-6}	3×10^{-7}	5.8×10^{-6}	5.8×10^{-6}
Effective aeolian porosity	0.28	0.2	0.28	0.28
Gradient of hydraulic head	0.0015	0.001	0.0015	0.0015
Dispersivity (m)	0.05	0.01	0.1	0.05
$[Cl^-]$ in the source term ($mmol.L^{-1}$)	0.1	0.05	0.2	0.05
$[^{36}Cl]$ in the source term ($mmol.L^{-1}$)	4×10^{-9}	2×10^{-9}	8×10^{-9}	4×10^{-10}

As too high simulated $[^{36}Cl]$ concentrations were observed downgradient of the trench dividing the $[^{36}Cl]$ term source by two in the sensitivity analysis and as an increase of simulated velocities is expected with the increase of permeabilities, the "optimized" source term $[^{36}Cl]$ is lowered at 4×10^{-10} $mmol.L^{-1}$, according to the highest values observed downgradient of the trench.

Simulated velocities are presented in Figure III-20, comparison between simulated and measured $[Cl^-]$ in Figure III-21 and simulated and measured $[^{36}Cl]$ in Figure III-22.

If $[^{36}Cl]$ fit better with observed values (particularly with May 2011 campaign) and the velocities are closer to the observed values, the $[Cl^-]$ contaminant plume is still diving too deep in groundwater and is not shifted far enough downgradient. Thus, the question of the contamination by ^{36}Cl measured in groundwater upgradient of trench T22 remains unexplained.

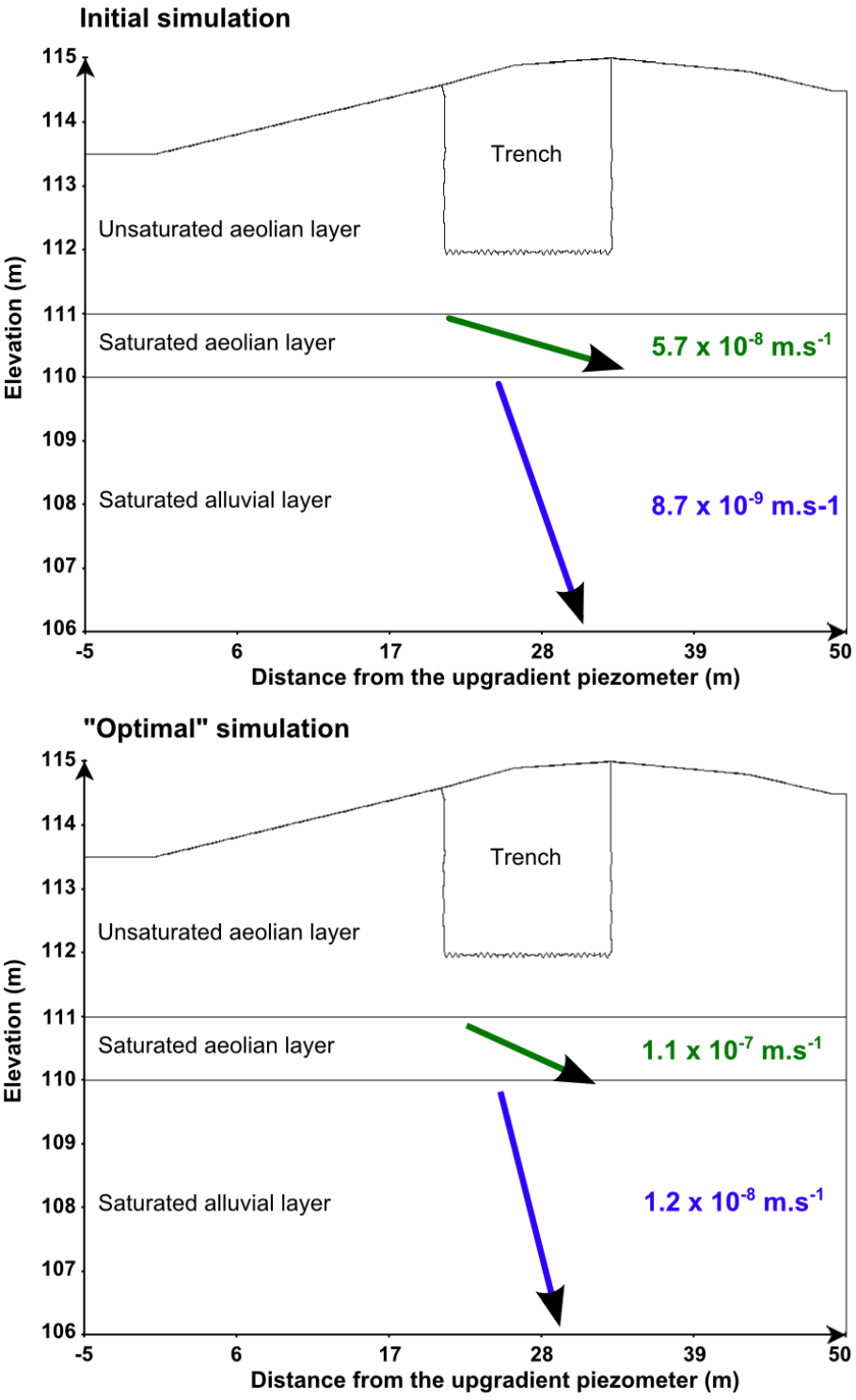

Figure III-20: Simulated velocities and flow directions

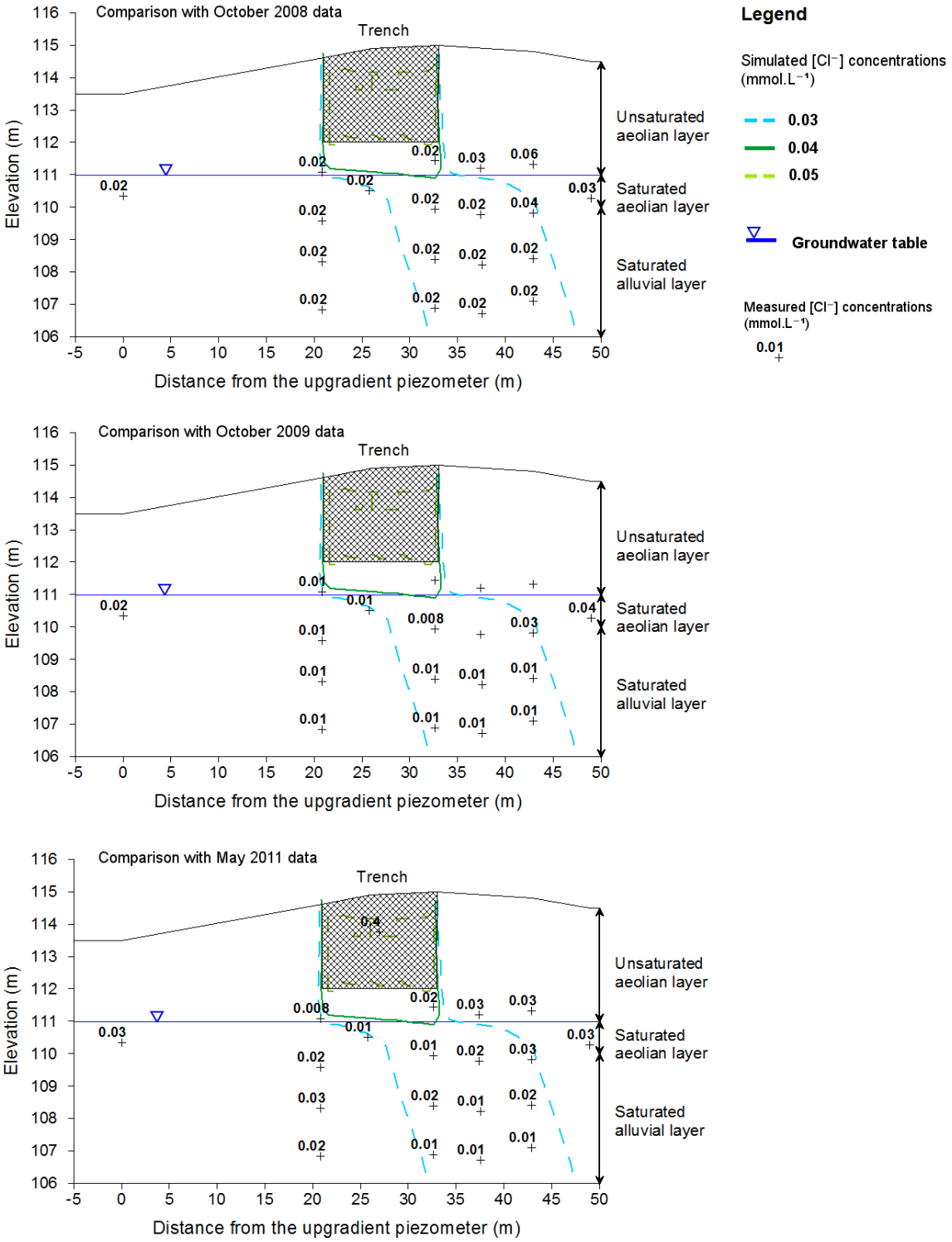

Figure III-21: Comparison of [Cl⁻] concentrations

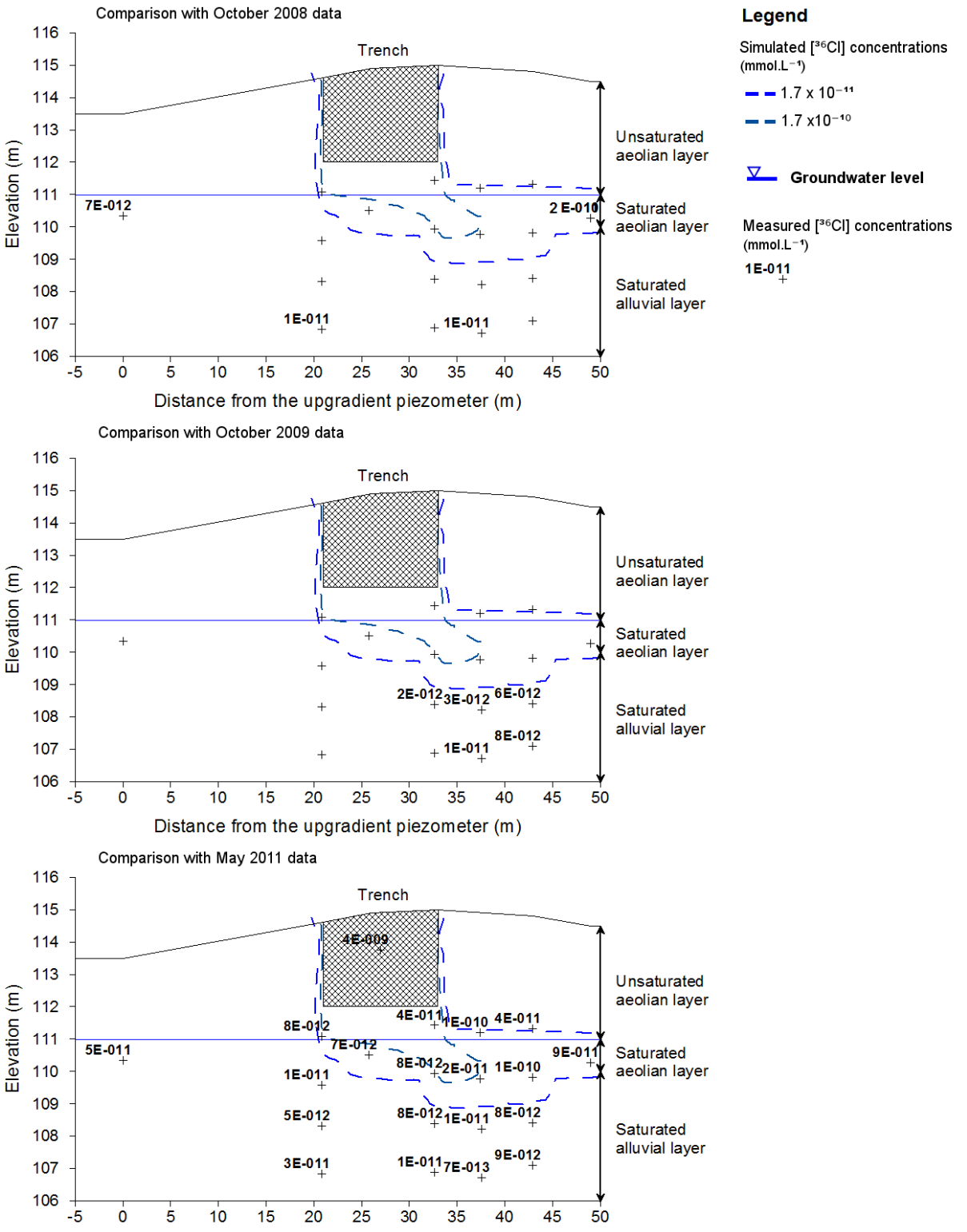

Figure III-22: Comparison of [^{36}Cl] concentrations

III.6.2.4 Perspectives

The sensitivity analysis showed that the simulation can be optimized changing hydraulic parameters and source term. However, the simulation of [Cl^-] is still a

problem and an upgradient contamination of ^{36}Cl is not taken account in the previous simulations.

There are some primary hypotheses underlying the simulation that can be questioned. Up to now the simulations considered a constant source term, i.e. a constant release with a constant concentration over time. As the source term has not been studied independently with respect to the release of chloride, an alternative tested here is proposed to simulate punctual release of chloride.

III.6.2.4.1 Punctual release of Cl from the trench

One of the main problems in the previous simulations is the too high [Cl^-] simulated in groundwater, particularly in the alluvial layer. In order to reduce [Cl^-] in the aquifer, the two initial hypotheses are questioned: constant term source and steady state.

III.6.2.4.1.1 Migration of Cl from the trench during 1 year

One of the initial hypotheses was the consideration of a constant source term. However, this assumption may be wrong. Indeed it is possible that Cl is released punctually to the groundwater. Here, a temporary release of Chlorine is simulated in groundwater: an initial source term with a concentration of 0.1 mmol.L^{-1} is released during a year. The persistence of the plume in groundwater is followed over time, without supplementary input of C. The same parameters in the optimized simulation are used.

Results are shown after 1 year, 1.25 year, 2, 3 and 10 years in Figure III-23. Concentrations of up to 0.03 mmol.L^{-1} persist in groundwater after 3 years but no more trace of the plume is found after 10 years. It illustrates that for a Cl release over a year, a persistence over 10 years is shown.

Such punctually release can occur for instance, when the water table rises up to the bottom of the trench and leaches directly the Cl source.

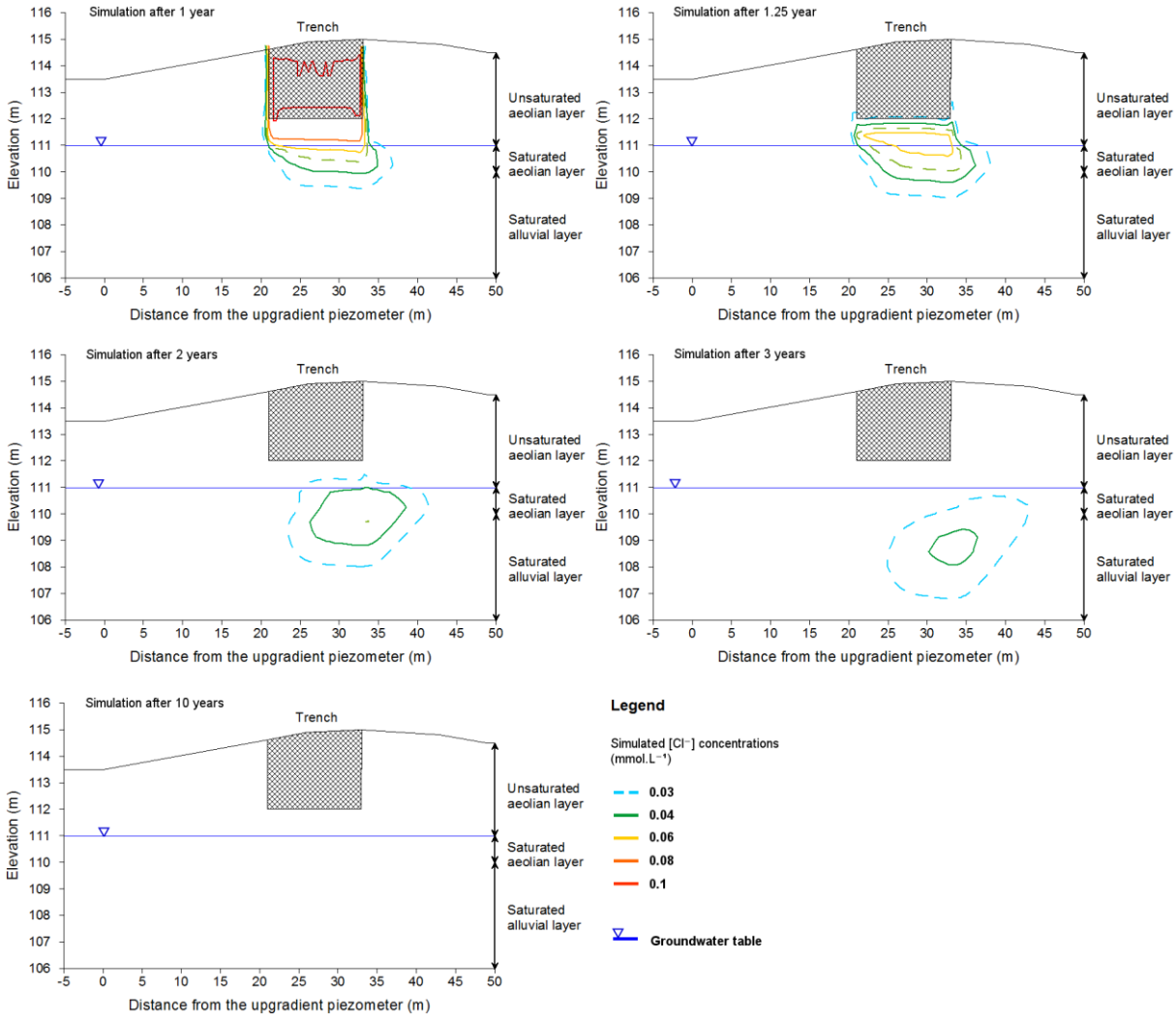

Figure III-23: Persistence of Cl plume in groundwater in time after a release from the trench during one year

III.6.2.4.1.2 Rising water table to fllod the trench

The influence of the trench flooding is then investigated: water table is risen to a very high level at 112.5 m.a.s.l. in steady state. The same parameters that in the optimized simulation are used. The Cl and ^{36}Cl source term is considered as constant again and the simulation runs over 25 years. Impact on [Cl^-] and [^{36}Cl] is shown in Figure III-24 and Figure III-23.

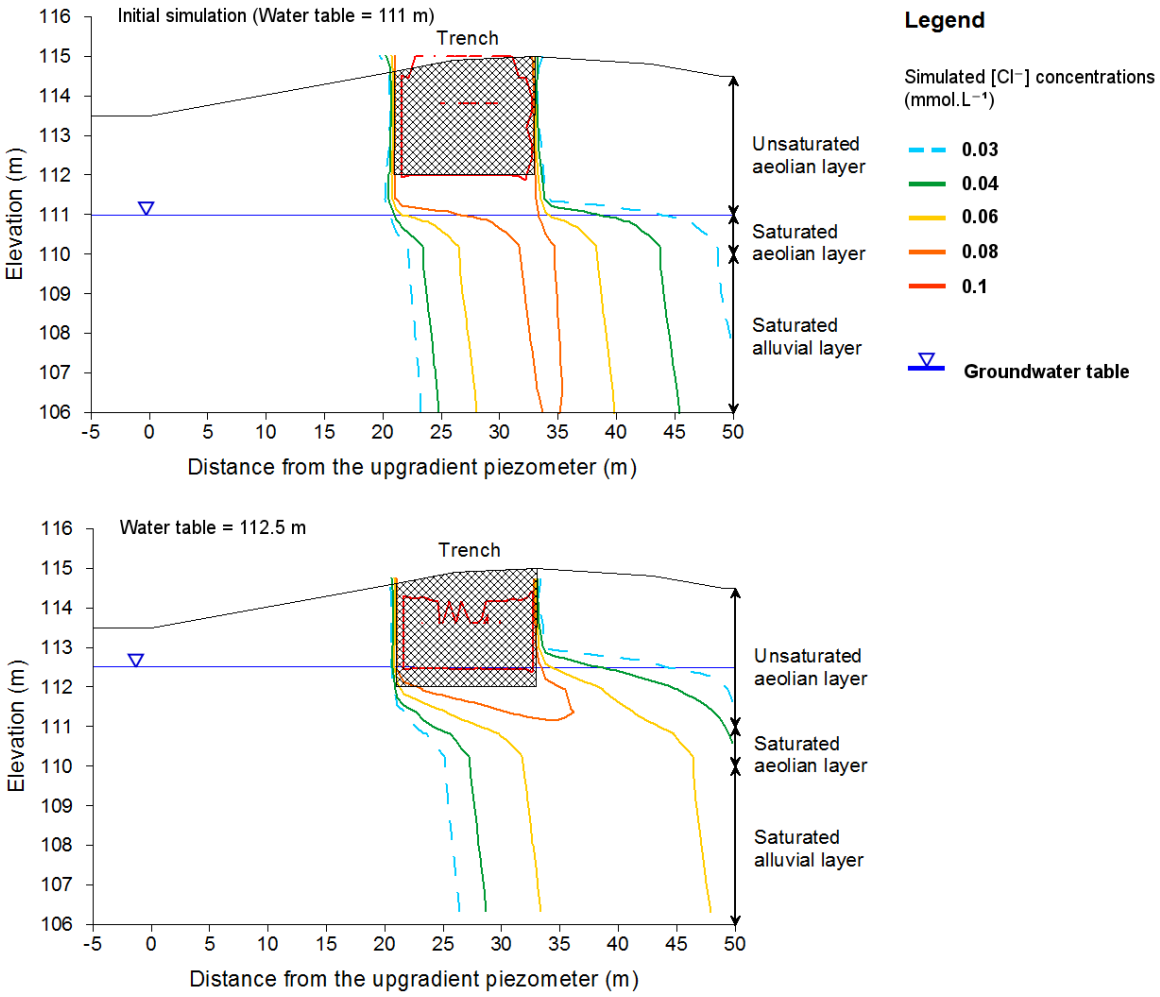

Figure III-24: Impact of the flooding of the trench on [Cl⁻] concentrations

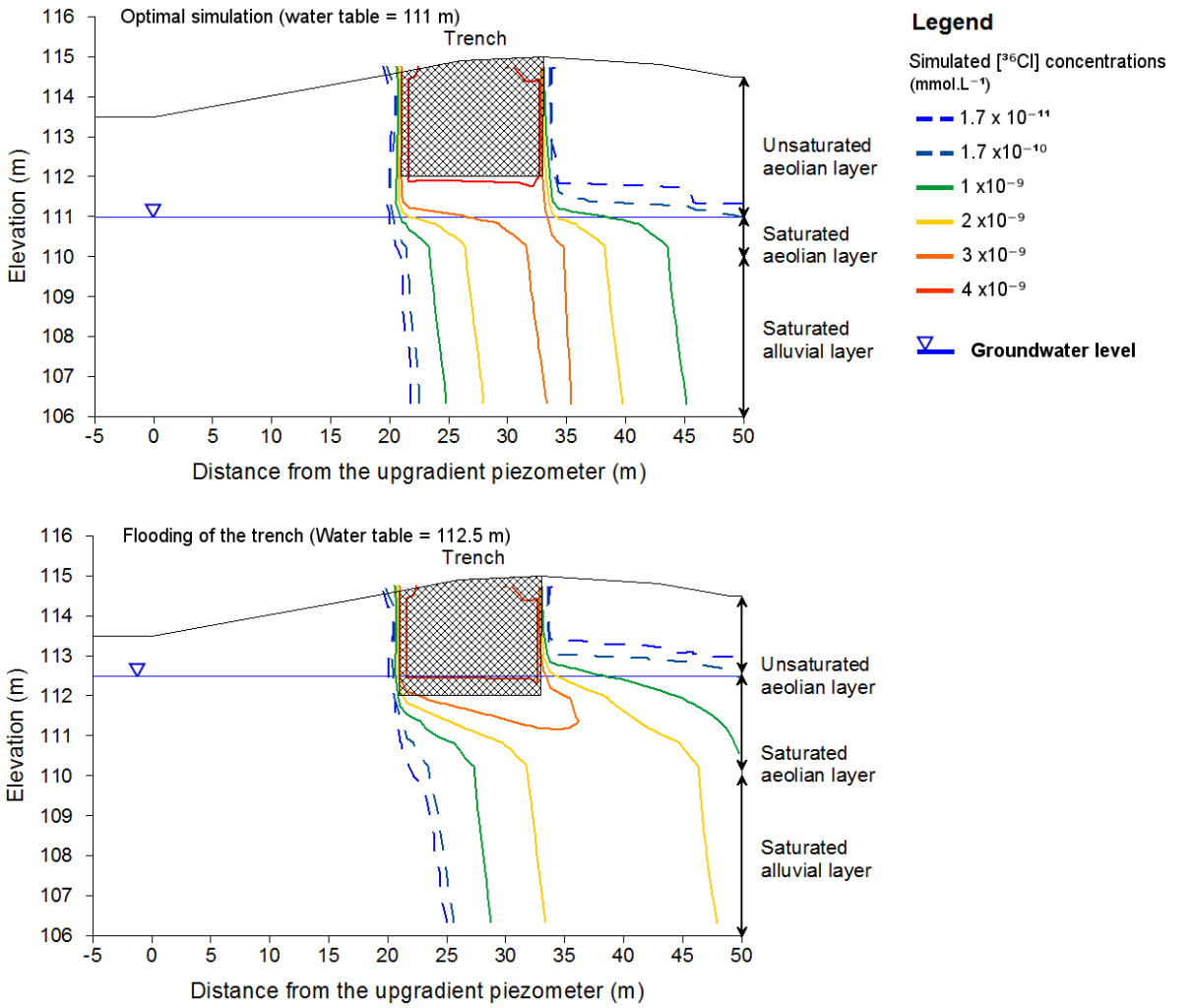

Figure III-25: Impact of the flooding of the trench on [^{36}Cl] concentrations

This change in flow conditions leads to shifting the Cl^- and ^{36}Cl plumes between the "optimized" simulation and the case where the water table is of 112.5 m. Concentrations decrease in groundwater when the trench is flooded. This is logic as the saturated aeolian layer is thicker and horizontal flow and transport away from the trench is, therefore, also increased. It is probable that such process is present on site as can be seen from the water table fluctuation observed since 2000 on site (Bugai et al., 2012b; Van Meir et al., 2007)

Trench T22 is not continuously flooded nevertheless flooding periods could lead to additional pulse releases of ^{36}Cl in groundwater.

The studies of the trench flooding and temporary release of Cl in groundwater show the impact of water table variations on contaminant plumes migration (velocities, concentrations…). Flooding of the trench is not permanent and will release more or less Cl and ^{36}Cl, with a signal that will persist in groundwater. It shows the limits of

the steady state consideration and suggests the investigation of migration of transient state to better constraint concentrations in groundwater.

III.6.2.4.2 Upgradient contamination

The upgradient contamination is one of the processes not simulated in the initial model. Two processes could explain such contamination: migration ^{36}Cl retained in soil or migration ^{36}Cl released by upgradient trenches. Both are simulated by the addition of a source term of $1x10^{-10}$ $mmol.L^{-1}$ (determined arbitrarily regarding concentrations in groundwater) at first in soil, and then in the upgradient groundwater. The "optimal" simulation conditions are used for these tests.

Results are presented in Figure III-26. ^{36}Cl contamination from the soil is shown at the top and ^{36}Cl contamination from upgradient trenches at the bottom of the figure.

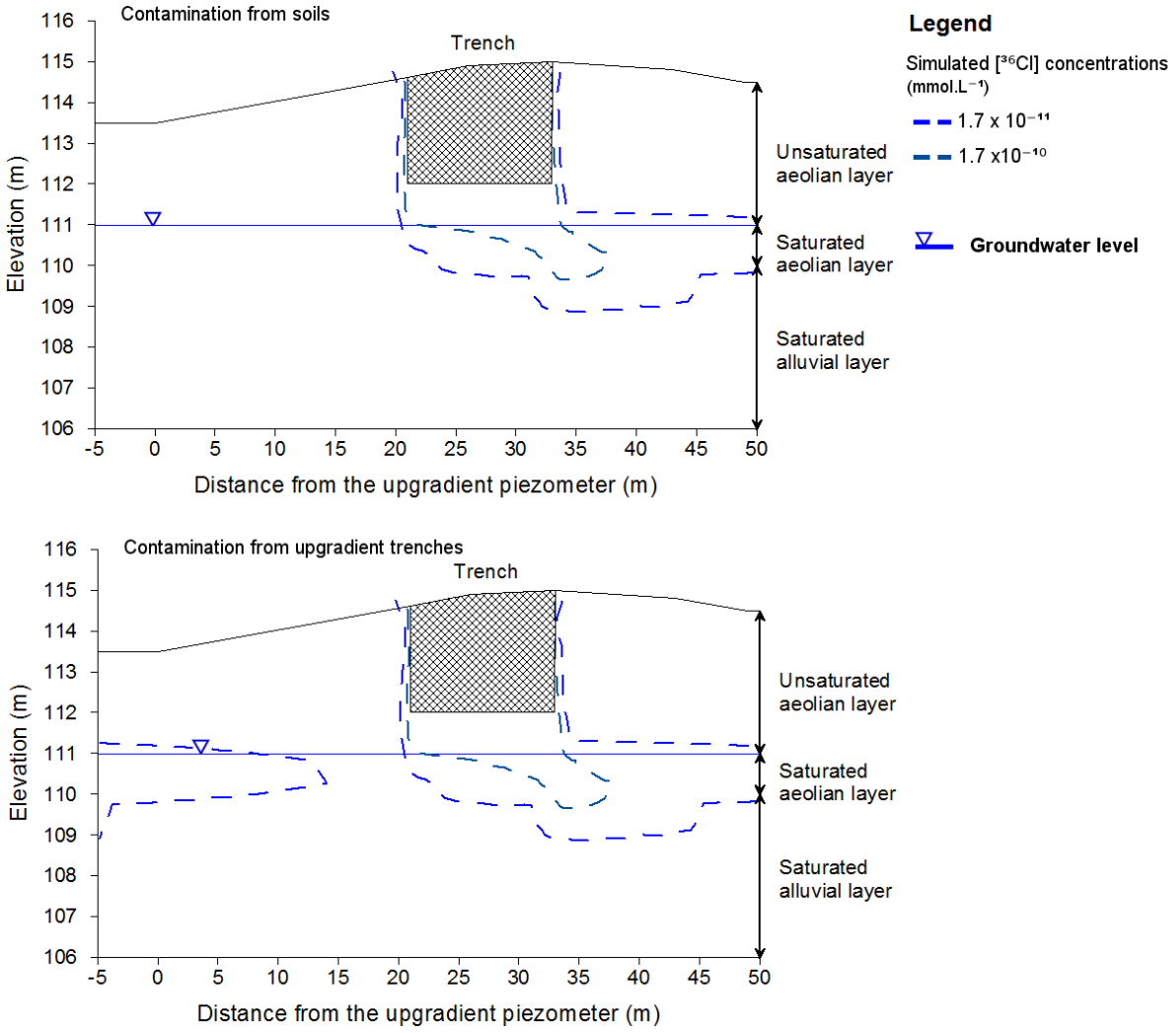

Figure III-26: ^{36}Cl upgradient contamination

With such ^{36}Cl concentrations in the source term, the ^{36}Cl from the soil never reach the groundwater. However, ^{36}Cl from upgradient groundwater contaminate the shallow groundwater but not the alluvial upgradient groundwater. This more or less arbitrary simulation shows that for a same contamination, ^{36}Cl originating from upgradient groundwater is more likely than $3^{6}Cl$ from soils. In order to support this hypothesis, soil water of the upgradient part and upgradient alluvial groundwater should be sampled.

III.6.2.5 Synthesis

In order to better constrain the maximal extension of the contaminant plume, ^{36}Cl release is simulated from trench T22 along the CD profile in groundwater. The aim is to study how and where ^{36}Cl migrates in groundwater according to the present hydrogeological knowledge of the groundwater flow.

Most of the initial hydrodynamic parameters derive from parameters used or measured by Bugai *et al.* (2012b), Van Meir *et al.* (2012) and Mazet, (2008). Initially, the source term was assumed using values close to concentrations observed in the trench soil water sample.

The initial simulation shows slightly lower velocities, too elevated $[Cl^-]$ and $[^{36}Cl]$, a large contamination of the alluvial layer, and an upgradient shift of the contaminant plume compared to the measured values. Thanks to the sensitivity analysis of this simulation, some improvements of the simulation are obtained decreasing the source term concentrations and increasing permeabilities in the aeolian and alluvial layer. However, $[Cl^-]$ still remain too high in the alluvial layer compared to measured concentrations.

Improvement of the simulation could also be made taking into account that the water table may have an influence on $[Cl^-]$ and $[^{36}Cl]$ release to groundwater. Consequently, the transient state should be considered. An upgradient contamination release from upgradient trenches is simulated too and this seems more realistic than ^{36}Cl release from soils.

III.7 CONCLUSION

In order to characterize the maximal extent of the contaminant plume from trench T22, the behavior of a conservative tracer, Chlorine-36, has been investigated in groundwater at the Chernobyl Pilot Site.

$^{36}Cl/Cl$ ratios were measured in groundwater samples, a soil water sample, leaf leachates and at the outlet of the Borshchii river, collected in October 2008, October 2009 and May 2011.

In groundwater, the obtained $^{36}Cl/Cl$ ratios are 1 to 4 orders of magnitude higher than the natural theoretical ratio. Such ratios show an anthropogenic origin for the ^{36}Cl in groundwater. According to groundwater apparent ages (Le Gal La Salle *et al.*, 2012), this high contamination of the groundwater mostly affect groundwater recharged after the Chernobyl explosion.

Trench T22 acts as an obvious point source of ^{36}Cl: soil water sampled in the trench body shows $^{36}Cl/Cl$ ratio 5 orders of magnitude higher than the natural theoretical ratio and one order of magnitude higher than the $^{36}Cl/Cl$ ratio in upgradient groundwater. Additional sources of ^{36}Cl are considered: diffuse contamination over the whole area at the time of the explosion, releases from upgradient trenches, release of ^{36}Cl by biogeochemical processes, nuclear activity at the Power Plant before the accident, thermonuclear tests. Even if Trench T22 is supposed to be the main source of ^{36}Cl contamination, these additional potential sources should be further investigated to better constrain the ^{36}Cl contamination of the Chernobyl Pilot Site groundwater. ^{36}Cl migration in groundwater is investigated based on the comparison of ^{36}Cl behavior relative to two other elements, Cl and ^{90}Sr. More specifically, the influence of potential mixing processes is studied. The dataset scattering can be explained by mixing processes between a contaminated end-member (trench soils water sample) and rainwater end-members. However, as ^{90}Sr contamination in groundwater just downgradient of the trench is close to the trench soil water ^{90}Sr contamination, [^{36}Cl] are lower in groundwater, suggesting some ^{36}Cl retention processes relatively to ^{90}Sr. Two different processes seem to occur in the aeolian and alluvial layers. In the aeolian layer, the contamination of the aeolian layer seems to result from the dilution of a contaminated end-member (contaminated shallow groundwater downgradient of trench T22 or soil water) by rainwater. In the shallow alluvial layer, ^{36}Cl contamination is constant while ^{90}Sr content decreases, most likely linked to retention and decay processes.

Based on this hypothesis, the migration of ^{36}Cl from trench T22 is simulated along the CD profile using the hydrodynamic parameters determined in previous studies (Bugai *et al.*, 2012b; Van Meir *et al.*, 2012 and Mazet, 2008) and using a source

term close to the soil water sampled in May 2011. An "optimal" simulation has been proposed with hydraulic parameters chosen the most possible in agreement with their natural range of variations, a constant adjusted source term, at steady state, in order to obtain results as close as possible of expected velocities and measured [^{36}Cl]. However, large discrepancies on [Cl^-] still remain. Improving the simulation results may reside reconsidering the two initial main hypotheses, which are: the consideration of a constant source term released by the trench and the flow in steady state conditions. Moreover, processes governing upgradient contamination need to be investigated.

Additional studies are necessary to determine the maximal extent of the contaminant plume horizontally and at depth. Particularly, the source term has to be better characterized through the biogeochemical processes involved in the present release of ^{36}Cl in groundwater in order to constrain this release. The influence of the water table variations, and the subsequent change in groundwater flow, on ^{36}Cl migration could also be potentially explained the ^{36}Cl migration. Once these issues investigated, a new simulation of ^{36}Cl should be carried out at a larger scale to determine the maximal extent of the contaminant plume.

IV. GEOCHEMICAL PROCESSES IN THE CHERNOBYL PILOT SITE GROUNDWATER

IV.1 MAIN GEOCHEMICAL REACTIONS

IV.1.1 INTRODUCTION

The previous section focused on the determination of the maximal extent of the contaminant plume from trench T22 into groundwater. Only non reactive processes were considered and they were investigated based on the low-reactive chlorine and chlorine-36 studies.

However, chemical reactions occurring in groundwater affect migration of elements. In groundwater, chemical concentrations depend on external and internal factors (Appelo and Postma, 2005). External factors are the composition of infiltrated meteoric water, evapotranspiration processes and vegetation uptakes of nutrient (Appelo and Postma, 2005). Internal factors are linked to reactive processes such as physical-chemical parameters in groundwater (conditioning acid-base and redox reactions) and water-rock interactions (dissolution/weathering and precipitation of mineral phases, ion exchanges) (Appelo and Postma, 2005; Michard, 1989). Furthermore, mixing of groundwater with other water (groundwater, meteoric water, seawater) has to be considered and also anthropogenic activities that are well known to impact groundwater chemistry (Appelo and Postma, 2005).

At the Chernobyl Pilot Site, studies were carried out to understand strontium-90 migration from trench T22 into groundwater (Dewière *et al.*, 2004; Szenknect, 2003; Mazet, 2008; Van Meir *et al.*, 2009; Bugai *et al.*, 2012a; Bugai *et al.*, 2012b; Martin-Garin *et al.*, 2012). Strontium-90 velocity was shown to be 9% of groundwater velocity and sorption processes were assumed to explain this retardation (Dewière *et al.*, 2004). These sorption processes can be simulated using a distributioncoefficient K_d (Szenknect, 2003). These K_d values in Chernobyl Pilot Site free aquifer were estimated by *in situ* tests and laboratory measurements. However, obtained values showed discrepancies with values used for simulation of strontium migration (Dewière *et al.*, 2004; Szenknect, 2003; Van Meir *et al.*, 2009; Bugai *et al.*, 2012b). In the aeolian layer (at the top of the aquifer), several

parameters were shown to influence these sorption processes, such as [Ca^{2+}] and stable [Sr^{2+}] concentrations in water, physical-chemical conditions (Szenknect, 2003). Cation exchange processes were assumed and corroborated by simulations (Szenknect, 2003; Mazet, 2008).

Nevertheless, gaps in understanding still persist for strontium-90 and other radionuclide migration. For instance, sorption processes were not investigated in the underlying alluvial layer, where a higher cation exchange capacity was shown (Matoshko *et al.*, 2004). Geochemical processes governing [Ca^{2+}] concentrations need to be investigated because of the influence of these concentrations on sorption processes (Szenknect, 2003). Moreover, the changes of physical-chemical conditions in Chernobyl Pilot Site groundwater and their impact on element speciation need to be investigated because element speciation may either promote or hinder migration in groundwater.

Consequently, the identification of the main geochemical processes occurring in groundwater is required to understand migrations from trench T22. This section aims at defining a conceptual model of these main geochemical processes, based on the interpretation of major element concentrations in groundwater: [Cl^-], [HCO_3^-], [SO_4^{2-}], [NO_3^-], [Na^+], [Ca^{2+}], [K^+] [Mg^2+] and [Si]. Some trace elements behaviors, such as Fe^{2+} and Mn^{2+}, are also investigated because their concentrations are dependent of physical-chemical conditions and their behavior may influence other major elements.

The discussion is organized in three parts. First, external factors are investigated based on:

- the comparison of groundwater composition with meteoric water composition and theoretical evapotranspiration processes (Bugai *et al.*, 2012a),
- the study of $\delta^{18}O$ and δ^2H (meteoric recharge characterization and water mass and transport processes)
- a review of hypotheses on reactions occurring in trench T22.

Then, internal aquifer factors are studied through the physical-chemical changes and geochemical processes governing these parameters are suggested to explain these changes. The impacts of potential water-rock interactions, cation-exchanges and mixing processes on groundwater geochemistry are then estimated and discussed.

IV.1.2 MATERIAL ET METHODS

IV.1.2.1 Sampling

During two field campaigns at the Chernobyl Pilot Site, one in October 2008 and one in October 2009, about 80 groundwater samples were collected along the AB and CD profiles (Annex 1 and 2).

After purging the piezometer and the pumping system by extracting between 3 and 5 L of groundwater, pH[4], Eh, temperature, dissolved O_2 and conductivity parameters were measured with a flow cell. The used Eh electrode is a Sentix ORP (WTW inc., in platinum), so values have to be corrected by between +217 and +214 mV (for temperatures between 10 and 15°C, according the user's manual). To simplify, a uniform correction of +216 was done.

Then, for sampling, 2 L of groundwater were extracted, and about 300 mL were used to rinse the filtration system. Then, samples were filtered at 0.45 µm and conditioned in two 125 mL polyethylene bottles, one for cation analyses and the other for anion analyses. Bottles for cation analyses were acidified to decrease the pH below 2.5 in order to hinder adsorption and precipitation of cations (Appelo and Postma, 2005). For analyses of the water molecule isotopes, samples were collected and conditioned in a fumed glass bottle of 30 mL, taking care that no bubbles were present in order to limit sample equilibration with atmosphere.

In the Chernobyl Pilot Site groundwater, [HCO_3^-] concentrations correspond to carbonate alkalinity because pH is always below 8. They were dosed immediately by titration with H_2SO_4 0.16 N (alkalimetric kit). Zone of changing pH was determined by colorimetric method using bromocresol green as colored indicator[5].

Other analyses were done few weeks to several months later. If the acidification of the cation bottles avoids most of the reactions, some redox changes may have occurred in anion bottles and impacted species sensitive to such changes, such as NO_3^-. Consequently, results of analyses are going to be discussed in Pourbaix diagrams, showing measured pH and redox potential pe with the stability field of the most concerned species.

---

[4] Potential hydrogen p*H* is defined by: $pH = -\log(H^+)$

Where (H^+) is H^+ activity, equals to the [H^+] concentration in subsurface conditions.

[5] For the analysis of 100 mL of sample, the detection limit of this method is 0.004 mmol.L^{-1} (addition of 1 digit of acid).

IV.1.2.2 Analyses

For major elements, concentrations of Cl^-, HCO_3^-, SO_4^{2-}, NO_3^-, Na^+, Ca^{2+}, K^+, Mg^{2+} were measured by ion chromatography, with an Ion Chromatograph IC 861 (Metrohm Inc.; Bassot *et al.*, 2010[6]) at the Analysis and Experimental facilities Laboratory (IRSN/LAME). Three measurements were performed to evaluate uncertainties. Concentrations of Si were also measured, with a spectrophotometer (Genesys 5, Spectronic Inc.; Bassot *et al.*, 2010).

For trace elements, analyzes were done with a Multi Collector Induced Coupled Plasma Mass Spectrometer X7 CCT (Thermoelectron Inc.; Bassot *et al.*, 2010[7]) at the Analysis and Experimental facilities Laboratory (IRSN/LAME).

$\delta^{18}O$ and $\delta^{2}H$ were measured by laser mass spectrometry at the "Interaction et Dynamique des Environnements de Surface" laboratory (UMR 8148, CNRS/Paris-Sud 11 University). Only samples with ^{90}Sr volumetric activities below 100 $Bq.L^{-1}$ were analyzed[8].

IV.1.3 RESULTS

IV.1.3.1 Results description

Results for physical-chemical parameters, major and trace element concentrations and water isotopes analysis are presented in Annex 9 in tabular format. The main results derived from the data are given here.

Field parameters

In both sampling campaigns, the depth-to-water was around 4 m, which was quite low in comparison with the long term evolution seen on site (Bugai *et al.*, 2012b; Van Meir *et al.*, 2007). In October 2008, mean water table was 111.3 m.a.s.l., while in October 2009, it was 110.9 m.a.s.l.

Groundwater conductivity ranges from 16 to 131 $\mu S.cm^{-1}$ and most samples show conductivity below 50 $\mu S.cm^{-1}$. Conductivity is higher for some groundwater samples collected downgradient from trench T22, reaching 100 $\mu S.cm^{-1}$ (4-02-1 piezometer - October 2008 – Annex 2) or in deep groundwater, with conductivities

[6] Detection limit: close to 0.001 $mmol.L^{-1}$

[7] Detection limit: 5 $ng.L^{-1}$

[8] These volumetric activities were analyzed by liquid scintillation on TRI-CARB 3170 TR/SL (Packard Inc., Bassot *et al.*, 2010)

increasing to 131 µS.cm^{-1} (1-022 piezometer –October 2008 - Annex 2), however this piezometer was not sampled because it was empty after the parameters measurements).

Chernobyl groundwater pH values range between 4.3 and 6.9, which is relatively acid (Figure IV-1 and Figure IV-2). The global trend seems to show an increase with depth. Moreover, in shallow groundwater downgradient of trench T22, pH reaches 6.0 for several piezometers (2-02-1 and 6-01-2 piezometers –October 2008 and October 2009 respectively - Annex 2).

Measured redox potential Eh values are reported in pe[9]. pe values are ranging between 1.8 and 9.7, increasing particularly between upgradient and downgradient groundwater (Figure IV-3 and Figure IV-4). Furthermore, a slight decreasing trend is observable with the depth.

[9] at 25°C (Appelo and Postma, 2005)
$Eh = 0.059 \times pe$

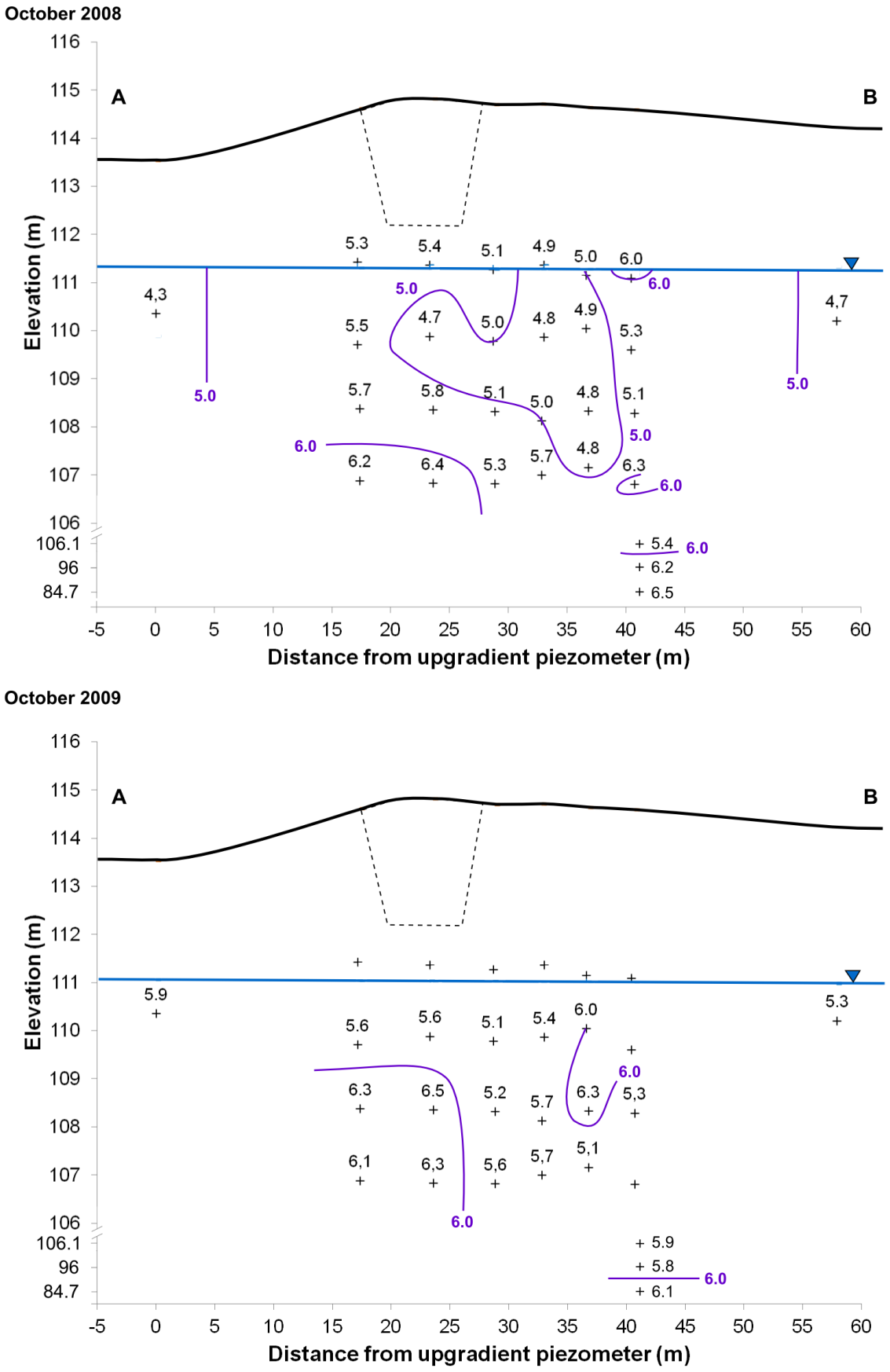

Figure IV-1: pH measured in AB-profile groundwater in October 2008 and October 2009

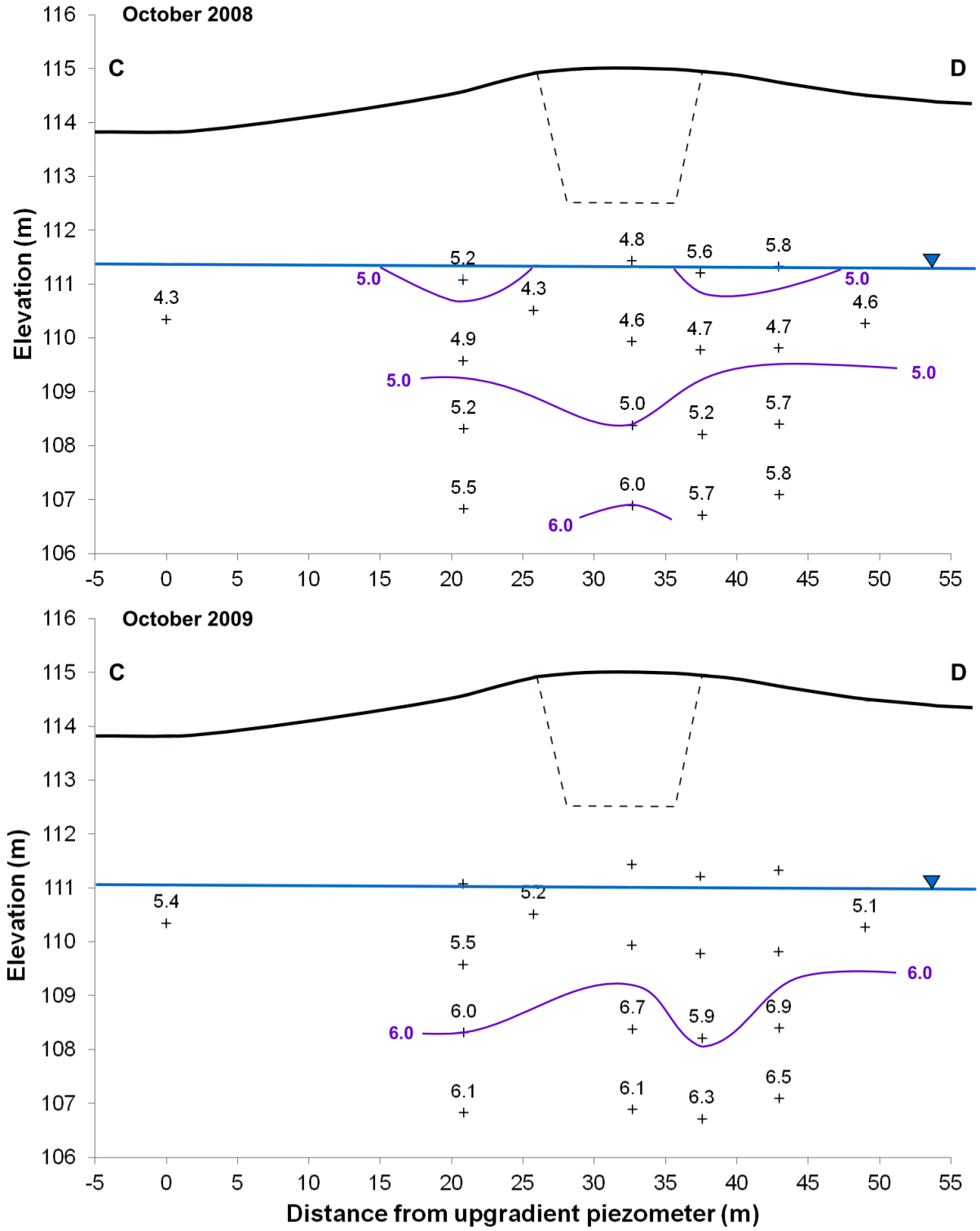

Figure IV-2: pH measured in CD-profile groundwater in October 2008 and October 2009

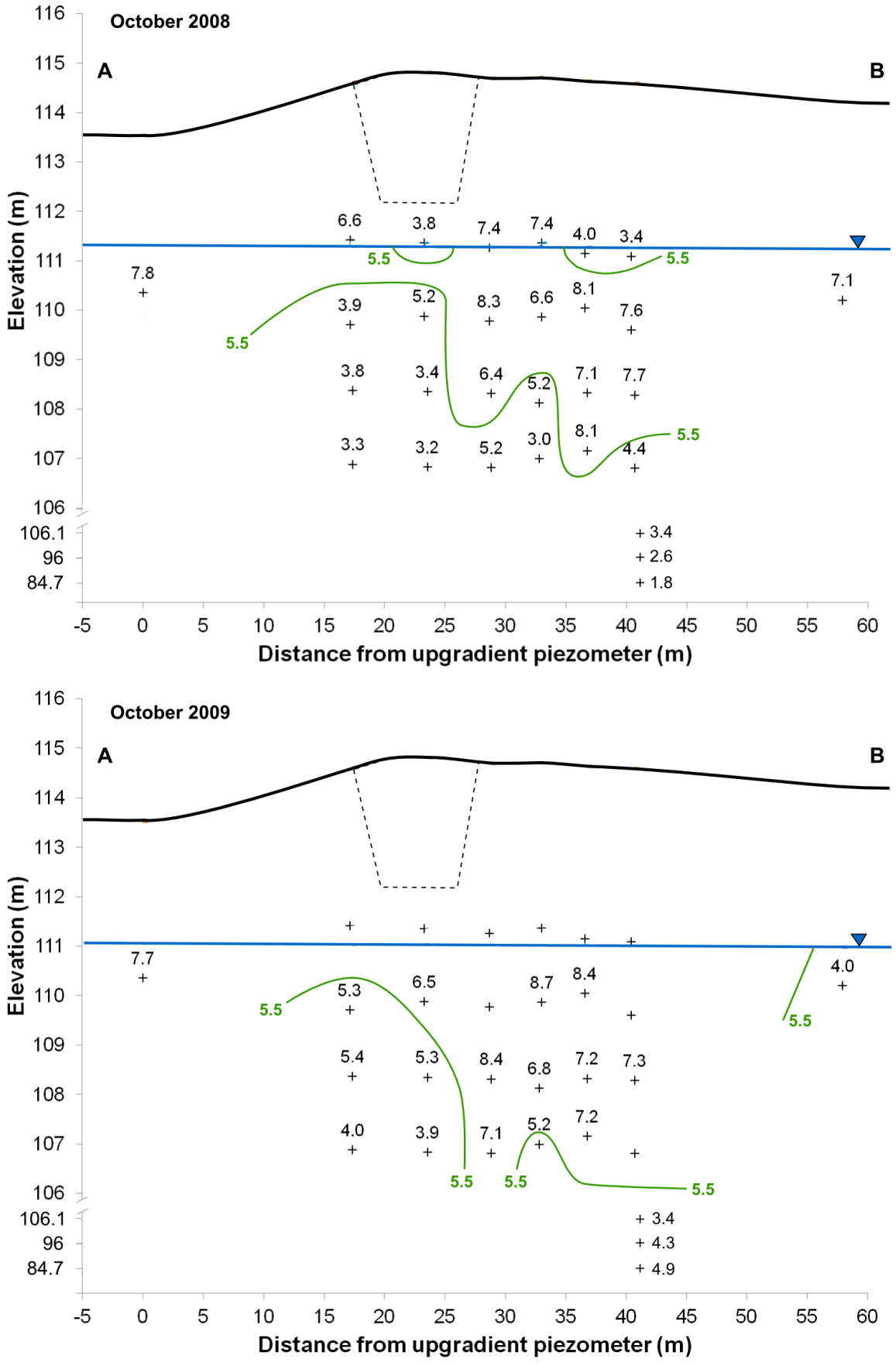

Figure IV-3: pe measured in AB-profile groundwater in October 2008 and October 2009

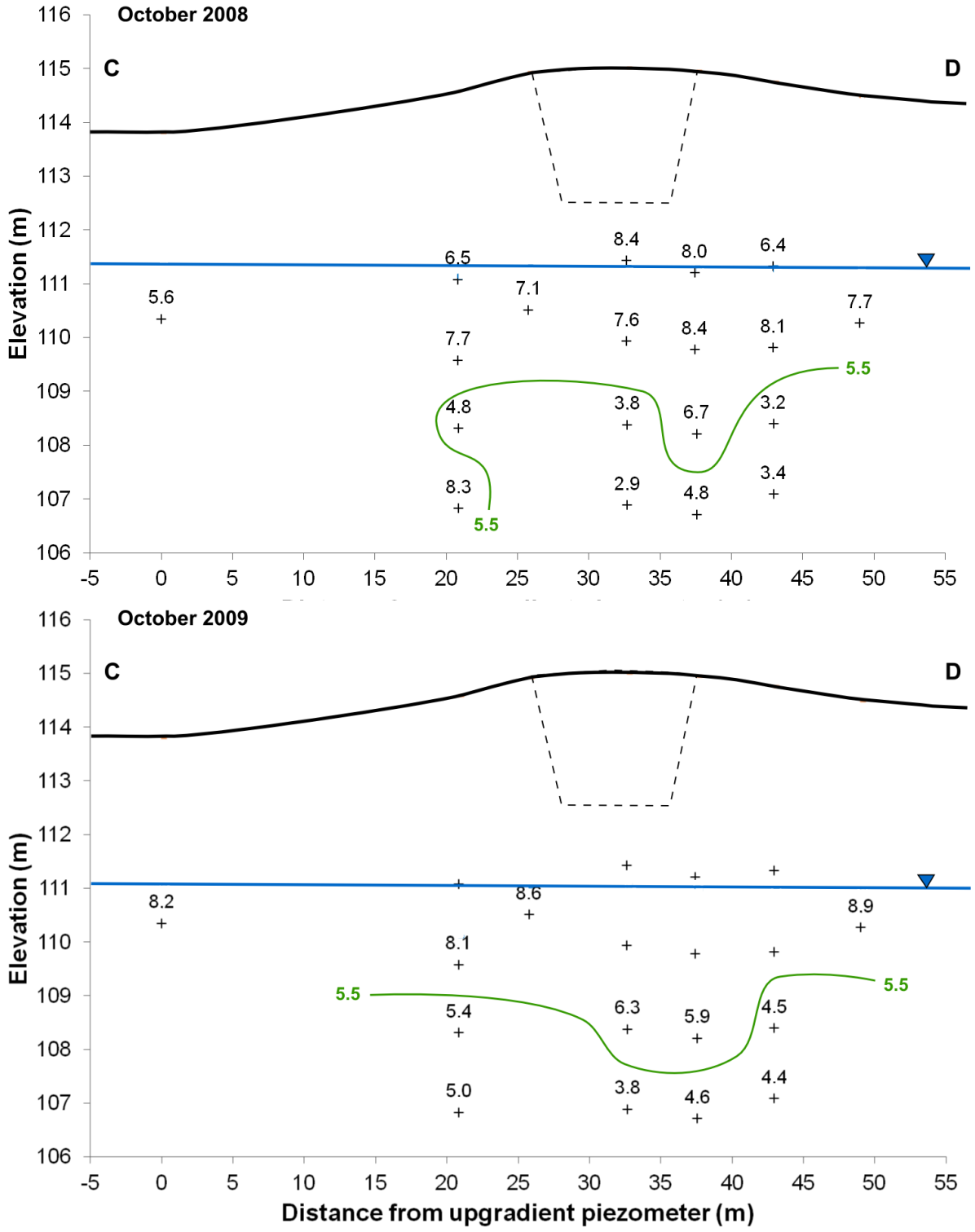

Figure IV-4: pe measured in CD-profile groundwater in October 2008 and October 2009

Dissolved O_2 concentrations in Chernobyl Pilot Site groundwater ranges between 0.014 and 0.315 mmol.L^{-1}. Most of [dissolved O_2] in samples ranges between 0.01 and 0.06 mmol.L^{-1}. The highest values are observed in samples just below trench T22 or downgradient, particularly in October 2008 data where [dissolved O_2] reaches 0.315 mmol.L^{-1} (6-02-1 and 2-02-1 piezometers - Annex 2).

Element concentrations

In order to present major element concentrations along both cross-sections (AB and CD), Stiff diagrams[10] with Na^++K^+, Ca^{2+}, Mg^{2+}, Cl^-, HCO_3^- and SO_4^{2-} concentrations were drawn for each sample using Diagrammes' software (developed at the "Laboratoire d'hydrologie d'Avignon"). Each sample diagram is then reported along AB and CD profiles (Figure IV-5 and Figure IV-6).

Sodium concentrations ([Na^+]) show values ranging from 0.015 ± 0.001 to 0.184 ± 0.014 mmol.L^{-1} (Annex 9). The highest [Na^+] are measured in deep piezometers however an increase up to 0.059 ± 0.001 mmol.L^{-1} is observable downgradient of trench T22 (10-02-1 piezometer –October 2008- Annex 2 and Figure IV-6). Groundwater sampled on AB profile in October 2008 shows slightly higher [Na^+] concentrations than those of the CD profile groundwater (Figure IV-5 and Figure IV-6).

Potassium concentrations ([K^+]) range from 0.016 ± 0.004 to 0.085 ± 0.008 mmol.L^{-1} (Annex 9). While most samples show [K^+] below 0.04 mmol.L^{-1} groundwater sampled downgradient of trench T22 shows concentrations reaching 0.085 ± 0.008 mmol.L^{-1} (4-02-1 piezometer– October 2008 - Annex 2 and Figure IV-6).

Calcium concentrations ([Ca^{2+}]) range from 0.027 ± 0.002 to 0.417 ± 0.005 mmol.L^{-1} (Annex 9). Most samples show [Ca^{2+}] below 0.15 mmol.L^{-1}. The samples with the highest values are located either downgradient of trench T22, with [Ca^{2+}] reaching 0.229 ± 0.003 mmol.L^{-1} (1-02-1 piezometer October 2009- Annex 2 and Figure IV-5) or deeper where concentrations reach 0.417 ± 0.005 mmol.L^{-1} (1-98-3 piezometer - AB profile – October 2009 – Annex 2 and Figure IV-5).

Magnesium concentrations ([Mg^{2+}]) range between 0.004 ± 0.000 and 0.114 ± 0.001 mmol.L^{-1} (Annex 9). An increase of [Mg^{2+}] with depth is shown and reaches a

[10] Stiff diagrams are used to show selected elements: concentrations are plotted on opposite axes, cations represented on the left and anions on the right side, in meq.L^{-1}.

maximum of 0.114 ± 0.001 mmol.L^{-1} in the deepest piezometer 1-98-3 (October 2009 - Annex 2 and Figure IV-5). A slight increase in concentrations is also observable downgradient of trench T22 in October 2008 (Figure IV-5).

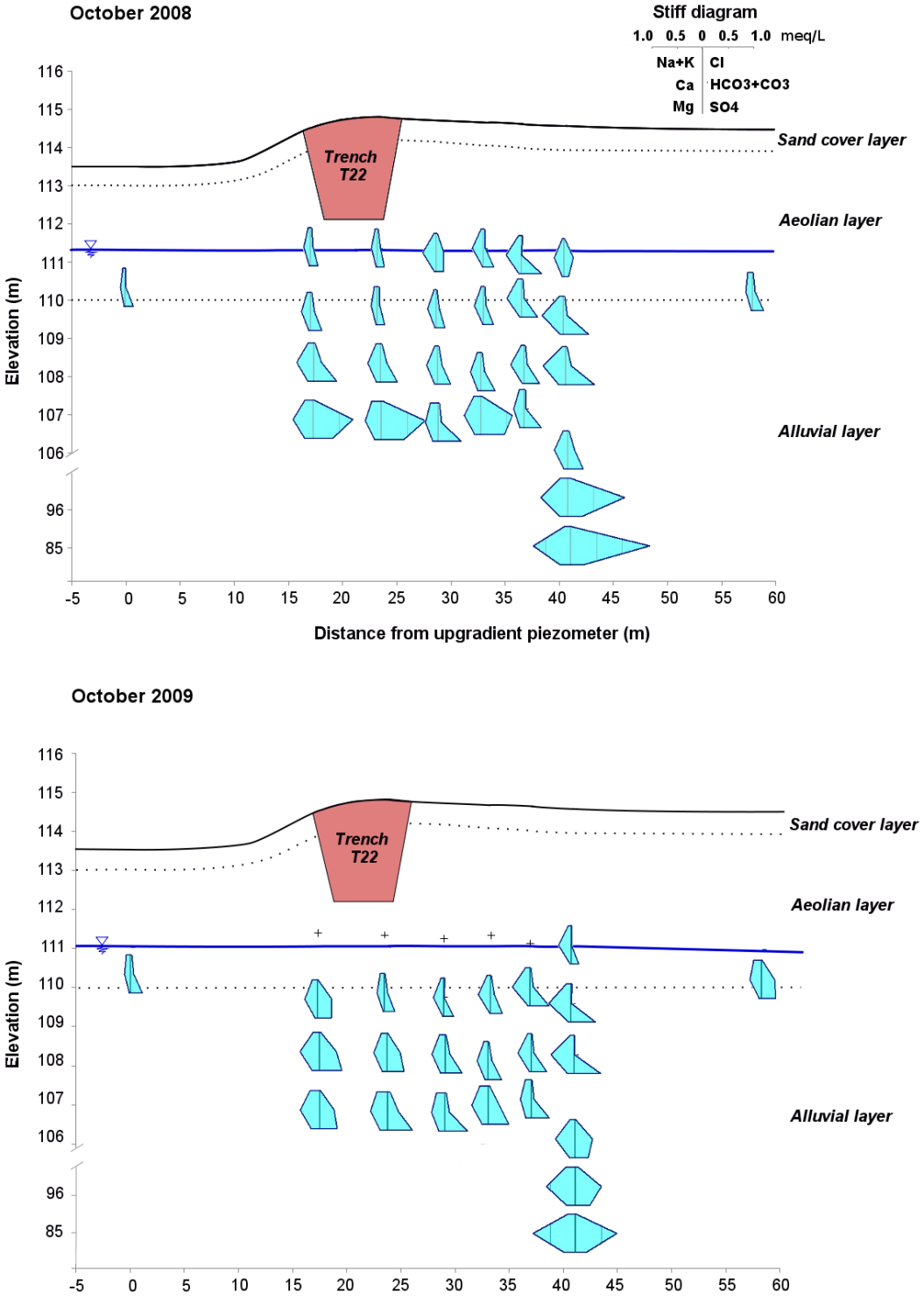

Figure IV-5: Stiff diagrams for the AB-profile groundwater samples in October 2008 and October 2009 (Stiff diagrams made with Diagrammes)

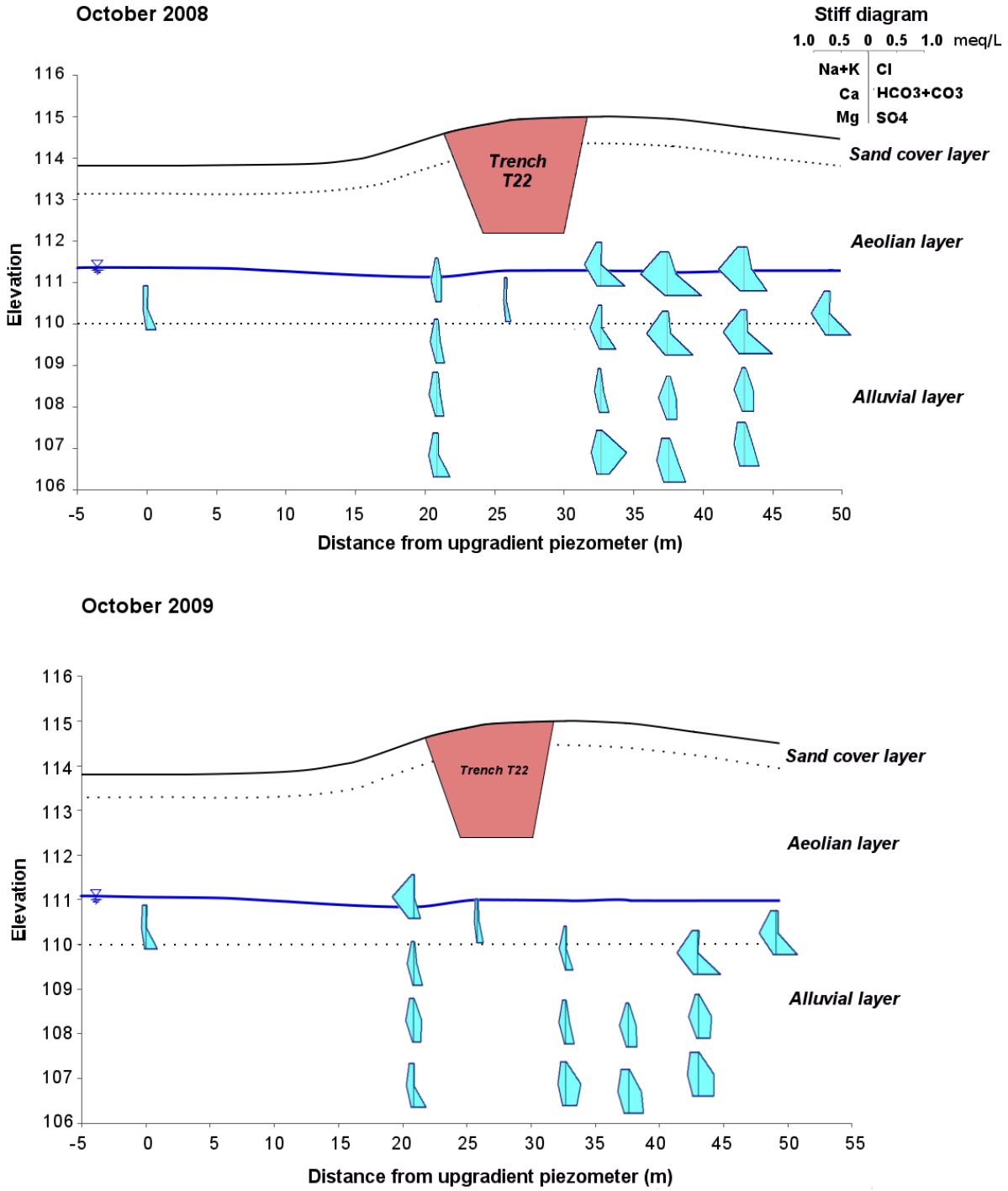

Figure IV-6: Stiff diagrams for the CD-profile groundwater samples in October 2008 and October 2009 (Stiff diagrams made with Diagrammes)

In Chernobyl groundwater, chlorine concentrations ($[Cl^-]$) range from 0.008 ± 0.001 $mmol.L^{-1}$ to 0.0606 ± 0.0006 $mmol.L^{-1}$ (Annex 9). Most samples show concentrations between 0.015 and 0.025 $mmol.L^{-1}$. Higher $[Cl^-]$ are found in groundwater sampled downgradient of trench T22, with maximum values of 0.0302 ± 0.0004 $mmol.L^{-1}$ on

the AB profile (19-00-1 piezometer – October 2008 – Annex 2 and Figure IV-5) and 0.0606 ± 0.0006 mmol.L^{-1} on the CD profile (10-02-1 piezometer – October 2008 - Annex 2 and Figure IV-6). Deep groundwater of the AB profile shows the highest concentrations, up to 0.04 mmol.L^{-1} (7-02-2 and 1-98-2 in October 2008 and 7-02-2, 7-01-2 and 1-98-2 in October 2009 - Annex 2 and Figure IV-5).

Bicarbonate concentrations ([HCO_3^-]) range from below 0.004 mmol.L^{-1} to 1.555 mmol.L^{-1} (Annex 9). Most of the samples show [HCO_3^-] between 0 and 0.1 mmol.L^{-1}, except for deep piezometers, where [HCO_3^-] increase to 1.555 mmol.L^{-1} in the deepest piezometer 1-98-3 (October 2008 - Annex 2 and Figure IV-5). Samples collected downgradient of trench T22 in October 2008 also show high values, up to 0.183 mmol.L^{-1} (2-02-1 piezometer - Annex 2 and Figure IV-5).

Sulfate concentrations([SO_4^{2-}]) range between 0.035 ± 0.004 and 0.269 ± 0.004 mmol.L^{-1} (Annex 9). Most of the [SO_4^{2-}] are below 0.15 mmol.L^{-1}. The most concentrated groundwater value is found downgradient of trench T22, with a [SO_4^{2-}] of 0.246 ± 0.002 mmol.L^{-1} (2-02-2 piezometer –October 2008 - Annex 2 and Figure IV-5). Groundwater sampled in deep piezometers located on the AB profile also shows high [SO_4^{2-}], up to 0.2 mmol.L^{-1} (7-02-2, 7-01-2 and 18-00-2 piezometers - Annex 2 and Figure IV-5). The possible redox condition changes between sampling and analysis[11] and the smell of some samples just before pumping may indicate H_2S presence, and Pourbaix diagram for sulfur shows that SO_4^{2-} is the predominant species in solution (Figure IV-7). However, during next campaigns, reduced S^{2-} concentrations were measured just after sampling and showed concentrations up to 0.006 mmol.L^{-1} (0.2 mg.L^{-1}).

[11] due to the lap of time between the sampling and the analysis carried out in France (between a few weeks and several months)

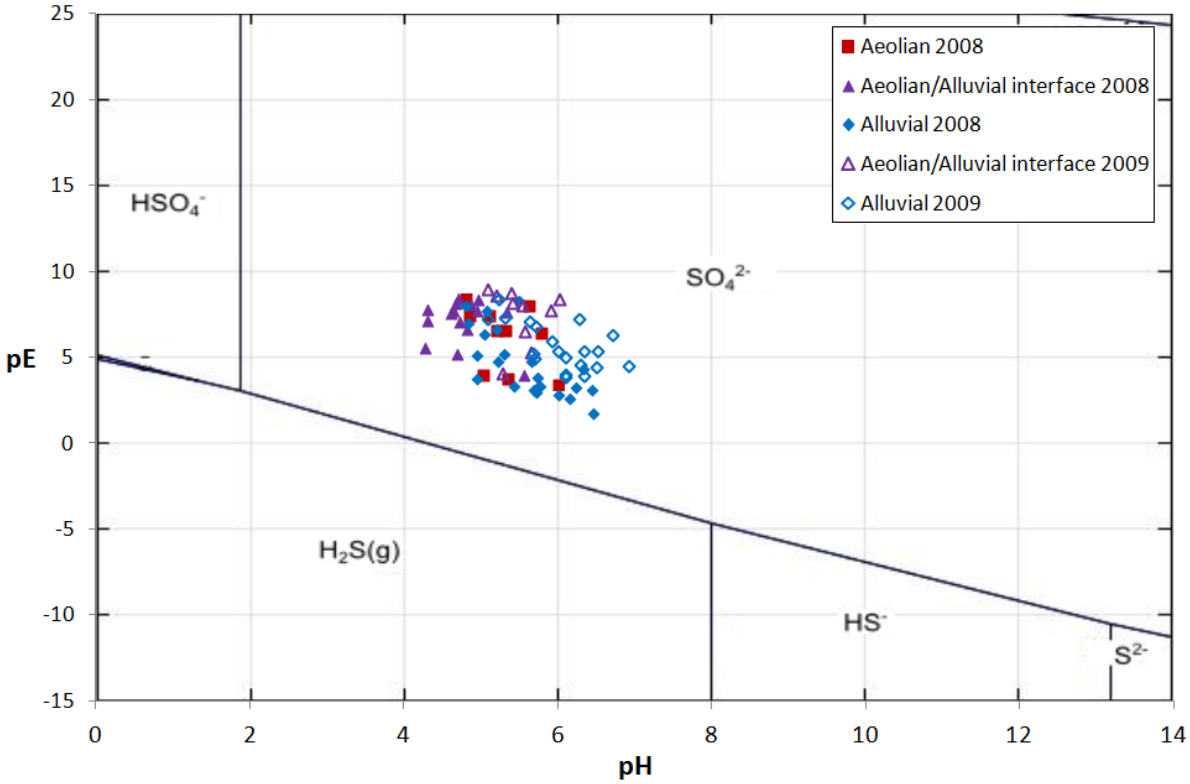

Figure IV-7: Pourbaix sulfate diagram

Only a few samples show nitrate concentrations ($[NO_3^-]$) above the detection limit (0.0007 $mmol.L^{-1}$; Bassot *et al.*, 2010) (Annex 9). These samples are located downgradient of trench T22, in the aeolian layer, with concentrations reaching 0.291 ± 0.002 $mmol.L^{-1}$ (4-02-1 piezometer – October 2008 – Annex 2). A Pourbaix diagram for dissolved nitrogen species shows that under groundwater conditions, ammonium (NH_4^+) is the most stable species. However, NO_3^- is the only analyzed nitrogen species and $[NH_4^+]$ are not available (Figure IV-8). As $[NO_3^-]$ are measured between few weeks and several months after sampling (instead of the 24 h advised by Appelo and Postma, 2005), it can be assumed that redox and pH conditions may have changed during the storage period. Consequently, nitrification processes of NH_4^+ in NO_3^- may have occurred, as well as denitrification processes of NO_3^- in N_2. Consequently, measured $[NO_3^-]$ represent concentrations of remaining NO_3^- in the bottle plus nitrified NH_4^+. Hereafter, those $[NO_3^-]$ will be labeled as "N-species" and represents minimum content of dissolved nitrogen species in groundwater samples. Even if it hinders any quantification of processes, main trends can be assumed.

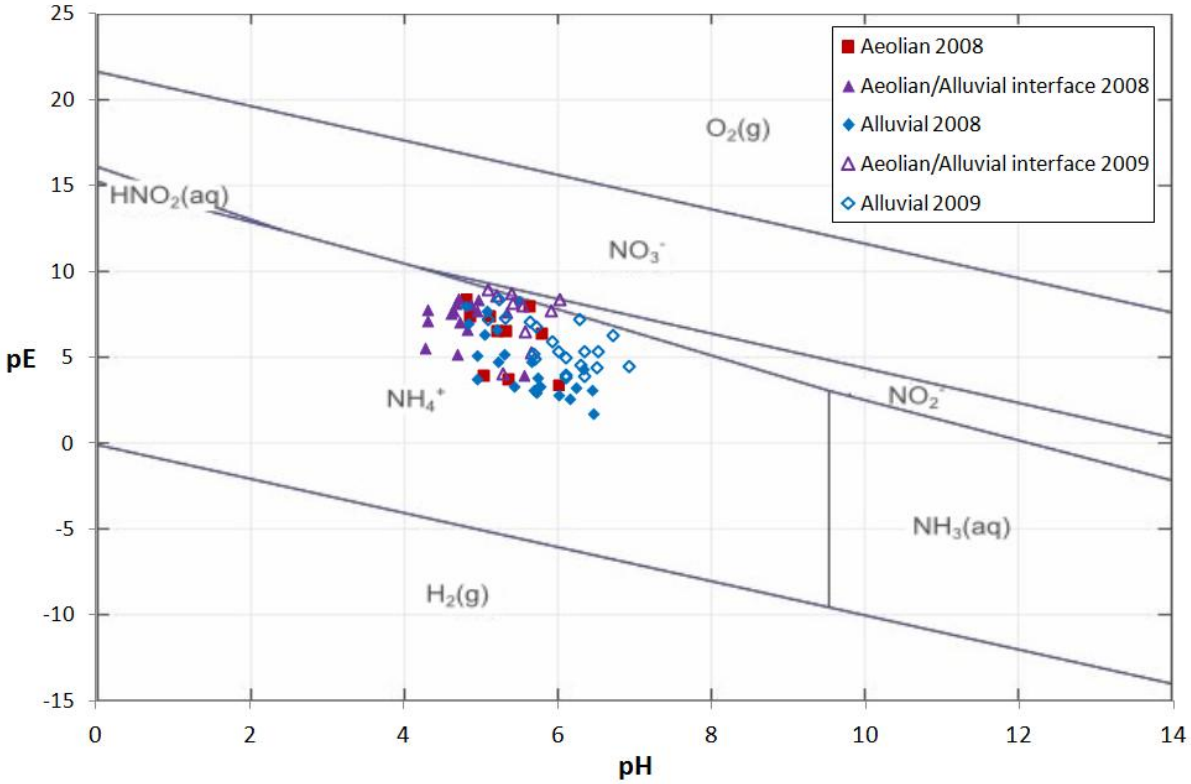

Figure IV-8: Pourbaix nitrogen diagram

From the above results of major elements concentrations previously presented, the Chernobyl Pilot Site groundwater can be classified as sulfated calcic for the shallow groundwater to bicarbonated calcic for alluvial groundwater (Piper diagrams[12], Figure IV-9). This change in classification is linked to the increase of [HCO_3^-] in alluvial groundwater.

[12] Piper diagram represent proportions of each major element from concentrations in meq.L^{-1}: cations and anions proportions are reported in two separate triangles and the obtained points are the reported in a central diamond.

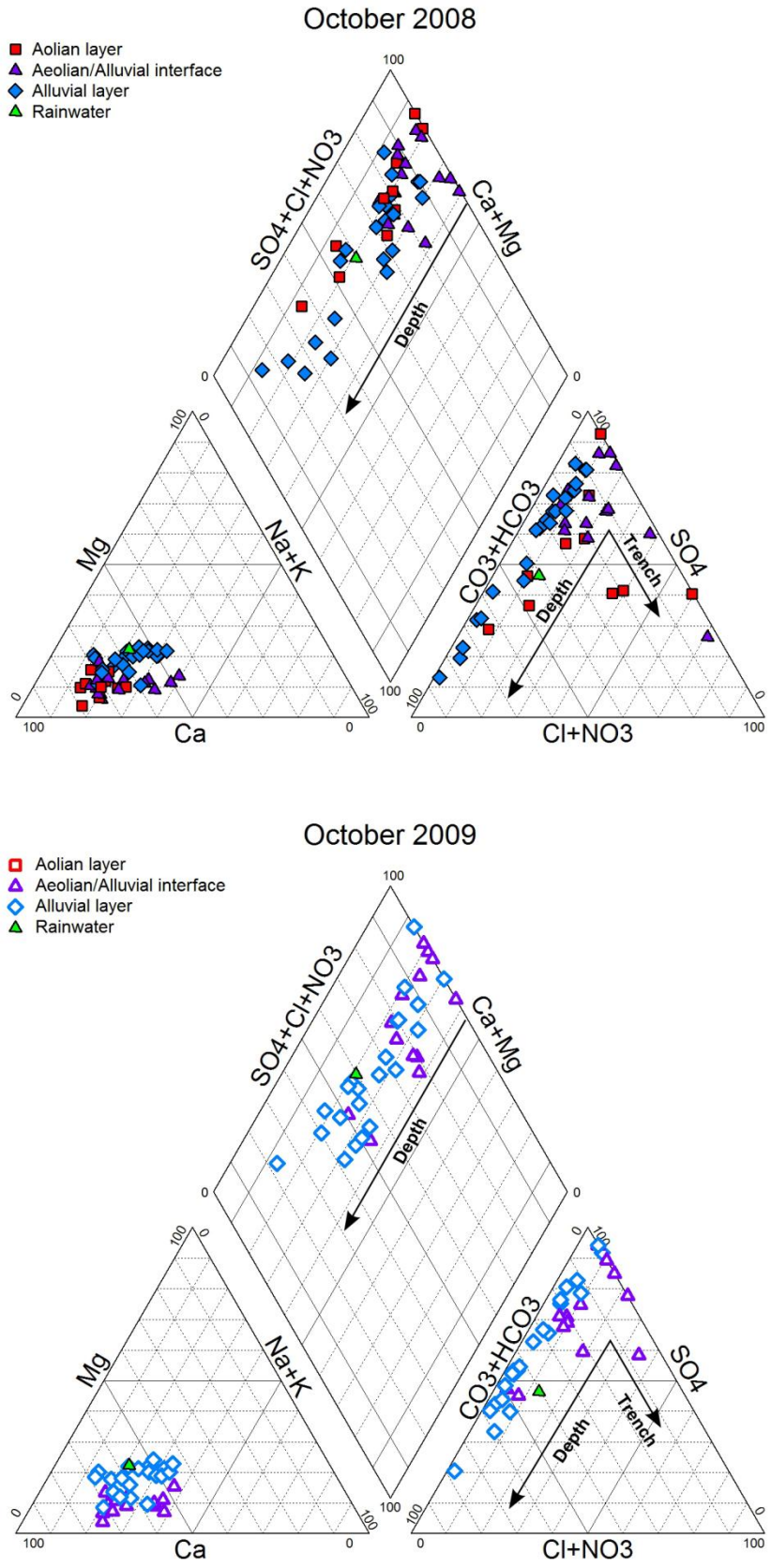

Figure IV-9: Piper diagrams for October 2008 and October 2009 samples

Si concentrations show values ranging from 0.093 ± 0.003 to 0.297 ± 0.001 mmol.L^{-1} (Annex 9). Concentrations increase slowly with depth for both profiles and for both sampling campaigns from 0.1 mmol.L^{-1} in the aeolian layer to more than 0.2 mmol.L^{-1} in the deepest piezometers in the alluvial layer. Aeolian groundwater downgradient from trench T22 seems to be more concentrated, with a maximum of 0.247 ± 0.000 mmol.L^{-1} in the 12-02-1 piezometer sampled in October 2008 (CD profile).

In order to better understand major element concentration interpretations, some trace element concentrations are also studied. Those trace elements are assumed to be more sensitive to processes that can affect major element concentrations, such as redox processes:

- Iron concentrations ([^{56}Fe]) range from 3.45×10^{-8} ± 0.2×10^{-8} to 1.45×10^{-4} ± 0.07×10^{-4} mol.L^{-1} (Annex 9). Most [$^{56}Fe^{2+}$] in groundwater range between 10^{-6} – 10^{-5} mol.L^{-1}. Groundwater sampled directly downgradient of trench T22 shows low concentrations, between 10^{-7} and 10^{-6} mol.L^{-1}. Deep piezometers show high concentrations in the order of 10^{-5} mol.L^{-1}. Analyses are carried out back in laboratory on samples acidified in field (some redox processes may have still occurred), consequently these concentrations represent total iron concentrations and will be labeled [Fe] hereafter (Appelo and Postma, 2005).
- Manganese concentrations ([^{55}Mn]) range from 3.29×10^{-8} ± 0.4×10^{-8} to 2.25×10^{-5} ± 0.02×10^{-5} mol.L^{-1} (Annex 9). Most of groundwater samples show [^{55}Mn] between 2.10^{-7} and 2.10^{-6} mol.L^{-1}. A few groundwater samples show different concentrations: downgradient of trench T22 and in the alluvial layer of the profiles, with concentrations up to 2.25×10^{-5} ± 0.02×10^{-5} mol.L^{-1}, and in the deepest piezometer (1-98-3), where concentrations are much lower, between 10^{-8} and 10^{-7} mol.L^{-1} order of magnitude. Analyses are carried out back in laboratory on samples acidified in field, consequently, like for [^{56}Fe] concentration; these concentrations represent the total iron concentration and will be labeled [Mn] hereafter.
- Strontium concentrations ([^{88}Sr]) range from 1.3×10^{-7}±0.1×10^{-7} to 9.0×10^{-7}± 0.3×10^{-7} mol.L^{-1}. Most of the sample show concentrations below 5×10^{-7} mol.L^{-1}, only concentrations in the shallow groundwater downgradient of the trench

show higher concentrations. Some upgradient deep groundwater samples (5-02-1 and 5-02-2 piezometers) show also higher concentrations.

Electrical balances are calculated considering only major element concentrations (Cl^-, HCO_3^-, SO_4^{2-}, NO_3^-, Na^+, Ca^{2+}, K^+ and Mg^{2+}). They often reach -10% or +10% whereas they are assumed to be close to 0. This can be due to the 10% analytic uncertainties, which are most likely due to the low concentrations measured. An additional explanation is that some trace elements could have concentrations high enough regarding the low concentrations of major elements to influence the electrical balance.

Isotopes of water molecule analyses show $\delta^{18}O$ between -11.8 ± 0.2 and -10.5 ± 0.2 ‰ *vs* SMOW and δ^2H between -86.0 and -75.2 ± 2 ‰ *vs* SMOW. An increase of both $\delta^{18}O$ and δ^2H seems to occur with depth (Annex 9).

IV.1.4 POTENTIAL PROCESSES GOVERNING GROUNDWATER GEOCHEMISTRY

Based on $[Na^+]+[K^+]$, $[Ca^{2+}]$, $[Mg^{2+}]$, $[Cl^-]$, $[HCO_3^-]$ and $[SO_4^{2-}]$ representation, Stiff diagrams (Figure IV-5 and Figure IV-6) show that concentrations in groundwater are globally higher in the deeper part of both profiles and downgradient of trench T22. The depth or the vicinity of the trench are shown to have also an impact on [N-species], $[SO_4^{2-}]$, [Fe-total], [Mn-total] and [Si].

In order to define the involved reactive processes, concentrations for each major element are compared with $[Cl^-]$, known to be a low reactive element that shows little variations in the Chernobyl Pilot Site groundwater (Figure IV-10). Cations diagrams are presented in the left column (Na^+, K^+, Ca^{2+} and Mg^{2+}) concentrations and anions diagrams are reported in the right column (N-species, SO_4^{2-} and HCO_3^-).

The same sample legend is used in each diagram. For October 2008 groundwater sample representation, full symbols are used: aeolian layer data are represented with red squares, data of the aeolian/alluvial interface with purple triangles and alluvial data with blue diamonds. For October 2009 groundwater sample representation, the same but void symbols are used: aeolian layer data are represented with a red outline, data of the aeolian/alluvial interface with a purple outline and alluvial data with blue outline. Mean meteoric water value is represented with a green triangle and the green rectangle is its range of concentrations. These meteoric data come from Bugai *et al.* (2012a), obtained by analyses on 30 meteoric samples (rainwater and snow) between 2005 and 2006). An

intermittent line with a slope of 1 passing through the mean meteoric water corresponds to a potential meteoric water evaporation process.

[Cl^-] concentrations in groundwater remain within the meteoric water range. However, it is important to note that the highest concentrations of groundwater sampled in the aeolian layer are found downgradient of trench T22 (10-02-1 and 4-02-1 piezometers - Annex 2).

Most of [K^+] and [N-species] are also in the meteoric water range, excepted for some samples located downgradient of trench T22, on the CD profile (12-02-1, 12-02-2, 4-02-1, 4-02-2, 10-02-1, 10-02-2, 4-00 piezometers - Annex 2). Some AB profile groundwater sampled downgradient of trench T22 show higher [K^+] (6-01-2, 7-00 piezometers - Annex 2). [K^+] are also locally higher in upgradient piezometers (6-99 piezometer - Annex 2) and in some alluvial piezometers (2-01-2, 7-02-2, 5-02-2 piezometers - Annex 2). In summary, K^+ and N-species concentrations are mostly impacted by the presence of trench T22.

The comparison of [Na^+] with [Cl^-] shows two different trends, reliable to the layer where the sample is collected. Groundwater sampled in the aeolian layer and at the aeolian/alluvial interface mostly falls within the meteoric water range. Groundwater sampled in the alluvial layer show a linear increasing trend, from the cloud of groundwater sampled in the aeolian layer to the deeper piezometers (5-02-2 and 1-98-2 piezometers), up to 8 times more concentrated in Na^+ than meteoric water. [Mg^{2+}] and [HCO_3^-] also show two different trends according to the layer where the sample is collected. Comparing [Mg^{2+}] with [Cl^-], groundwater sampled in the aeolian layer also mostly falls within the meteoric water range while [Mg^{2+}] in groundwater from the alluvial layer increase by up to 7 fold. Groundwater samples are mostly more concentrated in HCO_3^- than meteoric water; below 0.2 mmol.L^{-1} in groundwater sampled in the aeolian layer, [HCO_3^-] increase up to 1.55 mmol.L^{-1}. To summarize, [Na^+], [Mg^{2+}] and [HCO_3^-] seem to be mainly governed by geochemical processes occurring in the alluvial layer.

The trends observed comparing [Cl^-] with [Ca^{2+}] and [SO_4^{2-}] are similar. Most of the dataset fall outside the meteoric water range, showing an almost linear increasing trend with slope close to 10. Stiff diagrams (Figure IV-5 and Figure IV-6) suggest that those concentrations can be impacted by the presence of trench T22 and geochemical processes occurring in the alluvial layer.

To summarize, three groups of elements can be defined: those impacted by the presence of trench T22 (K^+, N-species), those impacted by geochemical processes occurring in the alluvial layer (Mg^{2+}, Na^+, HCO_3^-) and those impacted by both the presence of the trench and natural geochemical processes(Ca^{2+}, SO_4^{2-}).

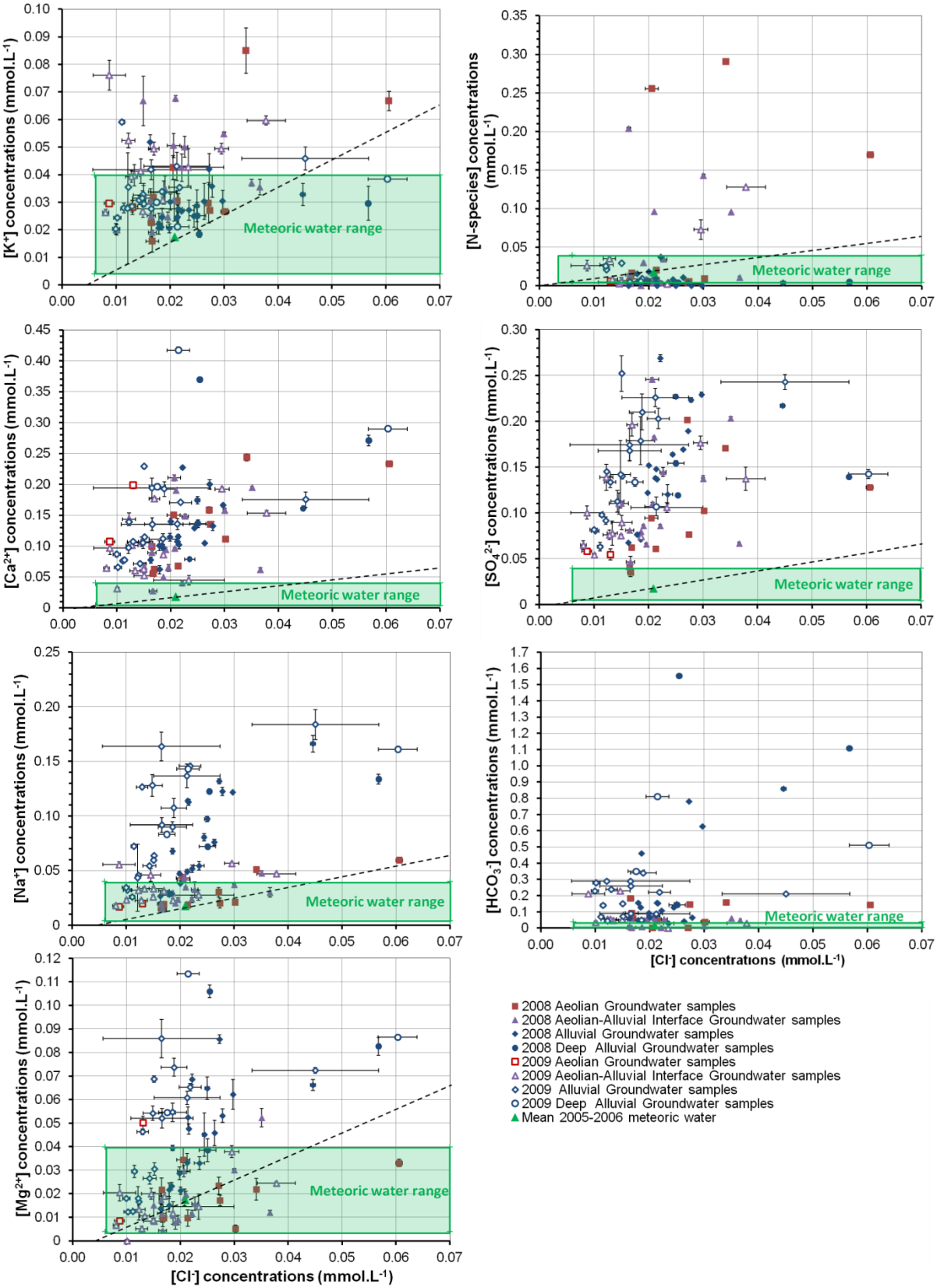

Figure IV-10: Major element concentrations versus [Cl^-]

IV.1.4.1 External factors: meteoric water and evapotranspiration processes

In order to understand geochemical processes occurring in the aquifer, the origin of groundwater has to be identified. As observed in Figure IV-10, shallow groundwater concentrations fall often in the meteoric water range: the main origin of groundwater is assessed to be the infiltration of a meteoric water mainly after snow thaw and during intense rainfall events in summer (Bugai *et al.*, 2012b; Bugai *et al.*, 2012a).

To confirm this origin, δ^2H and $\delta^{18}O$ were analyzed in several groundwater samples. δ^2H *vs* SMOW is compared with $\delta^{18}O$ *vs* SMOW in Figure IV-11. Samples are reported with orange diamonds. The global Meteoric water Line is also reported (dark line) (Craig, 1961). Using the data from the free WISER database (International Atomic Energy Agency, 2003-2008), local meteoric water lines can be drawn (purple and green lines). Average values for winter and summer are also reported.

The sample trend fits well with meteoric water lines, confirming the meteoric origin of the groundwater. No evaporation process seems to occur in this groundwater.

Sample values are closer to the average values for winter meteoric water, suggesting that the recharge is dominated by infiltration of winter meteoric water (rainwater, snowmelt), confirming observations made by Bugai *et al.* (2012a).

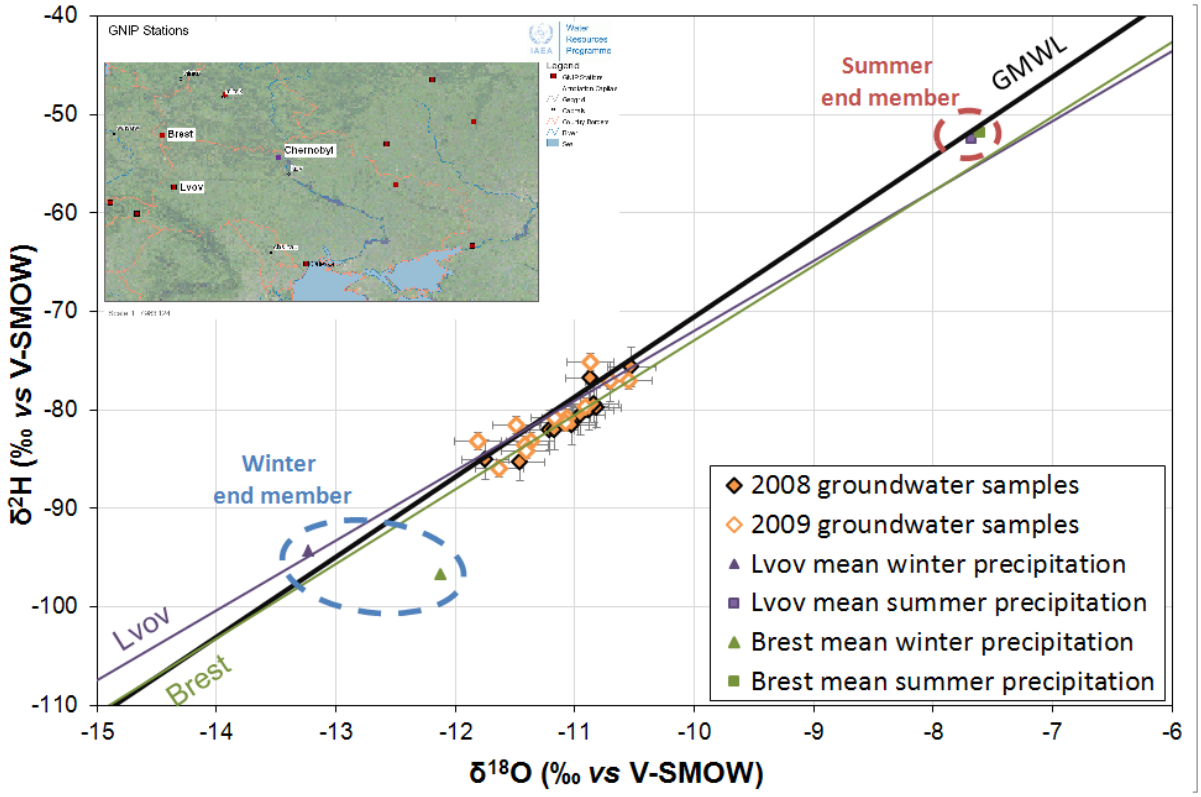

Figure IV-11: $\delta^{18}O$ and $\delta^{2}H$ diagram

Evaporation processes are suggested by Bugai *et al.* (2012a), based on the ratio of net yearly precipitation rate to net yearly infiltration recharge rate. A factor concentration of 2.5 ± 0.5 is expected. This process is could explain some increase of concentrations in groundwater. However, the water isotopes study suggests that the evaporation process is quite limited if inexistent. Finally, Cl^- is an element little impacted by geochemical processes except evapotranspiration processes, NaCl or KCl dissolution or anthropogenic pollutions. At the Chernobyl Pilot Site, in October 2008 and October 2009, [Cl^-] always remain between 0.006 and 0.071 mmol.L^{-1}, the meteoric water range published by Bugai *et al.* (2012a). Average rainwater [Cl^-] is 0.021 mmol.L-1 (Bugai *et al.*, 2012a), which is close to the [Cl^-] shown by most of the samples (0.015 and 0.025 mmol.L^{-1}). Even concentrations in groundwater sampled downgradient of trench T22 do not exceed 0.06 mmol.L^{-1}. Consequently, an evaporation process cannot be involved to explain increase of concentrations, particularly with the increase in the depth.

IV.1.4.2 Migration from the Trench

Potential biogeochemical processes occurring in the trench could explain the increase of concentrations downgradient of trench T22. Indeed, increases in [K^+], [Ca^{2+}], [N-species] and [SO_4^{2-}], decreasing pH and increasing Eh in groundwater downgradient of trench T22 were previously shown (Figure IV-5, Figure IV-6, Figure IV-10)

Processes of buried organic matter mineralization are known to result in acidification of soil solution due to CO_2 production and nitrification processes (Martin-Garin *et al.*, 2012).

The dissolution of produced CO_2 results in H_2CO_3 species formation. The equilibration of the carbonic system results in acidification of the soil solution and increase of [HCO_3^-] and [CO_3^{2-}]:

$$H_2O + CO_2 \leftrightarrow H_2CO_3 \leftrightarrow H^+ + HCO_3^- \leftrightarrow 2H^+ + CO_3^{2-} \qquad \textit{Equation IV-1}$$

Nitrification processes should explain increases of [N-species] concentrations downgradient of the trench T22 (Martin-Garin *et al.*, 2012). However, it was shown that under groundwater conditions, NH_4^+ is the dominant species. Consequently, to understand [N-species] concentrations in the Chernobyl Pilot Site groundwater, the nitrogen biogeochemical cycle should be deeper investigated.

Exchanges of H^+ with other cations in shallow soils should result in the release of those cations (Martin-Garin *et al.*, 2012). This process can explain increase of [K^+] and [Ca^{2+}] downgradient of trench T22. Different concentrations are observed downgradient of the trench comparing both profiles (Figure IV-1; Figure IV-2; Figure IV-3 ; Figure IV-4; Figure IV-5; Figure IV-6) which may be explained by heterogeneities in the buried material in trench T22 (Bugai *et al.*, 2005).

Biogeochemical processes involved in the oxidation of organic matter in trench T22 should be better investigated because no process assumed until now result in oxidizing redox conditions in groundwater as it is shown in Figure IV-3 and Figure IV-4. Since 2011, to assess the influence of organic matter on groundwater geochemistry, Total Organic Carbon analyses are carried out at the Analysis and Experimental facilities Laboratory (IRSN/LAME). The trench could also act as a preferential flow path, locally enhancing recharge, promoting oxidation of groundwater conditions.

IV.1.4.3 Variations of pH, redox changes and related processes

pH and pe vary a lot in space and in time from 4.3 to 6.9 and from 1.8 to 9.7 respectively. It was previously hypothesized that observed pH and pe variations result from migration of elements or chemical reactions linked to the presence of trench T22.

These parameters have an important impact on speciation of elements in aquatic environments and may have an influence on their mobility. For instance, regarding the Fe^{2+} speciation, in reduced environment Fe is in a mobile form whereas the oxidized Fe^{3+} form leads to the formation of iron oxides, mostly insoluble. Similar processes may influence the migration of some radionuclides, such as uranium and plutonium that could be mobilized or immobilized following the pe and pH changes. According to the pe-pH diagram built by Appelo and Postma (2005) to characterize natural water, the Chernobyl Pilot Site groundwater physical-chemical parameters lies in the classical range of groundwater, meaning they are mainly governed by common natural processes (Figure IV-12).

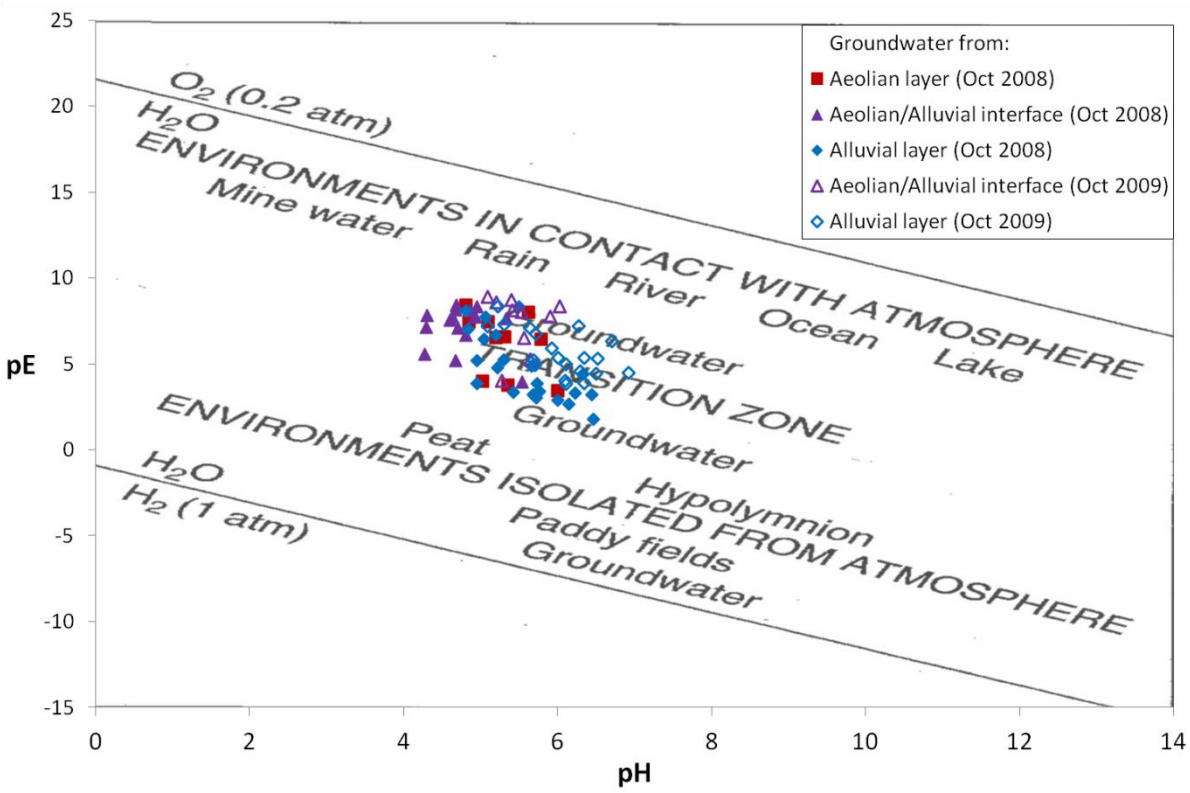

Figure IV-12: Chernobyl Pilot Site samples and Appelo and Postma's pe/pH diagram classifing natural water

This part aims to investigate geochemical processes related to pH and pe in groundwater.

IV.1.4.3.1 pH relation with carbonic system

In groundwater, the common system controlling pH is the carbonic system. In the absence of carbonate mineral, pH value is based on the dissolution of CO_2 in aqueous media (Equation IV-1).

Partial pressure of CO_2 (PCO_2) in the atmosphere is $10^{-3.5}$ atm whereas in groundwater PCO_2 is one or two orders of magnitude higher (Appelo and Postma, 2005), mainly due to biogeochemical processes occurring in soils. Overall, PCO_2 ranges between $10^{-3.0}$ and $1.0^{-1.4}$ atm in soils (Appelo and Postma, 2005). These changes in PCO_2 induce modifications in pH and $[HCO_3^-]$ to respect equilibrium given in Equation IV-1.

In order to investigate the impact of potential change in PCO_2 in the Chernobyl Pilot Site groundwater, pH values are represented versus $[HCO_3^-]$ in Figure IV-13.

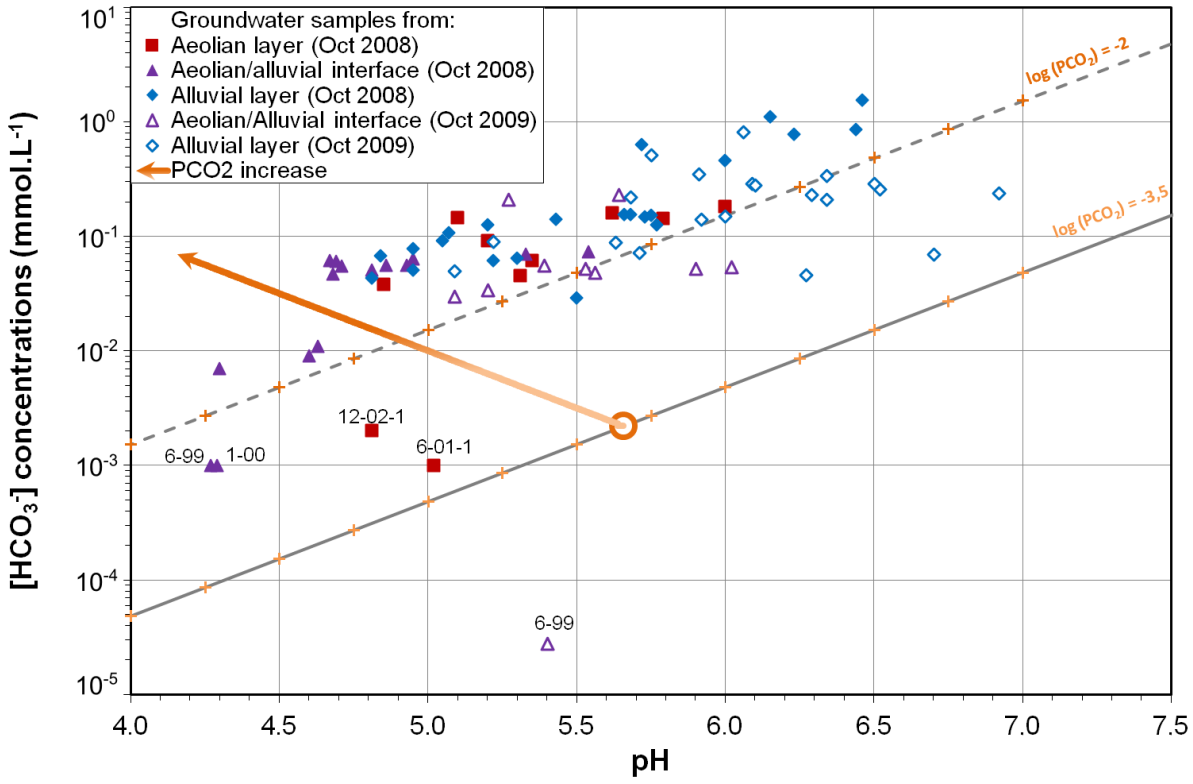

Figure IV-13: pH and $[HCO_3^-]$ concentrations in Chernobyl groundwater

For October 2008 groundwater sample representation, full symbols are used: aeolian layer data are represented with red squares while data of the aeolian/alluvial interface with purple triangles and alluvial data with blue diamonds. For October 2009 groundwater sample representation, the same but void symbols are used: aeolian layer data are represented with a red outline while data of the aeolian/alluvial interface with a purple outline and alluvial data with blue outline. The orange triangle represents a meteoric water end-member with pH and $[HCO_3^-]$ at equilibrium with PCO_2 ($10^{-3.5}$ atm), considering $[H^+]$ equals to $[HCO_3^-]$. The orange arrow shows the impact on pH and $[HCO_3^-]$ of a progressive increase of PCO_2 to 10^{-2} atm starting from rainwater (Bugai *et al.*, 2012a). This line is calculated to respect the equilibrium of the reaction in Equation IV-1:

$$K = \frac{(H^+)(HCO_3^-)}{P_{CO2}} \qquad \textit{Equation IV-2}$$

with K, the equilibrium constant equals to $10^{-7.81}$ at 25 °C (Lawrence Livemore National Laboratory database).

Another two lines are shown: $[HCO_3^-]$ are calculated in equilibrium with different pH values and PCO_2 equals to $10^{-3.5}$ atm and 10^{-2} atm respectively (Equation IV-1[13]). Most of groundwater samples are close to the line calculated for PCO_2 equal to 10^{-2} atm.

Some samples between those two lines and below the PCO_2 increasing arrow are identified on the figure, they correspond to piezometers sampled either downgradient of trench T22, or 6-99 piezometer, far upgradient of trench T22 (Annex 2).

pH and $[HCO_3]$ variations cannot be explained by the increase of PCO_2 with depth: instead of the theoretical decrease of pH and the increase of $[HCO_3^-]$ in meteoric water with the increasing PCO_2, groundwater sampled in the alluvial layer shows increasing pH and $[HCO_3^-]$ relative to shallow groundwater. These increases in pH and $[HCO_3^-]$ with depth may be the result of reactions occurring in the aquifer, as water rock-interactions.

The dissolution of carbonates can explain the increase of $[HCO_3^-]$ with depth. Dispersed calcite ($CaCO_3$) was identified in the fine fraction of the alluvial layer and the underlying Kiev suite is composed by marine carbonates silts and marls

[13] equilibrium constant: K = $10^{-7.81}$ at 25 °C (Lawrence Livemore National Laboratory database).

(Matoshko *et al.*, 2004), which could add some HCO_3^- by diffusion or leakage processes. Dissolution of calcite can be written as follow:

Equation IV-3

$$CaCO_3 + H_2O + CO_2 \Leftrightarrow Ca^{2+} + 2HCO_3^-$$

Dissolution of dolomite (Ca,Ma)CO_3 can be considered too, because of the quite similar trend to [HCO_3^-] shown by [Mg^{2+}] in Figure IV-10.

Figure IV-14 is composed by two diagrams: one represents [Ca^{2+}] relative to [HCO_3^-] and the other [Mg^{2+}] relative to [HCO_3^-].

The same legend as in the previous diagrams is used for the representation of the dataset in the two diagrams. Green curves represent progressive calcite and dolomite dissolution in the mean Chernobyl Pilot Site meteoric water (Bugai *et al.*, 2012a), calculated at equilibrium with $PCO_2 = 10^{-2}$ atm using PHREEQC code (Annex 10 and Annex 11). This PCO_2 is chosen according to the previous observations: in Figure IV-13, most samples are close to the line where [HCO_3^-] are calculated at equilibrium with pH for a PCO_2 equals to 10^{-2} atm. The dark green curve represents calcite dissolution and the light green curve represents dolomite dissolution.

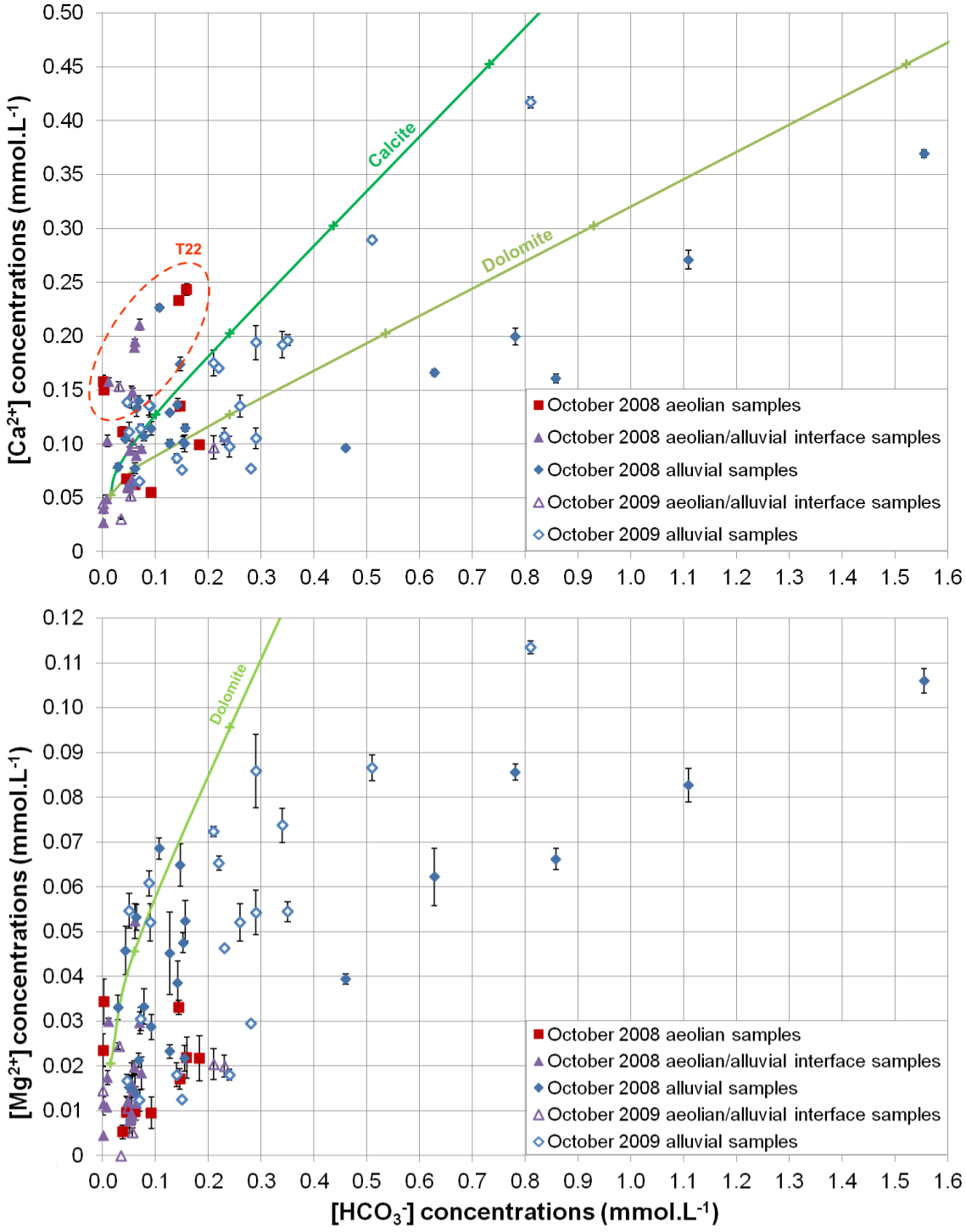

Figure IV-14: [Ca^{2+}] concentrations and [Mg^{2+}] concentrations evolutions as function of [HCO_3^-] concentrations

The main trend of the dataset shows a global increase of [Ca^{2+}] and [Mg^{2+}] with increasing [HCO_3^-]. [Ca^{2+}] seem to follow calcite and dolomite dissolution lines, with a slight overestimation of concentrations by the simulations. In the [Mg^{2+}] *versus* [HCO_3^-] diagram, concentrations simulated by dolomite dissolution are

always overestimated. However, the dataset trend could fit quite well with carbonates dissolution considering that the real proportions of Ca^{2+} and Mg^{2+} in the carbonate phase are not known. On the other hand, samples showing higher [Ca^{2+}] than the calcite dissolution simulation can be identified mainly as samples collected downgradient of the trench in shallow groundwater (circled by dashed orange line), so their "high" [Ca^{2+}] are probably not a consequence of calcite dissolution.

The impact of the dissolution of calcite on pH and [HCO_3^-] is shown in Figure IV-15. The green curve represents the simulation of carbonate dissolution in the Chernobyl Pilot Site mean meteoric water (Bugai *et al.*, 2012a), after equilibration with $PCO_2 = 10^{-2}$ atm. The dataset fit quite well with the simulation curve: pH and [HCO_3^-] in the alluvial layer can be explained by a carbonate mineral dissolution.

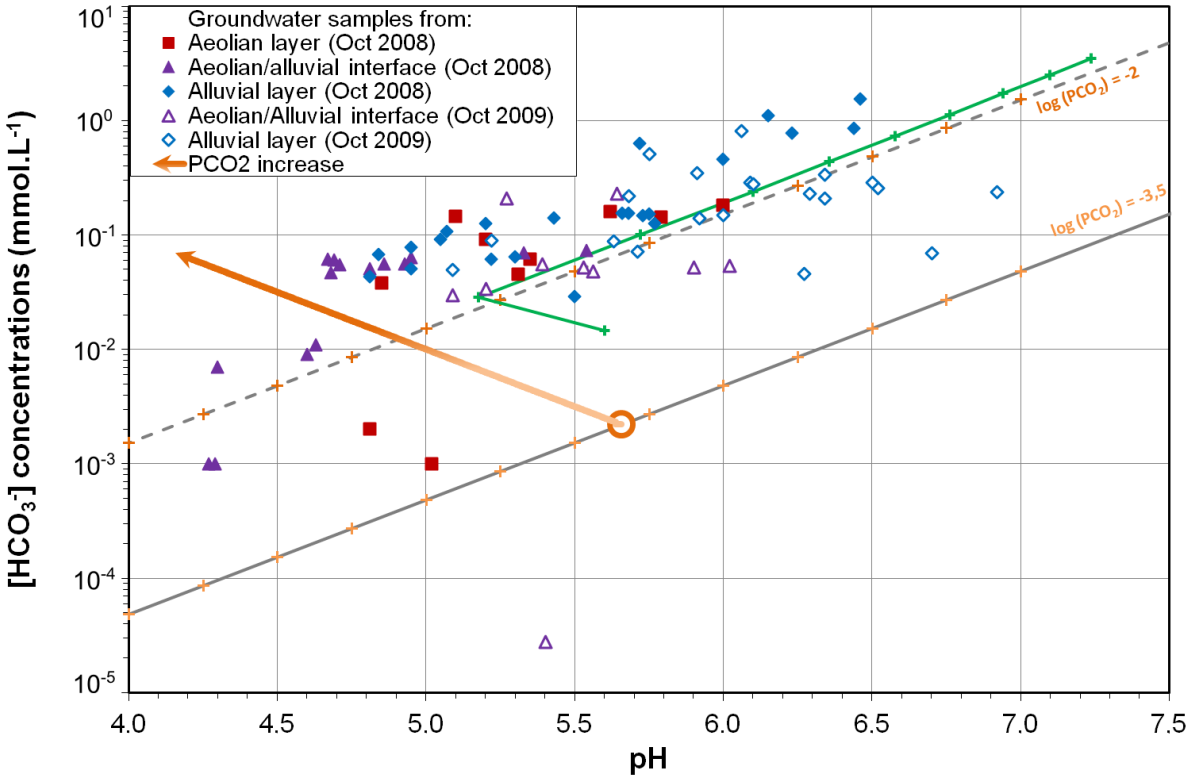

Figure IV-15: Impact of calcite dissolution on pH and [HCO_3^-] concentrations in Chernobyl Pilot Site meteoric water.

IV.1.4.3.2 Redox conditions variations and potential related processes

Redox changes are defined by electron transfer from one atom to another: in groundwater, redox changes occur by the addition of oxidizing species, such as O_2

or NO_3^- or a reducing species such as dissolved organic matter (Appelo and Postma, 2005).

All the following observations have to be interpreted with caution because of the sampling conditions where Eh values may have reequilibrate slightly with the atmosphere in the flow cell. As seen previously, Eh values are reported in pe values.

In order to investigate redox changes, pe variations are studied as a function of depth below the water table (Figure IV-16). Two diagrams are presented: one for data of the AB profile, one for the CD profile. The same legend as in the previous diagrams is used for the representation of the dataset. For October 2008 groundwater sample representation, full symbols are used: aeolian layer data are represented with red squares while data of the aeolian/alluvial interface with purple triangles and alluvial data with blue diamonds. For October 2009 groundwater sample representation, the same but void symbols are used: aeolian layer data are represented with a red outline while data of the aeolian/alluvial interface with a purple outline and alluvial data with blue outline. Piezometers are identified by their name. In natural systems, some processes are well known to govern redox conditions. The related pe range of these processes at pH 7 are shown below the diagrams on Figure IV-16 (according to Appelo and Postma, 2005). However, shown boundaries could be slightly shifted because pH ranges between 4.3 and 6.9 in Chernobyl Pilot Site groundwater.

Both diagrams of depth below the water table versus pe show the same trend: an overall decrease of pe with depth. Moreover, in the aeolian layer, groundwater downgradient of trench T22 is always more oxidizing than groundwater upgradient, suggesting migration of oxidizing element from the trench.

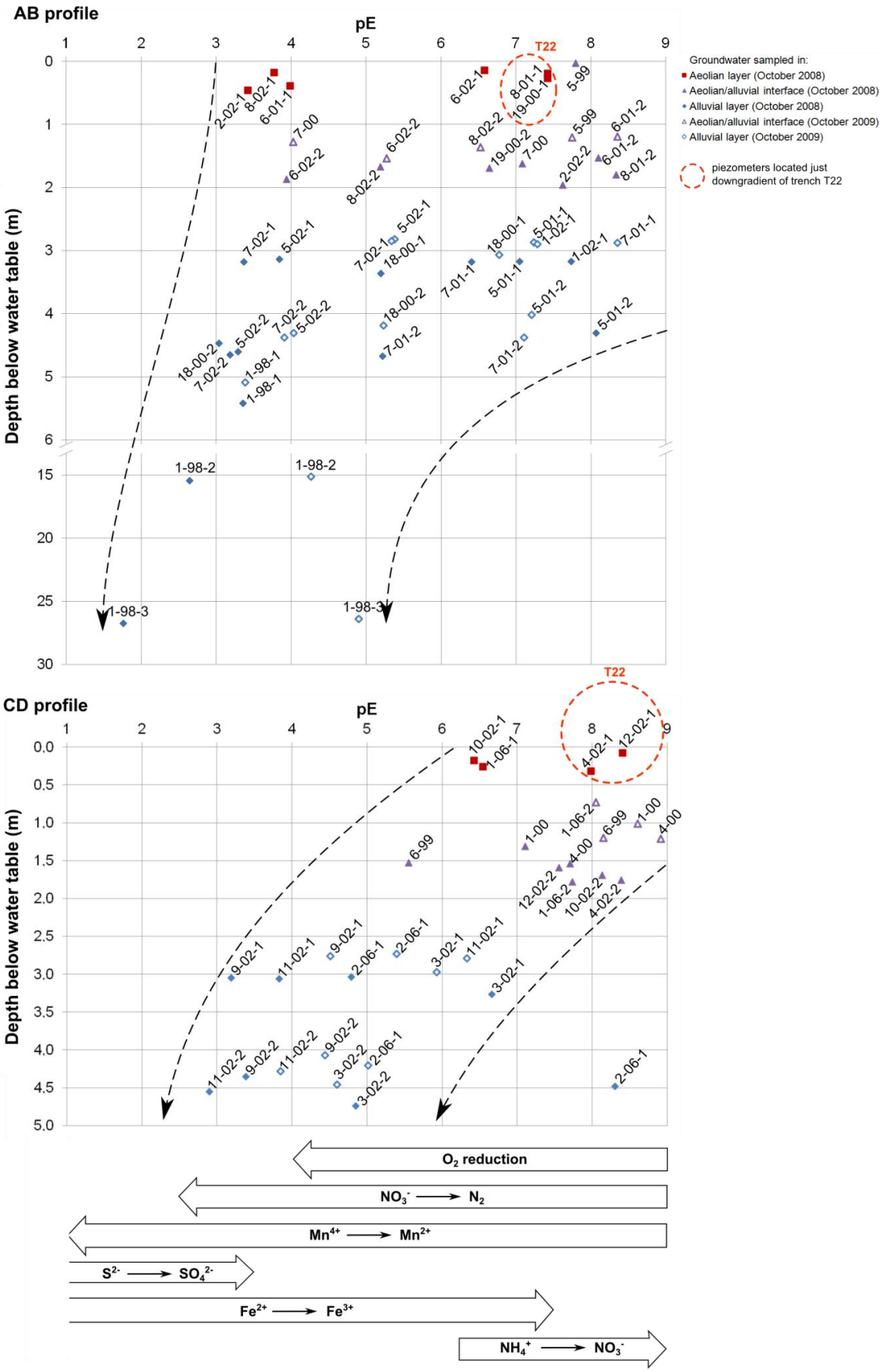

Figure IV-16: measured pe in function of the distance from the water table and potential redox reactions occuring in measured pe range at pH=7 (according to Appelo and Postma, 2005)

In order to better understand pe variations in Chernobyl Pilot site groundwater, impact of redox processes currently identified in natural system is then investigated. These processes govern dissolved O_2 concentrations, N-species concentrations, manganese concentrations, iron concentrations and sulfur concentrations, as detailed below:

- O_2 reduction

In groundwater, O_2, is not renewed because of the progressive sealing from the atmosphere, which is the main O_2 source. If reductant substances exist, O_2 reduction occurs, following the equation (Michard, 1989):

$$O_2 + 4e^- + 4H^+ \rightarrow 2H_2O \qquad \textit{Equation IV-4}$$

- Nitrification and denitrification processes.

Common nitrogen valences can be N^{5+} (under NO_3^- speciation), N^{3+} (under NO_2^- speciation), N^0 (under N_2 speciation) and N^{3-} (under NH_4^+ or NH_3 speciation). In solution, NH_4^+ is oxidized to NO_3^- following the equation (Michard, 1989):

$$NH_4^+ + 3H_2O \rightarrow NO_3^- + 8e^- + 10H^+ \qquad \textit{Equation IV-5}$$

At intermediate pe, N_2 is also a stable form of nitrogen (Michard, 1989; Appelo and Postma, 2005), however formation of N_2 is a slow reaction (Michard, 1989). Formation of N_2 results from the reduction of NO_3^-:

$$2NO_3^- + 10H^+ + 10e^- \rightarrow N_2 + 6H_2O \qquad \textit{Equation IV-6}$$

- Manganese reduction

Reduction of Mn^{4+} in Mn^{2+} leads to solubilization of Mn, initially immobilized under MnO_2 form (Michard, 1989; Appelo and Postma, 2005):

$$MnO_2 + 2e^- + 4H^+ \rightarrow Mn^{2+} + 2H_2O \qquad \textit{Equation IV-7}$$

- Iron oxidation

In Chernobyl Pilot Site groundwater, oxidation of Fe^{2+} should be promoted rather than Fe^{3+} reduction: it leads to the immobilization of iron under an insoluble oxidized Fe^{3+} form, not only depending on pe and pH conditions but also on [Fe^{3+}] concentrations and carbonates' presence (Michard, 1989). At pH between 3.3 and 9, the oxidizing condition can be (Michard, 1989):

$$Fe^{2+} + 3H_2O \rightarrow Fe(OH)_3 + e^- + 3H^+ \qquad \textit{Equation IV-8}$$

- Sulfur oxidation

In reduced conditions, sulfur valence is S^{2-}, as H_2S or HS^- species (following the pH) or immobilized as pyrite FeS_2. The oxidized valence S^{6+-} leads to the formation of sulfate SO_4^{2-} . Associated oxidation reaction are (Michard, 1989; Appelo and Postma, 2005):

$$HS^- + 4H_2O \rightarrow SO_4^{2-} + 9H^+ + 8e^- \qquad \textit{Equation IV-9}$$

$$H_2S_{(aq)} + 4H_2O \rightarrow SO_4^{2-} + 10H^+ + 8e^- \qquad \textit{Equation IV-10}$$

$$FeS_2 + 4H_2O \rightarrow SO_4^{2-} + 10H^+ + 8e^- \qquad \textit{Equation IV-11}$$

In order to investigate the influence of these reactions on redox conditions in Chernobyl Pilot Site groundwater, [dissolved O_2], [N-species], [Fe], [Mn] and [SO_4^{2-}] are compared with pe values in Figure IV-17.

October 2008 and October 2009 groundwater samples are shown separately. The same legend as in the previous diagrams is used to represent the dataset.

The overall trend describe by dissolved O_2 concentrations is a decrease from 0.315 mmol.L^{-1} in the shallow groundwater (aeolian layer and interface aeolian/alluvial) to 0.014 mmol.L^{-1} in deep groundwater with decreasing pe from 9 to 2. The main decrease of [Dissolved O_2] occurs in shallow groundwater independently from pe which range from 9 to 6. In deeper groundwater, [dissolved O_2] remain quite constant below 0.1 mmol.L^{-1}, while pe values decrease. Exceptions can be noticed for groundwater sampled in the aeolian layer in October 2008 with pe values between 3 and 4 various [dissolved O_2], located upgradient of the trench on the AB profile (8-02-1, 6-01-1, 2-02-1 piezometers).

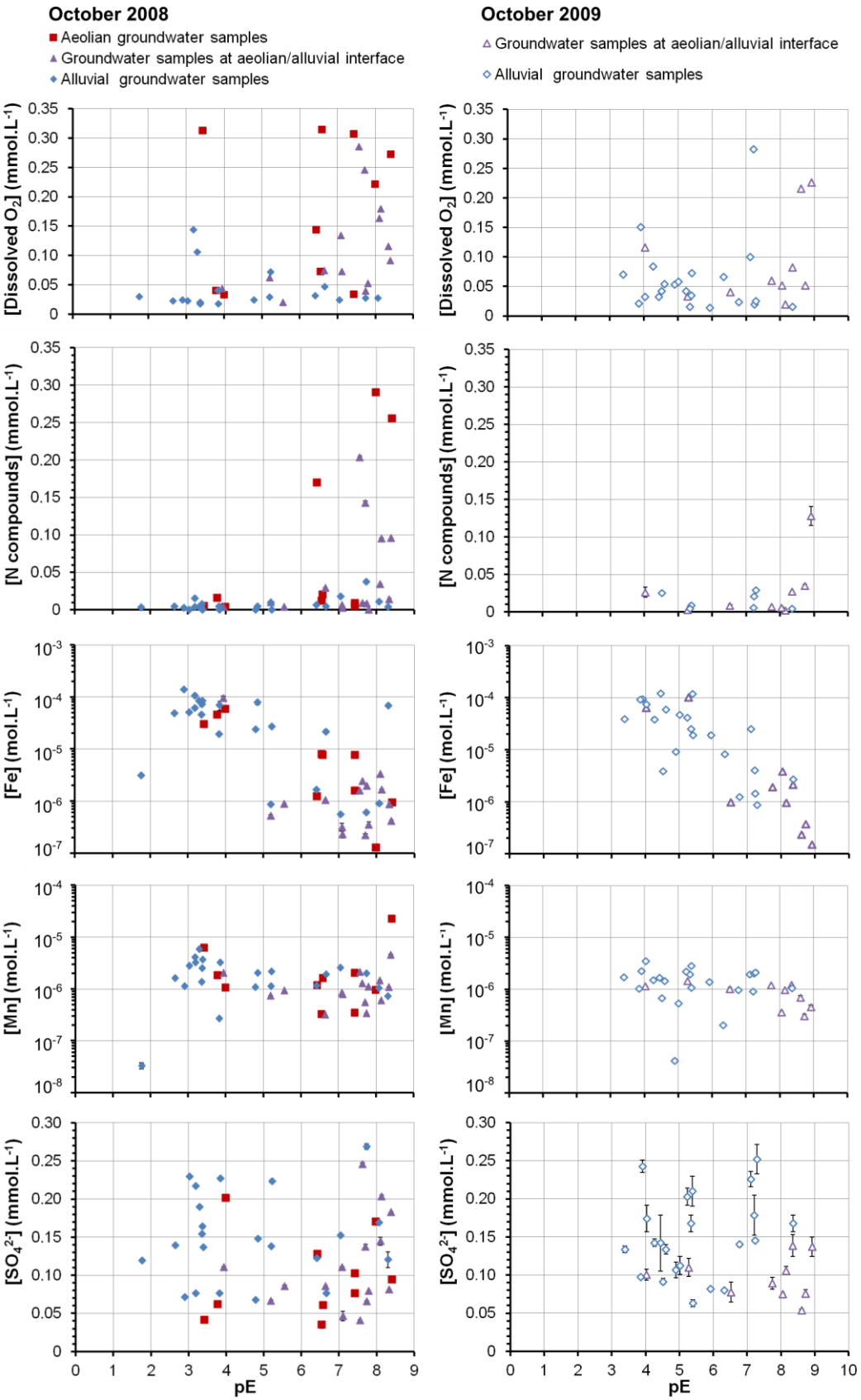

Figure IV-17: [Dissolved O_2], [N-species], [Fe], [Mn] and [SO_4^{2-}] concentrations in function of pe values.

To investigate the impact of decreasing [dissolved O_2] on pe values, rainwater is simulated in equilibrium with atmosphere (O_2 partial pressure equals to 0.21) with PHREEQC code and then, dissolved O_2 content is decreased progressively to simulate some microbial activity result. The results of the simulation are reported in the diagram of [dissolved O_2] versus pe values in Figure IV-18. Green circle shows the rainwater simulated in equilibrium with atmosphere (according to meteoric water composition of Bugai *et al.*, 2012a) and the green line show the result of decreasing O_2 starting from this rainwater (Annex 12).

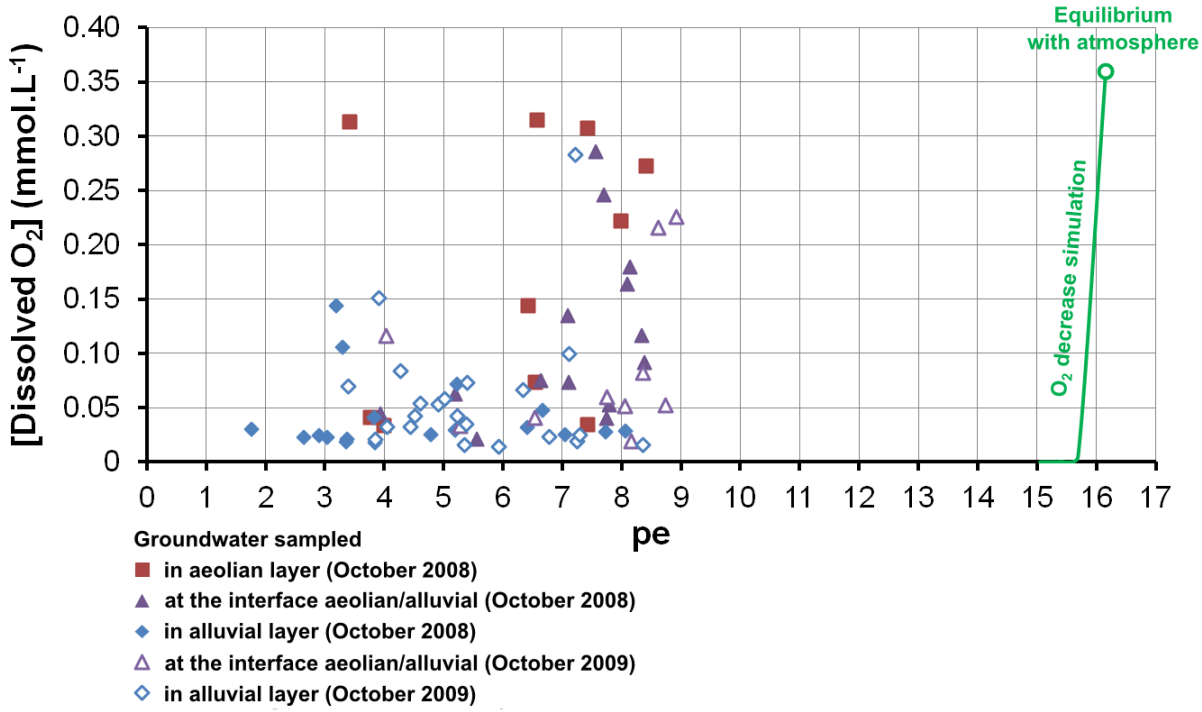

Figure IV-18: Simulation of [dissolved O_2] decreasing in rainwater in equilibrium with atmosphere and implications on pe values

The first observation is the shift of pe value in rainwater in equilibrium with atmosphere to higher values: theoretically, pe should be around 16. Then, O_2 decrease has only a slight impact on pe. The initial reductive species governing the lowering of pe in groundwater has to be identified.

Other oxidizing species decrease, such as NO_3^-, may explain pe decrease with the increasing depth below the water table. It was shown on the Pourbaix diagram of aqueous species that under the Chernobyl Pilot Site conditions, NH_4^+ seems to be the dominant aqueous species (Figure IV-8). However, under these conditions, N_2 is also a stable species (Michard, 1989; Appelo and Postma, 2005). Consequently, NH_4^+ should react to become N_2, which should result in a decrease of pe and pH:

$$2NH_4^+ \rightarrow N_2 + 6e^- + 10H^+$$ *Equation IV-12*

[N-compounds] concentrations are above the detection limit only in samples downgradient of trench T22 in the shallow groundwater. The presence of N-compounds does not persist in groundwater sampled in the underlying alluvial layer, suggesting that the reaction in Equation IV-12 is possible. However, it cannot be concluded that this reaction govern pe values because of the limited presence of this species. Moreover, if NH_4^+ is the dominant species, the origin of oxidizing conditions coming from the trench has to be explained.

[Fe] and [Mn] are highly dependent on redox conditions. [Fe] increase by 3 orders of magnitude with decreasing pe while [Mn] increase only slightly, by one order of magnitude. pe and [Fe] concentrations seem to show that Fe become more mobile in groundwater with increasing of depth below the water table and decreasing of pe (except for some upgradient samples), reduction of ferric minerals could explain such trend (Equation IV-8). Similarly, the slight increase of [Mn] with decreasing pe can be explained by Mn reduction under its mobile Mn^{2+} form (Equation IV-7) (Figure IV-17). This implies the presence of manganese oxides in the alluvial layer.

Finally, in [SO_4^{2-}] versus pe diagrams, sulfate [SO_4^{2-}] are very scattered. Some slight increase with the decrease of pe values seems to be observable in the October 2009 samples between groundwater samples showing the lowest and the highest pe values of 0.1 mmol.L^{-1}.

To study [SO_4^{2-}] variations, these concentrations are compared with [Fe] in Figure IV-19.

The same legend as in the previous diagrams is used for the representation of the dataset. Samples showing different trends than most of the samples located at the same depth are labeled on the diagram, as samples located upgradient of trench T22.

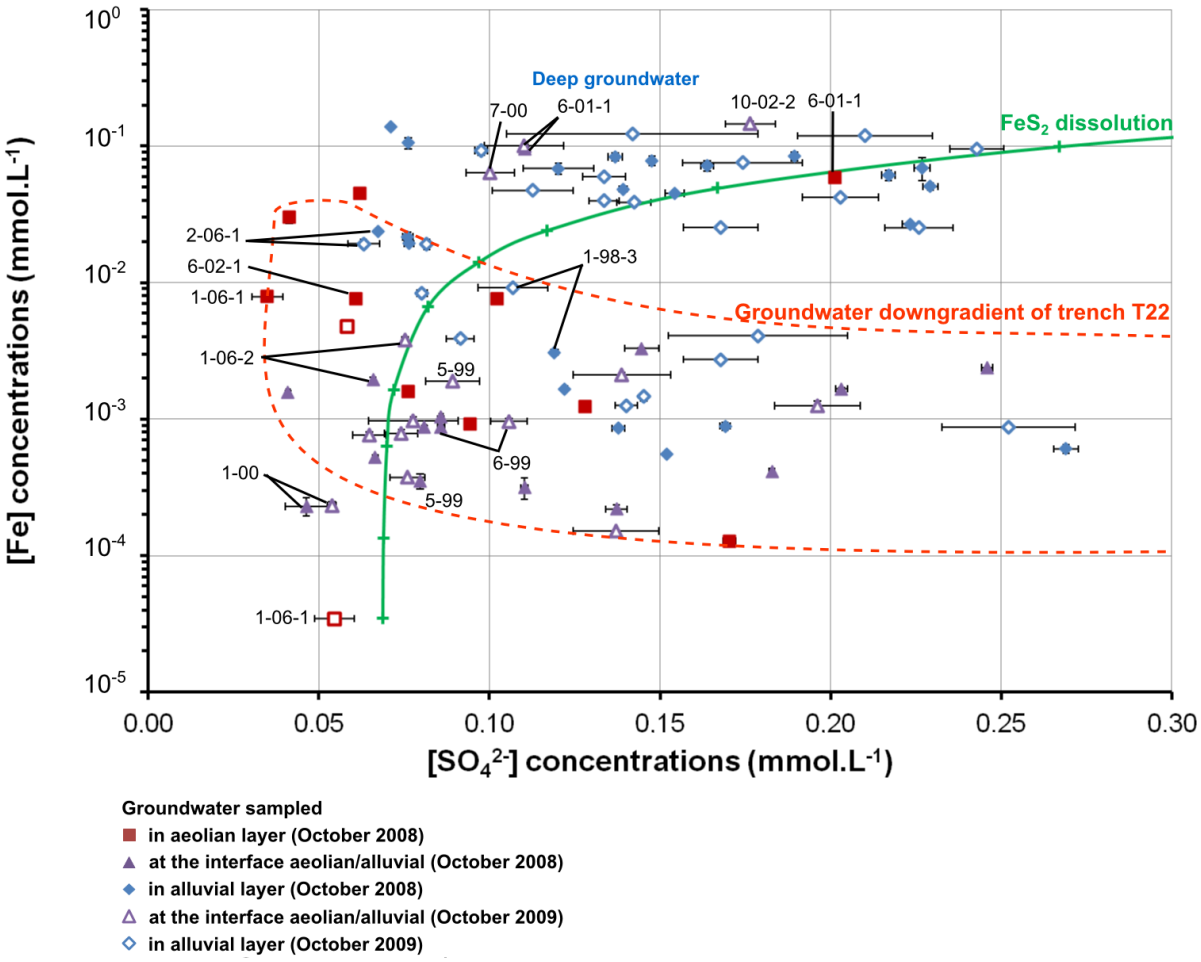

Figure IV-19: [Fe] concentrations versus [SO_4^{2-}] concentrations

Shallow groundwater and deep groundwater show different trends. Groundwater sampled in the aeolian layer or at the aeolian/alluvial interface show [Fe] decreasing with increasing [SO_4^{2-}]. Some groundwater samples from the alluvial layer also follow this trend. Other alluvial groundwater samples show increasing [Fe] with increasing [SO_4^{2-}].

The trend of the shallow groundwater could be explained by migration of elements from the trench: [SO_4^{2-}] increase downgradient of the trench whereas [Fe] remain mostly constant. To explain the trend of groundwater sampled in the alluvial layer, pyrite FeS_2 dissolution is simulated in the mean meteoric water[14] using the PHREEQC code (Annex 13). This mineral phase is chosen because it is composed only by Fe and S and is very sensitive to oxidation conditions. [Fe] is not known in

[14] From data published by Bugai *et al.*, 2012a

meteoric water; consequently, for the simulations, the lowest concentration measured in the Chernobyl Pilot Site groundwater is used. Results of this simulation are shown by the green line. Simulated concentrations fit quite well with the measured concentrations in the alluvial layer, excluding data downgradient of trench T22 which mostly show to low [Fe]. This implies that pyrite dissolution might occur in Chernobyl Pilot Site groundwater and might be impacted by migration of element and oxidizing conditions measured downgradient of trench T22 because.

To comfort this hypothesis, [Fe] are compared with [Dissolved O_2] in Figure IV-20 and the results of the pyrite dissolution simulation are reported.

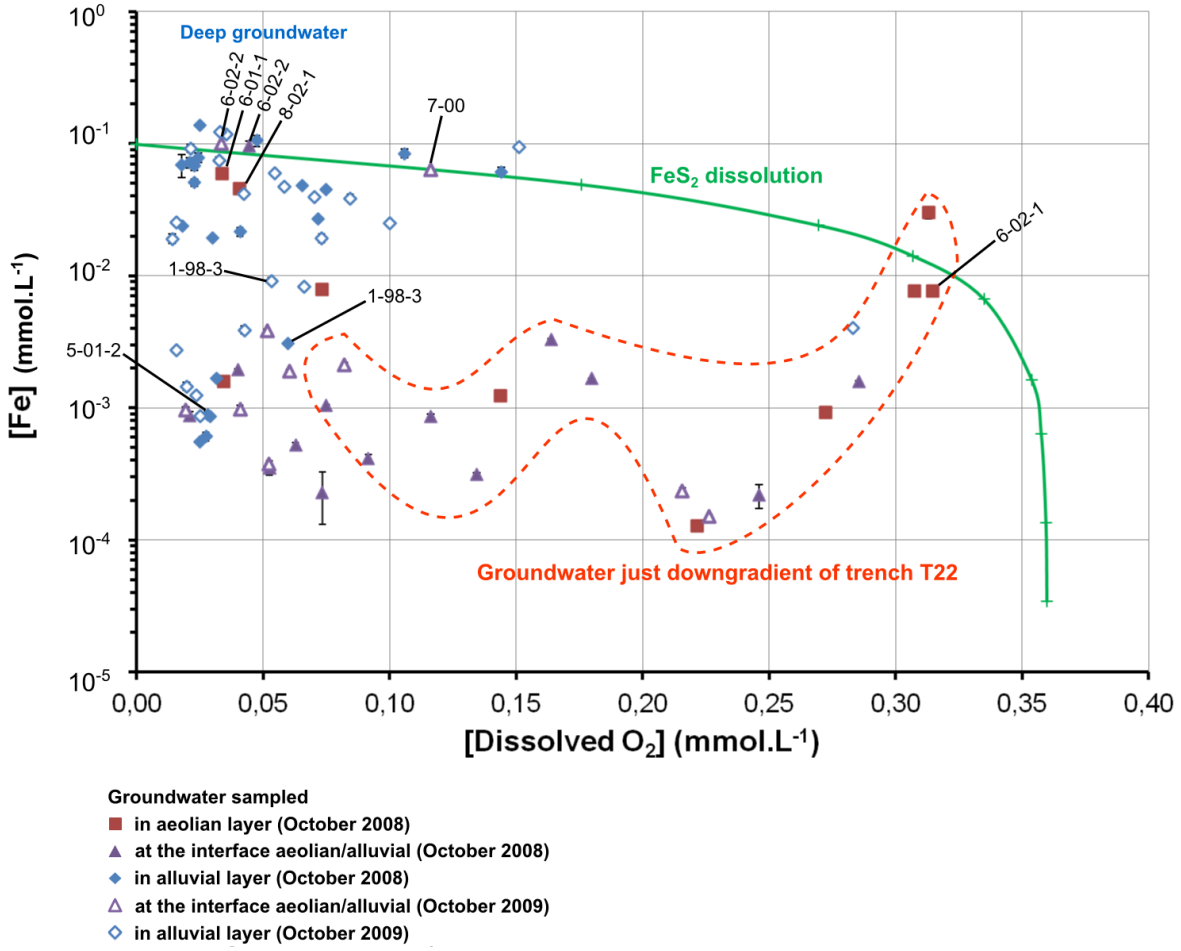

Figure IV-20: [Fe] concentrations and [dissolved O2] in the Chernobyl Pilot Site groundwater

Overall, [Fe] increase with decreasing of [dissolved O_2]. In shallow groundwater, [Fe] remains low, between 10^{-4} and 10^{-2} mmol.L^{-1} while [dissolved O_2] range from 0.01 upgradient of the trench to 0.032 mmol.L^{-1} downgradient of the trench. In groundwater downgradient of the trench, [Fe] increase with increasing [dissolved

O_2]. In deep groundwater, [Fe] drastically increases while [dissolved O_2] are below 0.1 mmol.L^{-1}. The results of the pyrite dissolution simulation seem coherent with concentrations observed in deep groundwater but not with shallow groundwater which is clearly highly influenced by the presence of the trench. In the considered simulation (Annex 13), pH decreases down to 3.6. However, it was assumed to be buffered by dissolution of a carbonate phase (§IV.1.4.3.1). As these two hypotheses are not enough well constrained, an overall simulation cannot be proposed.

However, pyrite was not identified in the mineral phases neither in the aeolian layer nor in the alluvial layer. A more detailed mineralogical study should be carried out, particularly in the alluvial layer and the Kiev suite layer to confirm this hypothesis.

In summary, following the study of the redox conditions and the potential associated processes, the following observations can be made:

- Redox conditions are more oxidizing downgradient of the trench. [Dissolved O_2], [N-species] and [SO_4^{2-}] are higher downgradient of this one. [Fe] mostly remain below 10^{-2} mmol.L^{-1}.
- pe values decrease with the increasing depth below the water table. In shallow groundwater, pe decrease with decrease of [Dissolved O_2] and [N-species]. This can be interpreted as the reduction of O_2 and denitrification processes because of microbial activity (Sposito, 2008). Most of these elements are potentially renewed by migration from the trench, feeding in the system.
- In deep groundwater, pe values decrease with increasing [SO_4^{2-}], [Fe] and [Mn]. [SO_4^{2-}] seem to be closely linked to [Fe] and their relationship can be interpreted as pyrite dissolution. This is comforted by [Dissolved O_2] decrease with increasing [Fe] in deep groundwater. However, to confirm this hypothesis, this mineral phase needs to be identified in mineralogy, particularly in deeper layers.

IV.1.4.4 Mineral weathering

The migration of elements from the trench, dissolution of carbonates and pyrite could explain variations of pe, pH, [HCO_3^-], [Ma^{2+}], [Ca^{2+}], [SO_4^{2-}] and [N-species]. As seen in Figure IV-10, [K^+] show the same trend as [N-species] concentrations: most concentrated samples are located downgradient of trench T22 and can consequently be explained by migration of elements from trench T22.

The only major element which is not explained yet is Na^+. In order to investigate processes which may govern [Na^+] in the Chernobyl Pilot Site groundwater, Figure IV-21 represents [Na^+] versus [Cl^-][15].

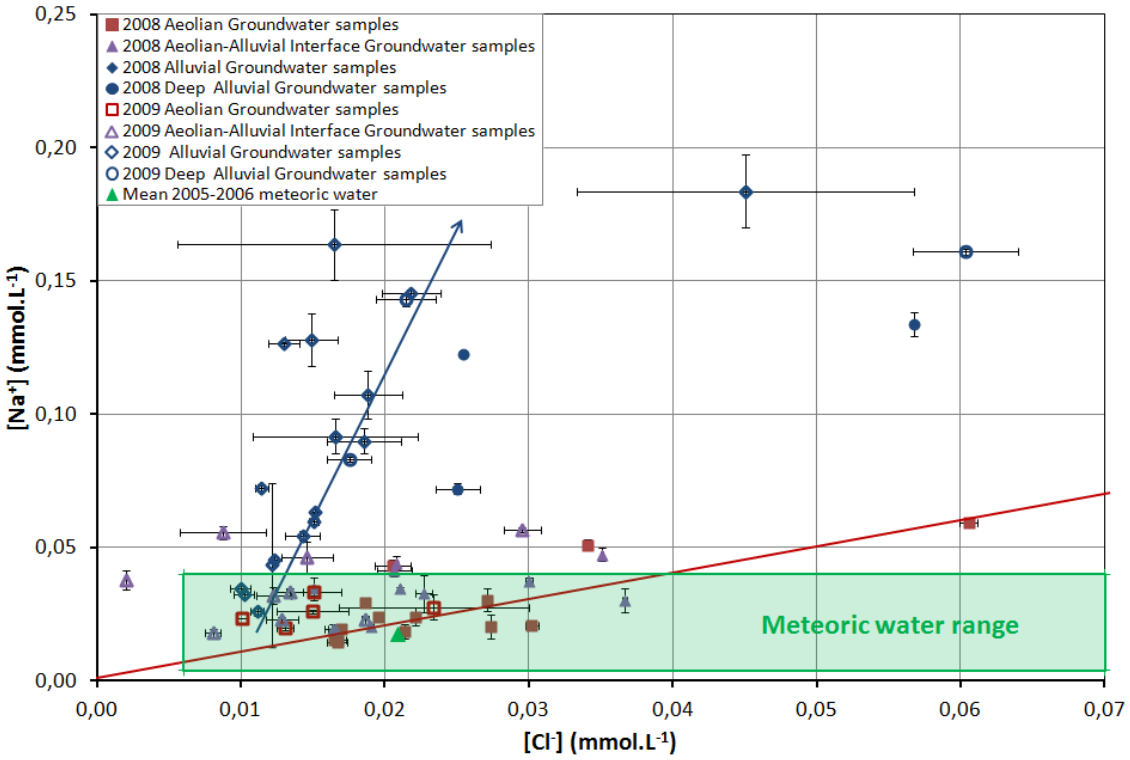

Figure IV-21: Sodium concentrations versus chloride concentrations

Red squares represent groundwater sampled in the aeolian layer, purple triangles are groundwater sampled at the aeolian/alluvial interface and blue diamonds represent alluvial groundwater. The green rectangle represents meteoric water concentration range[16] .

Two trends can be distinguished, corresponding to groundwater sampled in a specific geological formation:

- Groundwater from the aeolian layer and at the aeolian/alluvial interface follow a linear trend, mainly within the range of the meteoric water, except for a few samples, located downgradient of trench T22 (potentially impacted by its presence). These small variations of concentrations may result from migration of elements from the trench.

[15] [Cl^-] concentrations are assumed to be only impacted by migrations from the trench (see §III)

[16] From data published by Bugai *et al.*, 2012a

- Groundwater from the alluvial layer follow another trend: [Cl^-] remains within the meteoric water range but [Na^+] increase progressively with depth from about 0.025 mmol.L^{-1} up to 0.15 mmol.L^{-1}.

The increase of [Na^+] in the alluvial layer can be explained be several processes: mixing with a more concentrated groundwater or water-rock interaction processes. Water-rock interaction processes can be dissolution of mineral phases or cation-exchange with the matrix. Mixing processes and cation exchange processes will be investigated thereafter.

The aeolian and alluvial layers are mainly composed by quartz (Szenknect, 2003; Matoshko *et al.*, 2004). Due to its slow kinetics, its dissolution is probably of low influence on the hydrochemistry. Nevertheless, in the aeolian layer, some accessory minerals are identified and in the alluvial facies, mineralogy shown sodic and potassic feldspars and different heavy minerals, representing 5-9% and <0.5% of the mineralogy respectively (Matoshko *et al.*, 2004). In the finest fraction of the alluvial layer (particle size below 0.01 mm), quartz, phyllosilicates (montmorillonite, hydromica), fine-dispersed calcite and amorphous ferrous oxides are reported (Matoshko *et al.*, 2004). These minerals may have been altered or dissolved. Particularly, the weathering of sodic feldspar $NaAlSi_3O_8$ (albite) could result in Na^+ release in groundwater. In soils, hydrolysis of feldspars results in the formation of gibbsite, kaolinite and montmorillonite as secondary mineral phases. The formed mineral phase depends on the climate and the hydrological conditions (Appelo and Postma, 2005). A dry climate and long residence time of water in soil will result in the formation of montmorillonite whereas intense rainfall and low residence time of water in soils will result in the formation of aluminum oxides (Appelo and Postma, 2005).

Tardy's diagram of stability (1971) for these mineral phases is presented in Figure IV-22.

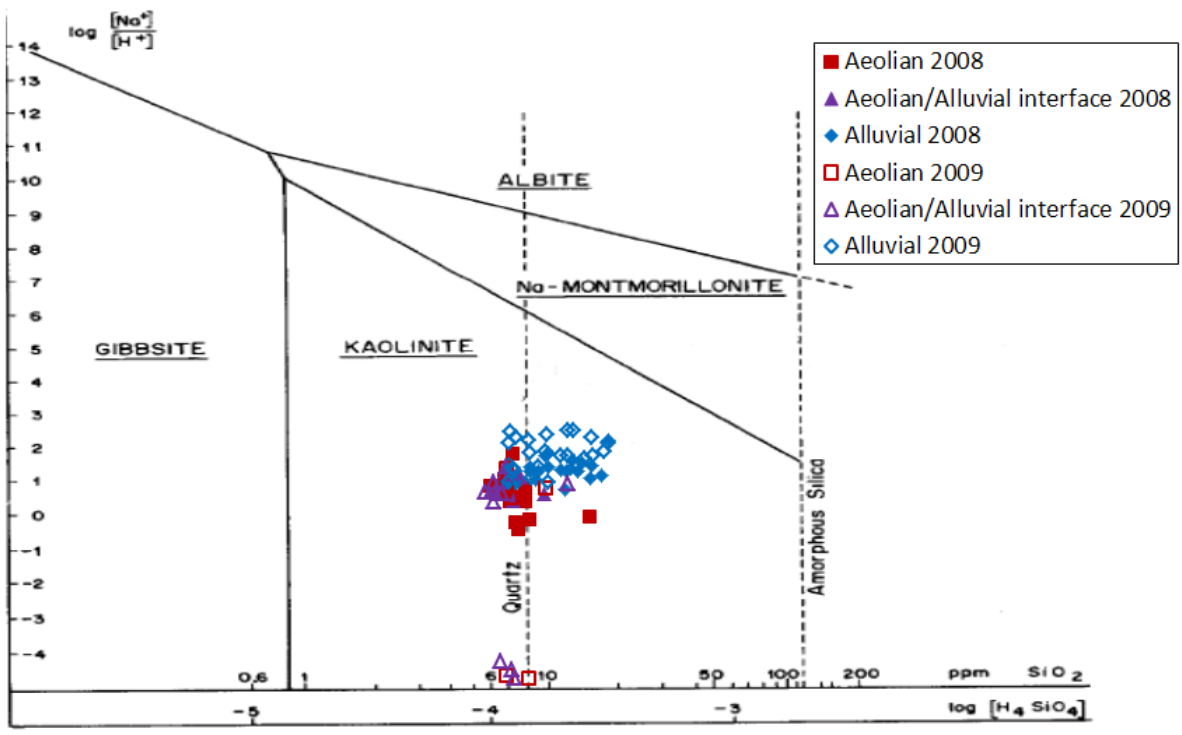

Figure IV-22: albite, montmorillonite, kaolinite and gibbsite diagram of stability (from Tardy, 1971) and Chernobyl Pilot Site groundwater

The entire dataset is located in the kaolinite stability domain. Consequently, the potential weathering of albite in Chernobyl Pilot Site free aquifer should result in the kaolinite formation. This reaction is written as:

$$2NaAlSi_3O_8 + 2H^+ + 9H_2O \rightarrow Al_2Si_2O_5(OH)_4 + 2Na^+ + 4H_4SiO_4$$ *Equation IV-13*

Kaolinite's saturation indices increasing with the depth in Chernobyl Pilot Site groundwater are in agreement with such a process (Annex 9). For instance, Figure IV-23 shows the evolution of albite and kaolinite saturation indices along a theoretical flow line (1-06-1, 1-00, 12-02-2, 11-02-1 and 11-02-2 piezometers).

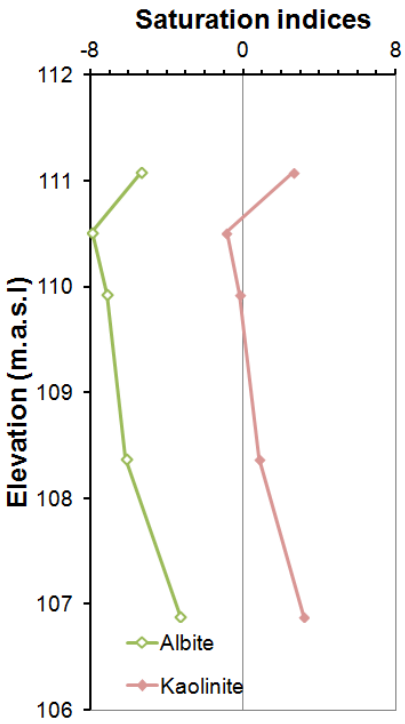

Figure IV-23: Albite and Kaolinite saturation indices along a theoretical flow line of the CD profile (October 2008)

To substantiate this hypothesis, albite hydrolysis is simulated through albite dissolution in mean meteoric water, using CHESS code[17]. The dissolution of 0.15 mmol of albite, excluding precipitation of SiO_2, is compared with [Na^+] and [H_4SiO_4] concentrations measured in groundwater in Figure IV-24. Simulation results are represented by purple line whereas the dataset is represented with red circles.

[17] Geochemical code developed by Mines-Paris Tech. EQ36 database, derived from Laurence Livemore National Laboratory database, is used here.

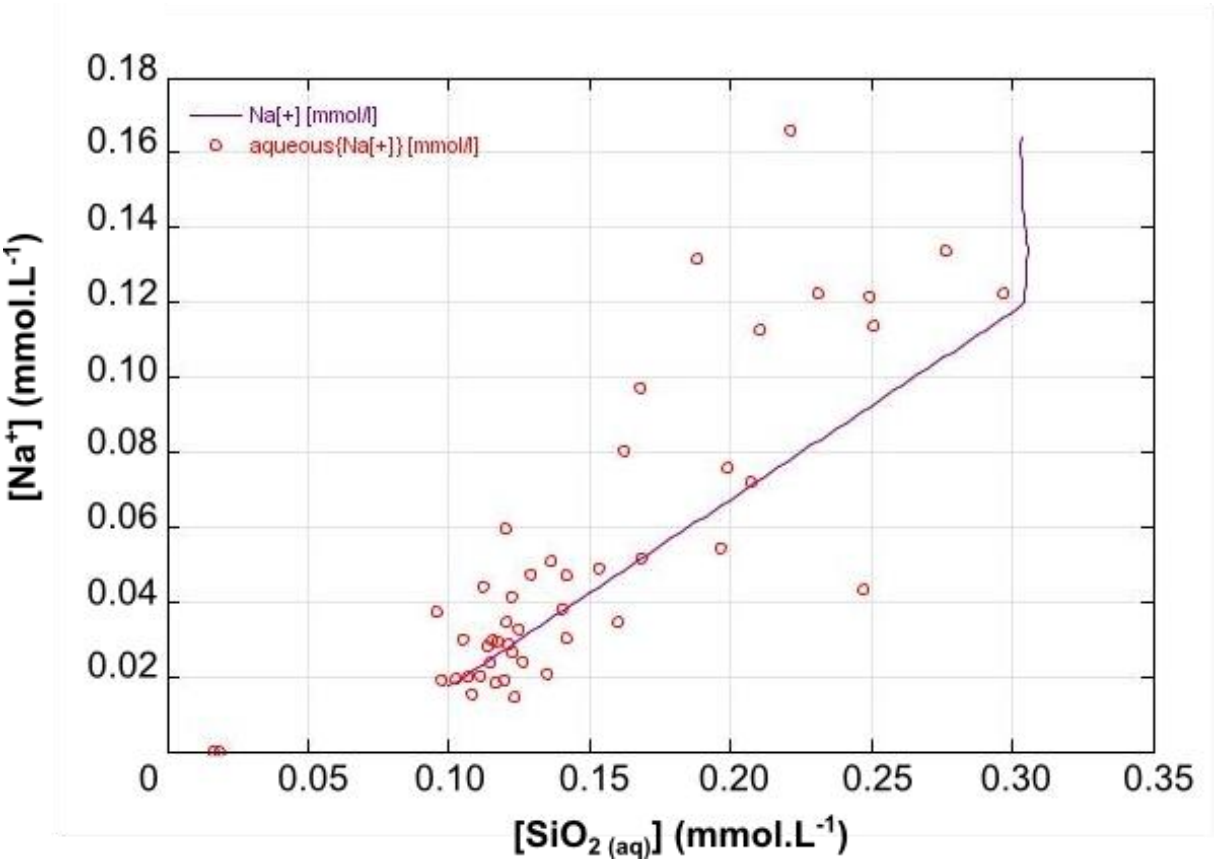

Figure IV-24: Albite dissolution simulation

The simulation fits quite well with the dataset scattering. Consequently, albite dissolution may explain increasing $[Na^+]$ in the groundwater sampled in the alluvial layer.

IV.1.4.5 Cation exchanges

Several hypotheses can be made to explain most of the major ion concentration variations in Chernobyl Pilot Site groundwater. However, cation exchange process shown to occur in the Chernobyl Pilot Site groundwater (Szenknect, 2003) has not been investigated yet. These processes may explain discrepancies in the simulation of $[Ca^{2+}]$ and $[Mg^{2+}]$ in solution by calcite and dolomite dissolution (cf. IV.1.4.3.1).

Ion exchanges occur at the solid surface: one element adsorbed on an exchange site is replaced by one from the solution. Solids with high specific surfaces are favorable to this type of process (Appelo and Postma, 2005).

This process is quantified by the cation exchange capacity (CEC). It corresponds to the number of exchangeable cations in meq per 100 g of soil. This parameter is closely linked to clay, organic matter and oxyhydroxides contents (Appelo and Postma, 2005). One of the clay minerals' properties, and particularly of montmorillonite, is the presence of exchangeable cations in the interlayer (Appelo and Postma, 2005). At the Chernobyl Pilot Site, CEC increases from less than 1 meq per 100 g of soil in the aeolian layer to almost 10 meq1 meq per 100 g of soil in the alluvial layer (Matoshko *et al.*, 2004). Cation exchanges were shown with laboratory experiments and simulations in the Pripyat Zaton aeolian sands, a geological analogue of the Chernobyl Pilot Site aeolian sands (Szenknect, 2003). The quantity of accessible exchange sites and the retardation factor were estimated for strontium and cesium. To illustrate the cation exchange processes, compositions of a synthetic water representative of Chernobyl Pilot Site groundwater average composition and a deionized water in contact with the aeolian sand during 3 days are shown in Table IV-1, according to the laboratory results (Szenknect, 2003). Potassium, calcium and strontium are particularly impacted.

Table IV-1: Major cations concentrations in initial synthetic water and in synthetic and deionized water in contact during 3 days with the synthetic water (mol.L^{-1})

	K^+	Na^+	Ca^{2+}	Mg^{2+}	Sr^{2+}
Initial composition of the synthetic water	$5.9.10^{-5}$ $\pm 1.10^{-5}$	$5.7.10^{-5}$ $\pm 1.10^{-5}$	$7.7.10^{-5}$ $\pm 1.10^{-5}$	$2.1.10^{-5}$ $\pm 0.5.10^{-5}$	0
Synthetic water in contact with sand	$1.05.10^{-4}$	$6.5.10^{-5}$	$1.35.10^{-4}$	$1.9.10^{-5}$	3.10^{-7}
Deionized water in contact with sand	$7.9.10^{-5}$	$2.2.10^{-5}$	$6.2.10^{-5}$	8.10^{-6}	1.10^{-6}

With the increase of CEC and the presence of clay minerals in the alluvial layer (Matoshko *et al.*, 2004), cation exchanges can be assumed in this layer too.

In order to investigate the impact of cation exchange processes on groundwater geochemistry, cation exchanges are simulated in Chernobyl Pilot Site groundwater using the PHREEQC code using Lawrence Livemore National Laboratory database

(Annexes 14, 15, 16 and 17). The simulation is considered along a flow line, assumed to be the least impacted by the presence of the trench, according to Stiff diagrams in Figure IV-6. This flow line is located upgradient from the Trench, on the CD profile (Figure IV-25).

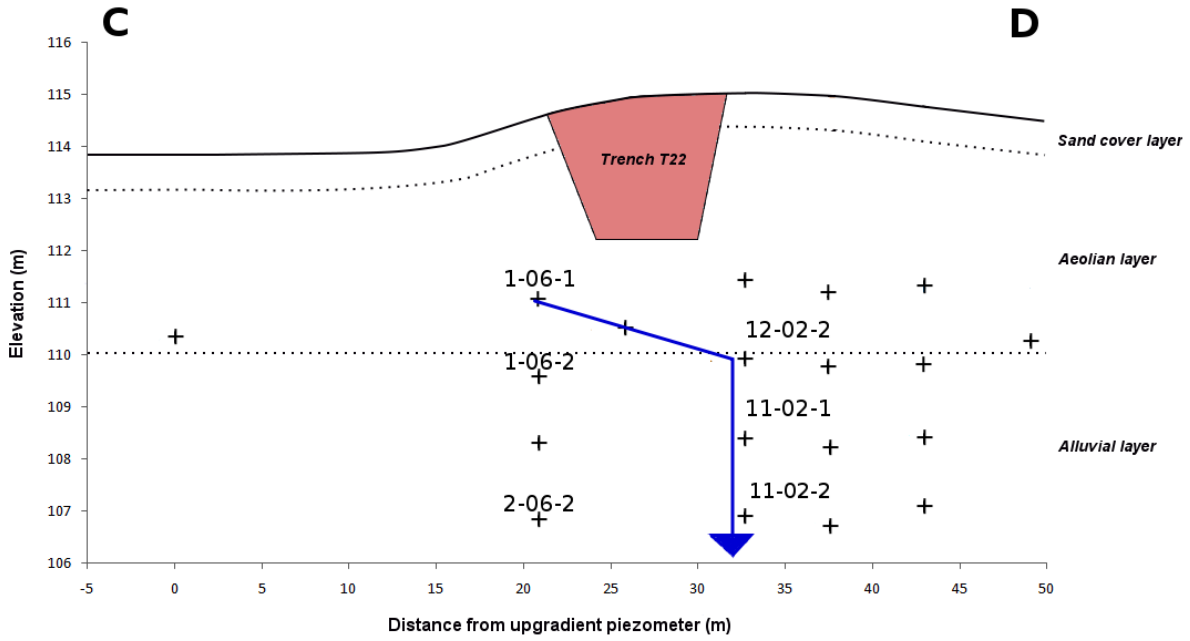

Figure IV-25: Considered flow line for simulations

Cation exchanges are simulated in the aeolian layer, from the groundwater sampled in the 1-06-1 piezometer in October 2008 (T8 1-06-1) to obtain concentrations of the groundwater sampled in the 12-02-2 piezometer (T8 12-02-2) (Figure IV-25).

The amount of exchange sites is required and can be calculated from the CEC measurements as:

Equation IV-14

$$X = CEC \times \frac{\rho_{solid}}{\rho_{water}} \times \frac{(1-\eta)}{\eta}$$

with X the amount of exchange sites in $mol.kg^{-1}$, CEC the cationic exchange capacity reported in $eq.kg^{-1}$, ρ_{solid} the volumetric mass of the mineral phase (2650 $kg.m^{-3}$ for quartz), ρ_{water} the volumetric mass of water (1000 $kg.m^{-3}$) and η the porosity.

In the aeolian layer, with a CEC of 1 meq per 100 g of soil, composed mainly by quartz and with a total porosity of 0.35 (Matoshko *et al.*, 2004), $X_{aeolian}$ is estimated to be 0.049 mol.kg^{-1}.Then, the exchanger is equilibrated with a solution.

The difficulty is then to define the cation exchanger in PHREEQC. As a first approximation, the composition of the solution obtained from synthetic water in contact with aeolian sand during 3 days in a batch reactor is used (Szenknect, 2003). In a second approximation, the exchanger is equilibrated with a solution closer to *in situ* conditions: an upgradient sample, approximately at the same altitude than the targeted composition and less concentrated (concentrations of groundwater sampled in 1-06-2 piezometer in October 2008). Only pH, major cations and Sr are considered because they are the only cations in the synthetic solution. Results are shown in Figure IV-26 and Figure IV-27.

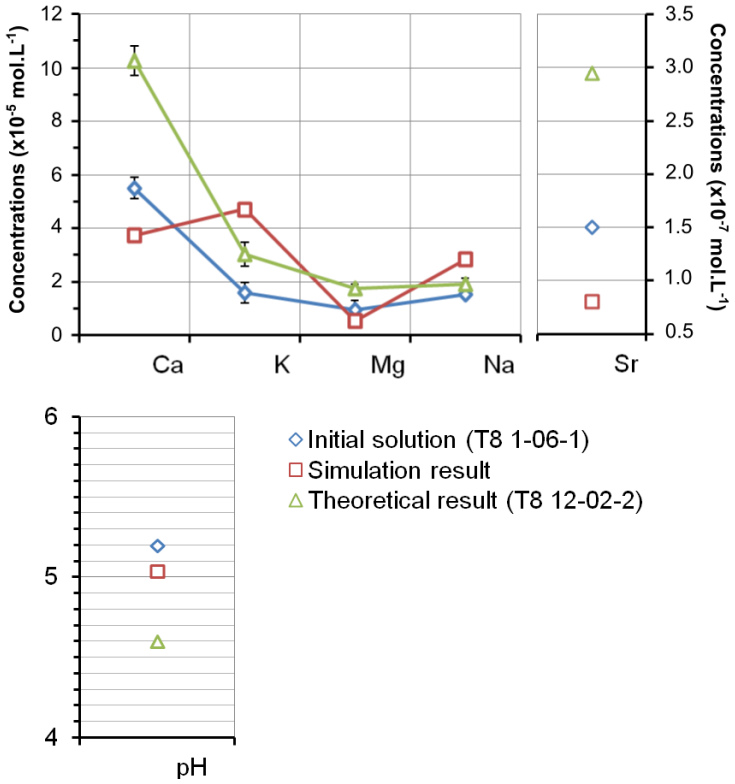

Figure IV-26: Results of cation exchange simulation in the aeolian layer following Szenknect's results (2003)

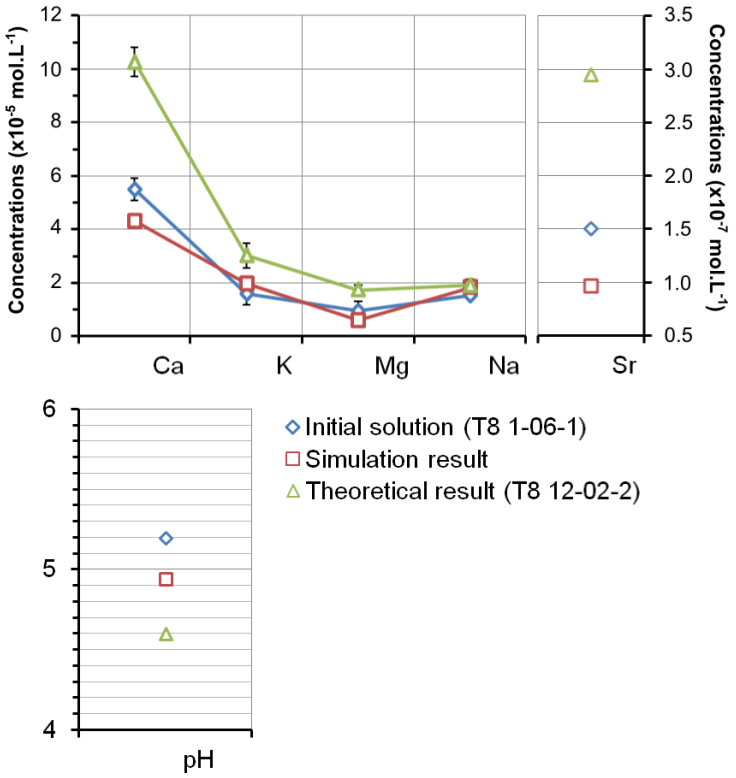

Figure IV-27: Results of cation exchange simulation in the aeolian layer using calibration of exchanger on upgradient sample

In both cases, the simulation concentrations are except in the first simulation, where potassium and sodium concentrations are overestimated.

For the alluvial layer, as no laboratory experimental results are available, the exchanger is only equilibrated with an upgradient sample: groundwater sampled in the 2-06-2 piezometer in October 2008. Following the same calculation as for the aeolian study, the amount of exchange sites in the alluvial layer can be calculated based on CEC measurements. A CEC of 5 meq per 100 g of soil, mineralogy composed mainly by quartz and a porosity of 0.35 are considered (Matoshko *et al.*, 2004). So, $X_{alluvial}$ is estimated to be 0.245 mol.kg^{-1}.

pH, major cations and Sr concentrations are considered. Results are presented in Figure IV-28.

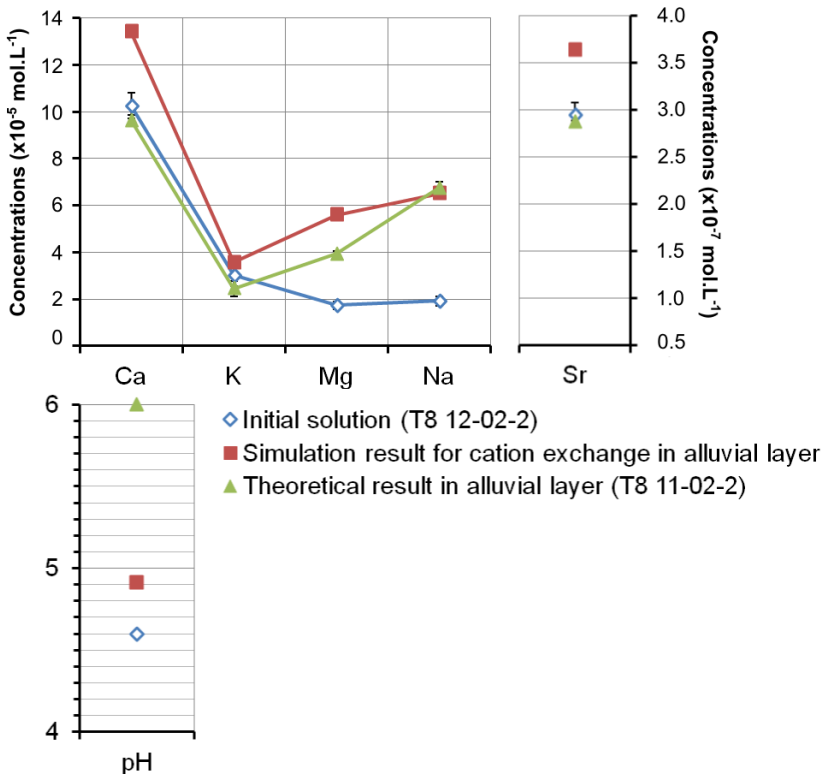

Figure IV-28: Results of cation exchange simulation in the alluvial layer using calibration of exchanger on upgradient sample

Sodium, potassium, and strontium fit quite well with the observed concentrations. Calcium and magnesium are overestimated.

The next simulation combines the two cation-exchange simulations for the aeolian and the alluvial layers, considering exchangers in equilibrium with upgradient piezometers. The results are shown below (Figure IV-29)

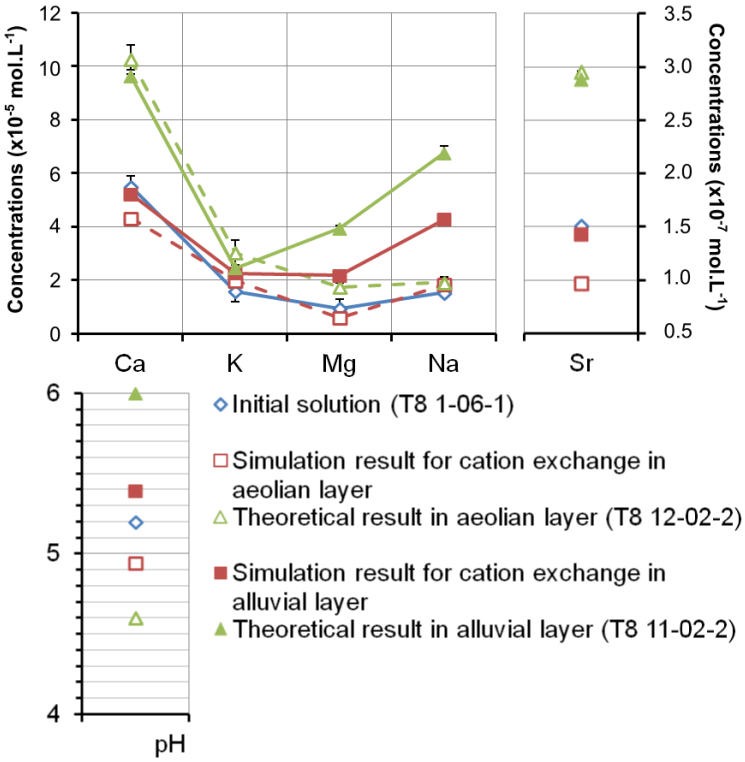

Figure IV-29: Results of cation exchange simulation using calibration of exchanger on upgradient samples

Simulated potassium concentrations, that remain constant, are in agreement with the observed values. For other species, measured concentrations are often underestimated, particularly in the alluvial layer. Magnesium and sodium concentrations fit quite well in the aeolian layer while they are then underestimated in the alluvial layer. Whereas $[Na^+]$ are well reproduced by albite hydrolysis in the alluvial layer (Figure IV-24), simulated $[Na^+]$ by cation exchange are underestimated by 0.02 $mmol.L^{-1}$ (concentrations in groundwater range from 0.015 to 0.184). Calcium and strontium concentrations are largely underestimated in the aeolian layer and in the alluvial layer: in alluvial layer, $[Ca^{2+}]$ and $[Sr^{2+}]$ are too low by 0.05 $mmol.L^{-1}$ and 0.0002 $mmol.L^{-1}$, respectively. In the simulation of calcite dissolution, $[Ca^{2+}]$ are overestimated by maximum 0.1 $mmol.L^{-1}$ in the deepest groundwater. In the simulation in the aeolian layer, a bigger influence of the trench (still lower than in the other non considered samples of the profile) could be supposed in 12-02-2 piezometer than the other considered piezometers (cf. Figure IV-6) and could explain the discrepancy.

Based on these results, cation-exchange cannot be the only geochemical process to explain groundwater cation geochemistry. However, it is an additional process and more specifically, if carbonate dissolution occurs in groundwater (cf. §IV.1.4.3.1), cation exchanges could explain the fact that, in the [Ca^{2+}] and [Mg^{2+}] versus [HCO_3^-] study (Figure IV-14), measured concentrations in the alluvial layer are lower than the simulated concentrations. The hypothesis is that dissolution of carbonate mineral release Ca^{2+} and Mg^{2+}, which are then exchanged on the surface sites with other cations, such as Na^+ or H^+, for instance. To confirm this hypothesis, the alluvial layer has to be better characterized (laboratory experiments on cation exchange processes, exchange sites determination, clay phase determination…). The origin of the potential carbonate dissolution has to be identified (fine dispersed calcite of alluvial layer or marine carbonate of the Kiev suite) as well as its composition (Ca, Mg and Sr content particularly). New simulations have to be run based on these studies.

IV.1.4.6 Mixing processes

Mixing processes are assessed in the interpretation of CFC-112, CFC-113, ^3H concentrations and $^3H/^3He$ ratios measured in 2008 groundwater samples on the AB profile (Le Gal La Salle *et al.*, 2012). These mixing processes seem to occur in the alluvial part of the aquifer but not in the aeolian part.

These mixing processes could be the result of some ascendant leakage processes from the underlying confined aquifer, as the underlying groundwater is known to be artesian at the regional scale (Dzhepo and Skal'skii, 2002). Consequently, the alluvial groundwater chemistry may be influenced by this deep groundwater geochemistry. The Kiev suite is mainly composed of marine carbonates, consequently, [Ca^{2+}], Mg^{2+}] and [HCO_3^-] could be impacted by carbonates dissolution due to potential groundwater leakage processes…

Piezometric data of the Kiev suite groundwater are needed to confirm this hypothesis.

IV.1.5 CONCLUSION

To constraint the fate of radionuclides and more particularly the fate of strontium, a conceptual model of the potential geochemical processes governing the Chernobyl Pilot Site groundwater geochemistry is proposed.

The model is developed based on the study of [Na^+], [K^+], [Ca^{2+}], [Mg^{2+}], [Cl^-], [HCO_3^-], [SO_4^{2-}] and [N-species], which are the major ions in groundwater, pH and redox potential are studied, focusing on groundwater sampled in October 2008 and October 2009.

These elements can be classified in two groups:

- Those influenced by the presence of the trench: [K^+], [N-species], [Ca^{2+}] and [SO_4^{2-}], which show significant increases of concentrations downgradient of trench T22. pH and pe are increasing too. [Cl^-] is much less influenced but also shows a slight increase in concentrations downgradient of the trench, remaining within the meteoric water range.
- Those influenced by deep geochemical processes: [Na^+], [Ca^{2+}], [Mg^{2+}], [HCO_3^-], [SO_4^{2-}] and pH are increasing with depth while pe decreases.

Potential geochemical processes are infered from these observations and confirmed, by other element behavior (O_2, Fe, Mn, Al, Si, $\delta^{18}O$, δ^2H) and the hypotheses are simulated with geochemical codes, when it is possible.

First, external factors are investigated. Water isotopes suggest that groundwater is recharged mainly by the infiltration of winter meteoric water. Evaporation processes seemed to be quite limited in October 2008 and October 2009. Degradation of buried material, particularly organic matter and migration of released elements is assessed by the increase of concentrations downgradient of the trench of K^+, Ca^{2+}, N-species and SO_4^{2-}, and the acidification of groundwater. High organic matter content could imply more reductive conditions in groundwater downgradient of the trench, the exact opposite is observed: pe values and [dissolved O_2] show increases. Consequently, biogeochemical processes occurring in the trench need to be better understood (reactions, kinetics, distance of influence) including whether if the trench should promote preferential flow path for rainwater infiltration.

Next, the study focuses on internal factors, starting with parameters controlling element speciation in groundwater. Following observations are made:

- pH is shown to be linked to [HCO_3^-]. Both are dependent on the carbonic system equilibrium. Increase in PCO_2 from the atmosphere to the soil and carbonate dissolution can explain pH and [HCO_3^-]

variations in groundwater. However, simulated [Ca^{2+}] and [Mg^{2+}] are slightly overestimated and are then supposed to be impacted by cation exchanges.

- Detailed study of the common redox processes occurring at the measured pe range showed that redox conditions seem to be related to decreasing [O_2] and [N-species] in the shallow groundwater downgradient of trench T22, most likely because of microbial activity, and by pyrite dissolution in deeper layers. However, pyrite was not reported in the alluvial mineral phases and this needs to be confirmed.

Weathering of Na-Feldspar, can explain the increase of [Na^+] with depth, based on the albite, montmorillonite, kaolinite and gibbsite diagram of stability (Tardy, 1971), saturation indices and albite dissolution simulation in meteoric water.

Cation exchange processes are assessed to have an influence on groundwater geochemistry, according to their proven occurrence in the aeolian layer (Szenknect, 2003) and considering an increase of CEC in the alluvial layer (Matoshko *et al.*, 2004). Cation exchange processes were simulated based on these observations and results show that it cannot be considered as the only processes involved in the increase of cation concentrations with depth. Further investigations are required to assess its role in the discrepancy between measured concentrations and simulated [Ca^{2+}] and [Mg^{2+}] in the hypothesis of carbonate dissolution.

Mixing processes could also be considered taking account of the underlying captive groundwater which may induce draining processes.

The conceptual model is summarized in Figure IV-30.

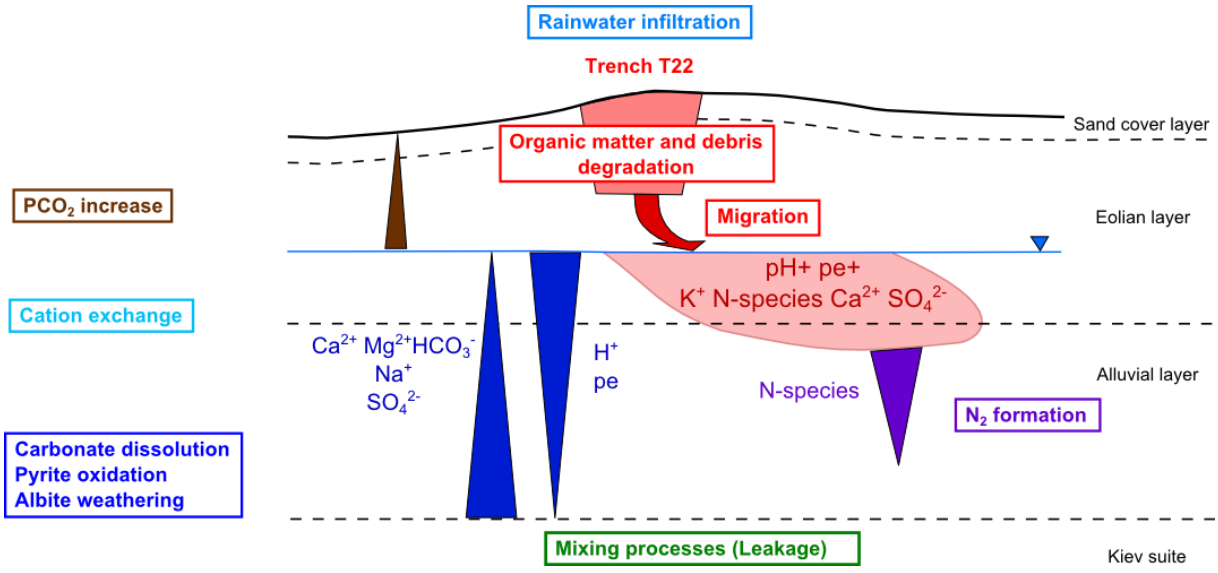

Figure IV-30: Main concentration variations and potential associated geochemical processes

Future perspectives to support this conceptual model include a more detailed mineralogical study, searching for dissolution trace on albite, presence of pyrite, kaolinite and investigation on carbonate phase characterization (dispersed calcite and marine carbonates of Kiev suite). It could contribute to characterize weathering of silicates and potential leakage processes. Those leakage processes could also be supported by piezometric and chemical data of the underlying groundwater. This potential process is important to investigate because it can bring Ca^{2+} ions, of which the concentrations are known to influence cation exchanges, and more specifically Sr (Szenknect, 2003). In addition, in the continuity of Szenknect's (2003) work, laboratory experiments of cation exchange in the alluvial layer should be carried out in order to characterize the composition of the exchanger composition.

Biogeochemical processes and preferential flow path in the trench should be better identified to explain particularly oxidizing conditions downgradient of the trench. It could be considered in the radionuclide migration forecast. For instance, uranium -which may be released by buried fuel particles dissolution at the Chernobyl Pilot Site (Ahamdach and Stammose, 2000 ; Kashparov *et al.*, 2000; Kashparov *et al.*, 2004)- is known to be really sensitive to pH/pe conditions (Langmuir, 1978)

IV.2 URANIUM MOBILITY

IV.2.1 INTRODUCTION

Fuel particles were identified among the fallout of the unit 4 explosion at the Chernobyl Nuclear Power Plant and are among the contaminated material buried in trench T22.

Since deposition, fuel particles have been weathered and their dissolution depends on their nature, their specific surface and on p*H* of the weathering solution and soils (Kashparov *et al.*, 2000; Kashparov *et al.*, 2004). Different types of fuel particles were identified (Ahamdach and Stammose, 2000; Kashparov *et al.*, 2000; Kashparov *et al.*, 2004):

- U-O particles (UO_2 and UO_{2+x}) which are fuel particles with the original structure, showing signs of cracking, as a result of a more or less pronounced oxidation.
- U-Zr-O particles, formed following the fusion of the reactor's core, resulting from the interaction between nuclear fuel and the combustible sheath in zircalloy (Zr-Nb alloy).

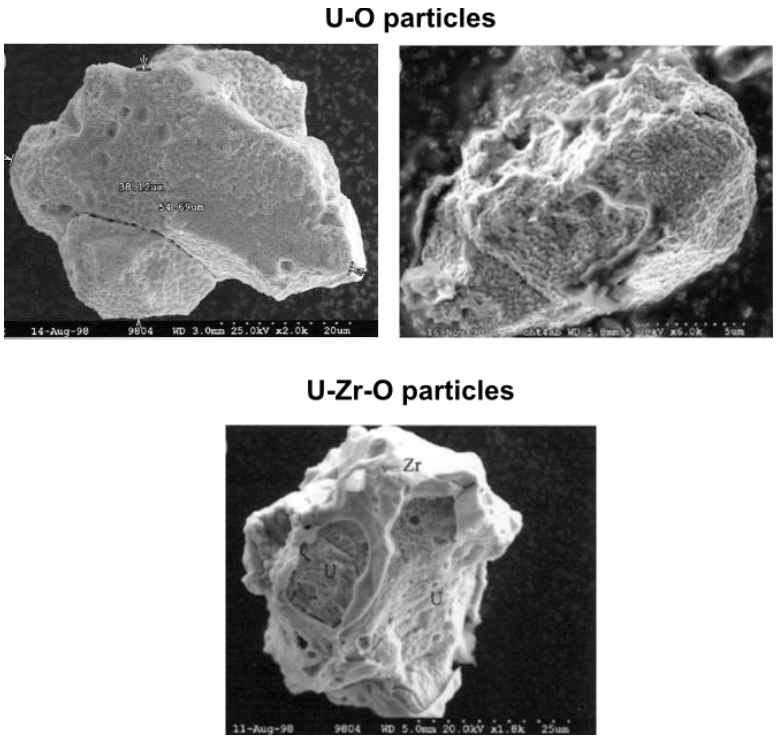

Figure IV-31: Fuel particles identified as fallout of the explosion (from Ahamdach and Stammose, 2000)

A fuel particle dissolution model was run under trench T22 conditions and showed that most oxidized particles UO_{2+x} should have dissolved today (Kashparov *et al.*, 2000; Kashparov *et al.*, 2009; Van Meir *et al.*, 2009). However, all types of particles (UO_2, UO_{2+x} and ZrU_yO_x) are still identified in the trench (Van Meir *et al.*, 2009; Kashparov *et al.*, 2012).

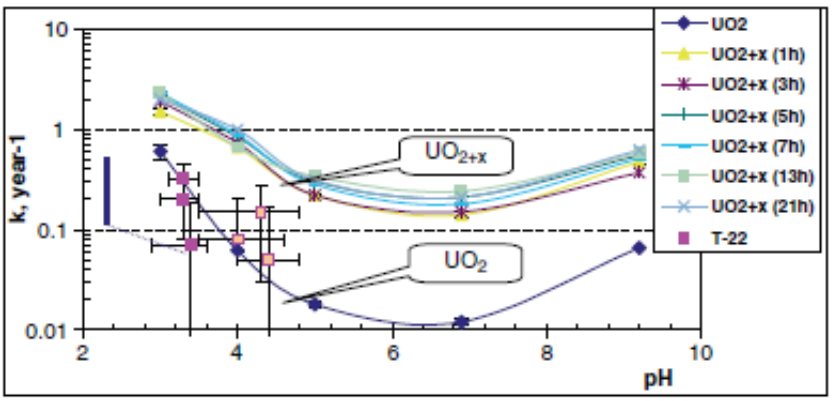

Figure IV-32: Dissolution kinetics of more-or-less annealed fuel particles, following pH of solution (figure from Van Meir et al., 2009)

The consequence of the fuel particles dissolution is the release of elements composing these particles, particularly uranium, which could then migrate in the soil and groundwater.

Uranium is a high reactive element and its migration is complex because of favored sorption processes, speciation highly depending on redox conditions and on present aqueous species, etc (Langmuir, 1978).

In order to investigate the migration of uranium released by fuel particle dissolution buried in trench T22 into groundwater, an isotopic approach was considered. Indeed, fuel particles are known to have a specific $^{238}U/^{235}U$ ratio: they were theoretically 1.1% enriched in ^{235}U content in the unit 4 core of the Chernobyl Nuclear Power Plant (Sobotovitch and Bondarenko, 2001). After the accident, $^{238}U/^{235}U$ ratio analyses were carried out on soil leachates of the near-field zone of the Chernobyl Nuclear Power Plant. Measured $^{238}U/^{235}U$ ratios ranged between 39.18 and 124.67 (Sobotovitch and Bondarenko, 2001) contrasting with the natural ratio of 137.88 ± 0.04 (Rosman and Taylor, 1998). In the Red Forest area, measured $^{238}U/^{235}U$ ratios after leaching with hydrochloric acid were 57.07 (Sobotovitch and Bondarenko, 2001). Hence, an anthropogenic uranium contamination from the trench should be easily identified in soils and groundwater.

This section aims at investigating the fate of uranium released by fuel particle dissolution in groundwater through the study of [^{238}U] concentrations and $^{238}U/^{235}U$ ratios in groundwater.

IV.2.2 MATERIAL AND METHODS

IV.2.2.1 Sampling

Two field campaigns were carried out at the Chernobyl Pilot Site, in October 2008 and in October 2009. AB profile was samples (Annex 2)

Firstly, piezometer and sampling device were purged pumping between 3 and 5 L of groundwater. Then, pH, Eh, dissolved O_2 and conductivity parameters were measured with a flow cell. The used Eh electrode is a Sentix ORP (WTW inc., in platinum), so values have to be corrected by between +217 and +214 (for temperatures between 10 and 15°C, according the user's manual). To simplify, a uniform correction of +216 is done. Then, Eh variations were reported in pe[18].

For [^{238}U] concentration were measured in the bottles used for all cation analyses (*c.f.* §IV.1.2.1). 2 L of groundwater were collected then, samples were filtered, acidified to pH below 2.5 and conditioned in 125 mL polyethylene bottles.

For $^{238}U/^{235}U$ analyses, 14 piezometers were sampled in the AB profile (7 in each campaign) with volumes ranging from 3 to 18 L. These samples were filtered and acidified at pH below 2.5.

IV.2.2.2 Uranium Analyses

[^{238}U] concentrations were analyzed at the LAME laboratory on a Multi Collector Induced Coupled Plasma Mass Spectrometer X7 CCT (Thermoelectron Inc.; Bassot *et al.*, 2010) on the acidified sampled.

IV.2.2.3 Thermo-ionisation Mass Spectrmeter method for uranium isotopic ratios analyses

$^{235}U/^{238}U$ ratios were measured on a Thermal Ionization Mass Spectrometer (TIMS) TRITON TI (ThermoScientific inc.).

Firstly, uranium is separated from the other elements on ion-exchange resin.

Then, the total evaporation is chosen for the analyses using double-filaments in rhenium (Re). That means that the uranium sample is deposited on a first Re

[18] at 25°C (Appelo and Postma, 2005)
$Eh = 0.059 \times pe$

filament (called "Evaporation" filament), heated and ionized with the help of the second Re filament (called "Ionization" filament). The ionized uranium is focused on the Mass Spectrometer magnet thanks to a lens system and isotopes are deviated depending on their respective masses. Faraday cups are placed on their trajectories and an electrical signal is emitted when isotopes hit the Faraday cups. This electrical signal is then amplified. In the total evaporation method, the whole sample electrical signal is measured and integrated. Several isotopes are analyses in the same time and the ratio of integrated signals gives isotopic ratios.

Initially, chemical separation and analysis methods on TIMS were tested in order to optimize protocols and to obtain the best possible precision and repeatability on the $^{238}U/^{235}U$ ratio measurement. Analyses are carried out for uranium quantities of 20-25 ng. This quantity was chosen to correspond to the lowest quantity of uranium in the samples, calculated from the analyses of [^{238}U] concentrations in the Chernobyl Pilot Site groundwater samples and the collected volumes of samples. Analyzing such quantities also allow limiting the time of analyses.

IV.2.2.3.1 Chemistry for uranium separation

Chemical separation protocol for uranium separation was determined according to optimal parameters defined by the constructor for the selected ion-exchange resin, *i.e.* UTEVA resin (Eichrom technologies inc.) (personal communication C.PIN).

First, samples had to be evaporated to dryness in Teflon beakers and dissolved in 0.5°mL of nitric acid [HNO_3] 5.5M.

Columns with a diameter of 2.5 mm were filled with 100 µL of UTEVA resin and were rinsed with 2x0.3 mL of nitric acid [HNO_3] 5.5M, 2x1 mL of tridistilled water, 2x0.3 mL of nitric acid [HNO_3] 3M, 2x1 mL of tridistilled water, 2x0.3 mL of nitric acid [HNO_3] 1M, 2x1 mL of tridistilled water and 2x0.3 mL of nitric acid [HNO_3] 0.05M. The column was then conditioned with 2x0.1 mL of nitric acid [HNO_3] 5.5M. The sample was then introduced in the column. Other elements were eluted with 3x0.2 mL of nitric acid [HNO_3] 5.5M. For U elution, resin aqueous solution acidity was progressively changed with the introduction of 0.1 mL of nitric acid [HNO_3] 3M, 0.1 mL of nitric acid [HNO_3] 1M and 2x1 mL of nitric acid [HNO_3] 0.05M. These elution solutions were collected in a Teflon beaker and evaporated to dryness.

Tests were carried out on natural uranium and measurements of uranium concentrations by ICP-MS before and after chemical separation showed that most of uranium was collected (more than 97%).

IV.2.2.3.2 TIMS analyses protocol description

The chosen filaments for $^{235}U/^{238}U$ ratio analyses were double-filaments in Re. For the sample analyses, the evaporation filament was hand-made whereas the ionization filament was industrial (Thermo Scientific inc.). To avoid uranium oxides formation and promote ionization, colloidal graphite was deposited "in sandwich" on the evaporation filament.

All filaments were previously degassed using the following protocol: at a pressure under 9.10^{-9} bar, intensity in filaments is increased to 4.5 A at a rate of 3 A/min and stabilized during 15 minutes. Then, the intensity in filaments is increased to 5 A at a rate of 0.5 A/min and stabilized during 15 minutes. Finally, intensity is decreased progressively at a rate of 3 A/min. Filaments are left to cool down for 2 hours before use.

For deposition of the sample, an intensity of 0.5 A is applied to the filaments. Colloidal graphite deposits were loaded with pipette whereas uranium deposit is loaded with a syringe equipped with a catheter. Then, 1 µL of colloidal graphite is deposited on the 2/3 of the surface of the rhenium filament. When this deposit is dry, another µL of colloidal graphite is deposited at the top and dried. The uranium sample is taken with diluted nitric acid HNO_3 and deposited slowly at the center of the graphite deposit to have the smallest deposit possible. When the uranium deposit has dried, 1 µL of colloidal graphite is deposited at the top and when this deposit has dried, another µL of colloidal graphite is deposited at the top and dried (Figure IV-33). The deposit is then dried at 1.5 A during 1 minute and intensity was increased until the glow of the filament for a few seconds. The inconvenience of this method is that graphite may not stick well to the Re filament, may break and fall. Nevertheless, graphite is assessed to promote uranium ionization and was shown to be essential as tests performed without graphite and no signal was visible.

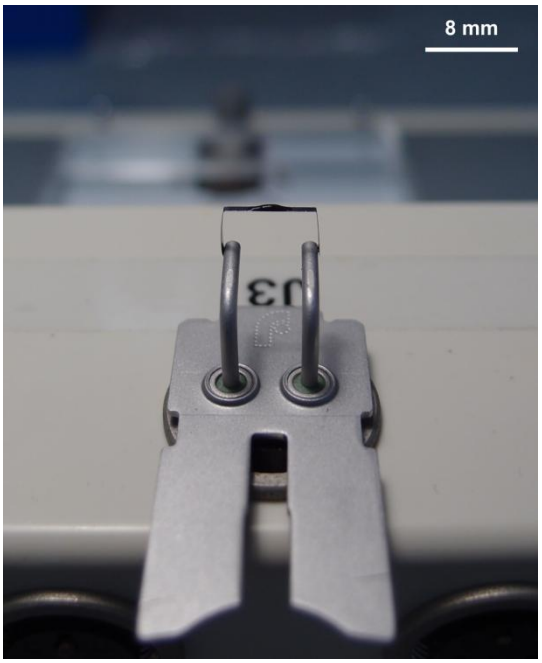

Figure IV-33: Uranium and graphite deposit on Re double-filament

After several tests to optimize the method, the following protocol was established. The central Faraday cup was the 234 mass. Intensity of the evaporation filament was raised to 800 mA at a rate of 800 mA/min. Then, intensity of the ionization filament was raised to 4500 mA at a rate of 1500 mA/min. Then, the intensity was raised progressively until ^{187}Re signal was high enough to do a first focalization on this signal: source lenses were adjusted to optimize the flux focalization and to obtain the best signal possible. Theoretically, this focalization had to be made on the analyzed element. Here, as the analysis was carried out on the total signal, a first focalization on ^{187}Re allowed losing less uranium in the steps of signal optimization. Then, the evaporation filament intensity was raised at a rate of 300 mA/min until reaching a ^{238}U signal of 1 mV. A second focalization and a peak center[19] were done on this signal. Then, the filament intensity was heated at a rate of 200 mA/min until the ^{238}U signal reached 10 mV. Then, the analysis began with the following parameters: the evaporation filament was heated until the maximal instant emission of the main isotope (Max Pilot signal) reached 800 mV, with a rate

[19] A peak center is useful to focus the isotope in the center of the Faraday cup

of 20 mA/cycle[20] (heatslope). When the Max Pilot value was reached or exceeded, intensity in the evaporation filament was decreased. The analysis stopped when the signal of the main isotope reached 0 mV. Intensity was set to not exceed 6000 mA in the evaporation filament and 4500 mA in the ionization filament. Figure IV-34 presents an example of ^{238}U signal evolution during the analysis.

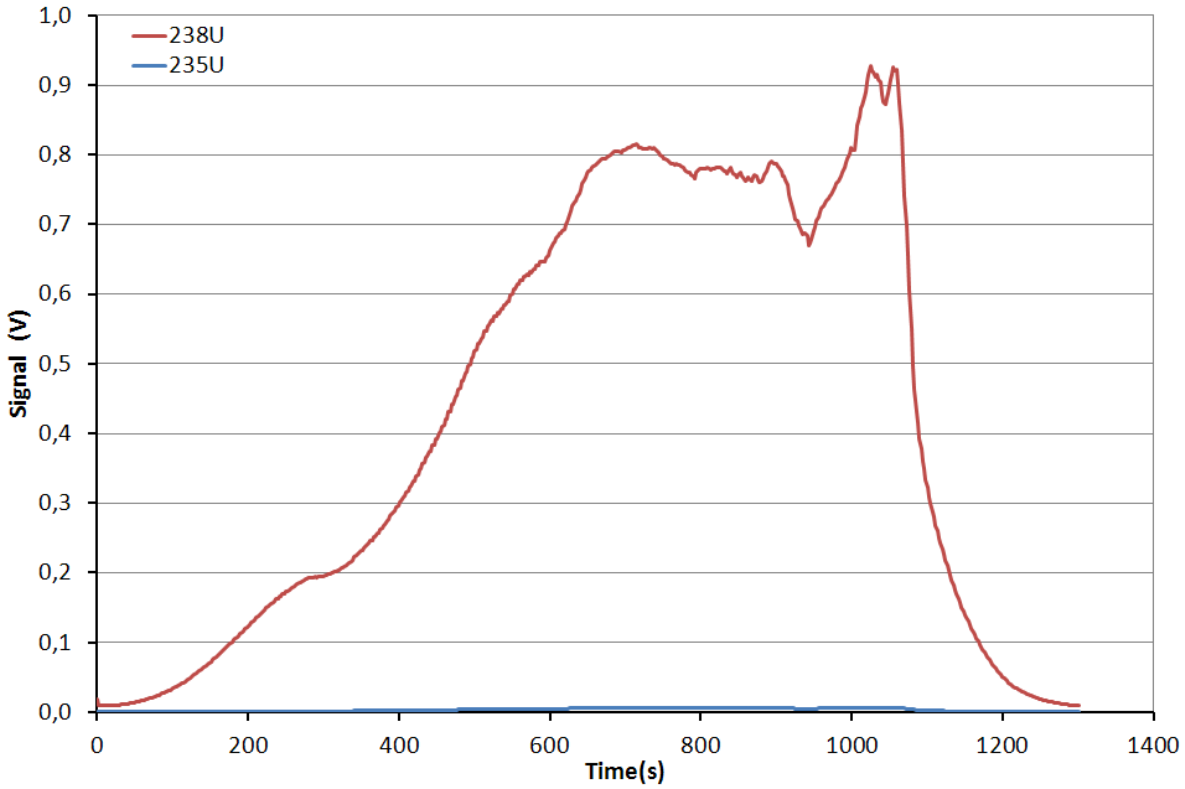

Figure IV-34: Example of signal evolution with time during an analysis

The repeatability of this analytical method was estimated based on a total of 36 analyses made on two isotopic standards: U010 ($^{238}U/^{235}U$ = 98.62; 25 analyses) and natural uranium ($^{238}U/^{235}U$ = 137.88 ; 11 analyses), respectively. The description of each standard analysis is reported in Annex 0. Figure IV-35 shows the standard measurements, giving $^{238}U/^{235}U$ ratios (in $at.at^{-1}$) in function of the final ^{235}U cumulated signal (in V). Because the ^{235}U isotope is less abundant than ^{238}U isotope, the analysis is validated when ^{235}U is enough high to be measured.

[20] Filament was heated by increasing the intensity by 20 mA, then after 2.097 sec a measurement of cumulative signal was done.

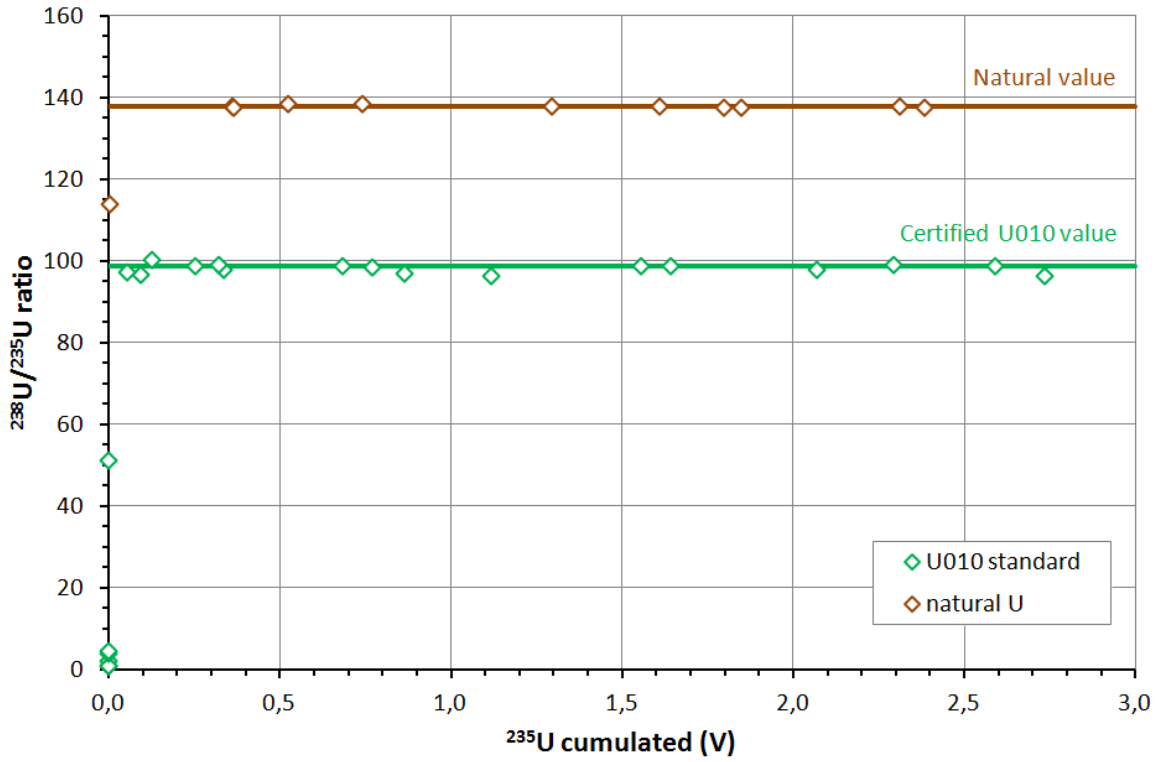

Figure IV-35: repeatability of the method of analysis

Figure IV-35 shows the measured $^{238}U/^{235}U$ ratios in the standards versus the cumulated ^{235}U signal. Repeatability of the results is good when cumulative ^{235}U signal is above 0.1 V. Table IV-2 compares mean values obtained for both standards and the standard deviation set at 2σ. At first, all the analyses are considered and then, only those with cumulative ^{235}U signal above 0.1 V are considered.

Table IV-2: Mean values and standard deviation of the method

	All the dataset		Cumulative ^{235}U above 0.1 V	
	Mean $^{238}U/^{235}U$	Standard deviation 2σ	Mean $^{238}U/^{235}U$	Standard deviation 2σ
U010	90.23	± 48.22	98.20	± 2.25
Unat	135.63	± 14.47	137.81	± 0.66

The accuracy and the standard deviation are dramatically improved considering only analysis with a cumulated ^{235}U signal above 0.1 V. Consequently, only sample analyses satisfying this requirement are hereafter taken into account.

The variability of the cumulated ^{235}U signal may be linked to the quality of the deposit, particularly of the graphite deposit, in spite of precautions taken to obtain the best possible deposit.

IV.2.2.3.3 Samples preparation

Samples were evaporated to dryness in Teflon beakers and dissolved in 0.5 mL of nitric acid [HNO_3] 5.5M. The volume of the evaporated sample is chosen to obtain 20-25°ng of uranium. Evaporated volumes for each sample are reported in Table IV-3 and Table IV-4.

Table IV-3: Evaporated volumes for each sample (October 2008)

	OCTOBER 2008		
	Concentration in [^{238}U] (mol/L)	Estimation of evaporated volume (L)	Estimated quantity of U (ng)
8-01-1	2.10^{-09}	0.1	50
19-00-2	3.10^{-09}	0.1	61
6-01-2	7.10^{-10}	0.34	60
2-02-2	5.10^{-10}	0.375	42
1-98-1	3.10^{-11}	6	48
1-98-2	3.10^{-11}	6	36
1-98-3	2.10^{-11}	6	24

Table IV-4: Evaporated volumes for each sample (October 2009)

	OCTOBER 2009		
	Concentration in [^{238}U] (mol/L)	Estimation of evaporated volume (L)	Estimated quantity of U (ng)
8-01-2	5.10^{-10}	0.275	33
19-00-2	2.10^{-09}	0.15	66
7-00	5.10^{-11}	5	62
7-01-1	7.10^{-10}	1	167
7-01-2	3.10^{-10}	1	68
18-00-1	1.10^{-09}	0.5	123
5-01-2	3.10^{-10}	1	73

IV.2.2.3.4 Blank analyses

In order to avoid any external contamination of the samples, their preparation was done using a specific installation. At Nimes University, samples were prepared in a clean room Class 100: incoming air is filtered to remove particles. At the CEA-Marcoule, no clean room was associated to the TIMS. Consequently a specific installation was set up in order to filter the incoming air to approach conditions prevailing in a Class 100 clean room: a fume cupboard is modified with the addition of a Plexiglas seal equipped with two filters H14 type[21] at the front of the fume cupboard (Figure IV-36).

[21] Filtration efficiency : 99.995%

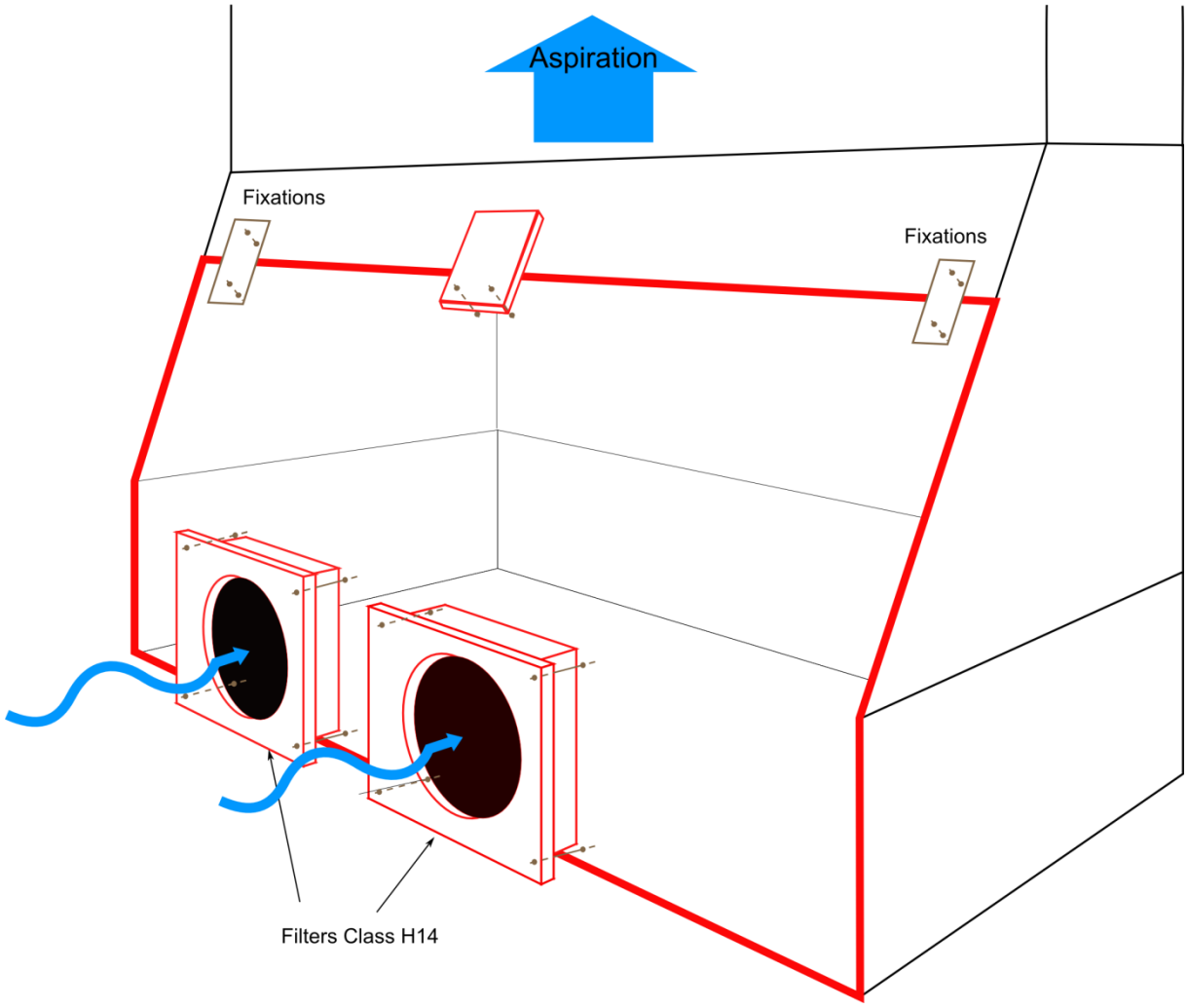

Figure IV-36: Equipment to hinder external contamination at the CEA-Marcoule designed at the University of Nîmes (Laboratory of Environmental Isotopic Geochemistry laboratory)

In both cases, standards and blanks were prepared under the same conditions in order to evaluate potential contamination.

In addition to standard analyses, one groundwater sample (from the 18-00-1 piezometer in October 2009) was analyzed several times at Nîmes University and at the CEA-Marcoule in order to compare both environments. This sample was chosen because of its high volume available considering the volume needed to obtain 25 ng of uranium. Figure IV-37 shows results obtained on the repeated analyses of the groundwater sampled in the 18-00-1 piezometer in October 2009.

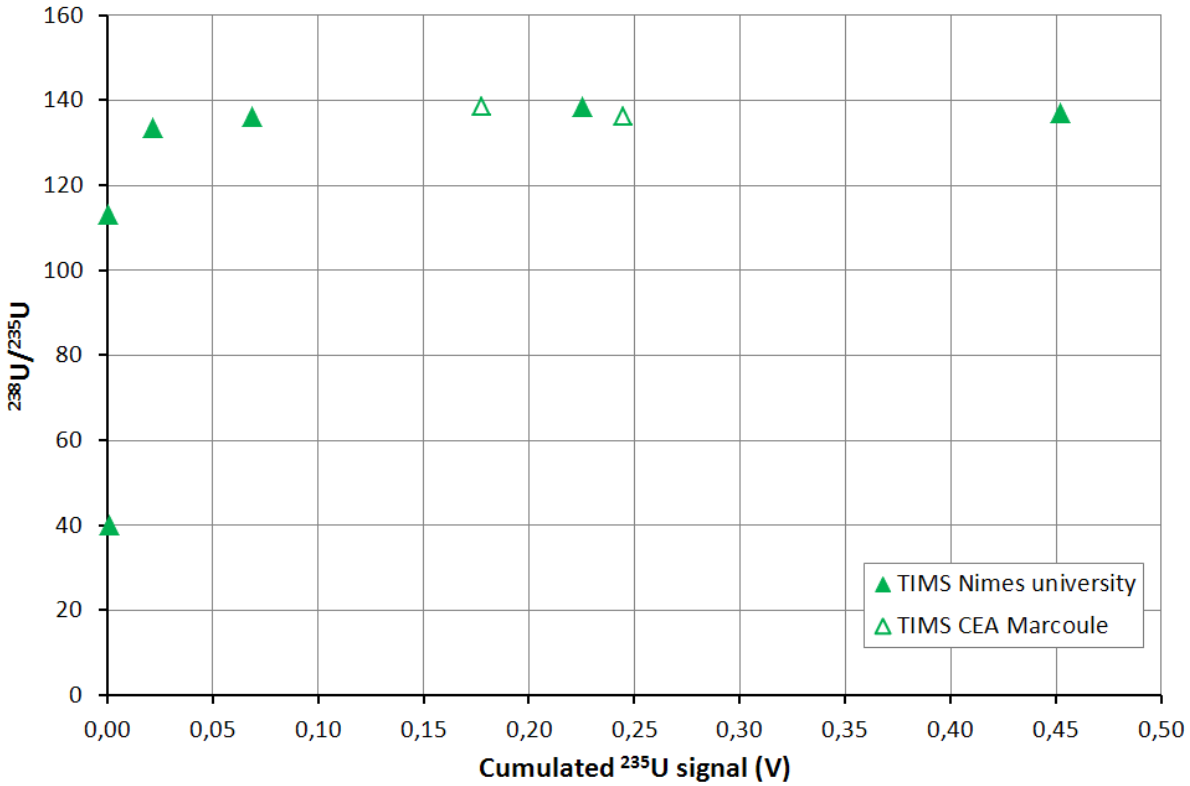

Figure IV-37: Duplicates analyses of sample collected in 18-00-1 piezometer in October 2009

Similar results were obtained at both facilities.

Finally, to validate of the protocol, chemical blanks were analyzed for U concentrations on ICP-MS. Hence, 7 mL-beakers (one at Nîmes University, and one at the CEA-Marcoule) without sample were left opened during the whole evaporation step nearby evaporating samples and were used as blanks for the chemistry. They received the same acid doses as those used for sample preparation, which had been passed through a new column. Then, the liquid phase was evaporated, similarly as for the samples. These beakers were then rinsed with 1.5 mL of a solution of HNO_3 2% and this solution was analyzed by MC ICP-MS at the IRSN/LAME laboratory to determine the uranium content. To assess the uncertainty on the measure, five analyses were performed on "blank" instead of the three performed classically (Bassot *et al.*, 2010). Uranium content remained under the detection limit or slightly above, showing a minimal contamination. Results are shown in Table IV-5.

Table IV-5: Blanks analyses

	^{238}U content of chemistry blanks (ng)
Nimes University blank	0.002 Estimated uncertainty: 0.0002
CEA-Marcoule blank	<0.002 (under detection limit) Estimated uncertainty: 0.0002

However, the impact of such "contamination" on the $^{238}U/^{235}U$ measured can be estimated from the equation (Equation IV-1) below:

Equation IV-1

$$\left(\frac{^{235}U}{^{238}U}\right)_{mix} = \frac{^{235}U_{ini} + ^{235}U_{nat}}{^{238}U_{tot}} = \frac{^{235}U_{ini}}{^{235}U_{tot}} \times \frac{^{238}U_{ini}}{^{238}U_{ini}} + \frac{^{235}U_{nat}}{^{238}U_{tot}} \times \frac{^{238}U_{nat}}{^{238}U_{nat}}$$

Equation IV-2

$$\left(\frac{^{235}U}{^{238}U}\right)_{mix} = \left(\frac{^{235}U}{^{238}U}\right)_{ini} \times \frac{^{238}U_{ini}}{^{238}U_{Tot}} + \left(\frac{^{235}U}{^{238}U}\right)_{nat} \times \frac{^{238}U_{nat}}{^{238}U_{Tot}}$$

where

- $(^{235}U/^{238}U)_{mix}$ is the ratio in the sample "contaminated" by natural uranium during the preparation of the sample
- $(^{235}U/^{238}U)_{ini}$ is the initial ratio in sample (for instance, $^{235}U/^{238}U$ = 0.0175 or $^{238}U/^{235}U$ = 57.07) (Sobotovitch and Bondarenko, 2001).
- $(^{235}U/^{238}U)_{nat}$ is the ratio in the potential added Uranium, theoretically natural: $^{235}U/^{238}U$ = 0.0072527 ($^{238}U/^{235}U$ = 137.88) (Rosman and Taylor, 1998).
- $^{238}U_{nat}$ is the concentration measured in the sample, in $at.L^{-1}$.

Considering a maximum contamination of 0.002 ng (5.10^9 atoms) in 20 ng of ^{238}U (5.10^{13} atoms):

Equation IV-3

$$\left(\frac{^{235}U}{^{238}U}\right)_{mix} = 0.0175 \times \frac{5\times10^{13}}{5\times10^{13}+5\times10^{9}} + 0.0072527 \times \frac{5\times10^{9}}{5\times10^{13}+5\times10^{9}}$$

Then, $^{235}U/^{238}U$ equals to 0.01752 and $^{238}U/^{235}U$ = 57.073)

Such contamination would be negligible with respect to the standard deviation of 2.25 characterizing the method of analyses.

IV.2.3 RESULTS AND DISCUSSION

IV.2.3.1 Results

Measured Eh values, pe, uranium-238 concentrations and measured $^{238}U/^{235}U$ ratios are given in Annex 20 and 21.

pe variations were already discussed in the section IV.1.4.3.2. As U speciation is affected by redox condition pe variations are reminded below. In October 2008 and October 2009 on the AB profile, pe values range between 1.8 and 9.7. A slight decrease in pe is observed with increasing depth and more oxidizing conditions are shown in groundwater downgradient of the trench T22 (Figure IV-38). pe is closely linked to dissolved O_2 concentrations, [Fe] and $[SO_4^{2-}]$ and microbial activity and pyrite oxidation were suggested to explain such trends.

Uranium-238 concentrations ($[^{238}U]$) in Chernobyl Pilot Site groundwater range between 1.7×10^{-11} (sampled in the 1-98-3 piezometer in October 2008) and 5.7×10^{-9} $mol.L^{-1}$ (sampled in the 1-06-1 piezometer in October 2008). Concentrations above 10^{-9} $mol.L^{-1}$ are sampled downgradient of trench T22 while groundwater sampled upgradient and in deeper part show concentrations in the order of 10^{-11} $mol.L^{-1}$.

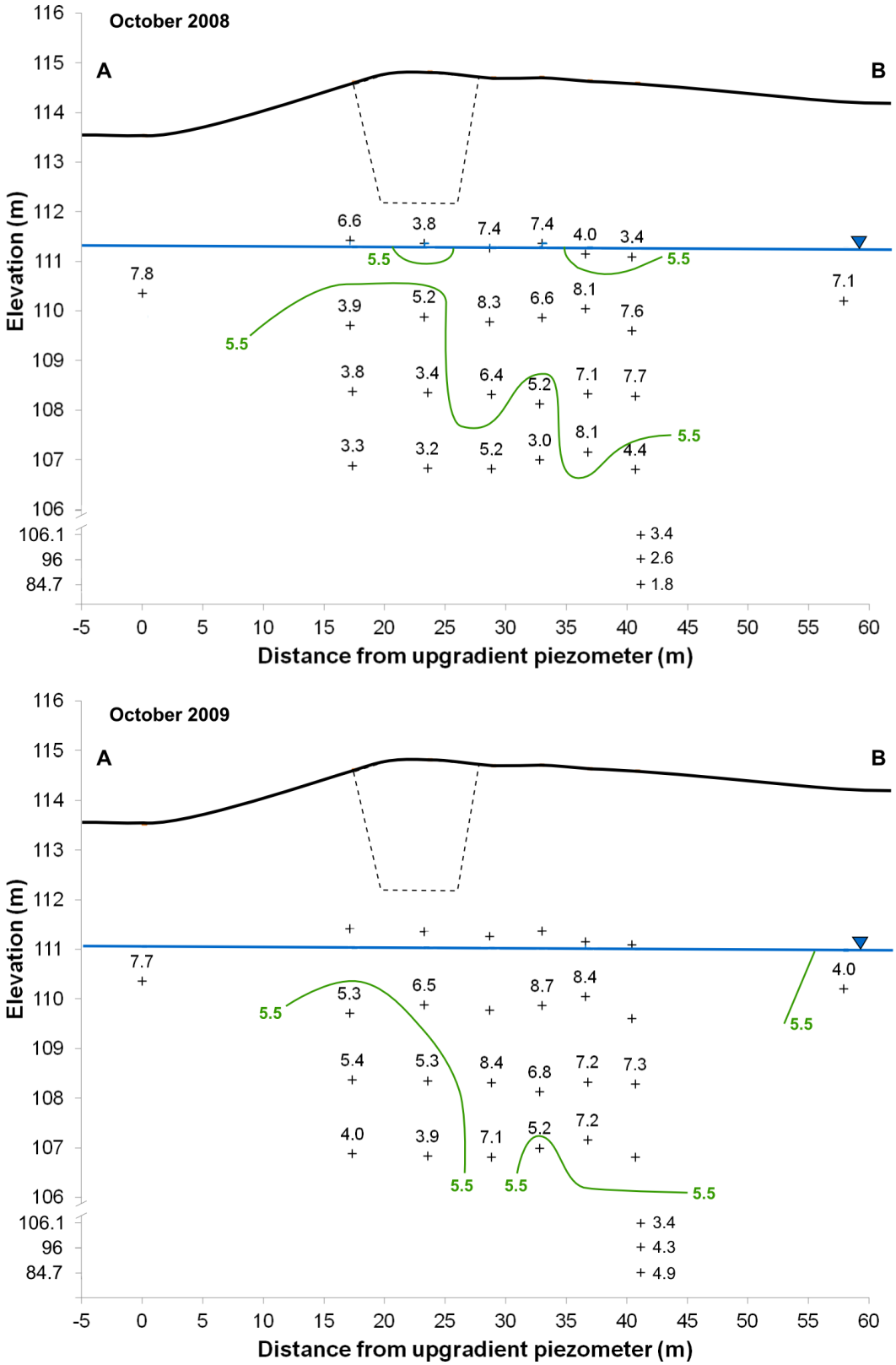

Figure IV-38: pe values observed in October 2008 and October 2009 in piezometers of the AB-profile

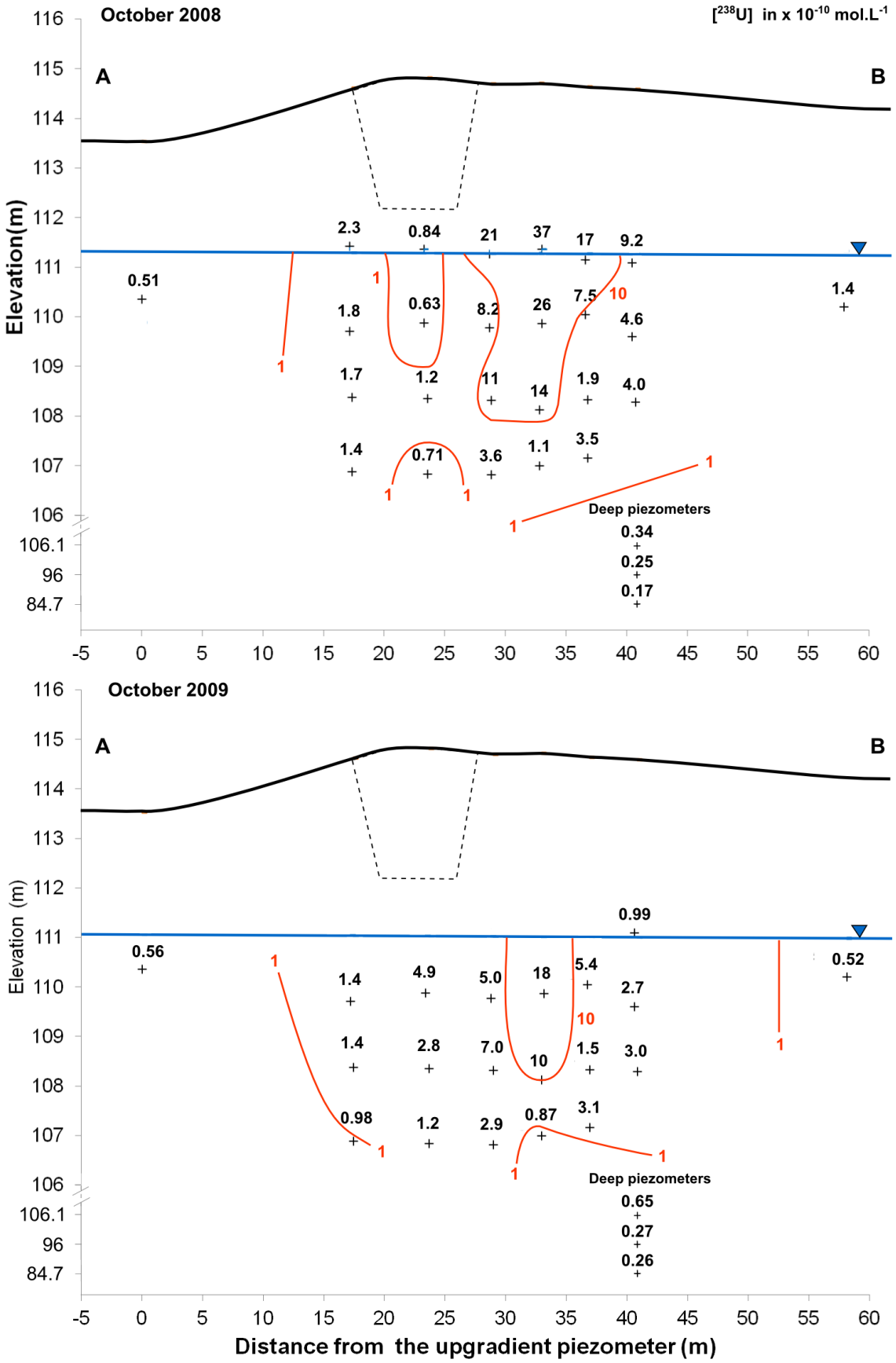

Figure IV-39: [^{238}U] along the AB profile in October 2008 and in October 2009

$^{238}U/^{235}U$ ratio analyses on Thermal ionization mass spectrometer (TIMS) with cumulated ^{235}U signal up to 0.1 V show ratios ranging from 136.3 (piezometer 18-00-1 sampled in October 2009) to 140.0 (piezometer 8-01-1 sampled in October 2008) (Figure IV-40). Surprisingly, these ratios are within the range of natural U, taking into account the analytical uncertainties based on the standard deviation of isotopic standard analyses. On Figure IV-40, $^{238}U/^{235}U$ ratios measured in Chernobyl Pilot Site groundwater are reported versus their cumulated ^{235}U signal, the natural $^{238}U/^{235}U$ ratio and 2σ standard deviation around the natural value are shown in red for comparison.

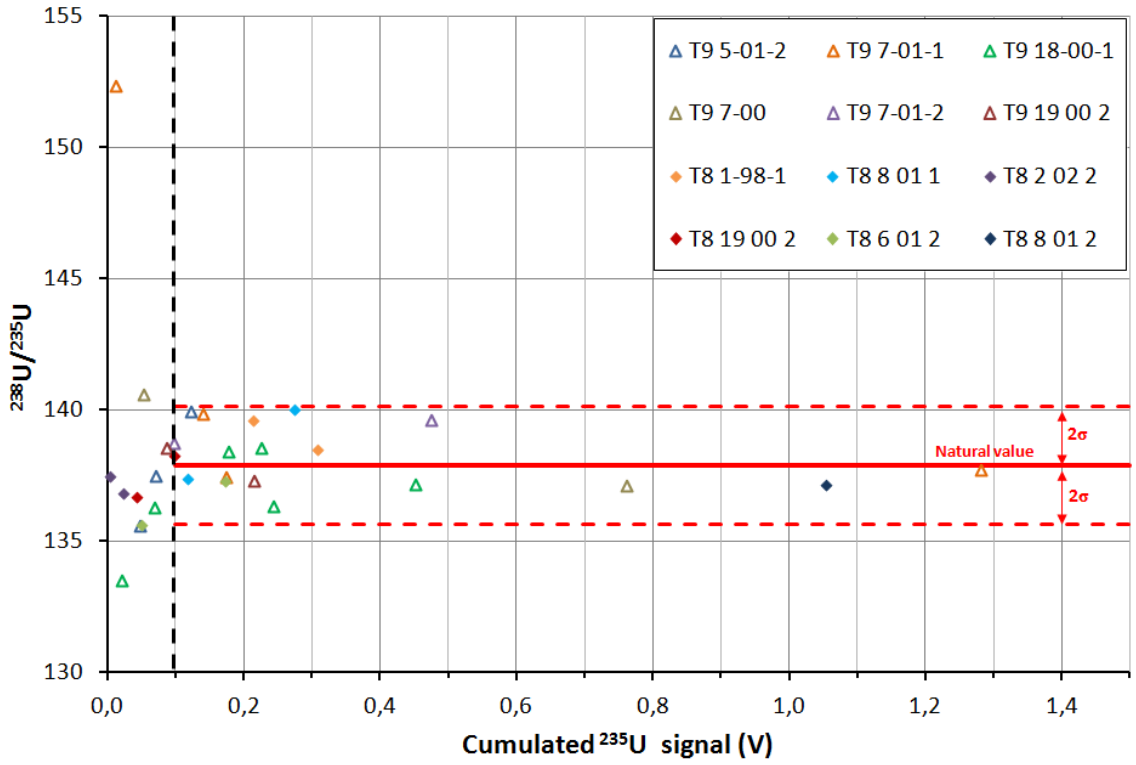

Figure IV-40: $^{238}U/^{235}U$ ratios in Chernobyl Pilot Site groundwater samples

IV.2.3.2 Implication of the natural $^{238}U/^{235}U$ ratios measured in groundwater

The first observation is that [^{238}U] increase by two orders of magnitude downgradient of trench T22, as it is shown on Figure IV-39. This increase in [^{238}U] could be explained by the migration of uranium released by dissolution of the fuel particles buried in the trench (Kashparov *et al.*, 2004), maybe facilitated by the redox changes in the trench. However, this increase in [^{238}U] seems to be closely

linked to the oxidation conditions downgradient of the trench (Figure IV-38; Figure IV-39). Following this hypothesis, the impact of U from fuel particle dissolution on the $^{238}U/^{235}U$ ratio in groundwater can be calculated as follows:

Equation IV-15

$$\left(\frac{^{235}U}{^{238}U}\right)_{GW} = \frac{^{235}U_{FP} + ^{235}U_{nat}}{^{238}U_{FP+nat}} = \frac{^{235}U_{FP}}{^{235}U_{FP+nat}} * \frac{^{238}U_{FP}}{^{238}U_{FP}} + \frac{^{235}U_{nat}}{^{238}U_{FP+nat}} * \frac{^{238}U_{nat}}{^{238}U_{nat}}$$

Equation IV-16

$$\left(\frac{^{235}U}{^{238}U}\right)_{GW} = \left(\frac{^{235}U}{^{238}U}\right)_{FP} * \frac{^{238}U_{FP}}{^{238}U_{FP+nat}} + \left(\frac{^{235}U}{^{238}U}\right)_{nat} * \frac{^{238}U_{nat}}{^{238}U_{FP+nat}}$$

where

- $(^{235}U/^{238}U)_{GW}$ is the theoretical ratio in groundwater, downgradient of the trench, in the piezometer showing the highest $[^{238}U]$ concentration;
- $(^{235}U/^{238}U)_{FP}$ is the ratio of 0.0175 ($^{238}U/^{235}U$ = 57.07) measured in solutions-leachates from the fuel particles in the red forest soils (Sobotovitch and Bondarenko, 2001).
- $(^{235}U/^{238}U)_{nat}$, the natural ratio of 0.0072527 ($^{238}U/^{235}U$ = 137.88) (Rosman and Taylor, 1998).
- $^{238}U_{FP+nat}$ is the highest quantity of ^{238}U measured in groundwater, downgradient of the trench. It corresponds to the maximum $[^{238}U]$ concentration measured in the present groundwater samples, around 4 $x10^{-9}$ $mol.L^{-1}$.
- If the increase in $[^{238}U]$ concentration is entirely due to the migration of uranium released by the dissolution of fuel particl[es, $^{238}U_{nat}$ is the ^{238}U quantity in the area less impacted by the presence of the trench, i.e. in groundwater just upgradient of trench T22 (groundwater sampled in 19-00-1 piezometer in October 2008). It corresponds to the $[^{238}U]$ measured upgradient of the trench: in the present dataset this value is approximately $1x10^{-10}$ $mol.L^{-1}$.
- $^{238}U_{FP}$ [is] the ^{238}U quantity which should have migrated from the trench to the groundwater. It corresponds to $^{238}U_{FP+nat}$ - $^{238}U_{nat}$, which is equals to 3.9 $x10^{-9}$ $mol.L^{-1}$.

Consequently, according to Equation IV-16, the $^{235}U/^{238}U$ theoretical ratio in groundwater showing the highest $[^{238}U]$ should be 0.0173, equivalent to a theoretical $^{238}U/^{235}U$ ratio of 57.9. The released uranium would dominate and $^{238}U/^{235}U$ ratio would be close to that of the fuel particles. Even considering the analytical uncertainty, the impact on $^{238}U/^{235}U$ ratio should be detectable.

However, measured $^{238}U/^{235}U$ ratios show values higher than this theoretical ratio: these ratios are close to the natural $^{238}U/^{235}U$ ratio of 137.88 (Rosman and Taylor, 1998), considering the standard deviation on measurement of approximately 2.25, as it is shown in Figure IV-40. The increase in [^{238}U] downgradient of the trench T22 cannot be linked to the migration of uranium released by the dissolution of fuel particles.

This is quite surprising considering that previous studies have shown that oxidized fuel particles are most likely altered if not entirely dissolved in the contaminated area (Ahamdach and Stammose, 2000 ; Kashparov *et al.*, 2000; Kashparov *et al.*, 2004a; Kashparov *et al.*, 2009; Van Meir *et al.*, 2009 ; Kashparov *et al.*, 2012).

Several hypotheses can be made to explain the lack of anthropogenic signal in the $^{238}U/^{235}U$ ratio in groundwater in spite of the assessed dissolution of fuel particles. The first is that natural leaching by rainwater, with a pH around 5-5.5, is not acid enough to leach uranium with sufficient efficiency to change $^{235}U/^{238}U$ ratio in groundwater. Indeed, leaching studies on fuel particles of the fallout have been performed and it was shown that depending on the acid used and the successive leachings, $^{238}U/^{235}U$ ratio range from the fuel particles theoretical ratio to higher ratio: Sobotovitch and Bondarenko, 2001 measured 238U/235U ratios ranging from 94.9 to 114.5 in several successive leachate solutions of a fuel fragment (1N HCl, 6.8N HCl + 7.5N HNO_3, 6.8N HCl, 6.8N HCl and HCl 7N). The second is that uranium of the dissolved oxidized particles has been released but moves under another form than dissolved uranium, with colloids for instance. Indeed, as groundwater is filtered before sampling, an important fraction of colloids may be removed from the groundwater sample and their U content cannot be measured. The third hypothesis is that the anthropogenic signal could be already out of the represented trench profile (velocity in the aeolian layer: 11 $m.y^{-1}$, Bugai *et al.*, 2012b). The last hypothesis is the retention of uranium in biosphere. Uranium could be trapped because of the bacteria activity present in the trench (Chapon *et al.*, 2012). For instance, sulfate-reductive bacteria were shown to promote uraninite precipitation because of redox changes they impose (Phrommavanh, 2008). Uranium uptake by growing vegetation is also shown, particularly by root uptake (Thiry *et al.*, 2005; Shtangeeva, 2010). This root uptake depends on uranium bioavailability and soil type (Shtangeeva, 2010). In pines, the uranium is mainly stored in the root zone

and humus: an uranium amount of 11020 µg.kg^{-1} was measured in 35-year-old Scots pine roots growing on a revegetated uranium mining heap (Thiry *et al.*, 2005). Similar studies could be carried out on uranium compartments in vegetation at the Chernobyl Pilot Site and coupled with isotopic approaches to understand the uranium migration, determining the fluxes involved.

IV.2.3.3 Potential origins of [^{238}U] increases downgradient of trench T22

As the anthropogenic uranium is not shown in groundwater, other processes have to be considered to explain the increase in [^{238}U] downgradient of trench T22. One of the hypotheses is the mobilization of naturally immobile uranium by changes in redox conditions downgradient of the trench. Indeed, in the aquifer, uranium content is controlled by the leachable uranium, the proximity of the water to uranium-bearing minerals, the degree of isolation of water from dilution by surface water, evapotranspiration parameters, pH and Eh conditions, the potential insoluble Uranium complexes which depend on concentrations in C, P, V, F, S, Si, Ca, K and the presence of sorptive materials as organic matter, oxides of Fe, Mn, Ti or clays (Langmuir, 1978). In order to investigate the dependence of [^{238}U] with redox condition evolution, [^{238}U] are compared with pe values in Figure IV-41.

For October 2008 groundwater sample representation, full symbols are used: the aeolian layer data are represented with red squares while data of the aeolian/alluvial interface with purple triangles and alluvial data with blue diamonds. For October 2009 groundwater sample representation, the same but void symbols are used: the aeolian layer data are represented with a red outline while data of the aeolian/alluvial interface with a purple outline and alluvial data with blue outline. Names of piezometers located downgradient of trench T22, either in the aeolian layer or at the aeolian/alluvial interface, are reported.

[^{238}U] seem to increase with the increasing pe values. The increase in [^{238}U] might be linked to the mobilization of uranium under oxidizing conditions: it could be under an immobile form in reductive conditions in the aquifer and become soluble under the increasing oxidizing conditions.

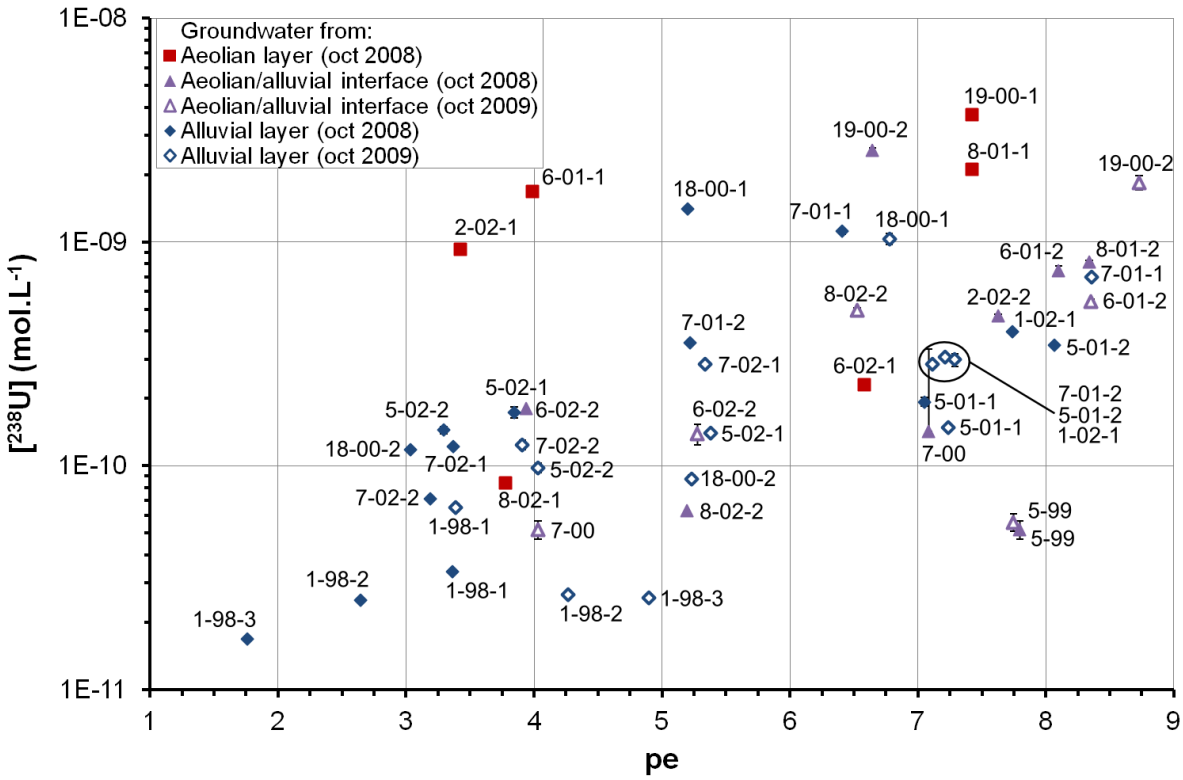

Figure IV-41: [^{238}U] concentrations evolution with pe variations

The Pourbaix diagram of uranium in the groundwater conditions may support the dependence of uranium mobility following redox changes downgradient of trench T22. Indeed, speciation of uranium has a high influence on uranium mobility, as shown by the Pourbaix diagram in (Figure IV-42) for uranium concentrations of 10^{-9} mol.L^{-1}. Groundwater samples are reported for comparison.

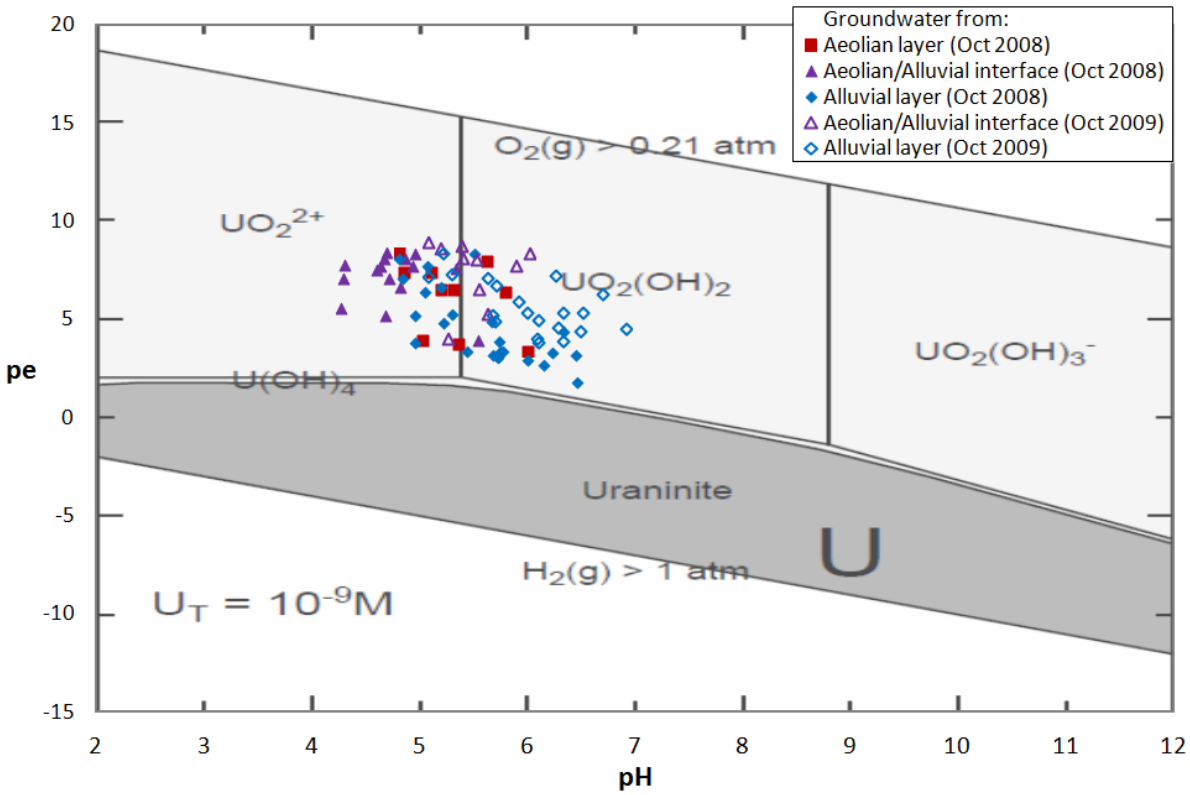

Figure IV-42: Uranium speciation for uranium concentrations of 10^{-9} mol.L^{-1} (database lnll.dat). Only uranium is considered.

Physical-chemical conditions in groundwater are favorable to uranium speciation under UO_2^{2+}/$UO_2(OH)_2$ species, which are soluble. Some groundwater samples collected in alluvial layer are close to the uraninite domain boundary. Locally more reductive conditions may prevail, potentially because of microbial activity (Phrommavanh, 2008; Ahmed *et al.*, 2012) or if the Eh measurement is overestimated, then uraninite may be stable.

Uranium speciation also depends on other species in solution (Langmuir, 1978). Two diagrams are built, each considering a particular uranium concentration: 10^{-9} mol.L^{-1} (Figure IV-43) or 10^{-11} mol.L^{-1} (Figure IV-44). Si, HCO_3, S (activity: 0.0001 each) and Fe (activity: 0.00001) are added to the system, according to their mean concentrations in the Chernobyl Pilot Site groundwater (see §IV.1).

Both diagrams show similar domains and groundwater samples still fall within the soluble domains, most likely due to the low concentrations considered. This information limits the hypothesis of the mobilization/precipitation of uranium because of a redox changes.

The question remaining is if these redox changes might increase the kinetic of dissolution of potential uranium minerals or might have an impact on desorption of uranium retained on mineral surfaces. Such releases of uranium complexed at mineral surfaces were shown at the Hanford site 300A to explain the persistence of uranium plume (Zachara *et al.*, 2013). To support this hypothesis, additional studies have to be carried out. As [^{238}U] seem to stay closely linked to the Eh/pe values (Figure IV-41), it could be interesting to study the influence of an increase of pe on [^{238}U] in water in contact with the aeolian and alluvial sands and then, if an increase of [^{238}U] is observed, searching to identify the origin of uranium.

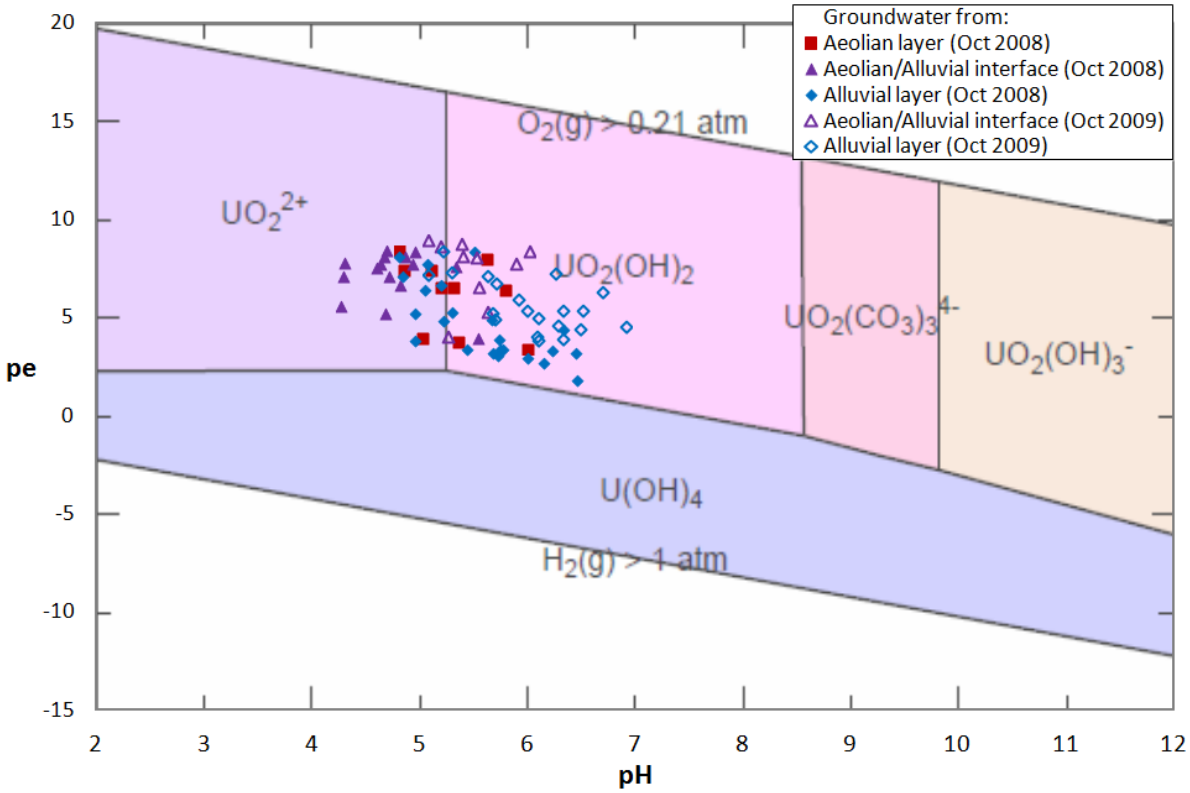

Figure IV-43: Pourbaix diagram for [U] = 10^{-11} mol.L^{-1}, considering possible complexations with Si, HCO3, S and Fe (database lnll.dat)

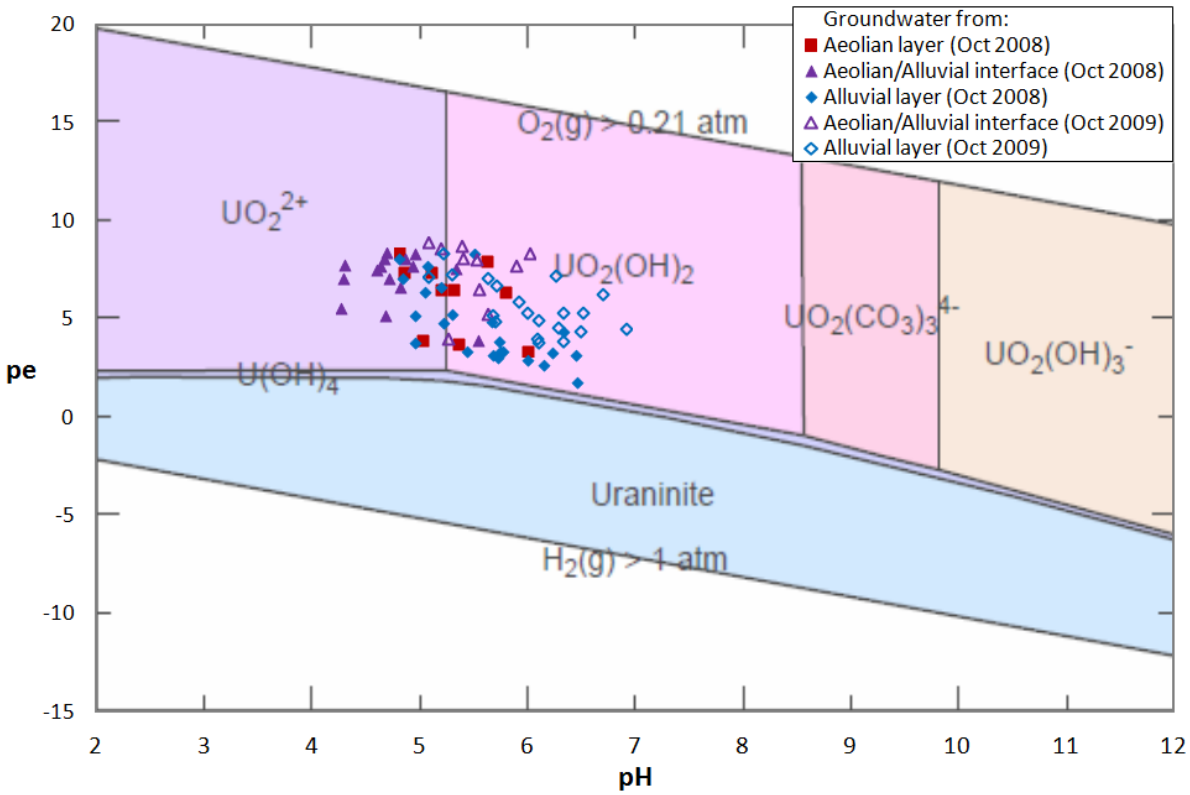

Figure IV-44: Pourbaix diagram for [U] = 10^{-9} mol.L^{-1}, considering possible complexations with Si, HCO3, S and Fe (database lnll.dat)

IV.2.4 CONCLUSION

Uranium migration is investigated based on the study of the isotopic variation of $^{238}U/^{235}U$ ratio in groundwater. This ratio is supposed to be highly impacted by the migration of uranium released by the dissolution of fuel particles from the trench T22.

$^{238}U/^{235}U$ ratios were analyzed on Thermal Ionization Mass Spectrometer by the total evaporation method using double rhenium filaments with addition of colloidal graphite. An analytical method was optimized and good precision and repeatability of the method was shown for analyses of two isotopic standards.

Results showed that $^{238}U/^{235}U$ ratios in groundwater are in the range of the natural ratio, despite of [^{238}U] increasing in groundwater by two orders of magnitude downgradient of trench T22. Consequently, this increase of [^{238}U] downgradient of the trench is not linked to the migration of uranium released by the dissolution of fuel particles.

As fuel particles dissolution was previously shown, several hypotheses may explain that the fuel particle $^{238}U/^{235}U$ signal is not shown in groundwater:

- weathering of fuel particles could not be enough to modify $^{238}U/^{235}U$ ratio in soils solution and groundwater,
- the uranium could be trapped in soils and biosphere (microbial activity, vegetation),
- the anthropogenic signal has already left the profile
- uranium migrate attached to colloids.

Then, the origin of the increase of [^{238}U] downgradient of the trench has to be answered. Uranium seems to be mobile in groundwater. Hence, the question remains if the dissolution of uranium minerals or the release of uranium sorbed on mineral surfaces could be intensified by oxidizing conditions.

These hypotheses are summarized in Figure IV-45.

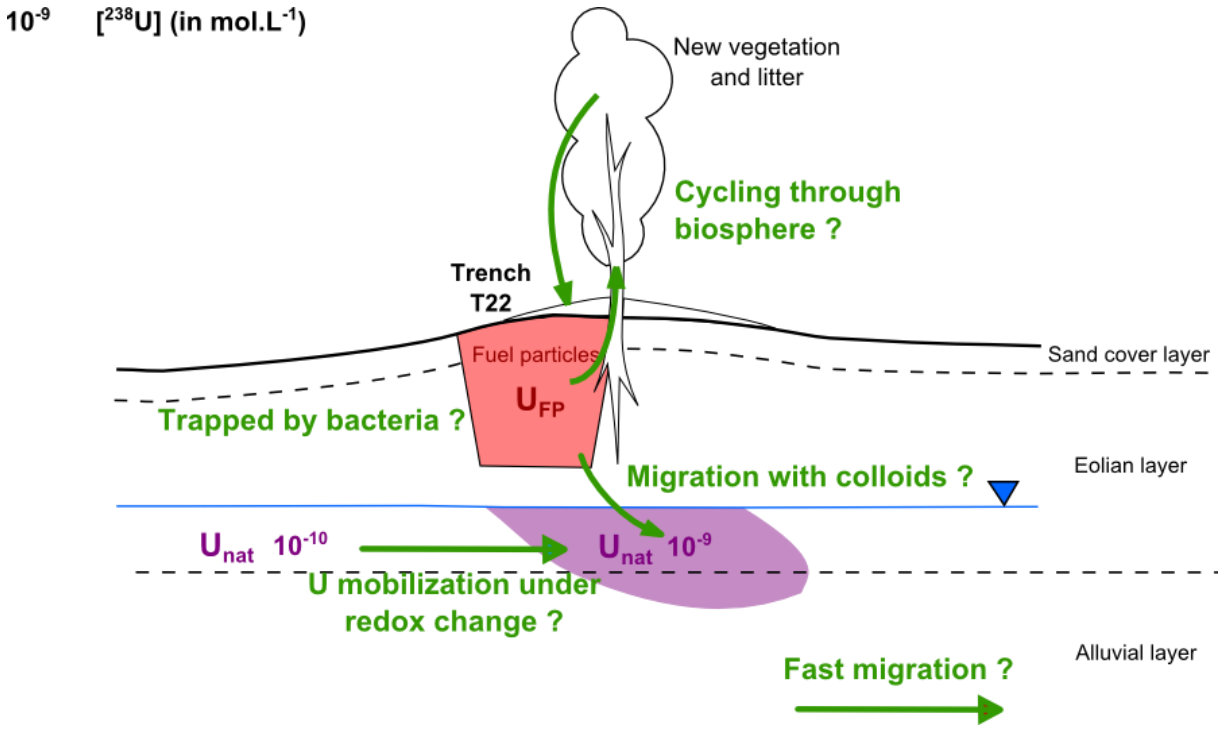

Figure IV-45: Main results and hypotheses

Such issues could be answered by laboratory experiments on impact of redox changes on [^{238}U] concentrations in water in contact with aeolian and alluvial sands. A more detailed study of uranium content and $^{238U}/^{235}U$ ratios in the different compartments (biosphere, soils, soil water, groundwater) should help to understand uranium behavior.

IV.3 STRONTIUM BEHAVIOR

IV.3.1 INTRODUCTION

At the Chernobyl Pilot Site, an important groundwater contamination results from strontium-90 migration from the trench T22.

This ^{90}Sr is assessed to be leached from the trench, tempered by biosphere uptakes (Thiry *et al.*, 2009, Bugai et al., 2012a, Martin-Garin *et al.*, 2012). In groundwater, a ^{90}Sr plume is shown downgradient of the trench with volumetric activities of 1000 $Bq.L^{-1}$ up to 15 meters far from the trench (Dewiere et al., 2004). ^{90}Sr migration velocity was shown to be 9% of the groundwater flow velocity (Dewiere et al., 2004). To explain that delay, cation exchange processes were assumed to govern ^{90}Sr retention (Dewière et al., 2004 ; Bugai et al., 2012a). In the upper aeolian layer, these processes were investigated and quantified by laboratory experiments (Szenknect, 2003). In the underlying alluvial layer, a higher cation exchange capacity was shown: values are of 5-10 meq/100g while they are of ~1 meq/100g in the aeolian layer. Consequently cation exchange processes are assumed to be more important (Matoshko *et al.*, 2004). However, ^{90}Sr retention by cation exchange processes may be influenced by competition on exchange sites with other strontium isotopes and calcium, as suggested by Szenknect (2003) and Mazet (2008). The concentrations in these elements may be influenced by additional geochemical processes, such as carbonate dissolution (see Chapter IV.1).

In order to better constrain the strontium behavior in Chernobyl Pilot Site groundwater, an isotopic approach can be considered. The most abundant strontium isotopes are ^{84}Sr, ^{86}Sr, ^{87}Sr and ^{88}Sr (Nier, 1936; Rosman and Taylor, 1998). As a relatively heavy element, strontium is assessed to be less impacted by fractionation processes than lighter elements, and strontium isotopic ratios are considered to be independant of temperature and biological processes (Capo *et al.*, 1998). Consequently, most of these natural isotopes exist in relatively stable proportions in environment. However, ^{87}Sr content is influenced by the presence of ^{87}Rb in the studied material, because ^{87}Rb is non stable and decays in ^{87}Sr. In rocks, ^{87}Sr content increases with rock age because the decay of the lithophilic ^{87}Rb produces ^{87}Sr (Capo *et al.*, 1998). Marine carbonates are also known to record $^{87}Sr/^{86}Sr$ ratio of seawater at the time of rock formation, ranging between 0.708

and 0.709 for the past 6 Ma (Capo *et al.*, 1998). In groundwater, $^{87}Sr/^{86}Sr$ ratios are closely linked to bedrock weathering and precipitations. Based on these principles, $^{87}Sr/^{86}Sr$ ratio is commonly used as tracer of origins of natural material (Capo *et al.*, 1998). At the Chernobyl Pilot Site, anthropogenic strontium could also impact on strontium isotopic ratios because ^{87}Sr, ^{88}Sr and ^{90}Sr are produced by uranium fission (Naudet, 1991).

However, this potential anthropogenic production implies a change in the analytical method of strontium isotopic ratio measurement. On Thermal-Ionization Mass Spectrometer (TIMS), the common method for $^{87}Sr/^{86}Sr$ ratio analysis is based on a correction by the natural constant $^{86}Sr/^{88}Sr$ ratio, as ^{88}Sr may be produced by uranium fission (Naudet, 1991), consequently, this method cannot be used here.

The following section describes the analytical development for $^{87}Sr/^{86}Sr$ measurement and investigates the impact of anthropogenic strontium input in the Chernobyl Pilot Site groundwater.

IV.3.2 Analytical method optimization

The usual method used for strontium isotopes ratios analyses on TIMS is the dynamic method. In contrast with the total volatilization method (c.f. §IV.2.2.3), analysis by dynamic method integrates the signal on a short time span, when the isotope emissions are stable and the isotopic ratios are then measured from the several integrations. Thereafter, as light isotopes are emitted before heavy isotopes, the measured isotopic ratios are corrected from mass discrimination. This correction of the mass discrimination is based on the deviation from a known ratio, most often corresponding to a ratio constant in natural materials. In the case of $^{87}Sr/^{86}Sr$ ratio measurement, mass discrimination is corrected based on the naturally constant $^{86}Sr/^{88}Sr$ ratio. The admitted value of this ratio is 0.1194 (Nier, 1936). This dynamic method is not recommended in the case of Chernobyl Pilot Site groundwater because the natural constant $^{86}Sr/^{88}Sr$ ratio could be modified by the addition of the fission product ^{88}Sr.

Consequently, the total volatilization method is chosen here again. Isotopic ratios are theoretically directly measured integrating the whole signals of isotopes. However, as no protocol for Sr isotope analyses is available in the literature, it has to be developed with isotopic standards. Several tests were performed to develop

the analytical method by total volatilization on TIMS and to obtain the best repeatability. The strontium isotopic standard NIST SRM987 was used in these to tests (National Institute of Standards and Technology, 2010-2013). Analyses were carried out on TRITON TI (ThermoScientific inc.) at the University of Nîmes. However, because some groundwater samples showed too high ^{90}Sr volumetric activities (above 100 $Bq.L^{-1}$), the same analytical method was used on TRITON TI (ThermoScientific inc.) at the CEA-Marcoule.

IV.3.2.1 Tested filament configurations

Rhenium (Re) filaments were used for analyses.

First, the filament configuration which promoted the better Sr ionization needed to be defined. Several tests were performed analyzing the SRM987 standard on double Re filaments without activator, on double Re filaments with tantalum (Ta) activator, on single filament with Ta "in sandwich" or with "flashed" Ta. As for uranium ratio analyses (*c.f.* §IV.2.2.3), in the double filament configuration, two Re filaments were used: one where the standard was deposited (evaporation filament) and another one, placed in front of the evaporation filament (ionization filament). Ionization filament and Ta deposits were both supposed to promote ionization of Sr.

All the filaments were previously degassed under a pressure of 9.10^{-9} bar on the degassing ramp, following the procedure of filament preparation for uranium ratio analyses, described in §IV.2.2.3.2.

NIST SRM987 standard was deposited as follow on Re filaments:

- For double Re filaments without activator, no additional preparation was needed before the deposition of the standard. Sample deposition was done under a 0.5 A current. Then, intensity was increased until the filament started to glow slightly. This intensity was then maintained for a few seconds.
- For double Re filaments with Ta activator tests, Ta was added on the evaporation filament "in sandwich": under a 0.5 A current, 1 µL of Ta solution was deposited and dried, then the standard was deposited and dried and another 1 µL of Ta solution was added and dried. Current intensity was increased for a minute at 1.8 A and increased until the filament glows.

- For Ta deposits “in sandwich”, 1 µL of Ta was deposited on the Re filament at 0.5 A and dried. Then, 1 µL of the standard was deposited and dried and finally, 1 µL of Ta was deposited and dried. Intensity of the filament was increased to 1.8 A and dried during 1 minute. Then, intensity was increased until the filament started to glow slightly. This intensity was then maintained for a few seconds.
- For deposits on “flashed” Ta filament, 1 µL of Ta were deposited and dried twice on the filament. The deposit was then dried at 1.8 A during 1 minute (Figure IV-46). Then, on the degassing ramp, under a pressure of 9.10^{-9} bar, intensity of filament was at first increased to 4.5 A at a rate of 3 A/min and stabilized during 15 minutes and then, briefly increased to 6 A during less than 1 second. Filaments were then let to cool during 2 hours. The aim of this procedure was to smooth Ta deposit.

To obtain the best reproducibility, Ta and standard deposits had to be the smallest possible, so they were preferentially deposited with a syringe with a catheter.

Figure IV-46: Dried Ta deposit on Re single filament

IV.3.2.2 Analytical parameters

The filament heating procedure was optimized to lose as little Sr signal as possible before the analysis started. Indeed, the filament temperature and the rate of

temperature increasing were assessed to be the most important parameters (they are closely linked to the intensity of the filament and the increase of intensity in the filament). The aim was to get a stable Sr signal as soon as possible, but low enough to lose as little Sr as possible during the focalization of the Sr flux on Faraday cups (peak center) and adjusting sources lenses localization (lenses focalization). The different heating procedures are reported in Annexes 22 and 23.
These tests lead to the main following heating procedure.
Regarding double Re filaments, the heating procedure was specific: first, evaporation filament was heated rising the intensity up to 400 mA at a rate of 100 mA/min. In the meantime, the ionization filament was heated rising the intensity up to 2800 or 3000 mA at a rate of 450 mA/min and then rising the intensity up to 3200-3300 mA at a rate of 100 mA/min. For a single Re filament with Ta activator, evaporation filament heating was done increasing current to 2400 mA with a heatslope of 150 mA/min. If the signal was too low, intensity was increased to 2800 mA at a rate of 100 mA/min and eventually to 3400 mA with a rate of 50 mA/min. Evaporation filaments with Ta as activator were more heated. For the last tests and samples analyses, procedures were done automatically.
These heating procedures aimed at having the best stable isotope signal. First, filaments were heated until a ^{85}Rb signal, element which could still remain in the sample in spite of all the precautions, was observable and strong enough to make first signal focalization of source lenses on this signal. Sometimes, Rb signal was not found. Then filaments were heated until ^{88}Sr signal was observable and strong enough, commonly above 1 mV, to make the peak center and the focalization. Then, when the ^{88}Sr signal was just enough to assure that the Sr flux was focused, analysis started. At this step, the ^{88}Sr signal was commonly above 10 mV.
The following analysis parameters were assessed as the best. The maximal instant emission of the main isotope (Max Pilot value) was set to 8000 mV. During the analysis, the intensity in the evaporation filament was increased by 20 mA/cycle (heatslope), until the Max Pilot value was reached by the main isotope emission. Other values were tested however they did not show improvements in measured ratios. ^{84}Sr, ^{85}Rb, ^{86}Sr, ^{87}Sr and ^{88}Sr signal were measured by integration of the signal from the beginning of measurement to ^{88}Sr signal reached 0 V. ^{85}Rb was measured in order to correct the 87 mass signal, from possible interference of the

remaining ^{87}Rb with ^{87}Sr. ^{87}Rb signal correction was calculated from the ^{85}Rb cumulative signal and the theoretically constant natural $^{85}Rb/^{87}Rb$ ratio of 0.3857 (Rosman and Taylor, 1998). In most cases, this correction had a minimal impact on measurements because most of the Rb was previously theoretically removed from Sr sample by chemical separation.

IV.3.2.3 Comparison

Figure IV-47 shows measurements of $^{87}Sr/^{86}Sr$ ratios versus $^{86}Sr/^{88}Sr$ ratios for all tests. Filament configuration was supposed to be the most influent on the strontium emission.

Results obtained on double-filaments without Ta activator show the highest dispersivity. Figure IV-48 represents the same values without these tests. Double-filaments with Ta activator and single filaments with "flashed" Ta are showing the lowest dispersivity and the obtained ratios fall on a linear trend, passing through the certified value of the NIST standard, 0.11935 ± 0.00005 for $^{86}Sr/^{88}Sr$ ratio and 0.71034 ± 0.00026 for $^{87}Sr/^{86}Sr$ ratio (National Institute of Standards and Technology, 2010-2013).The use of single filaments with "flashed" Ta was preferred because obtained signals were the most stables.

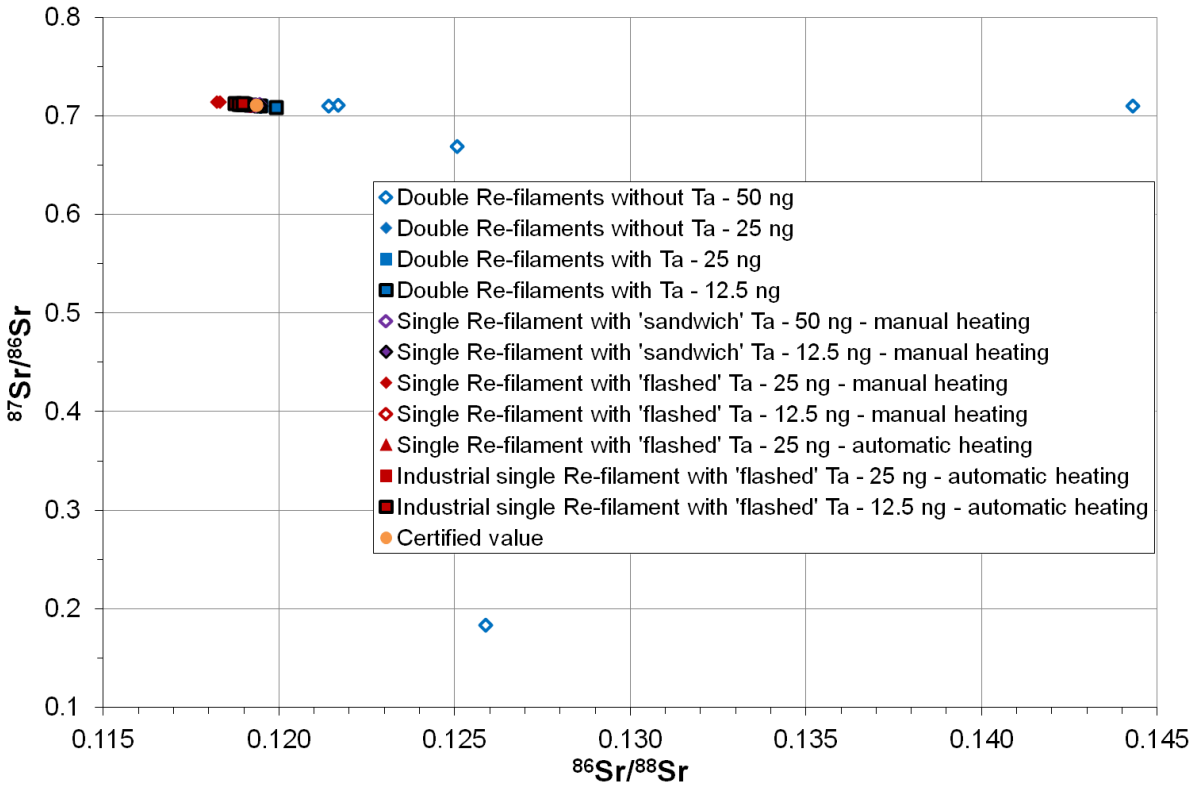

Figure IV-47: Measured $^{87}Sr/^{86}Sr$ ratios vs $^{86}Sr/^{88}Sr$ ratios for all NBS987 standard analyses

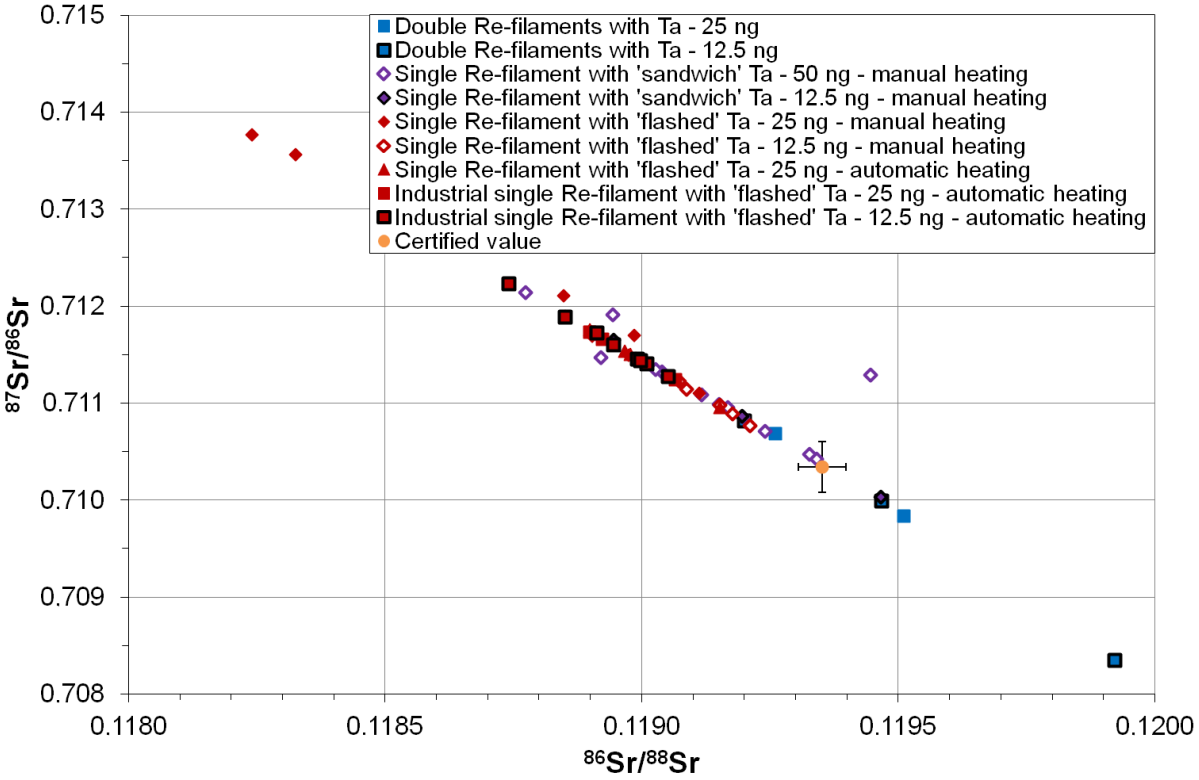

Figure IV-48: Measured $^{87}Sr/^{86}Sr$ ratios vs $^{86}Sr/^{88}Sr$ ratios for NBS987 standard analyses on Re filament with Ta activator

IV.3.2.4 Repeatability of the chosen method

The measurement repeatability of analyses on single Re filament with "flashed" Ta was assessed with the analysis of 11 filaments with NIST SRM987 standard. Heating procedure was automated. $^{86}Sr/^{88}Sr$ and $^{87}Sr/^{86}Sr$ mean values and standard deviations are given in Table IV-6.

Table IV-6

	Number of analyzed standards	Mean	2 σ	Certified value
$^{86}Sr/^{88}Sr$	11	0.1189	0.0002	0.11935 ± 0.00005
$^{87}Sr/^{86}Sr$ (Rb corrected)	11	0.7116	0.0006	0.71034 ± 0.00026

IV.3.2.5 Analytical bias and corrections

In order to improve results, analytical bias correction was envisaged based on the alignment of results in Figure IV-48. As ^{84}Sr cumulative signal was not negligible in most of the analyses, this correction would be based on $^{84}Sr/^{86}Sr$ ratio measurements: this ratio was certified to be 0.5655 in the NBS987 standard (National Institute of Standards and Technology, 2010-2013) and assessed to be 0.5724 ± 0.0022 in natural environments (Rosman and Taylor, 1998). This ratio should not be impacted by fission products because ^{84}Sr and ^{86}Sr were not produced during ^{235}U fission in nuclear reactors (Naudet, 1991).

In order to define this correction, $^{87}Sr/^{86}Sr$ ratios and $^{86}Sr/^{88}Sr$ ratios were compared to $^{84}Sr/^{86}Sr$ ratios for all the analyses of NIST SRM987 standards on single filaments with "flashed" Ta (Figure IV-49). Both $^{87}Sr/^{86}Sr$ and $^{86}Sr/^{88}Sr$ ratios show linear trend *versus* $^{84}Sr/^{86}Sr$ ratios with good correlation (R^2= 0.9345 and 0.9453 respectively). In addition, both regression lines intercept the certified values for $^{87}Sr/^{86}Sr$ and $^{86}Sr/^{88}Sr$ ratio (0.71034 and 0.11935 respectively) at a $^{84}Sr/^{86}Sr$ ratio of 0.05647. Hence, this $^{84}Sr/^{86}Sr$ ratio was here after preferred for the correction of the $^{86}Sr/^{88}Sr$ and $^{87}Sr/^{86}Sr$ ratios rather than the certified value.

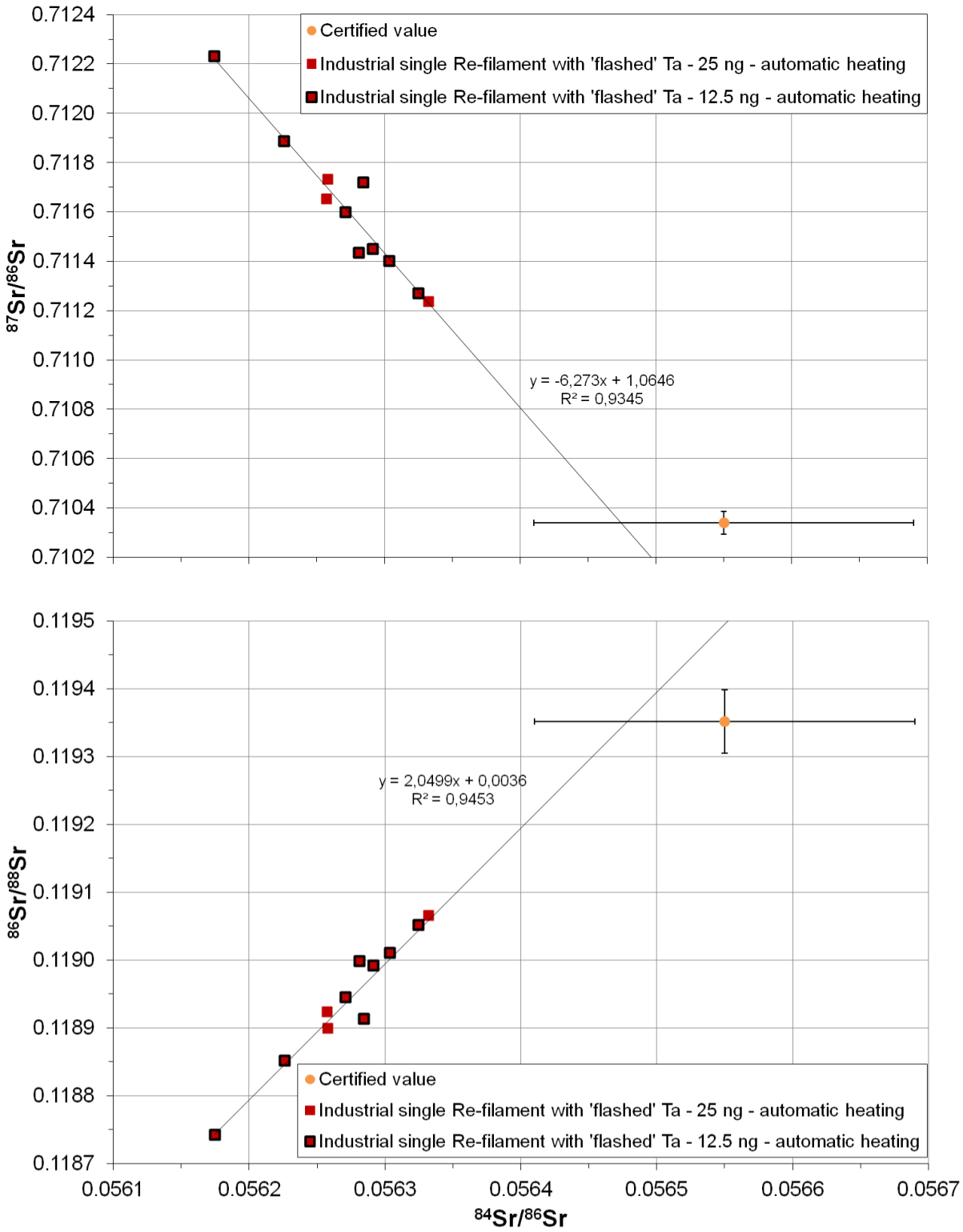

Figure IV-49: Measured 87Sr/86Sr ratios and 86Sr/88Sr ratios versus 84Sr/86Sr ratios (NBS987 standard analyses on single Re filament with "flashed" Ta)

The mass discrimination correction of $^{87}Sr/^{86}Sr$ and $^{86}Sr/^{88}Sr$ ratios by $^{84}Sr/^{86}Sr$ ratio was based on Habfast's study (1998). This work compared measured isotopic ratios (r) to theoretical isotopic ratios (S) for three isotopes of the same element. Several equations were proposed to calculate a r_1/S_1 ratio from a known r_2/S_2 ratio, based on the combination of Rayleigh's diffusion equation and Langmuir' evaporation equation (physical law) and common equations used in the literature (empirical laws). The linearized Rayleigh law was chosen here for the correction of the mass discrimination (Habfast, 1998):

$$\frac{r_1}{S_1} = (1-x) + x \times \frac{r_2}{S_2}$$ *Equation IV-17*

where $x = \frac{\beta_1 - 1}{\beta_2 - 1}$

In the strontium case, $\beta_1 = \sqrt{\frac{84}{86}}$ and $\beta_2 = \sqrt{\frac{84}{87}}$ *or* $\sqrt{\frac{84}{88}}$

Following this equation (Equation IV-17), theoretical $^{84}Sr/^{87}Sr$ (S_2) was calculated from measured $^{84}Sr/^{86}Sr$ (r_1), $^{84}Sr/^{87}Sr$ (r_2), ratios and theoretical $^{84}Sr/^{86}Sr$ ratio (S_1=0.05647) according to:

Equation IV-18

$$S_2 = \frac{x \times r_2}{\left(\frac{r_1}{S_1} + x - 1\right)}$$

Then, $^{87}Sr/^{86}Sr$ ratio was calculated from the theoretical $^{84}Sr/^{86}Sr$ ratios (0.05647) and this calculated $^{84}Sr/^{87}Sr$ ratio.

The same approach was used to determine $^{86}Sr/^{88}Sr$ from measured $^{84}Sr/^{86}Sr$ and $^{84}Sr/^{88}Sr$ ratios.

Mean values and standard deviation with this correction implemented to results of SRM987 analyses on filament with "flashed" Ta are given in Table IV-7. These values show a significant improvement with respect to the uncorrected value and are considered as sufficiently accurate.

Table IV-7

	effective	Mean	2 σ	Certified value
$^{86}Sr/^{88}Sr$	11	0.11935	0.00005	0.11935 ± 0.00005
$^{87}Sr/^{86}Sr$	11	0.7104	0.0001	0.71034 ± 0.00026

IV.3.2.6 CEA-Marcoule standards

Four NIST SRM987 standards were analyzed on TIMS at the CEA-Marcoule, which allowed analyzing sample with ^{90}Sr volumetric activity above 100 $Bq.L^{-1}$. Conditions of sample preparation were the same as for uranium sample preparation, in a fume cupboard equipped with systems of air filtration (§IV.2.2.3.4). The first two were deposited with a syringe equipped with a catheter. As the syringe broke, the following two and the samples were deposited using a pipette.

Table IV-8: NIST SRM987 analyzes at the CEA-Marcoule

Quantity (ng)	$^{86}Sr/^{88}Sr$	$^{87}Sr/^{86}Sr$ Rb corrected	$^{84}Sr/^{86}Sr$	$^{84}Sr/^{87}Sr$	$^{84}Sr/^{88}Sr$
25	0.11893	0.71242	0.04669	0.06553	0.00555
12.5	0.11897	0.71244	0.05051	0.07089	0.00601
25	0.11890	0.71273	0.04192	0.05881	0.00498
25	0.11884	0.71277	0.05114	0.07174	0.00608

These analyzes were close to the measured ratio ranges without correction (Table IV-7). However, they do not fall on the previous linear trends shown by standards analyzed at the University of Nîmes in the $^{87}Sr/^{86}Sr$ and $^{86}Sr/^{88}Sr$ ratios versus $^{84}Sr/^{86}Sr$ ratios diagrams, respectively (Figure IV-48 and Figure IV-49). This may be linked to the low measured ^{84}Sr signal, inducing a higher uncertainty in the $^{84}Sr/^{86}Sr$ ratio. Moreover, the number of standard analyzed was too low to emphasize a correlation and hence to the appropriate correction. Further tests would have to

be carried out to determine a reliable correlation and improve the statistics. However, as analytical time was limited on the machine at the CEA-Marcoule, these additional analyses could not be carried out within the scope of this study. Consequently, standard analyzes carried out at the CEA-Marcoule were not corrected from this mass discrimination. However, the results still remained close to the range of uncorrected standard analyzes carried out at the University of Nîmes: $^{86}Sr/^{88}Sr$ ratios were within the range of 0.1189 ± 0.0002 while $^{87}Sr/^{86}Sr$ ratios were slightly higher than the range of 0.7116 ± 0.0006 (Table IV-6). Hence, samples analyzed at the CEA-Marcoule were not corrected and their interpretation is made with caution because if $^{86}Sr/^{88}Sr$ ratios can be considered as correct as they give results within the standard analysis range carried out at the University of Nîmes, $^{87}Sr/^{86}Sr$ ratios are supposed to be overestimated: the maximal difference between the mean value obtained on standard analyses at the University of Nîmes and standard values obtained at the CEA-Marcoule is close to 1 on the 3rd decimal. This value of 0.001 is used as uncertainty on the presentation of sample analyses hereafter. All analyses carried out at the CEA-Marcoule are given in Annex 26.

IV.3.3 STRONTIUM BEHAVIOR IN CHERNOBYL PILOT SITE GROUNDWATER

In order to better constraint Sr behavior in the Chernobyl Pilot Site groundwater, particularly cation exchanges and anthropogenic impacts, samples were collected for the analyses of $^{87}Sr/^{86}Sr$ and $^{86}Sr/^{88}Sr$ ratios.

IV.3.3.1 Sampling

Groundwater samples were collected on the AB-profile (Annex 2).

First, the cleaning of each piezometer and pumping system was done pumping between 3 and 5 L of groundwater. Then, pH, Eh, dissolved O_2 and conductivity parameters were measured with a flow cell.

For cation concentration analyses, 2 L of all piezometers on each profile were sampled. Then, samples were filtered, acidified at pH under 2.5 and conditioned in 125 mL polyethylene bottles.

For strontium isotopes ratios analyses, 16 piezometers were sampled in October 2008 and 2 in October 2009. Hereafter, samples are named according the year of sampling and the piezometer sampled: for instance, “T8 1-98-3” means the piezometer “1-98-3” was sampled at Tchernobyl in 2008 (“T8”). Volumes of these

groundwater samples range from 50 to 350 mL. These samples were filtered and acidified at pH below 2.5.

IV.3.3.2 Analyses

IV.3.3.2.1 Strontium separation

The protocol used for strontium separation from other elements is the one developed by Pin *et al.*, 2003.

Samples were evaporated to dryness in Teflon beakers. Evaporated volumes ranged from 1 to 2 mL of Chernobyl groundwater samples. Then, samples were dissolved in 0.5 mL of [HNO_3] 2M. After 100 µL of Sr-resin (Eichrom technologies inc.) were poured into columns and rinsed with 2 mL of [HCl] 6M and 2mL [HNO_3] 0.05M. Then, resins were conditioned with 0.2 mL of [HNO_3] 2M. Samples were then introduced into the column by successive addition of 0.1 mL. Most of the elements were eluted with the addition of 0.4 mL of [HNO_3] 2M. For Ba elution, 1 mL [HNO_3] 7M was introduced in the column. The column was conditioned with 0.2 mL of [HNO_3] 2M. For Sr elution, 1 mL of [HNO_3] 0.05M was added in the column and the solution is collected in a Teflon beaker. Finally, this solution was evaporated to dryness.

Recovered Sr precipitate was diluted in a few µL of [HNO_3] 0.02M, in order to obtain either 12.5 ng or 25 ng of Sr in 1µL of solution. This 1 µL was deposited at the center of the prepared single Re filament with "flashed" Ta, under a current of 0.5 A and dried. Intensity was first increased to 1.8 A for 1 minute and then raised again until filament started to glow.

IV.3.3.2.2 Analyses of samples

$^{87}Sr/^{86}Sr$ and $^{86}Sr/^{88}Sr$ ratios were analyzed in these samples on TIMS TRITON TI (ThermoScientific inc.) according the optimized procedure described previously (*c.f.* §IV.3.2). Groundwater samples showing ^{90}Sr activity below 100 $Bq.L^{-1}$ were then analyzed at the University of Nîmes (11 groundwater samples). Other samples were analyzed at the CEA-Marcoule: as some groundwater analyses were duplicated, a total of 13 samples were analyzed.

At the University of Nîmes, several sample preparations and analyses were carried out, with different Sr quantities (12.5 ng or 25 ng). Eight samples were analyzed twice. The first time, intensity in filaments was increased manually before each

analysis started. The second time, it was automated. Analyzes were carried out automatically at the CEA-Marcoule and some sample analyzes failed. In several cases, some analyses failed, most likely because the automatic procedure did not find the ^{88}Sr signal.

IV.3.3.3 Results and discussion

^{88}Sr concentrations measured in October 2008 in Chernobyl Pilot Site groundwater along the AB profile range between 1.4 and 8.8 $x10^{-7}$ $mol.L^{-1}$. For the two samples collected in October 2009, [^{88}Sr] are of $3.50\times10^{-7} \pm 0.02\times10^{-7}$ $mol.L^{-1}$ for 5-01-2 piezometer and $3.76\times10^{-7} \pm 0.05\times10^{-7}$ $mol.L^{-1}$ for 7-01-2 piezometer. These values are close to values observed in October 2008, of $4.40\times10^{-7}\pm0.02\times10^{-7}$ $mol.L^{-1}$ and $4.14\times10^{-7}\pm0.09\times10^{-7}$ $mol.L^{-1}$, respectively.

[^{88}Sr] increase downgradient of the trench and with depth, excepted for the three deeper piezometers.^{90}Sr volumetric activities range between under the detection limit (piezometers are not colored when ^{90}Sr volumetric activity is below 10 $Bq.L^{-1}$) and 1380 $Bq.L^{-1}$.

Figure IV-50 represents [^{88}Sr] along the AB-profile and ^{90}Sr volumetric activity (samples are colored from white to red according to the ^{90}Sr activity) in October 2008. Groundwater sample analyzed for $^{86}Sr/^{88}Sr$ and $^{87}Sr/^{86}Sr$ ratios at the University of Nîmes are shown with thick open circles. Other groundwater samples with ^{90}Sr activity up to 100 $Bq.L^{-1}$ were collected and analyzed at the CEA-Marcoule (doted open circles).

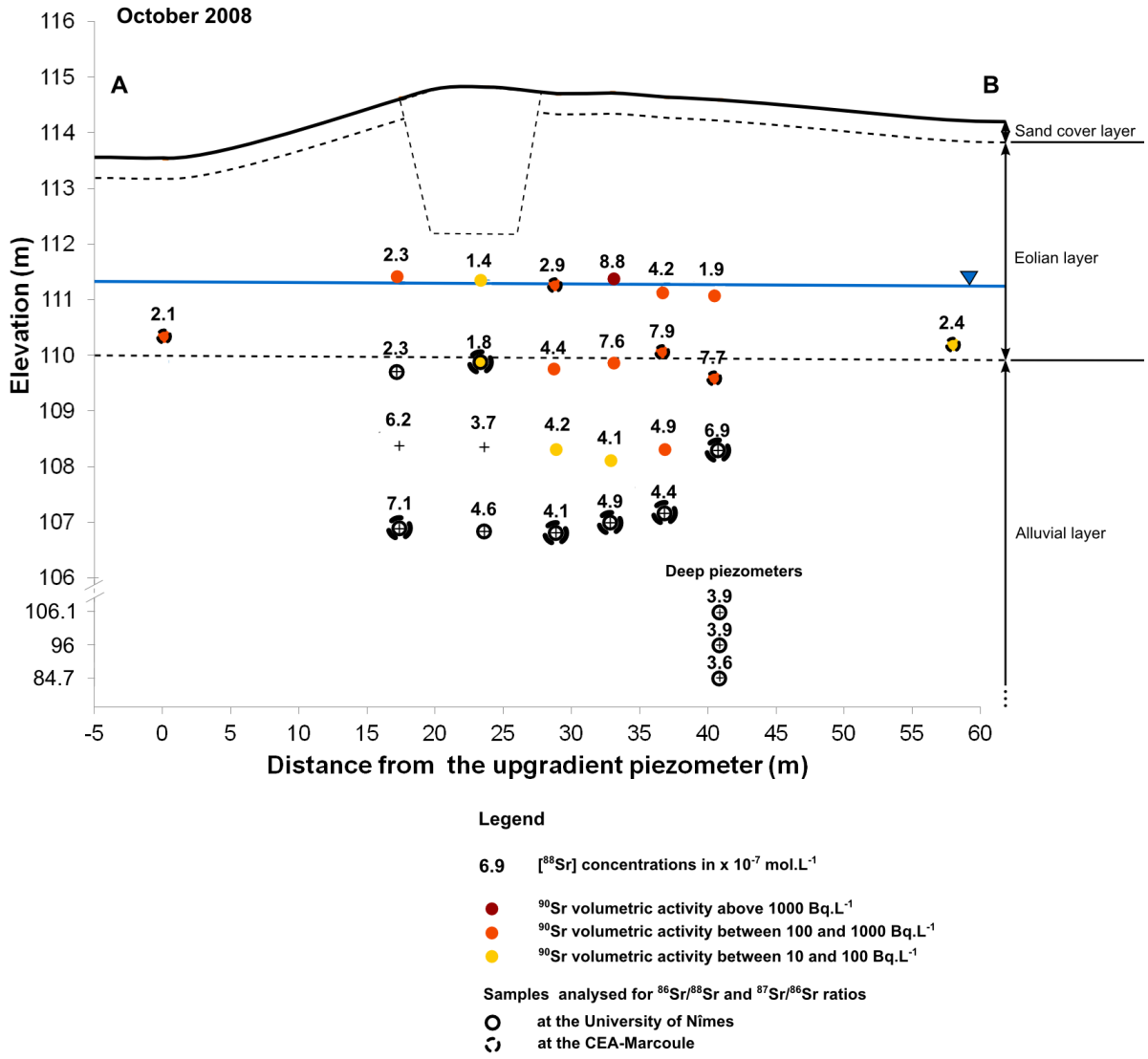

Figure IV-50: [^{88}Sr] concentrations, ^{90}Sr volumetric activities measured in October 2008 and goundwater sampled for isotopic analyses along the AB-profile

In the aeolian layer, [^{88}Sr] and ^{90}Sr volumetric activities both increase downgradient of the trench. [^{88}Sr] measured in groundwater collected in the shallow aquifer downgradient of the trench are at least twice more concentrated than groundwater collected in the aeolian layer upgradient of the trench. In the alluvial layer, ^{90}Sr volumetric activities fall below the detection limit with increasing depth.

At the University of Nîmes, obtained isotopic ^{84}Sr/^{86}Sr, ^{87}Sr/^{86}Sr and ^{86}Sr/^{88}Sr ratios by TIMS analysis (with the correction of ^{87}Sr by the ^{87}Rb content) and ^{87}Sr/^{86}Sr and ^{86}Sr/^{88}Sr ratios corrected from mass discrimination by the ^{84}Sr/^{86}Sr ratio, calculated

following the calculations described in section §IV.3.2.5 are shown in Annex 25. Duplicate analyses show mostly variations above 0.0001 and these discrepancies are just slightly higher than the standard deviation established on measurement repeatability by the NIST SRM987 analyses (Table IV-7). Some results can be discarded because they show r1/S1 ratio below 0.9 ($^{84}Sr/^{86}Sr$) (see §IV.3.2.5) and consequently, the linearized Rayleigh law is probably less adapted for the correction (samples from 7-01-2, 7-02-2 and 18-00-2 piezometers, analyzed in September 2011). Most likely, this results of a too low ^{84}Sr signal.

For analyses carried out at the CEA-Marcoule, the results are not corrected and have to be taken with caution: $^{87}Sr/^{86}Sr$ ratios are supposed to be slightly overestimated, by 1 on 3rd decimal (see §IV.3.2.6). Duplicates analyzed at the University of Nîmes and at the CEA-Marcoule confirm this trend, but still remain close. CEA-Marcoule results are reported in Annex 25.

For analyzes carried out at the University of Nîmes, Chernobyl Pilot Site groundwater $^{86}Sr/^{88}Sr$ ratios, corrected by the $^{84}Sr/^{86}Sr$ ratios mass discrimination ratios, range between 0.1167 (quite surprisingly low value compared with the natural ratio) and 0.1197. The mean value is of 0.1192 for a standard deviation (2σ) of 0.0007. $^{87}Sr/^{86}Sr$ ratios corrected of ^{87}Rb and by the $^{84}Sr/^{86}Sr$ ratios deviation range between 0.7089 and 0.7151. The mean value is of 0.713 for a standard deviation (2σ) of 0.002. For the analyses carried out at the CEA-Marcoule, uncorrected $^{86}Sr/^{88}Sr$ ratios range between 0.1184 and 0.1193 and uncorrected $^{87}Sr/^{86}Sr$ ratios range between 0.71116 and 0.71579.

IV.3.3.3.1 $^{86}Sr/^{88}Sr$ ratios

In the literature, the $^{86}Sr/^{88}Sr$ ratios measured in natural waters show values ranging from 0.11935 to 0.11937 in 13 river waters sampled all over the world (Krabbenhöft et al., 2010). The variation of measured ratios in the Chernobyl Pilot Site groundwater is quite high compared to this range of values. This variation may be attributed to the presence of anthropogenic ^{88}Sr, produced by uranium fission. The theoretical impact of the radiogenic ^{88}Sr migrating from the trench on the $^{86}Sr/^{88}Sr$ ratio in groundwater may be calculated based on estimations of ^{88}Sr produced by uranium fission and migrating from the trench. This estimation will hereafter be compared with observed values. First, the ^{88}Sr migrating from the trench can be calculated from the uranium fission yield of ^{90}Sr and ^{88}Sr, according

to Naudet (1991) and the ^{90}Sr volumetric activity measured in groundwater following the equation:

Equation IV-19

$$^{88}Sr_{FP} = {}^{90}Sr_{ini} \times \frac{^{88}Sr\ fission\ yield}{^{90}Sr\ fission\ yield}$$
$$= \frac{A_{Sr-90(t)}}{\lambda} \times e^{\lambda t} \times \frac{^{88}Sr\ fission\ yield}{^{90}Sr\ fission\ yield}$$

where:

- $^{90}Sr_{ini}$ is the initial ^{90}Sr issued from the trench, before decay in $Bq.L^{-1}$;
- $A_{Sr-90(t)}$ is the volumetric activity in ^{90}Sr measured at a time *t* (21 years for sampling in 2008)
- ^{88}Sr fission yield and ^{90}Sr fission yield are respectively 3.65% and 5.93% according to Naudet (1991).

Considering that $A_{Sr-90(t)}$ equals to 15000 $Bq.L^{-1}$ (maximal observed value), the $^{88}Sr_{FP}$ equals to $2.00x10^{13}$ $at.L^{-1}$ or $3.33x10^{-11}$ $mol.L^{-1}$. This value is small regarding [^{88}Sr] concentrations measured in groundwater which is in the order of 10^{-7} $mol.L^{-1}$.

Then, the impact of this increase in ^{88}Sr content on the $^{86}Sr/^{88}Sr$ ratio can be estimated considering three potential sources: Sr naturally present in groundwater and Sr released by the trench, including Sr released by degradation of buried organic matter and Sr released by the alteration of fuel particles.

Equation IV-20

$$\left(\frac{^{86}Sr}{^{88}Sr}\right)_{GW} = \frac{^{86}Sr_{nat} + {}^{86}Sr_{D} + {}^{86}Sr_{FP}}{^{88}Sr_{tot}}$$
$$= \frac{^{86}Sr_{nat}}{^{88}Sr_{tot}} + \frac{^{86}Sr_{D}}{^{88}Sr_{tot}} + \frac{^{86}Sr_{FP}}{^{88}Sr_{tot}}$$

where

- $(^{86}Sr/^{88}Sr)_{GW}$ is the ratio impacted by the migration of radiogenic ^{88}Sr, issued from the trench;
- $^{88}Sr_{tot}$ is the ^{88}Sr in groundwater influenced by migration ^{88}Sr issued from the trench, radiogenic or not, added to the natural ^{88}Sr.
- $^{86}Sr_{nat}$ is the ^{86}Sr naturally present in groundwater;
- $^{86}Sr_{D}$ is the ^{86}Sr issue from the degradation of natural materials buried in the trench;

- $^{86}Sr_{FP}$ is the ^{86}Sr produced by the fission of uranium and assessed to be 0.

Consequently,

Equation IV-21

$$\left(\frac{^{86}Sr}{^{88}Sr}\right)_{GW} = \frac{^{86}Sr_{nat}}{^{88}Sr_{tot}} + \frac{^{86}Sr_{D}}{^{88}Sr_{tot}}$$
$$= \frac{^{86}Sr_{nat}}{^{88}Sr_{nat}} \times \frac{^{88}Sr_{nat}}{^{88}Sr_{tot}} + \frac{^{86}Sr_{D}}{^{88}Sr_{D}} \times \frac{^{88}Sr_{D}}{^{88}Sr_{tot}}$$
$$= \left(\frac{^{86}Sr}{^{88}Sr}\right)_{nat} \times \frac{^{88}Sr_{nat}}{^{88}Sr_{tot}} + \left(\frac{^{86}Sr}{^{88}Sr}\right)_{D} \times \frac{^{88}Sr_{D}}{^{88}Sr_{tot}}$$

where

- $(^{86}Sr/^{88}Sr)_{nat}$ in the ratio in natural environment, set at 0.1194 by Nier (1936); as the uncertainty of this value is not known, the value 0.119400 is considered.
- $(^{86}Sr/^{88}Sr)_{D}$ is the ratio of strontium issue of the degradation of natural material buried in the trench, equal to the ratio in natural environment , *i.e.* 0.119400 (Nier, 1936);
- $^{88}Sr_{nat}$ the ^{88}Sr naturally present in groundwater and can be assimilated to the $[^{88}Sr]$ in groundwater not impacted by the trench, as in the upgradient groundwater where $[^{88}Sr]$ is around $2x10^{-7}$ $mol.L^{-1}$;
- $^{88}Sr_{tot}$ is the ^{88}Sr in groundwater influenced by migration ^{88}Sr issued from the trench, radiogenic or not, added to the natural ^{88}Sr. $^{88}Sr_{tot}$ can be assimilated to $[^{88}Sr]$ in groundwater impacted by the trench, as in the groundwater just downgradient of the trench, where $[^{88}Sr]$ is around $9x10^{-7}$ $mol.L^{-1}$;
- $^{88}Sr_{D}$ is the ^{88}Sr issue from the degradation of natural material buried in the trench and equals to

Equation IV-22

$$^{88}Sr_{D} = {}^{88}Sr_{Tot} - {}^{88}Sr_{nat} - {}^{88}Sr_{FP}$$

Consequently,

$$\left(\frac{^{86}Sr}{^{88}Sr}\right)_{GW} = \left(\frac{^{86}Sr}{^{88}Sr}\right)_{nat} \times \frac{^{88}Sr_{nat} + ^{88}Sr_{D}}{^{88}Sr_{tot}}$$
$$= \left(\frac{^{86}Sr}{^{88}Sr}\right)_{nat} \times \frac{^{88}Sr_{nat} + ^{88}Sr_{Tot} - ^{88}Sr_{nat} - ^{88}Sr_{FP}}{^{88}Sr_{tot}}$$
$$= \left(\frac{^{86}Sr}{^{88}Sr}\right)_{nat} \times \frac{^{88}Sr_{Tot} - ^{88}Sr_{FP}}{^{88}Sr_{tot}}$$
$$= \left(\frac{^{86}Sr}{^{88}Sr}\right)_{nat} \times \left(1 - \frac{^{88}Sr_{FP}}{^{88}Sr_{tot}}\right)$$

Considering that:

- the ^{90}Sr volumetric activity of 15000 $Bq.L^{-1}$, maximal value measured downgradient of the trench, the $^{88}Sr_{FP}$ is $3.33x10^{-11}$ $mol.L^{-1}$ (Equation IV-19) ;
- A $^{88}Sr_{Tot}$ corresponding to $9x10^{-7}$ $mol.L^{-1}$; $(^{86}Sr/^{88}Sr)_{nat}$ equals to 0.119400 (Nier, 1936);

$^{86}Sr/^{88}Sr$ in groundwater impacted by migration of Sr released from the trench is calculated to be equals to 0.119396 for an initial natural ratio of 0.119400, assumed to be constant (Nier, 1936). Hence, the impact of the anthropogenic ^{88}Sr on the $^{86}Sr/^{88}Sr$ in the most contaminated groundwater is very low, on the 6th decimal, regarding the variation observed in the groundwater samples, on the 3rd decimal (Annex 25). The calculated variation induced by migration of ^{88}Sr from fission product in Chernobyl Pilot Site groundwater is also lower than the $^{86}Sr/^{88}Sr$ ratio natural variation in river waters, ranging from 0.11935 to 0.11937 as mentioned previously (Krabbenhöft *et al.*, 2010). These $^{86}Sr/^{88}Sr$ ratios were obtained by the double-spike method, developed by Krabbenhöft *et al.* (2009). A solution with a known high $^{87}Sr/^{84}Sr$ ratio, called double-spike solution, is added to the sample and $^{87}Sr/^{86}Sr$ and $^{86}Sr/^{88}Sr$ ratios are then recalculated based on an isotopic dilution equation (Krabbenhöft *et al.*, 2009). However, the precision obtained, on the 5th decimal, is still too high to assess the impact of migrations from the trench on the $^{86}Sr/^{88}Sr$ ratios.

Moreover, the $^{86}Sr/^{88}Sr$ ratio variations observed in the Chernobyl Pilot Site groundwater, mainly on the 4th decimal, are most likely linked to other processes than migration of ^{88}Sr from the trench. Several hypotheses can be made:

- Geochemical processes influence ^{88}Sr and ^{86}Sr contents. However, the variation, mainly on the 4th decimal, seems quite high regarding the

variations observed in natural environments, on the 5th decimal (Krabbenhöft *et al.*, 2010).

- Considered fission yields are underestimated and the ^{88}Sr produced may imply a variation on the 4th decimal of $^{86}Sr/^{88}Sr$ ratio.
- The analytical standard deviation is higher for measurements on natural samples due to the presence of other elements which may infer in spite of the chemical separation. Tests should have been carried on drinking water for instance to avoid or confirm this hypothesis.

IV.3.3.3.2 $^{87}Sr/^{86}Sr$ ratios

As presented before, $^{87}Sr/^{86}Sr$ ratios are commonly used to trace the origin of natural material. In groundwater, $^{87}Sr/^{86}Sr$ ratios are influenced by the nature of the bedrock and atmospheric inputs (Capo *et al.*, 1998). In Chernobyl Pilot Site groundwater, it is supposed to be also influenced by Sr migration from the trench.

To illustrate the influence of the sample locations on [^{88}Sr] and $^{87}Sr/^{86}Sr$ ratios, [^{88}Sr] and $^{87}Sr/^{86}Sr$ ratios in Chernobyl Pilot Site groundwater are reported along the AB profile (Annex 1). Both $^{87}Sr/^{86}Sr$ ratios measured at the University of Nîmes and at the CEA-Marcoule are presented. CEA-Marcoule analyses are shown but still have to be interpreted with caution

Most of [^{88}Sr] in the shallow groundwater (aeolian layer and interface aeolian/alluvial) are lower than ratios measured in the shallow alluvial layer, excepted downgradient of the trench where the highest [^{88}Sr] are measured. In the alluvial deeper part, $^{87}Sr/^{86}Sr$ ratios decrease with increasing depth while [^{88}Sr] seem to decrease. Decreasing $^{87}Sr/^{86}Sr$ ratios may be due to the influence of the underlying marine carbonates. These carbonate $^{87}Sr/^{86}Sr$ ratios are probably in the same range than that of the seawater when they were deposited along the Cenozoic era (Capo *et al.*, 1998). Seawater is known to have a quite constant $^{87}Sr/^{86}Sr$ ratio, between 0.708 and 0.709, which corresponds to ratio measured in the deepest groundwater from the 1-98-3 piezometer.

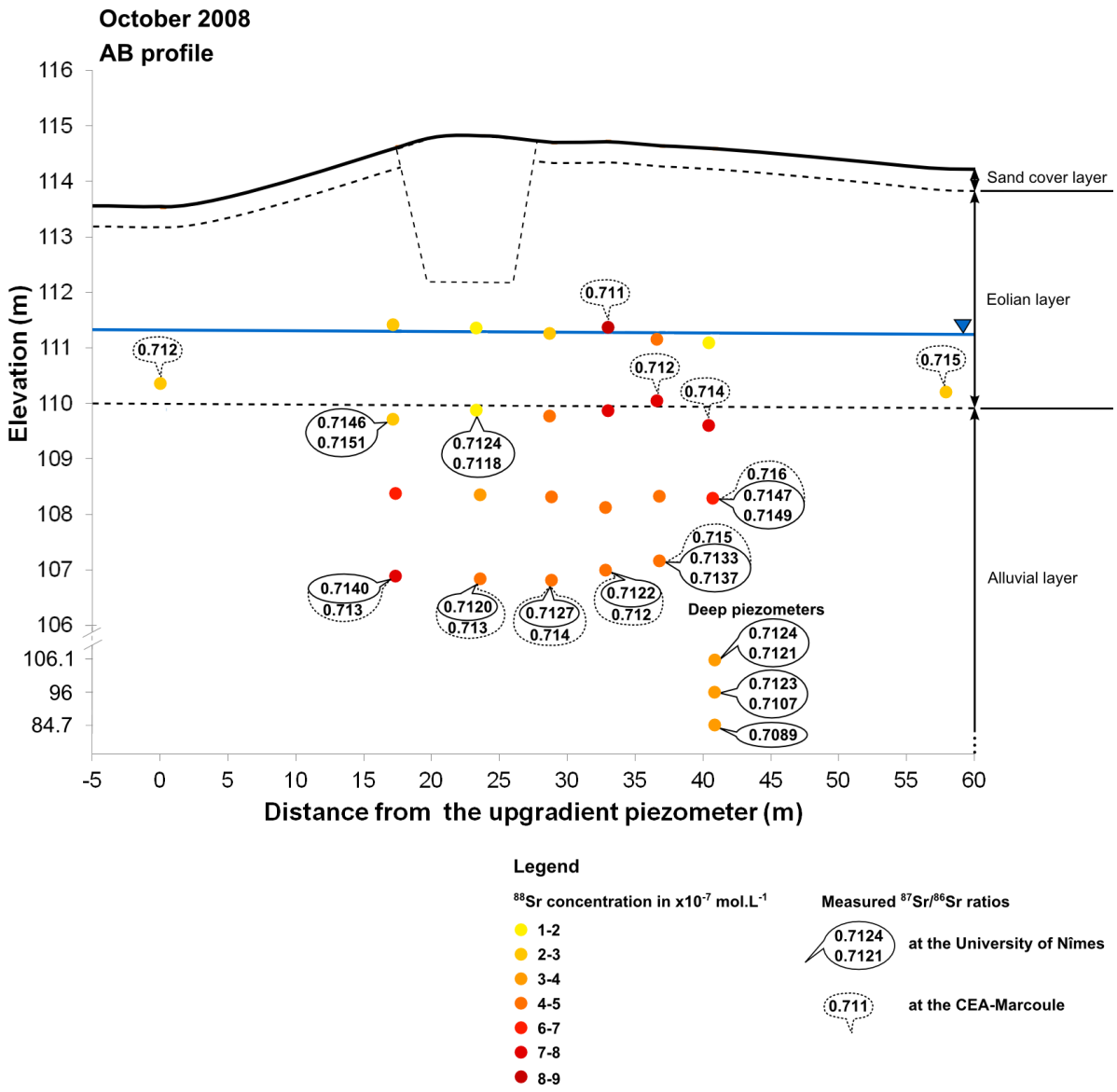

Figure IV-51: [^{88}Sr] measured in October 2008 and corrected ^{87}Sr/^{86}Sr ratios on the AB profile

To better investigate strontium behavior in groundwater, corrected ^{87}Sr/^{86}Sr ratios are compared respectively with [^{88}Sr] concentrations, in 1/[^{88}Sr] (Figure IV-52) and with ^{90}Sr volumetric activity corrected by the decay, calculated in mmol.L^{-1} and reported in 1/[^{90}Sr] (Figure IV-53). CEA-Marcoule analyses are shown but again have to be considered with caution. The ^{87}Sr/^{86}Sr ratio analyses of the sample from 1-98-2 piezometer, duplicated at the University of Nîmes and at the CEA-Marcoule, are the most incoherent (Annexes 25 and 26). The lower ^{87}Sr/^{86}Sr ratio seems to be more realistic, based on the ^{86}Sr/^{88}Sr ratio closer to the natural ratio. Colors and symbols are chosen as indications of samples location: groundwater samples the closest to the trench are colored in red, shallow samples are shown with triangles,

the deepest samples are shown with dots and other samples are shown with diamonds.

$^{87}Sr/^{86}Sr$ ratios are roughly constant for any [^{88}Sr], which was shown to increase downgradient of the trench and with increasing depth (Figure IV-50). In the shallow groundwater, samples show quite high $^{87}Sr/^{86}Sr$ ratios relatively to deeper samples: $^{87}Sr/^{86}Sr$ ratios decease with depth. The highest $^{87}Sr/^{86}Sr$ ratio is measured in groundwater downgradient of the trench with a quite high [^{88}Sr]. Consequently, three end-members could be identified: the deep groundwater with low $^{87}Sr/^{86}Sr$ ratio and intermediate [^{88}Sr], groundwater upgradient of the trench with low [^{88}Sr] and intermediate $^{87}Sr/^{86}Sr$ and finally, groundwater downgradient of the trench with high [^{88}Sr] and intermediate $^{87}Sr/^{86}Sr$ ratio.

In (Figure IV-53), $^{87}Sr/^{86}Sr$ ratios versus 1/[^{90}Sr] ($L.mmol^{-1}$) are shown. Groundwater showing the highest [^{90}Sr], collected downgradient of the trench does not show a higher $^{87}Sr/^{86}Sr$ ratio than other samples. The influence of anthropogenic Sr migration from the trench on $^{87}Sr/^{86}Sr$ ratio is difficult to assess taking into account that only few samples of the shallow groundwater, the most impacted by ^{90}Sr migration from the trench, were analyzed. Groundwater sample in the aeolian layer are required to better assess the influence of migrations from the trench.

Overall, a complete $^{87}Sr/^{86}Sr$ ratio study on the whole profile should help to characterize more precisely the Sr cycle and to determine the impact of Sr migration from the trench. Rainwater, biosphere and soil water sample as well as the whole profile groundwater could also be analyzed to obtain $^{87}Sr/^{86}Sr$ ratios. The comparison could be made with $^{90}Sr/^{86}Sr$ ratios to better characterize Sr originating from Chernobyl accident and the flux between the different compartments.

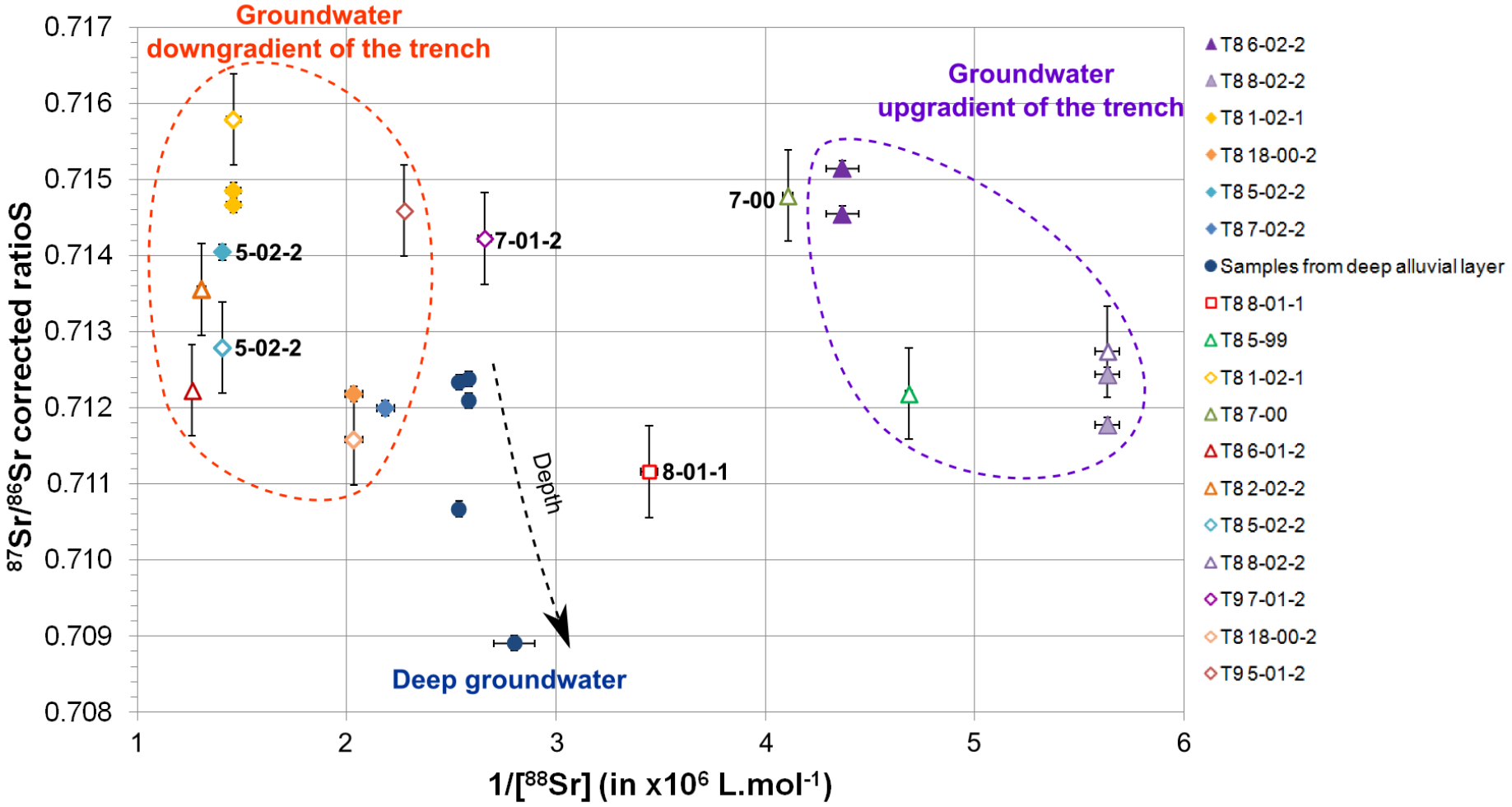

Figure IV-52: 87Sr/86Sr ratios versus 1/[88Sr]. Analyzes carried out at the University of Nîmes are shown with full symbols and analyzes carried out at the CEA-Marcoule are are shown with empty symbols.

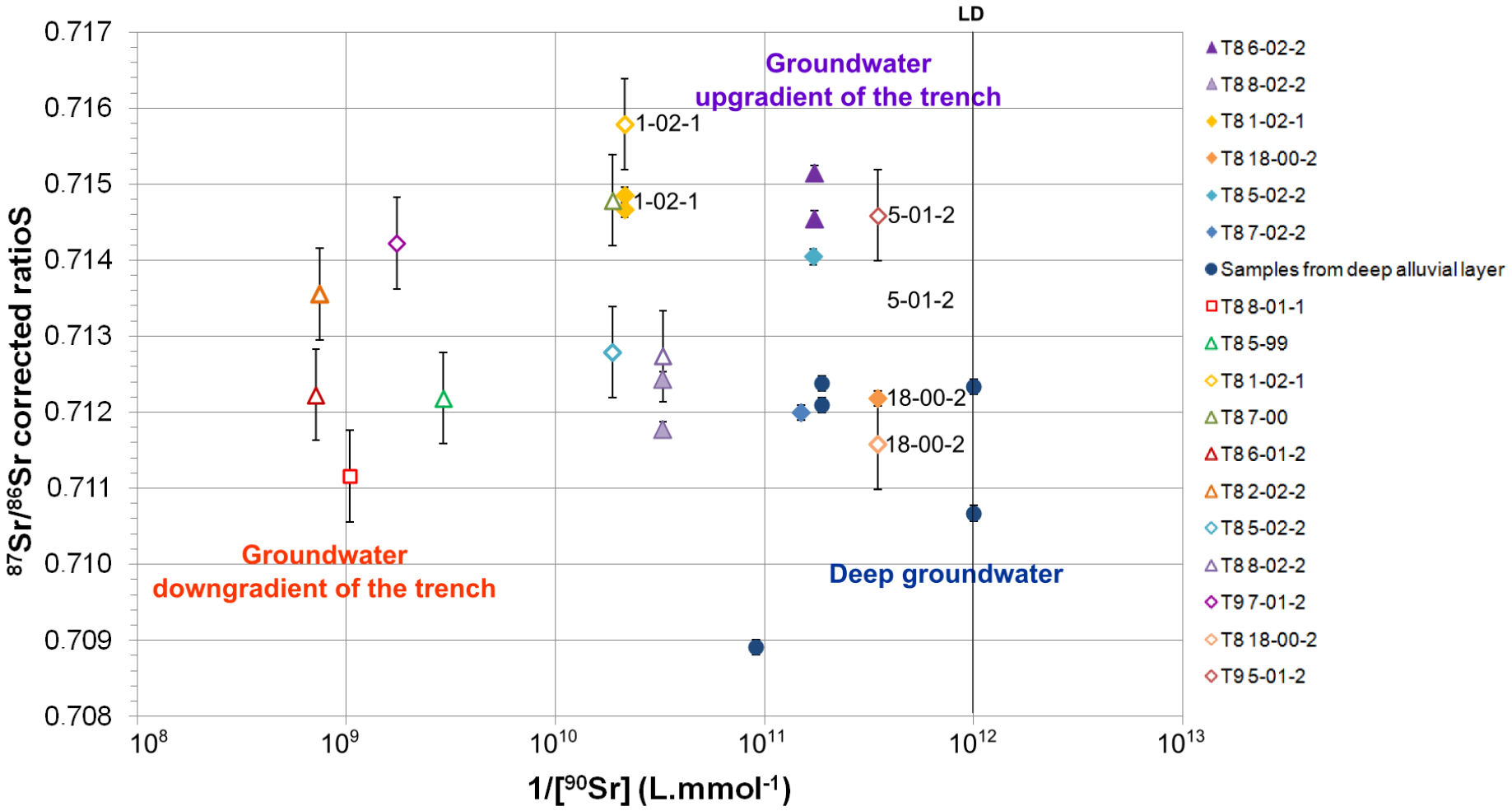

Figure IV-53: 87Sr/86Sr ratios versus 1/[90Sr]. Analyzes carried out at the University of Nîmes are shown with full symbols and analyzes carried out at the CEA-Marcoule are are shown with empty symbols.

IV.3.4 CONCLUSION

In order to better understand strontium behavior in the Chernobyl Pilot Site groundwater, $^{86}Sr/^{88}Sr$ and $^{87}Sr/^{86}Sr$ ratios were analyzed in few samples.

For $^{87}Sr/^{86}Sr$ ratios analysis, as the dynamic method on thermal ionization mass spectrometer was not recommended; consequently the total volatilization method was developed. Several filament configurations were tested to optimize the method and the repeatability was assessed (precision, standard deviation) based on analyses of strontium isotopic standard.

Increases in [^{88}Sr] concentrations and ^{90}Sr volumetric activities are shown downgradient of the trench, most likely due to migrations from the trench.

The theoretical anthropogenic impact on $^{86}Sr/^{88}Sr$ ratio calculated based on the estimated ^{88}Sr migration of the trenchremains too low to be quantified by used analytical methods.

The measured $^{86}Sr/^{88}Sr$ ratio variations are much higherthan the theoretical impact.

$^{87}Sr/^{86}Sr$ ratios seems to be little impacted by the migration of Sr from the trench T22, taking into account the low number of samples collected in the shallow groundwater. However, some geochemical processes can be supposed based on $^{87}Sr/^{86}Sr$ ratios variation: the decreasing trend with the depth seems to indicate the influence of the underlying carbonate layer $^{87}Sr/^{86}Sr$ ratio, supposed to be lower between 0.708 and 0.709 (seawater value, Capo *et al.*, 1998). Complementary analyses of deeper groundwater are needed to confirm the influence of the marine carbonates layer on $^{87}Sr/^{86}Sr$ ratios.

Furthermore, a complementary study of the $^{87}Sr/^{86}Sr$ ratio focusing on the strontium cycle from the atmosphere through the soil and biosphere could also be valuable to better characterize ^{90}Sr fluxes

V. GENERAL CONCLUSION AND PERSPECTIVES

The aim of this study was to identify processes occurring in the Chernobyl Pilot Site groundwater which may influence the migration of radionuclides released from trench T22. Non reactive processes and reactive processes were investigated separately.

First, the behavior of a conservative chlorine-36 was studied in groundwater in order to investigate the maximal extent of the contaminant plume under non-reactive processes. Indeed, ^{36}Cl, as a product of nuclear activity, was supposed to be an appropriate tracer to follow the groundwater contamination.

High chlorine-36 contamination of the groundwater, the trench soil water, leaf leachates and river water was shown with $^{36}Cl/Cl$ ratios 1 to 5 orders of magnitude higher than the natural theoretical ratio. Such ratios implied an anthropogenic ^{36}Cl. According to groundwater apparent ages (Le Gal La Salle *et al.*, 2012), this high contamination of the groundwater mostly affected groundwater recharged after the Chernobyl explosion. Trench T22 was shown to act as an obvious point source of ^{36}Cl: soil water sampled in the trench body shows $^{36}Cl/Cl$ ratio five orders of magnitude higher than the natural theoretical ratio and one order of magnitude higher than the $^{36}Cl/Cl$ ratio in upgradient groundwater. According to the comparison with $[Cl^-]$ and $[^{90}Sr]$, the dilution of the trench soil water by rainwater explained most of the Chernobyl Pilot Site groundwater ^{36}Cl contamination. Additional sources of ^{36}Cl were considered: diffuse contamination over the whole area at the time of the explosion, point source contamination release from upgradient trenches, release of ^{36}Cl by biogeochemical processes, nuclear activity at the Power Plant before the accident, thermonuclear tests. Even if Trench T22 was supposed to be the main source of ^{36}Cl contamination, these additional potential sources should be further investigated to better constrain the ^{36}Cl contamination of the Chernobyl Pilot Site groundwater.

Two different processes seemed to occur in the aeolian and alluvial layers. In the aeolian layer, the contamination seems to result from the dilution of a contaminated end-member (contaminated shallow groundwater downgradient of

trench T22 or soil water) by rainwater, depending on recharge intensity. In the shallow alluvial layer, ^{36}Cl contamination remains relatively constant, 3 orders of magnitude higher than the theoretical natural ratio while ^{90}Sr content decreases, most likely due to retention and decay processes. Further at depth, ^{36}Cl contamination is still noticeable.

Based on the hypothesis of release from trench T22 as the main ^{36}Cl source, the migration of ^{36}Cl is simulated along a profile using the hydrodynamic parameters determined in previous studies (Bugai *et al.*, 2012b; Van Meir *et al.*, 2012 and Mazet, 2008) and using a source term close to the trench soil water sampled in May 2011. In this first approximation, steady state was considered. An "optimal" simulation has been proposed with adjusted hydraulic parameters. In order to obtain results as close as possible of expected velocities and measured [^{36}Cl], the choice of the parameters is made in agreement with the natural range of variation of these parameters and an adjusted value for the source term. However, large discrepancies on [Cl^-] still remain. Improvement of the simulation results may be done by reconsidering the two main hypotheses: the consideration of a constant source term released by the trench and the steady state conditions. Moreover, studies of Cl release mechanisms and origin of upgradient contamination, as well as the impact of water table flooding the trench on Cl release should be investigated to better constrain the background ^{36}Cl level and the previous processes of groundwater contamination. A better consideration of the anisotropy in the alluvial layer should also improve simulation results. Once these processes better constrained and because the chlorine-36 plume extend outside of the boundaries of the profile considered in this study, a larger scale profile should be considered to investigate the ^{36}Cl plume maximal extent through *in situ* observations as well as through simulations..

Next, the main reactive geochemical processes occurring in groundwater were investigated. A conceptual model of the geochemical processes occurring in Chernobyl Pilot Site groundwater was proposed based on the study of major elements' behavior. Groundwater was shown to be recharged by infiltration of meteoric water (mainly winter) with limited influence of evaporation processes. Migration of elements from the trench was assumed to explain acidification and

oxidation of groundwater and increase of concentrations downgradient of the trench and particularly N-species. Water-rock interactions were supposed to explain most of the geochemical evolution with depth. Increase of CO_2 partial pressure in soils and the influence of the carbonated mineral dissolution were assumed to influence on pH, [HCO_3^-], [Ca^{2+}] and [Mg^{2+}] concentrations in the alluvial layer. The carbonated mineral dissolution could be the result of dispersed calcite dissolution in the alluvial layer, or alternatively the influence of the underlying layer composed by dense marine carbonates. Pyrite dissolution was supposed to be the main process to govern the decrease in pe values and the increase of [Fe] and [SO_4^{2-}] concentrations with increasing depth, however this mineral phase was not identified in the mineralogy. Silicates hydrolysis (albite) explained increase in [Na^+] and [Si] concentrations in the alluvial layer. Cations exchange processes were highly likely: they were shown in the aeolian layer (Szenknect, 2003) and the cation exchange capacity of the alluvial layer is higher (Matoshko *et al.*, 2004). However, the simulation carried out with the chemical PHREEQC code showed that they cannot account alone taking into consideration the observed chemical variations and that they had to be coupled to other processes to explain groundwater chemistry. Mixing processes were also possible considering potential upward leakage processes from the underlying carbonated layer. To confirm these observations, some additional studies are required, such as the fine characterization of the alluvial layer: the cation exchanger has to be defined by the precise composition of clay phases and pyrite phase has to be identified to confirm its implication on pe conditions. A focus of the involved carbonate phases should be done too, particularly on dispersed calcite in the alluvial layer and assessing the influence of the underlying marine carbonate layer.

Then, the impact of reactive processes was investigated on uranium and strontium behavior in groundwater. To investigate uranium migration, $^{238}U/^{235}U$ ratios were studied as they are supposed to be impacted by migration of uranium, released by the dissolution of fuel particles, enriched in ^{235}U. Surprisingly, $^{238}U/^{235}U$ ratios were shown to be close to the natural constant ratio, considering the precision of the optimized analytical method on Thermal Ionization Mass Spectrometer. This implied that migration of uranium released by the dissolution of fuel particles buried in trench T22 was not observable in the dissolved uranium in groundwater.

However, an increase of [^{238}U] concentrations by two orders of magnitude was observed downgradient of the trench and seemed to be due to oxidizing conditions downgradient of the trench. The fate of anthropogenic uranium released by the fuel particle dissolution must be investigated: whether released uranium was transported further than the considered area, whether uranium particles were no longer dissolved (unlikely) or if it was trapped in the trench and soils (microbial activity, adsorption processes…). The origin of the natural uranium concentration downgradient of the trench t22 need to be further investigated.

The strontium isotopic $^{86}Sr/^{88}Sr$ and $^{87}Sr/^{86}Sr$ ratios were studied aimed to emphasize the anthropogenic strontium signal in groundwater and geochemical processes that may have influence ^{90}Sr migration, such as cation exchange processes. However, considering the precision and the standard deviation of the considered analytical method on Thermal Ionization Mass Spectrometer, this anthropogenic signal is supposed to be too low on the $^{86}Sr/^{88}Sr$ ratio. $^{86}Sr/^{88}Sr$ ratio as well as $^{87}Sr/^{86}Sr$ ratio analyses did not allow evidencing influence of strontium migration from the trench. However, $^{87}Sr/^{86}Sr$ ratios significantly decreased with increasing depth and this decrease was attributed to the influence of the underlying marine carbonate layer. The investigation of strontium isotopic ratio variations could be completed by $^{87}Sr/^{86}Sr$ analyses of the different compartments: a whole groundwater profile, soil water samples, vegetation samples, rainwater and groundwater from the underlying layer. This will allow to the characterization of the strontium biogeochemical cycle and hence the ^{90}Sr plant uptake processes at the Chernobyl Pilot Site.

Several perspectives can be proposed to complete this study.

First, biogeochemical processes inside the trench (microbial activity, plant uptakes…), which result in migration of elements (H^+, O_2, N-species,…) in groundwater, need to be better constrained. ^{90}Sr fluxes to the vegetation were already supposed and uptakes by biosphere are most likely to explain such delay in radionuclide migration. Such processes should be evidenced by the study of the strontium cycle in the different compartments with $^{87}Sr/^{86}Sr$ measurements compared with ^{90}Sr contents. The fate of uranium released by the fuel particle dissolution is also an important issue because it is not observable in dissolved

uranium in groundwater. One of the hypotheses is that uranium could be trapped in soils and biosphere.

^{36}Cl, which is conservative in groundwater, is still released from the trench in important quantities. Further investigations on ^{36}Cl retention processes in the trench need to be investigated to characterize ^{36}Cl source term in the trench.Once ^{36}Cl released better characterized, the extent of ^{36}Cl in groundwater would be investigation considering a larger profile scale with in situ measurements and simulations.

Once the source term releases from the trench and non reactive processes in groundwater better constrained, simulations of reactive processes should be carried out based on the proposed conceptual model.

VI. BIBLIOGRAPHY

Ahamdach N. and Stammose D., 2000. Séparation et caractérisation microscopique des particules de combustible nucléaire presentes dans les sols contaminés de Tchernobyl. C. R. Acad. Sci. Paris, Sciences de la Terre et des planètes / Earth and Planetary Sciences 330, 415–422

Ahmed B., Coa B., Mishra B., Boyanov M. I., Kemmer K. M., Fredrickson J. K. and Beyenal H., 2012. Immobilization of U(VI) from oxic groundwater by Hanford 300 area sediments and effects of Columbia river water. Water Res. 46, 3989-3998. doi:10.1016/j.watres.2012.05.027.

Antropov V. M., Bugai D. A., Dutton M. C., Gerchikov M. Y., Kennett E. J., Ledenev A. I., Novikov A. A., Rudko V. and Ziegenhagen Y., 2001. Review and Analysis of Solid Long-Lived and High Level Radioactive Waste Arising at the Chernobyl Nuclear Power Plant and the Restricted Zone. European Commission, Nuclear Safety and the Environment. 294 p.

Appelo C. A. J. and Postma D., 2005. Geochemistry, Groundwater and Pollution - 2nd Edition. Balkema, 649 p.

Bassot S., Dupuis M. and Mifsud A., 2010. Descriptif des appareils et des techniques d'analyse utilisés au LAME. Note technique IRSN DEI/SARG/2010-035. *In French*.

Beasley T. M., Cecil L. D., Sharma P., Kubik P. W., Fehn U., Mann L. J. and Gove H. E., 1993. Chlorine-36 in Snake river plain aquifer at the Idaho National Engineering Laboratory: origin and implications. Ground Water 31. 302-310.

Bentley H. W., Phillips F. M. and Davis S. N. Chlorine-36 in the Terrestrial Environment. In *Handbook of Environmental Isotope Geochemistry, the Terrestrial Environment*. Fritz and Fontes (Eds.) (1986) p.427-480.

Bentley H. W., Phillips F. M., Davis S. N., Gifford S., Elmore D., Tubbs L. E. and Gove H. E., 1982. Thermonuclear 36Cl pulse in naturel water. Nature 300. 737-740.

Bessho K., Matsumura H., Miura T., Wang Q., Masumoto K., Hagura H., Nagashima N., Seki R., Takahashi T., Sasa K., Sueki K., Matsuhiro T. and Tosaki Y., 2007. Estimation of thermal netron fluences in the concrete of proton accelerator facilities from 36Cl production. Nuclear Instruments and Methods in Physics Research B 259. 702-707.

Bondar'kov M. D., Bondar'kov D. M., Maksimenko A. M., Zheltonozhskii V. A., Zheltonozhskaya M. V., Petrov V. V. and Savin A. I., 2009. Activity study of graphite from the Chernobyl NPP reactor. Bulletin of the Russian Academy of Sciences : Physics 73, 261-265. doi: 10.3103/S1062873809020300.

Bugai D. and Dewière L., 2004. Geology structure and hydrogeology conditions of the Chernobyl Pilot Site. Rapport IRSN 04-16. *In French*. 150p.

Bugai D., Kashparov V., Dewiére L., Khomutinin Y., Levchuk S. and Yoschenko V., 2005. Characterization of subsurface geometry and radioactivity distribution in the trench containing Chernobyl clean-up wastes. Environmental Geology 47, 869-881.

Bugai D., Kashparov V., Khomutinin Y., Levchuk S., Yoschenko V. and Dewiére L., 2005. Characterization of subsurface geometry and radioactivity distribution in the trench containing Chernobyl clean-up wastes. Environ Geol 47. 869-881

Bugai D., Skalskyy A., Dzhepo S., Kubko Y., Kashparov V., Van Meir N., Stammose D., Simonucci C. and Martin-Garin A., 2012b. Radionuclide migration at experimental polygon at red forest waste site in Chernobyl zone. Part 2: hydrogeological characterization and groundwater transport modeling. Applied geochemistry 27, 1359-1374. doi: 10.1016/j.apgeochem.2011.09.028.

Bugai D., Tkachenko E., Van Meir N., Simonucci C., Martin-Garin A., Roux C., Le Gal La Salle C. and Kubko Y., 2012a. Geochemical influences of the waste trench no.22t at Chernobyl Pilot Site at the aquifer: long-term trends, governing process, and implications for radionuclide migration. Applied geochemistry 27, 1320-1338. doi: 10.1016/j.apgeochem.2011.09.028.

Capo R. C., Stewart B. W. and Chadwick O., 1998. Strontium isotopes as tracers of ecosystem processes: theory and methods. Geoderma 82. 197-225.

Chant L. A., Andrews H. R., Cornett R. J., Koslowky V., Milton J. C. D., Van der berg J. G., Verburg T. G. and Wolterbeek H. T., 1996. 129I and 36Cl concentrations in lichens collected in 1990 from three regions around Chernobyl. Applied Radiation and Isotopes 47, 933-937.

Chapon V., Piette L., Vesvres M. H., Coppin F., Le Marec C., Christen R., Theodorakopoulos N., Février L., Levchik S., Martin-Garin A., Berthomieu C. and Sergeant C., 2012. Microbial diversity in contaminated soils alond the T22

trench of the Chernobyl experimental platform. Applied geochemistry 27, 1375-1383. doi:10.1016/j.apgeochem.2011.08.011.

Conard N. J., Elmore D., Kubik P. W., Gove H. E., Tubbs L. E., Chrunyk B. A. and Wahlen M., 1986. The chemical preparation of agcl for measuring 36Cl in polar ice with accelerator masse spectrometry. Radiocarbon 28. 556-560.

Cornett R. J., Andrews H. R., Chant L. A., Davies W. G., Greiner B. F., Imahori Y., Koslowsky V. T., Kotzer T., Milton J. C. D. and Milton G. M., 1997. Is 36Cl from weapons' test fallout still cycling in the atmosphere. Nuclear Instruments and Methods in Physics Research B 123, 378-381.

Cornett R. J., Cramer J., Andrews H. R., Chant L. A., Davies W., Greiner B. F., Imahori Y., Koslowski V., McKay J., Milton G. M. and Milton J. C. D., 1996. In situ production of 36Cl in uranium ore: a hydrogeological assessment tool. Water ressources research 32, 1511-1518. 0043-1397/96/95WR-03821$09.00.

Craig H., 1961. Isotopic variations in meteoric waters. Science 133. 1702-1703. .

Dewière L., Bugaï D., Grenier C., Kashparov V. and Ahamdach N., 2004. 90Sr migration to the geo-sphere from a waste burial in the Chernobyl exclusion zone. 74, 139-150. doi: 10.1016/j.jenvrad.2004.01.019.

Dzhepo S. and Skal'skii A. Radioactive Contamination of Groundwater within the Chernobyl Exclusion Zone. In *Chernobyl - Disaster and Groundwater*. Shestopalov V. (Ed.) (2002) p.25-70.

Elmore D., Tubbs L. E., Newmann D., Ma X. Z., Finkel R., Nishiizumi K., Beer J., Oeschger H. and Andree M., 1982. 36Cl bomb pulse measured in shallow ice core drom dye 3, greenland. Nature 300, 735-737.

Endt P. M. and Van der Leun C., 1973. Energy levels of a = 21-44 nuclei (v). Nuclear Physics A214, 1-625.

Ferrand E., **2011**. Bilan et perspectives des actions de recherches sur le transfert des radionucléides dans les sols et les nappes phréatiques. Note technique IRSN DEI/SARG/2011-016. *In French*.

Fetter C. W., 2008. Contaminant Hydrogeology - Second Edition. , Waveland Press. 330 p.

Finkel R. C., Nishiizumi K., Elmore D., Ferraro R. D. and Gove H. E., 1980. 36Cl in polar ice, rainwater ans seawater. Geophysical Research Letters 7, 983-986.

Fontes J., 1984. Hydrological implications of deep production of chlorine-36. Nuclear Instruments and Methods in Physics Research B 5, 303-307.

Green J. R., Cecil L. D., Synal H., Santos J., Kreutz K. J. and Wake C. P., 2004. A high resolution of chlorine-36 nuclear-weapons-tests fallout from central asia. Nuclear Instruments and Methods in Physics Research B 223-224, 854-857. doi: 10.1016/j.nimb.2004.04.157.

Green J. R., DeWayne Cecil L., Synal H., Kreutz K. J., Wake C., Naftz D. L. and Frape S. K., 2000. Chlorine-36 and cesium-137 in ice-core samples from mid-latitude glacial sites in the northern hemisphere. Nuclear Instruments and Methods in Physics Research B 172, 812-816.

Habfast K., 1998. Fractionation correction and multiple collectors in thermal ionization isotope ratio mass spectrometry. International Journal of Mass Spectrometry 176. 133-148.

Hou X., Frosig Ostergaard L. and Nielsen S. P., 2007. Determination of 36Cl in nuclear waste from reactor decommissing. Anal. Chem. 79. 3126-3134.

International Atomic Energy Agency, **2003-2008**. www.naweb.iaea.org/napc/ih/IHS_resources_isohis.html.

Kashparov V. A., Zvarich S. I., Yoschenko V. I., Maloshtan I. M., Ahamdach N. and Dewiere L., 2004. Kinetics of dissolution of Chernobyl fuel particles in soil in natural conditions. Journal of Environmental Radioactivity 72. 335-353.

Kashparov V., Ahamdach N., Levchuk S., Yoschenko V., Fesenko S. and Maloshtan I.. Dissolution of Particles of Irradiated Nuclear Fuel in the Temporary Storages of Radioactive Waste in Chernobyl Zone: Sources of Radionuclides Migration. In *Radioactive Particles in the Environment*. Deborah H. Oughton and Valery Kashparov (Eds.) (2009) p.139-156.

Kashparov V., Protsak V., Ahamdach N., Stammose D., Peres J. M., Yoschenko V. I. and Zvarich S. I., 2000a. Dissolution kinetics of particles of irradiated chernobyl nuclear fuel: influence of pH and oxidation state on the release of radionucleides in the contaminated soil of Chernobyl. 279. 225-233.

Kashparov V., Yoschenko V., Levchuk S., Bugai D., Van Meir N., Simonucci C. and Martin-Garin A., 2012. Radionuclide migration in the experimental polygon of the red forest waste site in the Chernobyl zone. Part 1: characterization of waste trench, fuel particle transformation processes in soils, biogenic fluxes and effects

on biota. Applied geochemitry 27, 1348-1358. doi:10.1016/j.apgeochem.2011.11.004.

Krabbenhöft A., Eisenhauer A., Böhma F., Vollstaedt H., Fietzke J., Liebetrau V., Augustin N., Peucker-Ehrenbrink B., Müller M. N., Horn C., Hansen B. T., Nolte N. and Wallmann K., 2010. Constraining the marine strontium budget with natural strontium isotope fractionations (87Sr/86Sr*, d88/86Sr) of carbonates, hydrothermal solutions and river waters. Geochimica et Cosmochemina Acta 74. 4097-4109.

Krabbenhöft A., Fietzke J., Eisenhauer A., Liebetrau V., Böhm F. and Vollstaedt H., 2009. Determination of radiogenic and stable strontium isotope ratios (87Sr/86Sr; d(88/86Sr)) by thermal ionization mass spectrometry applying an 87Sr/84Sr double spike. Journal of Analytical Spectrometry 24. 1267-1271.

Kuriny V. D., Ivanov Y. A., Kashparov V. A., Loshchilov N. A., Protsak V. P., Yudin E. B., Zhurba M. A. and Parsharov A. E., 1993. Particle-associated Chernobyl fall-out in the local and intermediate zonnes. Annals of Nuclear Energy 20, 415-420.

Langmuir D., 1978. Uranium solution-mineral equilibria at low temperatures with applications to sedimentary ore deposits. Geochemica et Cosmochemica Acta 42, 547-569.

Le Gal La Salle C., Aquilina L., Fourre E., Jean-Baptiste P., Michelot J. L., Roux C., Bugai D., Labasque T., Simonucci C., Van Meir N., Noret A., Bassot S., Dapoigny A., Baumier D., Verdoux P., Stammose D. and Lancelot J., 2012. Groundwater residence time down gradient of the T22 trench at the Chernobyl Pilot Site. constraints on groundwater models. Applied geochemistry 27, 1304-1319. doi: 10.1016/j.apgeochem.2011.12.006.

Martin-Garin A., Van Meir N., Simonucci C., Kashparov V. and Bugai D. Quantitative Assessment of Radionuclide Migration From Near-Surface Radioactive Waste Burial Sites: the Waste Dumps in the Chernobyl Exclusion Zone as an Example. In *Radionuclide Behaviour in the Natural Environment - Science, Implications and Lessons for the Nuclear Industry*. Poinssot C. and Geckeis H. (Eds.) (2012) p.570-600.

Matoshko A., Bugai D., Dewiere L. and Skalskyy A., 2004. Sedimentological study of the Chernobyl NPP site to schematise radionuclide migration conditions. Environmental Geology 46, 820-830. doi: 10.1007/s00254-004-1067-3.

Mazet P., **2008**. Influence des écoulements transitoires sur la mobilité du strontium dans les sols partiellement saturés en eau. Université Joseph Fournier - Grenoble 1. 288p. *In French.*

Michard G., 1989. Equilibre Chimique Dans les Eaux Naturelles, Publisud. 357 p. *In French.*

Milton G. M., Andrews H. R., Causey S. E., Chant L. A., Cornett R. J., Davies W. G., Greiner B. F., Koslowsky S. J., Imahori Y., Kramer S. J., McKay J. W. and Milton J. C. D., 1994. Chlorine-36 dispersion in the chalk river area. Nuclear Instruments and Methods in Physics Research B 92, 376-379.

Milton G. M., Milton J. C. D., Sciff S., Cook P., Kotzer T. G. and Cecil L. D., 2003. Evidence for chlorine recycling-hydrosphere, biosphere, atmosphere-in a forested wet zone on the canadian shield. Applied geochemistry 18, 1027-1042. doi: 10.1016/S0883-2927(02)00240-8.

National Institute of Standards and Technology, **2010-2013**.www.nist.gov.

Naudet R., 1991. Oklo : des Réacteurs Nucléaires Fossiles. Commissariat à l'Energie Atomique (Ed.), Eyrolles. *In French.*

Nier A., 1936. The isotopic constitution of strontium, barium, bismuth, thallium and mercury. Physical Review 5, 275-278.

Phillips F. M. Chlorine-36. In *Environmental Tracers in Subsurface Hydrology*. Peter Cook and Andrew L. Herczeg (Ed.) (2000) p.299-348.

Phrommavanh V., **Octobre 2008**. Etude de la migration de l'uranium en milieu naturel: approche expérimentale et modélisation géochimique. Université Joseph Fournier - Grenoble 1. 181p. *In French.*

Pin C., Joannon S., Bosg C., Le Fèvre B. and Gauthier J. P., 2003. Precise determination of Rb, Sr, Ba, and Pb in geological materials by isotope dilution and icp-quadrupole mass spectrometry following selective separation of the analytes. Journal of Analytical Atomic Spectrometry 18, 135-141. DOI: 10.1039/B211832G.

Pöllänen R., Valkama I. and Toivonen H., 1997. Transport of radioactive particles from the Chernobyl accident. Atmos. Environ. 31. 3575-3590.

Rosman K. J. R. and Taylor P. D. P., 1998. Isotopic compositions of the elements 1997. Pure and Applied Chemistry 70. 217-235.

Scanlon B. R., Kubik P. W., Sharma P., Richter B. C. and Gove H. E., 1990. Bomb chlorine-36 analysis in the characterization of unsaturated flow at a proposed radioactive waste disposal facility, Chihuahuan desert, Texas. Nuclear Instruments and Methods in Physics Research B 52. 489-492.

Schaeffer O. A., Thompson S. O. and Lark N. L., 1960. Chlorine-36 radioactivity in rain. Journal of Geophysical Research 65. 4013-4016.

Seki R., Matsuhiro T., Nagashima Y., Takahashi T., Sasa K., Sueki K., Tosaki Y., Bessho K., Matsumura H. and Miura T., 2007. Isotopic ratios of 36Cl/Cl in japanese surface soil. Nuclear Instruments and methods in Physics Research B 259. 486-490. doi: 10.1016/j.nimb.2007.01.227.

Shestopalov V., 2002. Chernobyl Disaster and Groundwater. 289 p.

Shtangeeva I., 2010. Uptake of uranium and thorium by native and cultivated plants. Journal of Environmental Radioactivity 101, 458-463. doi:/10.1016/j.jenvrad.2008.06.004.

Smith J. and Beresford N. A., 2005. Chernobyl. Catastrophe and Consequences. Smith J. and Beresford N. A. (Eds.), Springer Praxis. 310 p.

Sobotovitch E. V. and Bondarenko G. N. Isotopic Composition of Uranium in the Products of Accidental Ejection From the Chernobyl NPP. In *Radionuclides and Heavy Metals in Environment*. Frontasyeva M. V., Perelygin V. P. and Vater P. (Eds.) (2001) p.77-84.

Songsheng J., Shan J., Hong G. and Shubin D., 1994. Determination of 36Cl in the groundwaters and ores arounda uranium deposit. Nuclear Instruments and Methods in Physics Research B 92, 385-388.

Sposito G., 2008. The Chemistry of Soils, Oxford University Press. 330 p.

Stirling C. H., Andersen M. B., Potter E. and Halliday A. N., 2007. Low-temperature isotopic fractionation of uranium. Earth Planet. Sci. Lett. 264, 208-225.

Szenknect S., **2003**. Transferts de radioéléments en zone non saturée. etude expérimentale et modélisation appliquées au site pilote de tchernobyl. Université Joseph Fournier - Grenoble 1. 286p. *In French*.

Tardy Y., 1971. Characterization of the principal weathering types by the geochemistry of waters from some european and african crystalline massifs. Chem. Geol. 7, 253-271.

Thiry Y., Colle C., Yoschenko V., Levchuk S., Van Hees M., Hurtevent P. and Kashparov V., 2009. Impact of scots pine (pinus sylvestris l.) plantings on long term 137Cs and 90Sr recycling from a waste burial site in the chernobyl red forest. Journal of Environmental Radioactivity 100, 1062-1068. doi:10.1016/j.jenvrad.2009.05.003.

Thiry Y., Schmidt P., Van Hees M., Wannijn J., Van Bree P., Rufyikiri G. and Vandenhove H., 2005. Uranium distribution and cycling in scots pine (pinus sylvestris l.) growing on a revegetated u-mininge heap. Journal of Environmental Radioactivity 81. 201-219. doi:/10.1016/j.jenvrad.2004.01.036.

UNSCEAR (2000). Annex j: exposures and effects of the chernobyl accident.

Van Meir N., Ardois C., Bugai D., Kashparov V., Levchuk S., Yoschenko V. and Geckeis H., 2007. Water level fluctuations as a contributing factor to 90Sr release from a shallow waste trench at the chernobyl pilot site. Migration 2007, Munich

Van Meir N., Bugaï D. and Kashparov V..The Experimental Platform in Chernobyl: an International Research Polygon in the Exclusion Zone for Soil and Groundwater Contamination. In *Radioactive Particles in the Environment*. Deborah H. Oughton and V. Kashparov (Eds.) (2009) p.197-208.

Van Meir N., Gaudet J. P., Phrommavanh V., Laurent J. P., Bugai D. and Biron R., 2012. Flow in the unsaturated zone around a shallow subsurface radioactive waste trench: interpretation of an infiltration-dainage test at the Chernobyl Pilot Site. Applied Geochemistry 27. 1297-1303. doi: 10.1016/j.apgeochem.2011.08.009.

Van der Lee J., De Windt L., Lagneau V. and Goblet P., 2003. Module-oriented modeling of reactive transport with hytec. Computers & Geosciences 29, 265-275. doi:10.1016/S0098-3004(03)00004-9.

Zachara J., Long P. E., Bargar J., Davis J. A., Fox P., Fredrickson J. K., Freshlay M. D., Konopka A. E., Liu C., McKinley J. P., Rockhold M. L., Williams K. H. and Yabusaki S. B., 2013. Persistence of uranium groundwater plumes: contrasting mechanisms at two doe sites in the groundwater-river interaction zone. J. Contam. Hydrol. 147. 45-72. doi:/10.1016/j.jconhyd.2013.02.001.

VII. ANNEXES

1. Map of the Chernobyl Pilot Site

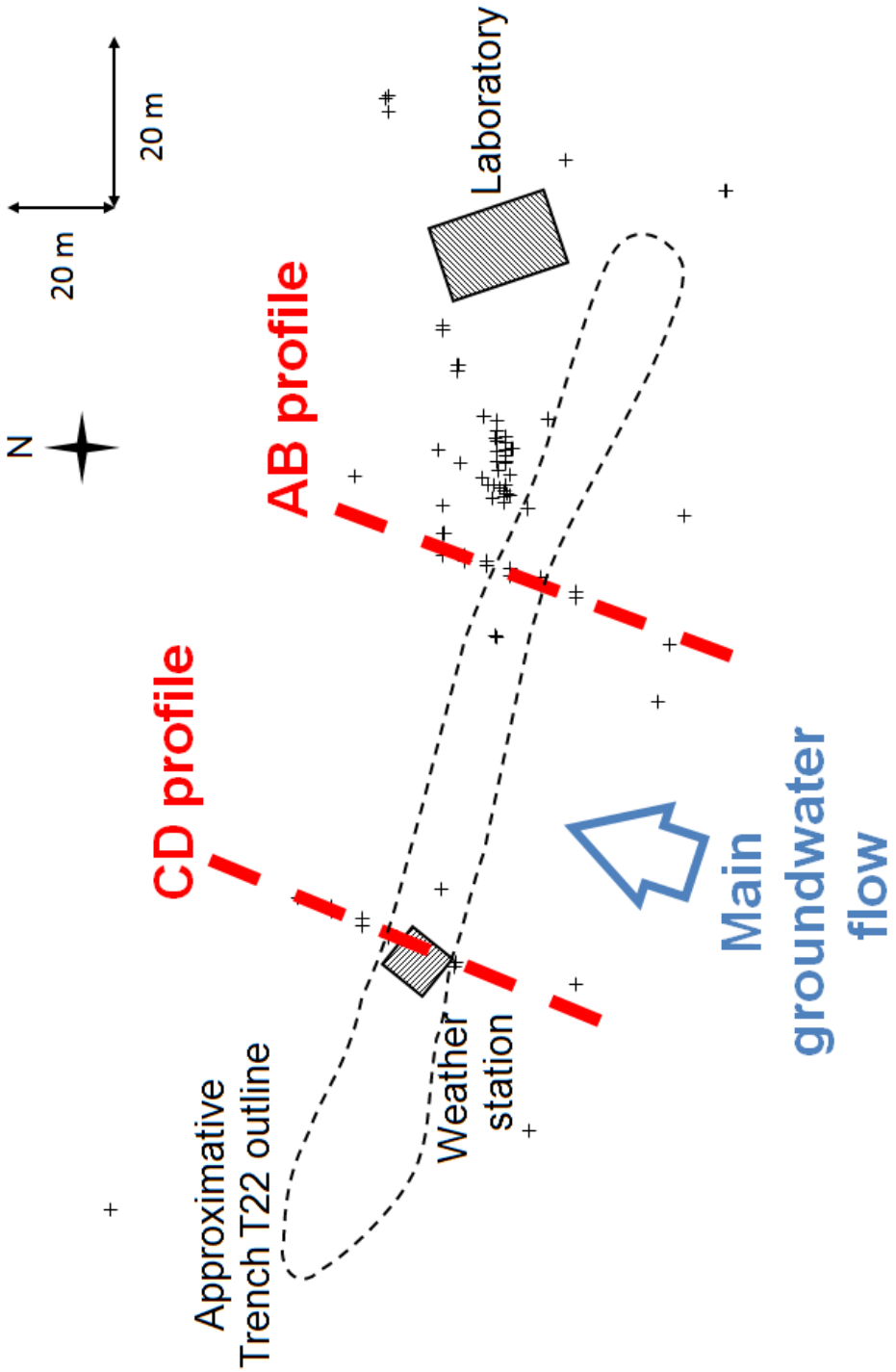

2. Piezometers profiles

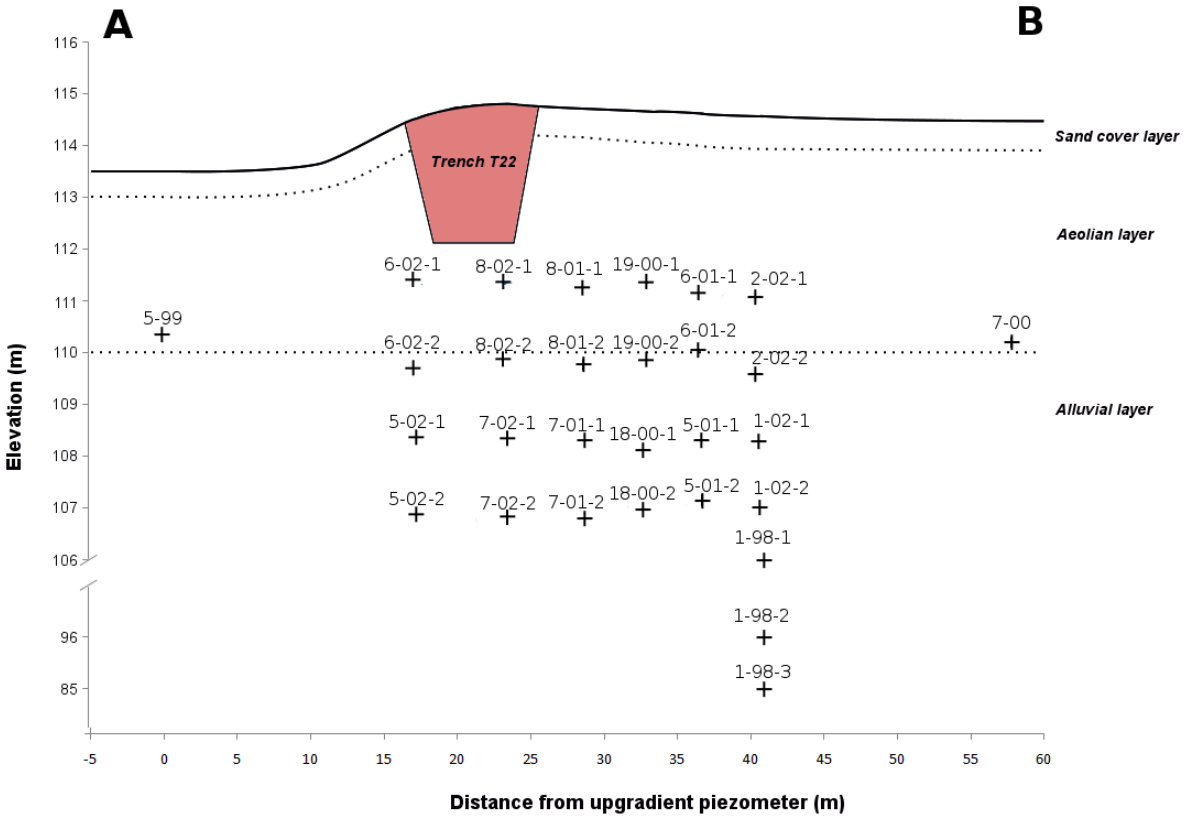

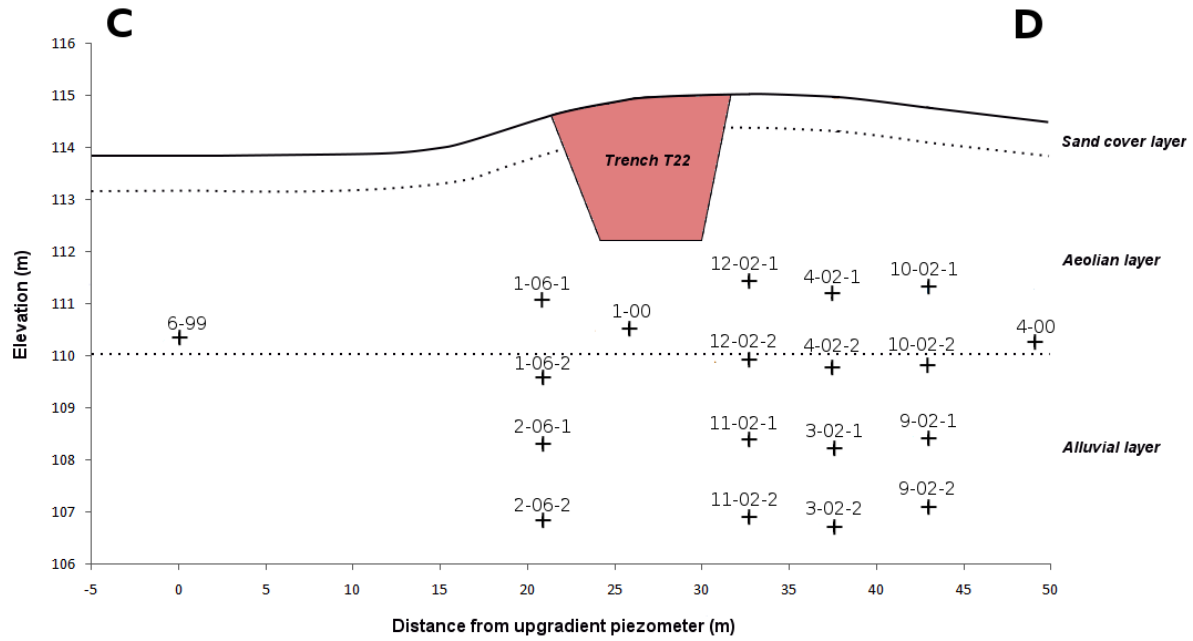

NON-REACTIVE TRANSPORT ANNEXES

3. Isotopic dilution

r = $^{36}Cl/Cl$; ech = sample; std = standard; ini = initial

Isotopic dilution tests on October 2008 samples

Sample	[Cl] $_{ini}$ (mol/L)	Uncertainty	Cl ech (mol)	Uncertainty (%)	Cl halite (mol)	Uncertainty (%)	measured r_{TOT}	Uncertainty (%)	measured r_{halite}	Uncertainty (%)	r ech	Uncertainty
1-98-2 10^{-12}	6×10^{-05}	2×10^{-07}	5.67×10^{-06}	0.36%	4.92×10^{-05}	0.95%	1.4813×10^{-12}	$\pm 3\times10^{-02}$	2.1158×10^{-15}	$\pm 3\times10^{-01}$	1.43×10^{-11}	$\pm 5\times10^{-12}$
4-00 10^{-12}	3×10^{-05}	3×10^{-07}	7.54×10^{-09}	1.40%	8.14×10^{-05}	0.94%	1.78666×10^{-13}	$\pm 3\times10^{-02}$	2.1158×10^{-15}	$\pm 3\times10^{-01}$	1.9×10^{-09}	$\pm 7\times10^{-10}$

Standards		Uncertainty (%)
r_{halite} daughter	2.116×10^{-15}	0.3171
	1.327×10^{-15}	

4. Isotopic dilution of May 2011 samples

Solutions used for the dilution

Used Standard	NIST SRM 999b			
Sample	[Cl] (mg/L)	±Uncertainty	[Cl] (mol/L)	±Uncertainty
solution mother	749	± 75.00	2.11×10^{-02}	$\pm 2.1\times10^{-03}$
solution daughter	28.9	± 2.90	8.15×10^{-04}	$\pm 8.2\times10^{-05}$

Analyses of samples

	Isotopic dilution A - Wished $R_{tot} = 1\times10^{-12}$ at.at^{-1}- solution used : daughter						Results			
Sample	Cl_{ech} (mol)	±Uncertainty	Cl_{std} (mol)	±Uncertainty	Cl_{tot} (mol)	±Uncertainty	measured R_{Tot}	±Uncertainty	R_{ech}	±Uncertainty
T11 4-02-2	7.63×10^{-08}	$\pm 7\times10^{-09}$	4.41×10^{-05}	$\pm 5\times10^{-06}$	4.42×10^{-05}	$\pm 5\times10^{-06}$				
T11 1-00	4.82×10^{-08}	$\pm 5\times10^{-09}$	4.38×10^{-05}	$\pm 5\times10^{-06}$	4.38×10^{-05}	$\pm 5\times10^{-06}$				
T11 1-06-2	1.05×10^{-07}	$\pm 1\times10^{-08}$	4.39×10^{-05}	$\pm 5\times10^{-06}$	4.40×10^{-05}	$\pm 5\times10^{-06}$				
T11 3-02-1	6.82×10^{-08}	$\pm 7\times10^{-09}$	4.39×10^{-05}	$\pm 5\times10^{-06}$	4.40×10^{-05}	$\pm 5\times10^{-06}$				
T11 6-99	1.75×10^{-07}	$\pm 2\times10^{-08}$	4.38×10^{-05}	$\pm 5\times10^{-06}$	4.40×10^{-05}	$\pm 5\times10^{-06}$				
T11 3-02-2	7.30×10^{-08}	$\pm 7\times10^{-09}$	4.40×10^{-05}	$\pm 5\times10^{-06}$	4.41×10^{-05}	$\pm 5\times10^{-06}$				
T11 2-06-1	1.49×10^{-07}	$\pm 2\times10^{-08}$	4.17×10^{-05}	$\pm 4\times10^{-06}$	4.19×10^{-05}	$\pm 4\times10^{-06}$	5.9×10^{-13}	$\pm \times10^{-14}$	$\mathbf{1.6\times10^{-10}}$	4×10^{-11}
T11 2-06-2	1.06×10^{-07}	$\pm 1\times10^{-08}$	4.42×10^{-05}	$\pm 5\times10^{-06}$	4.43×10^{-05}	$\pm 5\times10^{-06}$				
T11 1-01	1.59×10^{-07}	$\pm 2\times10^{-08}$	4.40×10^{-05}	$\pm 5\times10^{-06}$	4.41×10^{-05}	$\pm 5\times10^{-06}$				
T11 10-02-1	1.27×10^{-07}	$\pm 1\times10^{-08}$	4.31×10^{-05}	$\pm 5\times10^{-06}$	4.32×10^{-05}	$\pm 5\times10^{-06}$				
T11 9-02-2	6.87×10^{-08}	$\pm 7\times10^{-09}$	4.33×10^{-05}	$\pm 5\times10^{-06}$	4.33×10^{-05}	$\pm 5\times10^{-06}$				
T11 11-02-2	6.93×10^{-08}	$\pm 7\times10^{-09}$	4.34×10^{-05}	$\pm 5\times10^{-06}$	4.35×10^{-05}	$\pm 5\times10^{-06}$	1.21×10^{-12}	$\pm 2\times10^{-14}$	$\mathbf{8\times10^{-10}}$	2×10^{-10}
T11 11-02-1	9.26×10^{-08}	$\pm 1\times10^{-08}$	4.33×10^{-05}	$\pm 5\times10^{-06}$	4.34×10^{-05}	$\pm 5\times10^{-06}$				

Sample	Cl_{ech} (mol)	±Uncertainty	Cl_{std} (mol)	±Uncertainty	Cl_{tot} (mol)	±Uncertainty	measured R_{Tot}	±Uncertainty	**R_{ech}**	±Uncertainty
T11 IGS 33	6.06×10^{-08}	$\pm 3\times10^{-10}$	4.40×10^{-05}	$\pm 5\times10^{-06}$	4.40×10^{-05}	$\pm 5\times10^{-06}$	3.9×10^{-14}	$\pm 2\times10^{-15}$	**3×10^{-11}**	2×10^{-10}
T11 1-98-1	1.25×10^{-07}	$\pm 1\times10^{-08}$	4.46×10^{-05}	$\pm 5\times10^{-06}$	4.47×10^{-05}	$\pm 5\times10^{-06}$				
T11 12-02-1	9.00×10^{-08}	$\pm 9\times10^{-09}$	4.38×10^{-05}	$\pm 5\times10^{-06}$	4.39×10^{-05}	$\pm 5\times10^{-06}$	5.10×10^{-12}	$\pm 7\times10^{-14}$	**2.5×10^{-09}**	5×10^{-10}
T11 9-02-1	8.16×10^{-08}	$\pm 9\times10^{-09}$	4.39×10^{-05}	$\pm 5\times10^{-06}$	4.40×10^{-05}	$\pm 5\times10^{-06}$				
T11 10-02-2	1.49×10^{-07}	$\pm 2\times10^{-08}$	4.42×10^{-05}	$\pm 5\times10^{-06}$	4.43×10^{-05}	$\pm 5\times10^{-06}$				
TCV 11-1	3.95×10^{-07}	$\pm 4\times10^{-08}$	4.36×10^{-05}	$\pm 5\times10^{-06}$	4.40×10^{-05}	$\pm 5\times10^{-06}$				
TCV 11-2	1.44×10^{-06}	$\pm 1\times10^{-07}$	4.30×10^{-05}	$\pm 5\times10^{-06}$	4.44×10^{-05}	$\pm 5\times10^{-06}$				
T11 12-02-2	5.88×10^{-08}	$\pm 6\times10^{-09}$	4.38×10^{-05}	$\pm 5\times10^{-06}$	4.39×10^{-05}	$\pm 5\times10^{-06}$	9.1×10^{-13}	$\pm 2\times10^{-14}$	**7×10^{-10}**	2×10^{-10}
T11 4-02-1	1.73×10^{-07}	$\pm 2\times10^{-08}$	4.42×10^{-05}	$\pm 5\times10^{-06}$	4.43×10^{-05}	$\pm 5\times10^{-06}$				
T11 1-06-1	3.98×10^{-08}	$\pm 4\times10^{-09}$	4.39×10^{-05}	$\pm 5\times10^{-06}$	4.39×10^{-05}	$\pm 5\times10^{-06}$				
T11 4-00	1.70×10^{-07}	$\pm 2\times10^{-08}$	4.43×10^{-05}	$\pm 5\times10^{-06}$	4.44×10^{-05}	$\pm 5\times10^{-06}$				
T11 1-98-3	1.18×10^{-07}	$\pm 1\times10^{-08}$	4.43×10^{-05}	$\pm 5\times10^{-06}$	4.44×10^{-05}	$\pm 5\times10^{-06}$	9×10^{-15}	$\pm 1\times10^{-15}$	**2×10^{-12}**	2×10^{-12}
T11 1-98-2	2.90×10^{-07}	$\pm 3\times10^{-08}$	4.44×10^{-05}	$\pm 5\times10^{-06}$	4.47×10^{-05}	$\pm 5\times10^{-06}$	2.41×10^{-13}	$\pm 7\times10^{-15}$	**3.7×10^{-11}**	9×10^{-12}

Sample	Cl_{ech} (mol)	±Uncertainty	Cl_{std} (mol)	±Uncertainty	Cl_{tot} (mol)	±Uncertainty	measured R_{Tot}	±Uncertainty	R_{ech}	±Uncertainty
Borshi	8.47×10^{-07}	$\pm 9\times10^{-08}$	4.38×10^{-05}	$\pm 5\times10^{-06}$	4.46×10^{-05}	$\pm 5\times10^{-06}$				
TWS SWS 1.25m	1.74×10^{-06}	$\pm 2\times10^{-07}$	4.34×10^{-05}	$\pm 5\times10^{-06}$	4.51×10^{-05}	$\pm 5\times10^{-06}$				

	Isotopic dilution B- Wished R_{tot} = 1×10^{-14} at.at^{-1}- solution used : mother						Results			
Sample	Cl_{ech} (mol)	±Uncertainty	Cl_{std} (mol)	±Uncertainty	Cl_{tot} (mol)	±Uncertainty	measured R_{Tot}	±Uncertainty	R_{ech}	±Uncertainty
T11 4-02-2	1.52×10^{-08}	$\pm 1\times10^{-09}$	6.19×10^{-04}	$\pm 7\times10^{-05}$	6.19×10^{-04}	$\pm 7\times10^{-05}$	3.1×10^{-14}	$\pm 2\times10^{-15}$	1.2×10^{-09}	4×10^{-10}
T11 1-00	9.49×10^{-09}	$\pm 1\times10^{-09}$	6.17×10^{-04}	$\pm 6\times10^{-05}$	6.17×10^{-04}	$\pm 6\times10^{-05}$	1.3×10^{-14}	$\pm 1\times10^{-15}$	7×10^{-10}	3×10^{-10}
T11 1-06-2	2.09×10^{-08}	$\pm 2\times10^{-09}$	6.24×10^{-04}	$\pm 7\times10^{-05}$	6.24×10^{-04}	$\pm 7\times10^{-05}$	2.3×10^{-14}	$\pm 1\times10^{-15}$	6×10^{-10}	2×10^{-10}
T11 3-02-1	1.31×10^{-08}	$\pm 1\times10^{-09}$	6.24×10^{-04}	$\pm 7\times10^{-05}$	6.24×10^{-04}	$\pm 7\times10^{-05}$	1.9×10^{-14}	$\pm 2\times10^{-15}$	8×10^{-10}	3×10^{-10}
T11 6-99	3.42×10^{-08}	$\pm 4\times10^{-09}$	6.17×10^{-04}	$\pm 6\times10^{-05}$	6.17×10^{-04}	$\pm 6\times10^{-05}$				
T11 3-02-2	1.41×10^{-08}	$\pm 1\times10^{-09}$	2.36×10^{-05}	$\pm 2\times10^{-06}$	2.37×10^{-05}	$\pm 2\times10^{-06}$	3.3×10^{-14}	$\pm 2\times10^{-15}$	5×10^{-11}	2×10^{-11}
T11 2-06-1	2.94×10^{-08}	$\pm 3\times10^{-09}$	6.19×10^{-04}	$\pm 7\times10^{-05}$	6.19×10^{-04}	$\pm 7\times10^{-05}$				
T11 2-06-2	2.06×10^{-08}	$\pm 2\times10^{-09}$	6.26×10^{-04}	$\pm 7\times10^{-05}$	6.26×10^{-04}	$\pm 7\times10^{-05}$	4.7×10^{-14}	$\pm 2\times10^{-15}$	1.3×10^{-09}	4×10^{-10}
T11 1-01	3.19×10^{-08}	$\pm 3\times10^{-09}$	6.24×10^{-04}	$\pm 7\times10^{-05}$	6.24×10^{-04}	$\pm 7\times10^{-05}$	1.76×10^{-13}	$\pm 9\times10^{-15}$	3.4×10^{-09}	9×10^{-10}
T11 10-02-1	2.53×10^{-08}	$\pm 3\times10^{-09}$	6.18×10^{-04}	$\pm 6\times10^{-05}$	6.18×10^{-04}	$\pm 6\times10^{-05}$	6.3×10^{-14}	$\pm 2\times10^{-15}$	1.5×10^{-09}	4×10^{-10}
T11 9-02-2	1.36×10^{-08}	$\pm 1\times10^{-09}$	6.20×10^{-04}	$\pm 7\times10^{-05}$	6.20×10^{-04}	$\pm 7\times10^{-05}$	1.6×10^{-14}	$\pm 1\times10^{-15}$	6×10^{-10}	3×10^{-10}

Sample	Cl_{ech} (mol)	±Uncertainty	Cl_{std} (mol)	±Uncertainty	Cl_{tot} (mol)	±Uncertainty	measured R_{Tot}	±Uncertainty	R_{ech}	±Uncertainty
T11 11-02-2	1.37×10^{-08}	$\pm 1\times10^{-09}$	6.19×10^{-04}	$\pm 7\times10^{-05}$	6.19×10^{-04}	$\pm 7\times10^{-05}$				
T11 11-02-1	1.82×10^{-08}	$\pm 2\times10^{-09}$	6.20×10^{-04}	$\pm 7\times10^{-05}$	6.20×10^{-04}	$\pm 7\times10^{-05}$	1.5×10^{-14}	$\pm 1\times10^{-15}$	4×10^{-10}	2×10^{-10}
T11 IGS 33	1.20×10^{-08}	$\pm 6\times10^{-11}$	5.86×10^{-04}	$\pm 6\times10^{-05}$	5.86×10^{-04}	$\pm 6\times10^{-05}$				
T11 1-98-1	2.46×10^{-08}	$\pm 3\times10^{-09}$	6.29×10^{-04}	$\pm 7\times10^{-05}$	6.29×10^{-04}	$\pm 7\times10^{-05}$	9.6×10^{-14}	$\pm 3\times10^{-15}$	2.4×10^{-09}	6×10^{-10}
T11 12-02-1	1.77×10^{-08}	$\pm 2\times10^{-09}$	6.16×10^{-04}	$\pm 6\times10^{-05}$	6.16×10^{-04}	$\pm 6\times10^{-05}$	9.8×10^{-14}	$\pm 3\times10^{-15}$	3.3×10^{-09}	8×10^{-10}
T11 9-02-1	1.61×10^{-08}	$\pm 2\times10^{-09}$	6.25×10^{-04}	$\pm 7\times10^{-05}$	6.25×10^{-04}	$\pm 7\times10^{-05}$	1.6×10^{-14}	$\pm 1\times10^{-15}$	5×10^{-10}	2×10^{-10}
T11 10-02-2	2.95×10^{-08}	$\pm 3\times10^{-09}$	6.21×10^{-04}	$\pm 7\times10^{-05}$	6.21×10^{-04}	$\pm 7\times10^{-05}$				
TCV 11-1	7.84×10^{-08}	$\pm 8\times10^{-09}$	6.05×10^{-04}	$\pm 6\times10^{-05}$	6.05×10^{-04}	$\pm 6\times10^{-05}$	4.8×10^{-13}	$\pm 2\times10^{-14}$	3.7×10^{-09}	9×10^{-10}
TCV 11-2	2.87×10^{-07}	$\pm 3\times10^{-08}$	6.15×10^{-04}	$\pm 6\times10^{-05}$	6.15×10^{-04}	$\pm 6\times10^{-05}$				
T11 12-02-2	1.18×10^{-08}	$\pm 1\times10^{-09}$	6.18×10^{-04}	$\pm 6\times10^{-05}$	6.18×10^{-04}	$\pm 6\times10^{-05}$	1.8×10^{-14}	$\pm 1\times10^{-15}$	8×10^{-10}	3×10^{-10}
T11 4-02-1	3.46×10^{-08}	$\pm 4\times10^{-09}$	6.20×10^{-04}	$\pm 7\times10^{-05}$	6.20×10^{-04}	$\pm 7\times10^{-05}$	1.82×10^{-13}	$\pm 5\times10^{-15}$	3.2×10^{-09}	8×10^{-10}
T11 1-06-1	7.91×10^{-09}	$\pm 8\times10^{-10}$	6.25×10^{-04}	$\pm 7\times10^{-05}$	6.25×10^{-04}	$\pm 7\times10^{-05}$	1.4×10^{-14}	$\pm 1\times10^{-15}$	9×10^{-10}	4×10^{-10}

Sample	Cl_{ech} (mol)	±Uncertainty	Cl_{std} (mol)	±Uncertainty	Cl_{tot} (mol)	±Uncertainty	measured R_{Tot}	±Uncertainty	R_{ech}	±Uncertainty
T11 4-00	3.35×10^{-08}	$\pm 4\times10^{-09}$	6.21×10^{-04}	$\pm 7\times10^{-05}$	6.21×10^{-04}	$\pm 7\times10^{-05}$	1.48×10^{-13}	$\pm 4\times10^{-15}$	2.7×10^{-09}	7×10^{-10}
T11 1-98-3	2.33×10^{-08}	$\pm 2\times10^{-09}$	6.26×10^{-04}	$\pm 7\times10^{-05}$	6.26×10^{-04}	$\pm 7\times10^{-05}$				
T11 1-98-2	5.77×10^{-08}	$\pm 6\times10^{-09}$	6.25×10^{-04}	$\pm 7\times10^{-05}$	6.25×10^{-04}	$\pm 7\times10^{-05}$				
Borshi	1.69×10^{-07}	$\pm 2\times10^{-08}$	6.19×10^{-04}	$\pm 7\times10^{-05}$	6.19×10^{-04}	$\pm 7\times10^{-05}$	4×10^{-15}	$\pm 1\times10^{-15}$	1.4×10^{-11}	8×10^{-12}
TWS SWS 1.25m	3.30×10^{-07}	$\pm 3\times10^{-08}$	6.19×10^{-04}	$\pm 7\times10^{-05}$	6.20×10^{-04}	$\pm 7\times10^{-05}$				

	Isotopic dilution C - Wished $R_{tot} = 5\times10^{-15}$ at.at^{-1}- solution used : mother						Results			
Sample	Cl_{ech} (mol)	±Uncertainty	Cl_{std} (mol)	±Uncertainty	Cl_{tot} (mol)	±Uncertainty	measured R_{Tot}	±Uncertainty	R_{ech}	±Uncertainty
T11 4-02-2	1.43×10^{-09}	$\pm 1\times10^{-10}$	8.27×10^{-04}	$\pm 9\times10^{-05}$	8.27×10^{-04}	$\pm 9\times10^{-05}$				
T11 1-00	7.52×10^{-10}	$\pm 8\times10^{-11}$	8.21×10^{-04}	$\pm 9\times10^{-05}$	8.21×10^{-04}	$\pm 9\times10^{-05}$				
T11 1-06-2	1.80×10^{-09}	$\pm 2\times10^{-10}$	8.32×10^{-04}	$\pm 9\times10^{-05}$	8.32×10^{-04}	$\pm 9\times10^{-05}$				
T11 3-02-1	1.05×10^{-09}	$\pm 1\times10^{-10}$	8.22×10^{-04}	$\pm 9\times10^{-05}$	8.22×10^{-04}	$\pm 9\times10^{-05}$				
T11 6-99	1.90×10^{-09}	$\pm 2\times10^{-10}$	8.18×10^{-04}	$\pm 9\times10^{-05}$	8.18×10^{-04}	$\pm 9\times10^{-05}$	5.46×10^{-15}	$\pm 6\times10^{-16}$	$\mathbf{1\times10^{-09}}$	$\mathbf{1\times10^{-09}}$
T11 3-02-2	1.09×10^{-09}	$\pm 1\times10^{-10}$	8.22×10^{-04}	$\pm 9\times10^{-05}$	8.22×10^{-04}	$\pm 9\times10^{-05}$				
T11 2-06-1	2.79×10^{-09}	$\pm 3\times10^{-10}$	8.19×10^{-04}	$\pm 9\times10^{-05}$	8.19×10^{-04}	$\pm 9\times10^{-05}$	1.70×10^{-15}	$\pm 4\times10^{-16}$	$\mathbf{3\times10^{-10}}$	$\mathbf{3\times10^{-10}}$
T11 2-06-2	1.65×10^{-09}	$\pm 2\times10^{-10}$	8.34×10^{-04}	$\pm 9\times10^{-05}$	8.34×10^{-04}	$\pm 9\times10^{-05}$				
T11 1-01	2.58×10^{-09}	$\pm 3\times10^{-10}$	8.22×10^{-04}	$\pm 9\times10^{-05}$	8.22×10^{-04}	$\pm 9\times10^{-05}$				
T11 10-02-1	1.74×10^{-09}	$\pm 2\times10^{-10}$	8.15×10^{-04}	$\pm 9\times10^{-05}$	8.15×10^{-04}	$\pm 9\times10^{-05}$				
T11 9-02-2	1.23×10^{-09}	$\pm 1\times10^{-10}$	8.18×10^{-04}	$\pm 9\times10^{-05}$	8.18×10^{-04}	$\pm 9\times10^{-05}$				

Sample	Cl_{ech} (mol)	±Uncertainty	Cl_{std} (mol)	±Uncertainty	Cl_{tot} (mol)	±Uncertainty	measured R_{Tot}	±Uncertainty	R_{ech}	±Uncertainty
T11 11-02-2	9.69×10^{-10}	$\pm 1\times10^{-10}$	8.42×10^{-04}	$\pm 9\times10^{-05}$	8.42×10^{-04}	$\pm 9\times10^{-05}$				
T11 11-02-1	1.24×10^{-09}	$\pm 1\times10^{-10}$	8.22×10^{-04}	$\pm 9\times10^{-05}$	8.22×10^{-04}	$\pm 9\times10^{-05}$				
T11 IGS 33	1.08×10^{-09}	$\pm 8\times10^{-12}$	8.27×10^{-04}	$\pm 9\times10^{-05}$	8.27×10^{-04}	$\pm 9\times10^{-05}$				
T11 1-98-1	2.15×10^{-09}	$\pm 2\times10^{-10}$	8.41×10^{-04}	$\pm 9\times10^{-05}$	8.41×10^{-04}	$\pm 9\times10^{-05}$	5.32×10^{-12}	$\pm 7\times10^{-14}$	**2.1×10^{-06}**	**5×10^{-07}**
T11 12-02-1	1.45×10^{-09}	$\pm 1\times10^{-10}$	8.17×10-04	± 9×10-05	8.17×10-04	± 9×10-05				
T11 9-02-1	1.22×10^{-09}	$\pm 1\times10^{-10}$	8.29×10^{-04}	$\pm 9\times10^{-05}$	8.29×10^{-04}	$\pm 9\times10^{-05}$				
T11 10-02-2	2.10×10^{-09}	$\pm 2\times10^{-10}$	8.19×10^{-04}	$\pm 9\times10^{-05}$	8.19×10^{-04}	$\pm 9\times10^{-05}$	1.21×10^{-14}	$\pm 1\times10^{-15}$	**4×10^{-09}**	**2×10^{-09}**
TCV 11-1	5.82×10^{-09}	$\pm 6\times10^{-10}$	8.28×10^{-04}	$\pm 9\times10^{-05}$	8.28×10^{-04}	$\pm 9\times10^{-05}$	3.03×10^{-14}	$\pm 2\times10^{-15}$	**4×10^{-09}**	**1×10^{-09}**
TCV 11-2	2.04×10^{-08}	$\pm 2\times10^{-09}$	8.23×10^{-04}	$\pm 9\times10^{-05}$	8.23×10^{-04}	$\pm 9\times10^{-05}$	2.60×10^{-13}	$\pm 7\times10^{-15}$	**1.0×10^{-08}**	**2×10^{-09}**
T11 12-02-2	1.13×10^{-09}	$\pm 1\times10^{-10}$	8.27×10^{-04}	$\pm 9\times10^{-05}$	8.27×10^{-04}	$\pm 9\times10^{-05}$				
T11 4-02-1	3.30×10^{-09}	$\pm 4\times10^{-10}$	8.30×10^{-04}	$\pm 9\times10^{-05}$	8.30×10^{-04}	$\pm 9\times10^{-05}$				
T11 1-06-1	6.93×10^{-10}	$\pm 7\times10^{-11}$	8.33×10^{-04}	$\pm 9\times10^{-05}$	8.33×10^{-04}	$\pm 9\times10^{-05}$				

Sample	Cl_{ech} (mol)	±Uncertainty	Cl_{std} (mol)	±Uncertainty	Cl_{tot} (mol)	±Uncertainty	measured R_{Tot}	±Uncertainty	R_{ech}	±Uncertainty
T11 4-00	3.24×10^{-09}	$\pm 3\times10^{-10}$	8.36×10^{-04}	$\pm 9\times10^{-05}$	8.36×10^{-04}	$\pm 9\times10^{-05}$				
T11 1-98-3	2.00×10^{-09}	$\pm 2\times10^{-10}$	8.32×10^{-04}	$\pm 9\times10^{-05}$	8.32×10^{-04}	$\pm 9\times10^{-05}$				
T11 1-98-2	4.61×10^{-09}	$\pm 5\times10^{-10}$	8.34×10^{-04}	$\pm 9\times10^{-05}$	8.34×10^{-04}	$\pm 9\times10^{-05}$				
Borshi	1.13×10^{-08}	$\pm 1\times10^{-09}$	8.26×10^{-04}	$\pm 9\times10^{-05}$	8.26×10^{-04}	$\pm 9\times10^{-05}$	1.19×10^{-15}	$\pm 4\times10^{-16}$	$\mathbf{5\times10^{-11}}$	$\mathbf{7\times10^{-11}}$
TWS SWS 1.25m	1.67×10^{-08}	$\pm 2\times10^{-09}$	8.20×10^{-04}	$\pm 9\times10^{-05}$	8.20×10^{-04}	$\pm 9\times10^{-05}$	2.36×10^{-13}	$\pm 6\times10^{-15}$	$\mathbf{1.2\times10^{-08}}$	$\mathbf{3\times10^{-09}}$

5. Results used of the non reactive transport study

[Cl^-], ^{90}Sr volumetric activity, $^{36}Cl/Cl$ measured ratios and laboratory where $^{36}Cl/Cl$ were measured for samples collected in October 2008 and October 2009 at the CPS (from upgradient to downgradient)

Sampled piezometer (profile)	Date of sampling	Mean screen altitude (m)	[^{90}Sr] (mmol.L^{-1})	[Cl^-] (mmol.L^{-1})	Measured $^{36}Cl/Cl$ (Laboratory) (at.at^{-1})	[^{36}Cl] (mmol.L^{-1})
6-99 (CD)	Oct-2008	110.3	$4.0\times10^{-10} \pm 3\times10^{-11}$	0.0221 ± 0.0002	$3.1\times10^{-10} \pm 6\times10^{-11}$ (ANU)	$6.9\times10^{-12} \pm 1\times10^{-12}$
2-06-2 (CD)	Oct-2008	106.8	$5\times10^{-12} \pm 2\times10^{-12}$	0.0235 ± 0.0009	$4.5\times10^{-10} \pm 9\times10^{-11}$ (ANU)	$1\times10^{-11} \pm 3\times10^{-12}$
3-02-2 (CD)	Oct-2008	106.7	$4.8\times10^{-11} \pm 4\times10^{-12}$	0.0214 ± 0.0002	$5\times10^{-10} \pm 1\times10^{-10}$ (ANU)	$1\times10^{-11} \pm 2\times10^{-12}$
4-00 (CD)	Oct-2008	110.3	$8.3\times10^{-09} \pm 5\times10^{-10}$	0.0300 ± 0.0003	$5\times10^{-9} \pm 2.5\times10^{-9}$ (ANU)	$2\times10^{-10} \pm 8\times10^{-11}$
					$1.9\times10^{-9} \pm 7\times10^{-10}$ (ASTER)	$5.7\times10^{-11} \pm 2.0\times10^{-11}$
1-98-2 (AB)	Oct-2008	96.0	$<2.9\times10^{-12}$	0.0567 ± 0.0002	$1.68\times10^{-11} \pm 8\times10^{-13}$ (ANU)	$9.5\times10^{-13} \pm 5\times10^{-14}$
					$1.5\times10^{-11} \pm 5\times10^{-12}$ (ASTER)	$8.1\times10^{-13} \pm 2.6\times10^{-13}$
11-02-1 (CD)	Oct-2009	108.4	$<1.7\times10^{-12}$	0.0102 ± 0.0007	$2.2\times10^{-10} \pm 4\times10^{-11}$ (ANU)	$2.3\times10^{-12} \pm 6\times10^{-13}$
3-02-1 (CD)	Oct-2009	108.2	$6\times10^{-12} \pm 2\times10^{-12}$	0.0100 ± 0.0007	$2.8\times10^{-10} \pm 6\times10^{-11}$ (ANU)	$2.8\times10^{-12} \pm 8\times10^{-13}$
3-02-2 (CD)	Oct-2009	106.7	$5\times10^{-12} \pm 2\times10^{-12}$	0.0130 ± 0.0010	$7\times10^{-10} \pm 1\times10^{-10}$ (ANU)	$9.7\times10^{-12} \pm 3\times10^{-12}$
9-02-1 (CD)	Oct-2009	108.4	$2.5\times10^{-10} \pm 2\times10^{-11}$	0.0122 ± 0.0000	$4.6\times10^{-10} \pm 9\times10^{-11}$ (ANU)	$5.6\times10^{-12} \pm 1\times10^{-12}$
9-02-2 (CD)	Oct-2009	107.1	$6\times10^{-12} \pm 2\times10^{-12}$	0.0149 ± 0.0018	$5\times10^{-10} \pm 1\times10^{-10}$ (ANU)	$7.6\times10^{-12} \pm 2\times10^{-12}$

[Cl^-] concentrations, $^{36}Cl/Cl$ ratios measured on ASTER (CEREGE) for each isotopic dilution of samples collected in May 2011 outside the CPS

Sample (nature)	[^{90}Sr] ($mmol.L^{-1}$)	[Cl^-] ($mmol.L^{-1}$)	Calculated $^{36}Cl/Cl$ Dilution A ($at.at^{-1}$)	Calculated $^{36}Cl/Cl$ Dilution B ($at.at^{-1}$)	Calculated $^{36}Cl/Cl$ Dilution C ($at.at^{-1}$)	[^{36}Cl] ($mmol.L^{-1}$)
IGS33 (groundwater)	$8.0\times10^{-8} \pm 0.2\times10^{-8}$	0.012	3×10^{-11}			3×10^{-13}
Borschii (river water)	$2.1\times10^{-11} \pm 0.1\times10^{-11}$	0.17 ± 0.02		$1.4\times10^{-11} \pm 0.8\times10^{-11}$	$5\times10^{-11} \pm 7\times10^{-11}$	$2.4\times10^{-12} \pm 1.6\times10^{-12}$

$^{36}Cl/Cl$ ratios measured on ASTER (CEREGE) for each isotopic dilution of vegetal samples collected in May 2011

Sample (nature)	$^{36}Cl/Cl$ calculated ratio Dilution B ($at.at^{-1}$)	$^{36}Cl/Cl$ calculated ratio Dilution C ($at.at^{-1}$)
TCV 1 (leaves)	$3.7\times10^{-9} \pm 9\times10^{-10}$	$4\times10^{-9} \pm 1\times10^{-9}$
TCV 2 (leaves)		$1.05\times10^{-8} \pm 2\times10^{-9}$

[Cl^-], ^{90}Sr volumetric activity, $^{36}Cl/Cl$ ratios measured on ASTER (CEREGE) for each isotopic dilution of samples collected in May 2011 at the CPS

Sampled piezometer (profile)	Mean screen altitude (m)	[Cl^-] ($mmol.L^{-1}$)	[^{90}Sr] ($mmol.L^{-1}$)	Calculated $^{36}Cl/Cl$ Dilution A ($at.at^{-1}$)	Calculated $^{36}Cl/Cl$ Dilution B ($at.at^{-1}$)	Calculated $^{36}Cl/Cl$ Dilution C ($at.at^{-1}$)	[^{36}Cl] (Dilution) ($mmol.L^{-1}$)
TWS SWS 1.25m (CD)	1.25	0.35 ±0.04	4.1×10^{-8} $\pm1\times10^{-9}$		1.16×10^{-8} $\pm3\times10^{-9}$		4.1×10^{-9} $\pm1\times10^{-9}$ (B)
6-99 (CD)	110.3	0.035 ± 0.003	4×10^{-10} $\pm1\times10^{-11}$			1.3×10^{-9} $\pm1\times10^{-9}$	5×10^{-11} $\pm5\times10^{-11}$ (C)
1-06-1 (CD)	111.1	0.008 ± 0.001	5×10^{-11} $\pm2\times10^{-12}$		9×10^{-10} $\pm4\times10^{-10}$		8×10^{-12} $\pm4\times10^{-12}$ (B)
1-06-2 (CD)	109.6	0.021 ± 0.002	9×10^{-11} $\pm3\times10^{-12}$		6×10^{-10} $\pm2\times10^{-10}$		1×10^{-11} $\pm6\times10^{-12}$ (B)
1-00 (CD)	110.5	0.010 ± 0.001	6×10^{-10} $\pm2\times10^{-11}$		7×10^{-10} $\pm3\times10^{-10}$		7×10^{-12} $\pm4\times10^{-12}$ (B)
12-02-1 (CD)	111.4	0.018 ± 0.002	3.0×10^{-8} $\pm8\times10^{-10}$	2.5×10^{-9} $\pm5\times10^{-10}$	3.3×10^{-9} $\pm8\times10^{-10}$		4.5×10^{-11} $\pm1\times10^{-11}$ (A)
12-02-2 (CD)	109.9	0.012 ± 0.001	4×10^{-9} $\pm1\times10^{-10}$	7×10^{-10} $\pm2\times10^{-10}$			8×10^{-12} $\pm3\times10^{-12}$ (A)
4-02-1 (CD)	111.2	0.035 ± 0.003	3×10^{-8} $\pm8\times10^{-10}$		3.2×10^{-9} $\pm8\times10^{-10}$		1×10^{-10} $\pm4\times10^{-11}$ (B)

Sampled piezometer (profile)	Mean screen altitude (m)	$[Cl^-]$ ($mmol.L^{-1}$)	$[^{90}Sr]$ ($mmol.L^{-1}$)	Calculated $^{36}Cl/Cl$ Dilution A ($at.at^{-1}$)	Calculated $^{36}Cl/Cl$ Dilution B ($at.at^{-1}$)	Calculated $^{36}Cl/Cl$ Dilution C ($at.at^{-1}$)	$[^{36}Cl]$ (Dilution) ($mmol.L^{-1}$)
4-02-2 (CD)	109.8	0.015 ± 0.001	9.9×10^{-9} $\pm3\times10^{-10}$		1.2×10^{-9} $\pm4\times10^{-10}$		1.8×10^{-11} $\pm7\times10^{-12}$ (B)
10-02-1 (CD)	111.3	0.026 ± 0.003	2.4×10^{-9} $\pm7\times10^{-11}$		1.5×10^{-9} $\pm4\times10^{-10}$		3.8×10^{-11} $\pm1\times10^{-11}$ (B)
10-02-2 (CD)	109.8	0.030 ± 0.003	7×10^{-10} $\pm2\times10^{-11}$			4×10^{-9} $\pm2\times10^{-9}$	1×10^{-10} $\pm6\times10^{-11}$ (C)
4-00 (CD)	110.3	0.034 ± 0.003	1×10^{-8} $\pm3\times10^{-10}$		2.7×10^{-9} $\pm7\times10^{-10}$		9×10^{-11} $\pm3\times10^{-11}$ (B)
2-06-1 (CD)	108.3	0.030 ± 0.003	8×10^{-12} $\pm7\times10^{-13}$	1.6×10^{-10} $\pm 4\times10^{-11}$		3×10^{-10} $\pm3\times10^{-10}$	5×10^{-12} $\pm2\times10^{-12}$ (A)
2-06-2 (CD)	106.8	0.021 ± 0.002	$<2.4\times10^{-12}$		1.3×10^{-9} $\pm4\times10^{-10}$		2.9×10^{-11} $\pm1\times10^{-11}$ (B)
11-02-1 (CD)	108.4	0.019 ± 0.002	$<2.4\times10^{-12}$		4×10^{-10} $\pm2\times10^{-10}$		8×10^{-12} $\pm4\times10^{-12}$ (B)
11-02-2 (CD)	106.9	0.014 ± 0.001	$<2.4\times10^{-12}$	8×10^{-10} $\pm 2\times10^{-10}$			1.1×10^{-11} $\pm3\times10^{-12}$ (A)
3-02-1 (CD)	108.2	0.014 ± 0.001	2×10^{-11} $\pm9\times10^{-13}$		8×10^{-10} $\pm3\times10^{-10}$		1×10^{-11} $\pm5\times10^{-12}$ (B)

Sampled piezometer (profile)	Mean screen altitude (m)	$[Cl^-]$ ($mmol.L^{-1}$)	$[^{90}Sr]$ ($mmol.L^{-1}$)	Calculated $^{36}Cl/Cl$ Dilution A ($at.at^{-1}$)	Calculated $^{36}Cl/Cl$ Dilution B ($at.at^{-1}$)	Calculated $^{36}Cl/Cl$ Dilution C ($at.at^{-1}$)	$[^{36}Cl]$ (Dilution) ($mmol.L^{-1}$)
3-02-2 (CD)	106.7	0.015 ± 0.001	8×10^{-12} $\pm7\times10^{-13}$		5×10^{-11} $\pm2\times10^{-11}$		7×10^{-13} $\pm3\times10^{-13}$ (B)
9-02-1 (CD)	108.4	0.016 ± 0.002	2×10^{-10} $\pm7\times10^{-12}$		5×10^{-10} $\pm2\times10^{-10}$		8×10^{-12} $\pm4\times10^{-12}$ (B)
9-02-2 (CD)	107.1	0.014 ± 0.001	3×10^{-11}		6×10^{-10} $\pm3\times10^{-10}$		9×10^{-12} $\pm4\times10^{-12}$ (B)
1-98-1 (AB)	106.1	0.025 ± 0.003	5×10^{-12} $\pm6\times10^{-13}$		2.4×10^{-9} $\pm6\times10^{-10}$	2.1×10^{-6} $\pm5\times10^{-7}$	6×10^{-11} $\pm2\times10^{-11}$ (B)
1-98-2 (AB)	96.0	0.058 ± 0.006	$<2.4\times10^{-12}$	3.7×10^{-11} $\pm 9\times10^{-12}$			$.1\times10^{-12}$ $\pm7\times10^{-13}$ (A)
1-98-3 (AB)	84.7	0.024 ± 0.002	$<2.4\times10^{-12}$	2×10^{-12} $\pm 2\times10^{-12}$			6×10^{-14} $\pm4\times10^{-14}$ (A)
1-01	106.16	0.033 ± 0.003	$<2.4\times10^{-12}$		3.4×10^{-9} $\pm9\times10^{-10}$		1×10^{-10} $\pm4\times10^{-11}$ (B)

6. Non reactive transport initial simulation (HYTEC script)

```
#============================================================
# Geometry and hydrogeology
# # ------------------------
domain = -50,1060 -50,1135 0,1135 210,1146 260,1149 330,1150 380,1149 430,1148
490,1145 500,1145 500,1060 dm

flow-regime = unsaturated
unsaturated-model = van-genuchten {
  alpha = 3
  n = 2
}
storage = 1×10-2

nodes = 3000

# disturbed layer
# """""""""""
zone uz_soilL {
  geometry = polygon -50,1132 -50,1135 210,1146 210,1138 dm, density = 8
  diffusion-coeff = 1×10-10 m2/s
  dispersivity = 0.05 m
  permeability = 4.5×10-5 m/s
  porosity = 0.30
  unsaturated-model = van-genuchten {
    alpha = 7.5
    n = 2.5
  }
  water-content {
    start = 0.10
    minimum = 0.05
    maximum = 0.30
  }
  geochem = Eolian
}
zone uz_soilR {
  geometry = polygon 330,1141 330,1150 380,1149 430,1148 490,1145 500,1145
500,1140 dm, density = 3
  diffusion-coeff = 1×10-10 m2/s
  dispersivity = 0.05 m
  permeability = 4.5×10-5 m/s
  porosity = 0.30
  unsaturated-model = van-genuchten {
    alpha = 7.5
    n = 2.5
  }
```

```
  water-content {
    start = 0.10
    minimum = 0.05
    maximum = 0.30
  }
  geochem = Eolian
}
#trench T22
#""""""""""
zone trench {
  geometry = rectangle 270,1134 120,28 dm, density = 3
  diffusion-coeff = 1×10-10 m2/s
  dispersivity = 0.01 m
  permeability = 2.0×10-5 m/s
  porosity = 0.28
  unsaturated-model = van-genuchten {
    alpha = 3
    n = 2
  }
  water-content {
    start = 0.15
    minimum = 0.10
    maximum = 0.28
  }
  geochem = Trench
# A verifier/tester
  transport-constraint = constant-concentration
}
#eolian
#""""""""""
zone uz_eolL {
  geometry = polygon -50,1120 -50,1132 210,1138 210,1120 dm, density = 2 overgrid
= disabled
  diffusion-coeff = 1×10-10 m2/s
  dispersivity = 0.05 m
  permeability = 4.17×10-5 m/s
  porosity = 0.28
  unsaturated-model = van-genuchten {
    alpha = 6.5
    n = 1.8
  }
  water-content {
    start = 0.10
    minimum = 0.03
    maximum = 0.28
  }
  geochem = Eolian
```

```
}
zone uz_eolR {
  geometry = polygon 330,1120 330,1141 500,1140 500,1120 dm, density = 2,
overgrid = disabled
  diffusion-coeff = 1×10-10 m2/s
  dispersivity = 0.05 m
  permeability = 4.17×10-5 m/s
  porosity = 0.28
  unsaturated-model = van-genuchten {
    alpha = 6.5
    n = 1.8
  }
  water-content {
    start = 0.10
    minimum = 0.03
    maximum = 0.28
  }
  geochem = Eolian
}
zone eol_unsat {
  geometry = rectangle 225,1115 550,10 dm, density = 2, overgrid = disabled
  diffusion-coeff = 1×10-10 m2/s
  dispersivity = 0.05 m
  permeability = 4.17×10-5 m/s
  porosity = 0.28
   unsaturated-model = van-genuchten {
    alpha = 6.5
    n = 1.8
  }
  water-content {
    start = 0.25
    minimum = 0.03
    maximum = 0.28
  }
  geochem = Eolian
}
zone eol_sat {
  geometry = rectangle 225,1105 550,10 dm, density = 2, overgrid = disabled
  diffusion-coeff = 1×10-10 m2/s
  dispersivity = 0.05 m
  permeability = 4.17×10-5 m/s
  porosity = 0.28
   unsaturated-model = van-genuchten {
    alpha = 6.5
    n = 1.8
  }
  water-content {
```

```
    start = 0.28
    minimum = 0.03
    maximum = 0.28
  }
  geochem = Eolian
}

#satured-zone alluvial
#"""""""""""""""
zone sz_sand {
  geometry = rectangle 225,1080 550,40 dm, density = 1
  diffusion-coeff = 1×10-10 m2/s
  dispersivity = 0.05 m
# A verifier/tester
  permeability = 2×10-6 m/s
  porosity = 0.24
  unsaturated-model = van-genuchten {
    alpha = 20
    n = 2
  }
  water-content {
    start = 0.24
    minimum = 0.03
    maximum = 0.24
  }
  geochem = Alluvial
}

# Boundary conditions
# ------------------------
boundary Infiltration {
  coordinates = -50,1135 500,1145 dm
  flow-condition = constant-flow at 0,-0.250 m/y
  transport-condition = flux using rainwater
}
boundary eol-left {
  coordinates = -5,110 -5,111 m
  flow-condition = constant-head at 111.0825 m
  transport-condition = flux using mean_upstream_GW
}
boundary eol-right {
  coordinates = 50,110 50,111 m
  flow-condition = constant-head at 111 m
}
boundary alluvial-left {
  coordinates = -5,106 -5,110 m
  flow-condition = constant-flow at 0.27,0 m/y
```

```
  transport-condition = flux using mean_upstream_GW
}
boundary alluvial-right1 {
  coordinates = 50,106 50,110 m
  flow-condition = constant-flow at 0.27,0 m/y
}
boundary bottom {
  coordinates = -5,106 50,106 m
  flow-condition = constant-flow at 0,-0.250 m/y
}

#Geochemistry
# ------------
unit rainwater {
  tot Cl[-] = 0.02 mmol/l
  tot 36Cl[-] = 2×10-15 mmol/l
}
unit mean_upstream_GW {
  tot Cl[-] = 0.02 mmol/l
  tot 36Cl[-] = 2×10-15 mmol/l
}
unit Eolian {
  tot Cl[-] = 0.02 mmol/l
  tot 36Cl[-] = 2×10-15 mmol/l
}
unit Alluvial {
  tot Cl[-] = 0.02 mmol/l
  tot 36Cl[-] = 2×10-15 mmol/l
}
unit Trench {
  tot Cl[-] = 0.1 mmol/l
  tot 36Cl[-] = 4×10-9 mmol/l #Soil solution tws sws 1.25m in May 2011
}


# Simulation parameters
# ---------------------
duration = 25 y
timestep = variable {
  start = 2 hr
  maximum = 1 d
  courant-factor = 4
}

save grid

# Output specifications
```

```
# --------------------
sample = 50
verbose = enabled

select head in m
select pressure in m
select x-flowrate, y-flowrate in m/s
select water-content
select moistur×10-content
select pH
select aqueous{Cl[-]} in mmol/l
select aqueous{36Cl[-]} in mmol/l
```

7. Sensitivity analyses results

Changing aeolian permeability

Impact on velocities

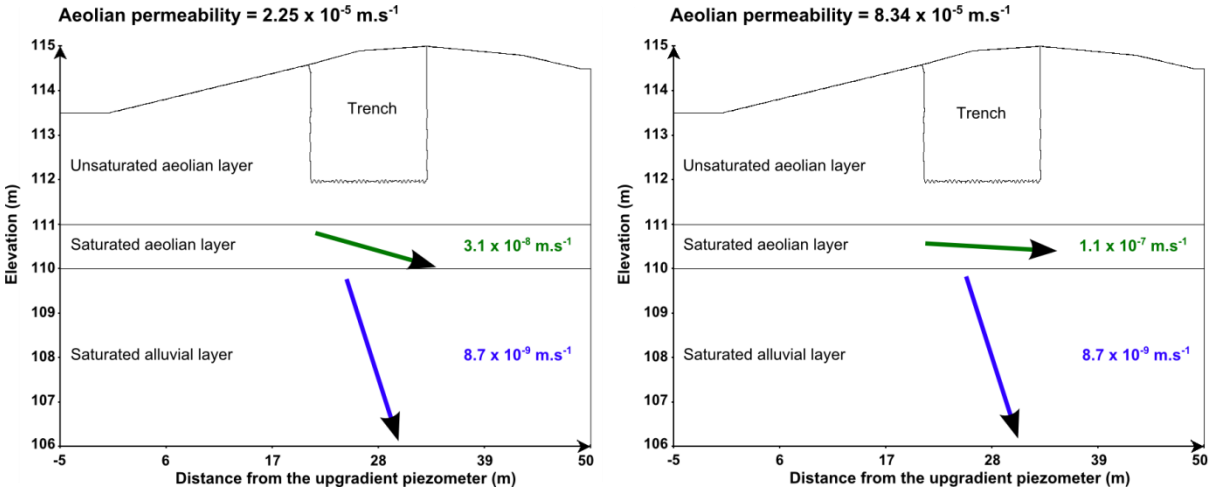

Impact on [Cl^-] concentrations

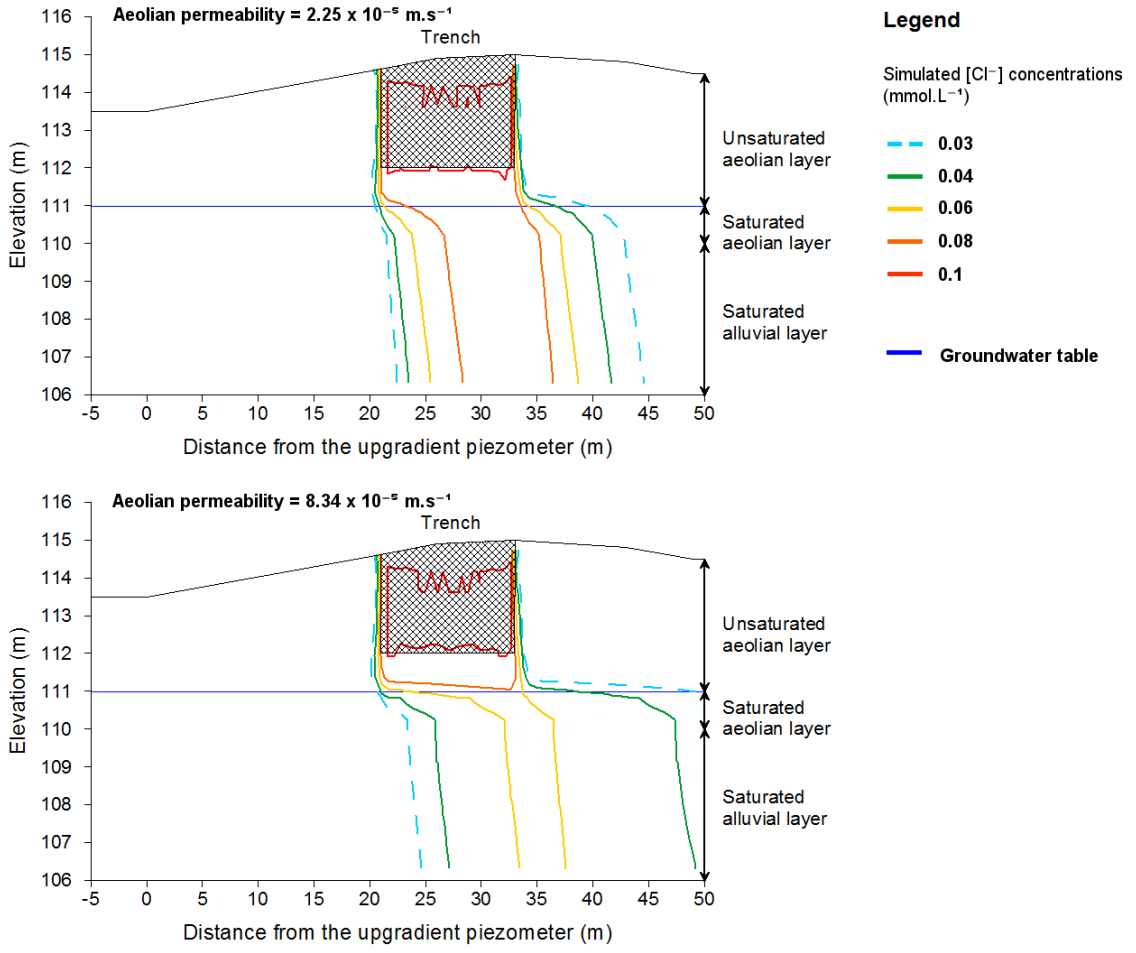

Changing alluvial permeability

$K = 5.8\times10^{-6}$ m.s^{-1} and $K = 3\times10^{-7}$ m.s^{-1}
Impact on velocities

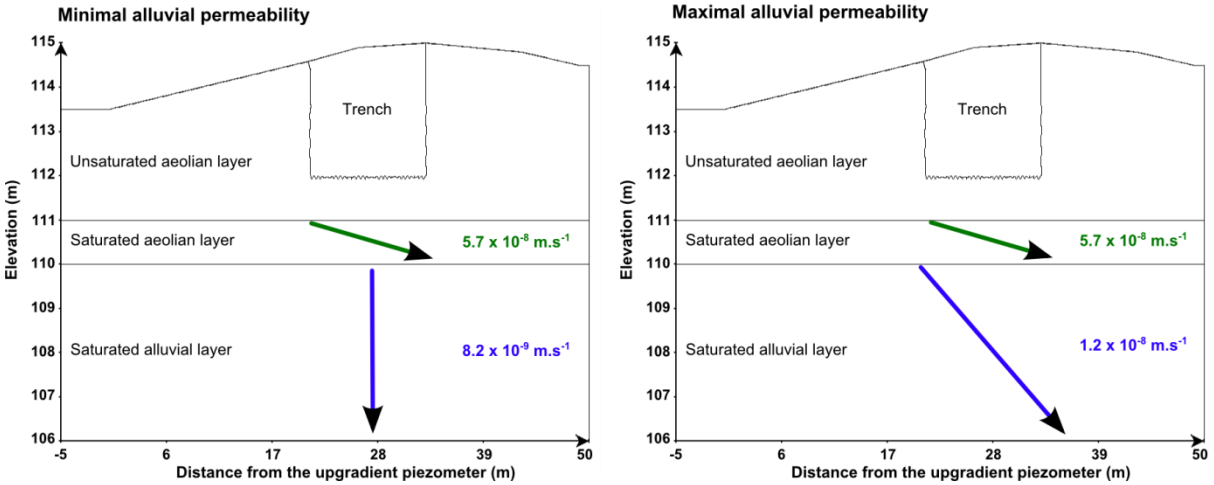

Impact on [Cl^-] concentrations

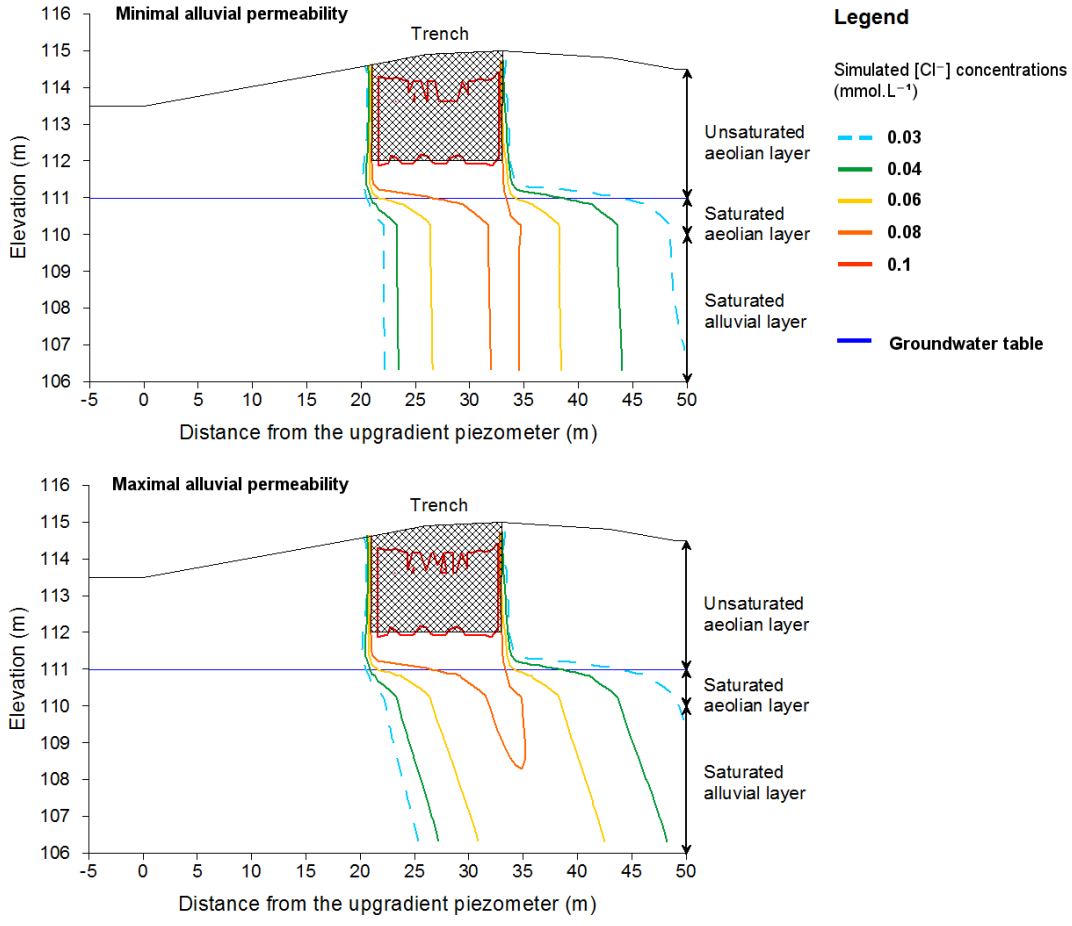

Changing effective porosity

Impact on velocities

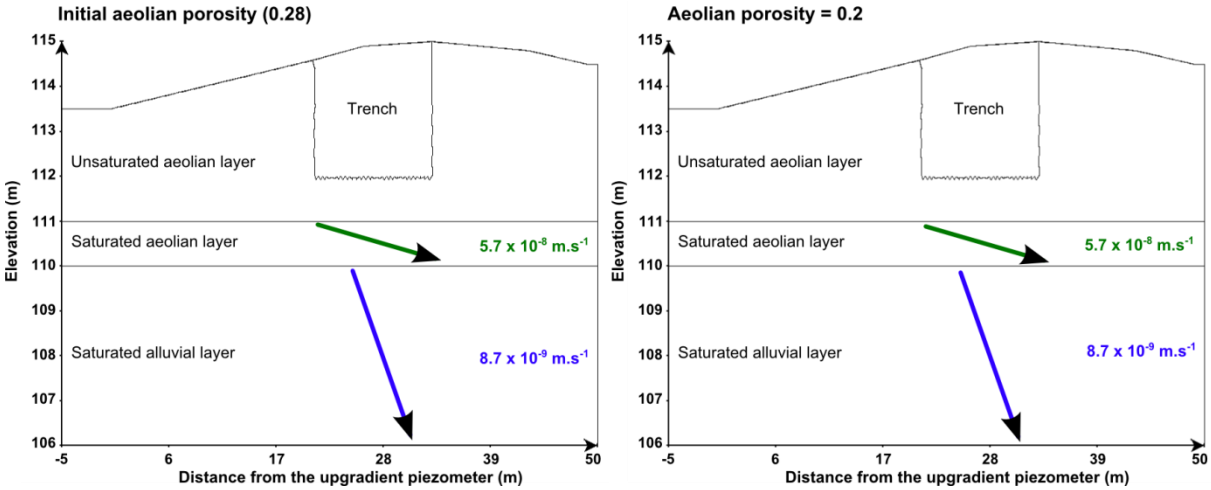

Impact on [Cl^-] concentrations

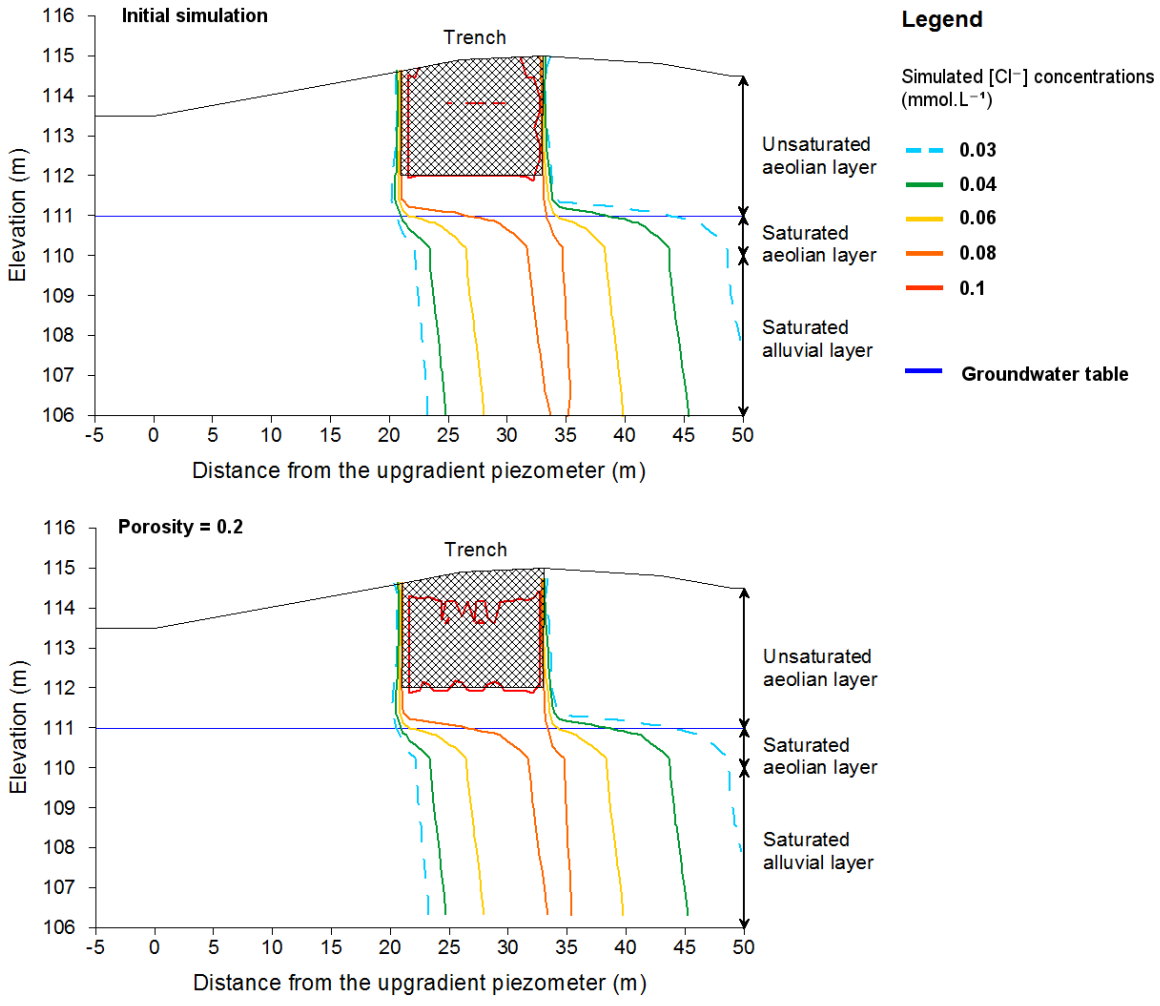

Changing gradient of hydraulic head

Impact on velocities

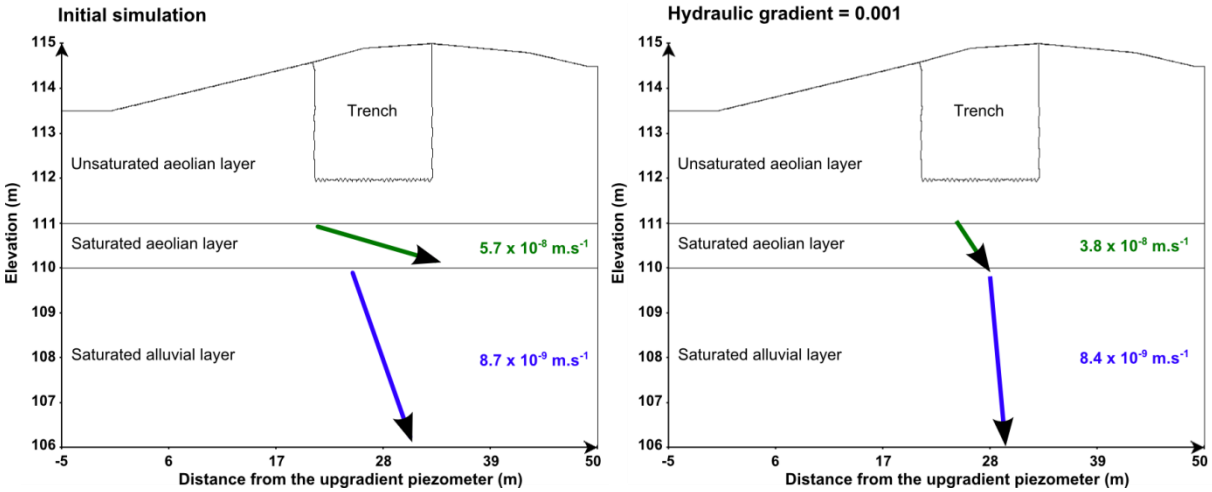

Impact on [Cl^-] concentrations

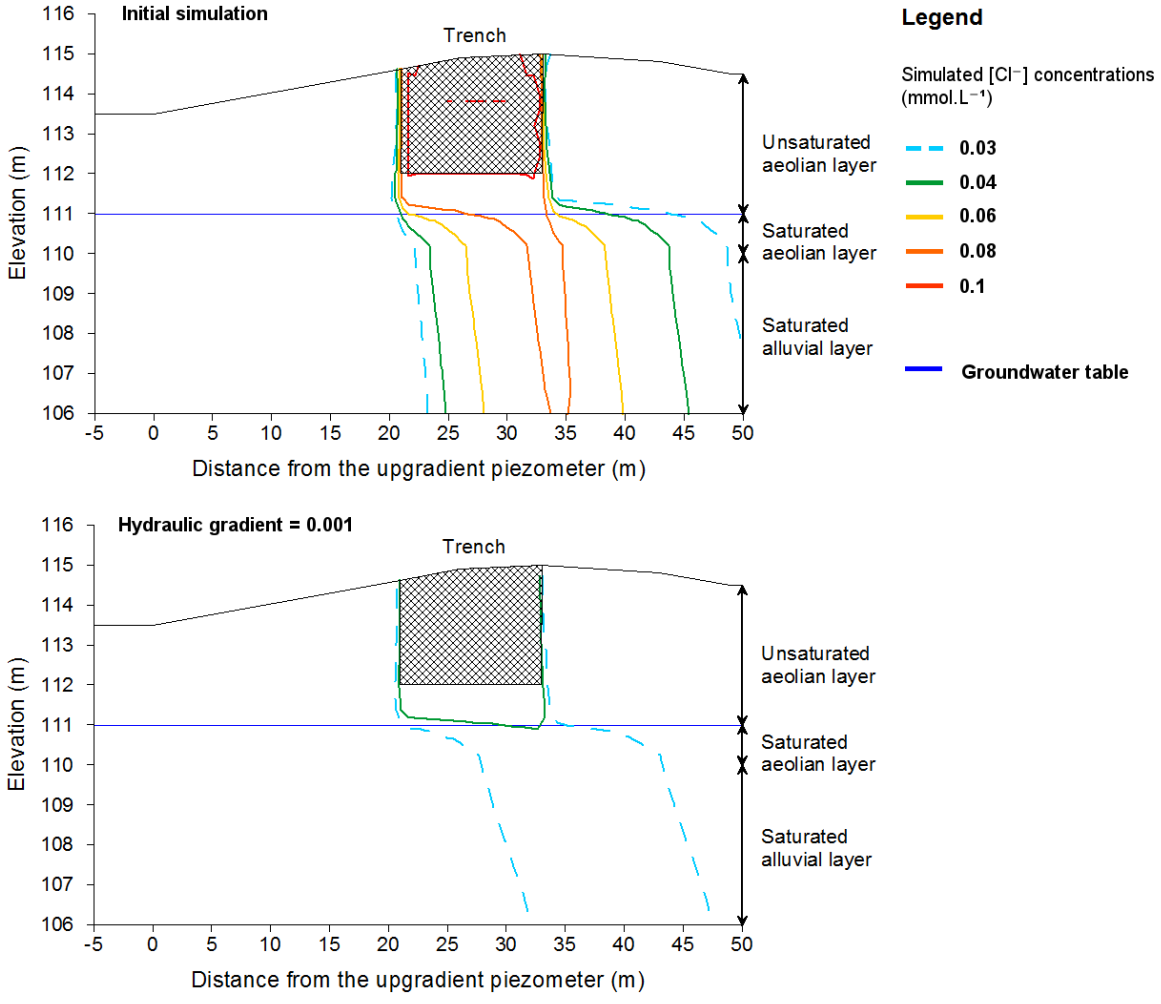

8. Optimal simulation (HYTEC script)

```
# Geometry and hydrogeology
# # ------------------------
domain = -50,1060 -50,1135 0,1135 210,1146 260,1149 330,1150 380,1149 430,1148
490,1145 500,1145 500,1060 dm

flow-regime = unsaturated
unsaturated-model = van-genuchten {
  alpha = 3
  n = 2
}
storage = 1×10-2

nodes = 3000

# disturbed layer
# """""""""""
zone uz_soilL {
  geometry = polygon -50,1132 -50,1135 210,1146 210,1138 dm, density = 8
  diffusion-coeff = 1×10-10 m2/s
  dispersivity = 0.05 m
  permeability = 9×10-5 m/s
  porosity = 0.30
  unsaturated-model = van-genuchten {
    alpha = 7.5
    n = 2.5
  }
  water-content {
    start = 0.10
    minimum = 0.05
    maximum = 0.30
  }
  geochem = Eolian
}
zone uz_soilR {
  geometry = polygon 330,1141 330,1150 380,1149 430,1148 490,1145 500,1145
500,1140 dm, density = 3
  diffusion-coeff = 1×10-10 m2/s
  dispersivity = 0.05 m
  permeability = 9×10-5 m/s
  porosity = 0.30
  unsaturated-model = van-genuchten {
    alpha = 7.5
    n = 2.5
  }
  water-content {
```

```
    start = 0.10
    minimum = 0.05
    maximum = 0.30
  }
  geochem = Eolian
}
#trench T22
#""""""""""
zone trench {
  geometry = rectangle 270,1134 120,28 dm, density = 3
  diffusion-coeff = 1×10-10 m2/s
  dispersivity = 0.01 m
  permeability = 2.0×10-5 m/s
  porosity = 0.28
  unsaturated-model = van-genuchten {
    alpha = 3
    n = 2
  }
  water-content {
    start = 0.15
    minimum = 0.10
    maximum = 0.28
  }
  geochem = Trench
# A verifier/tester
  transport-constraint = constant-concentration
}
#eolian
#""""""""""
zone uz_eolL {
  geometry = polygon -50,1120 -50,1132 210,1138 210,1120 dm, density = 2 overgrid
= disabled
  diffusion-coeff = 1×10-10 m2/s
  dispersivity = 0.05 m
  permeability = 8.34×10-5 m/s
  porosity = 0.28
  unsaturated-model = van-genuchten {
    alpha = 6.5
    n = 1.8
  }
  water-content {
    start = 0.10
    minimum = 0.03
    maximum = 0.28
  }
  geochem = Eolian
}
```

```
zone uz_eolR {
  geometry = polygon 330,1120 330,1141 500,1140 500,1120 dm, density = 2,
overgrid = disabled
  diffusion-coeff = 1×10-10 m2/s
  dispersivity = 0.05 m
  permeability = 8.34×10-5 m/s
  porosity = 0.28
  unsaturated-model = van-genuchten {
    alpha = 6.5
    n = 1.8
  }
  water-content {
    start = 0.10
    minimum = 0.03
    maximum = 0.28
  }
  geochem = Eolian
}
zone eol_unsat {
  geometry = rectangle 225,1115 550,10 dm, density = 2, overgrid = disabled
  diffusion-coeff = 1×10-10 m2/s
  dispersivity = 0.05 m
  permeability = 8.34×10-5 m/s
  porosity = 0.28
   unsaturated-model = van-genuchten {
    alpha = 6.5
    n = 1.8
  }
  water-content {
    start = 0.25
    minimum = 0.03
    maximum = 0.28
  }
  geochem = Eolian
}
zone eol_sat {
  geometry = rectangle 225,1105 550,10 dm, density = 2, overgrid = disabled
  diffusion-coeff = 1×10-10 m2/s
  dispersivity = 0.05 m
  permeability = 8.34×10-5 m/s
  porosity = 0.28
   unsaturated-model = van-genuchten {
    alpha = 6.5
    n = 1.8
  }
  water-content {
    start = 0.28
```

```
    minimum = 0.03
    maximum = 0.28
  }
  geochem = Eolian
}

#satured-zone alluvial
#""""""""""""""""
zone sz_sand {
  geometry = rectangle 225,1080 550,40 dm, density = 1
  diffusion-coeff = 1×10-10 m2/s
  dispersivity = 0.05 m
# A verifier/tester
  permeability = 5.8×10-6 m/s
  porosity = 0.24
  unsaturated-model = van-genuchten {
    alpha = 20
    n = 2
  }
  water-content {
    start = 0.24
    minimum = 0.03
    maximum = 0.24
  }
  geochem = Alluvial
}

# Boundary conditions
# ------------------------
boundary Infiltration {
  coordinates = -50,1135 500,1145 dm
  flow-condition = constant-flow at 0,-0.250 m/y
  transport-condition = flux using rainwater
}
boundary eol-left {
  coordinates = -5,110 -5,111 m
  flow-condition = constant-head at 111.0825 m
  transport-condition = flux using mean_upstream_GW
}
boundary eol-right {
  coordinates = 50,110 50,111 m
  flow-condition = constant-head at 111 m
}
boundary alluvial-left {
  coordinates = -5,106 -5,110 m
  flow-condition = constant-flow at 0.27,0 m/y
  transport-condition = flux using mean_upstream_GW
```

```
}
boundary alluvial-right1 {
  coordinates = 50,106 50,110 m
  flow-condition = constant-flow at 0.27,0 m/y
}
boundary bottom {
  coordinates = -5,106 50,106 m
  flow-condition = constant-flow at 0,-0.250 m/y
}

#Geochemistry
# ------------
unit rainwater {
  tot Cl[-] = 0.02 mmol/l
  tot 36Cl[-] = 2×10-15 mmol/l
}
unit mean_upstream_GW {
  tot Cl[-] = 0.02 mmol/l
  tot 36Cl[-] = 2×10-15 mmol/l
}
unit Eolian {
  tot Cl[-] = 0.02 mmol/l
  tot 36Cl[-] = 2×10-15 mmol/l
}
unit Alluvial {
  tot Cl[-] = 0.02 mmol/l
  tot 36Cl[-] = 2×10-15 mmol/l
}
unit Trench {
  tot Cl[-] = 0.05 mmol/l
  tot 36Cl[-] = 4×10-10 mmol/l #1 order of magnitude lower than Soil solution tws
sws 1.25m in May 2011
}


# Simulation parameters
# --------------------
duration = 25 y
timestep = variable {
  start = 2 hr
  maximum = 1 d
  courant-factor = 4
}

save grid

# Output specifications
```

```
# --------------------
sample = 50
verbose = enabled

select head in m
select pressure in m
select x-flowrate, y-flowrate in m/s
select water-content
select moistur×10-content
select pH
select aqueous{Cl[-]} in mmol/l
select aqueous{36Cl[-]} in mmol/l
```

GEOCHEMICAL PROCESSES IN THE CHERNOBYL PILOT SITE
GROUNDWATER ANNEXES

9. Field parameters and element concentration

October 2008 Field data (from Chernobyl database)

№ Well	Formation	Profile	Mean screen elevation	Distance from upgradient point	Hydraulic head	pH	T°	Conductivity	Eh (ENH)	pe	O_2	Alkalinity
			(m.a.s.l.)	*(m)*	*(m.a.s.l.)*	*(field)*	*(°C)*	*(µS/cm)*	*(mV)*		*(mg/L)*	*(mmol/L)*
5-99	Aeolian	AB	110.4	0	109.89	4.3	13.7	32	460	8	1.68	0.007
6-02-1	Aeolian	AB	111.4	17	111.36	5.3	16.5	30	388	7	10.06	0.045
6-02-2	Interface Aeolian/Alluvial	AB	109.7	17	111.38	5.5	13.2	57	232	4	1.42	0.073
8-02-1	Aeolian	AB	111.4	23	111.34	5.4	13.1	35	223	4	1.30	0.061
8-02-2	Interface Aeolian/Alluvial	AB	109.9	23	111.35	4.7	12.8	30	306	5	2.01	0.047
8-01-1	Aeolian	AB	111.3	29	111.33	5.1	13	43	438	7	1.10	0.146
8-01-2	Interface Aeolian/Alluvial	AB	109.8	29	111.37	5.0	12.7	34	492	8	3.72	0.063
19-00-1	Aeolian	AB	111.4	33	111.35	4.9	13.1	40	438	7	9.83	0.038
19-00-2	Interface Aeolian/Alluvial	AB	109.9	33	111.35	4.8	12.6	36	392	7	2.40	0.051
6-01-1	Aeolian	AB	111.1	37	111.34	5.0	13.3	30	235	4	1.08	0.001
6-01-2	Interface Aeolian/Alluvial	AB	110.0	37	111.38	4.9	12.3	50	478	8	5.24	0.056

№ Well	Formation	Profile	Mean screen elevation	Distance from upgradient point	Hydraulic head	pH	T° (pH)	Conductivity	Eh (ENH)	pe	O_2	Alcalinity
			(m.a.s.l.)	*(m)*	*(m.a.s.l.)*	*(field)*	*(°C)*	*(µS/cm)*	*(mV)*		*(mg/L)*	*(mmol/L)*
2-02-1	Aeolian	AB	111.1	40	111.35	6.0	12.9	38	202	3	10.01	0.183
2-02-2	Interface Aeolian/Alluvial	AB	109.6	40	111.36	5.3	11.7	72	450	8	-	0.070
7-00	Interface Aeolian/Alluvial	AB	110.2	58	111.33	4.7	14.1	40	418	7	4.30	0.055
5-02-1	Alluvial	AB	108.4	17	111.31	5.7	13.6	85	227	4	0.57	0.147
5-02-2	Alluvial	AB	106.9	17	111.28	6.2	17.5	98	194	3	3.39	0.781
7-02-1	Alluvial	AB	108.4	24	111.33	5.8	12.4	70	199	3	0.67	0.127
7-02-2	Alluvial	AB	106.8	24	111.28	6.4	17.5	111	188	3	4.61	0.858
7-01-1	Alluvial	AB	108.3	29	111.29	5.1	12.4	45	378	6	1.01	0.092
7-01-2	Alluvial	AB	106.8	29	111.28	5.3	12.7	70	308	5	2.30	0.064
18-00-1	Alluvial	AB	108.1	33	111.29	5.0	11.9	47	307	5	0.93	0.078
18-00-2	Alluvial	AB	107.0	33	111.27	5.7	11.5	83	179	3	0.73	0.628
5-01-1	Alluvial	AB	108.3	37	111.30	4.8	12.3	52	416	7	0.80	0.068
5-01-2	Alluvial	AB	107.2	37	111.27	4.8	12	53	476	8	0.90	0.043
1-02-1	Alluvial	AB	108.3	41	111.25	5.1	12.4	85	457	8	0.88	0.107
1-02-2	Alluvial	AB	106.8	41	111.17	6.3	13.6	131	259	4	4.99	

№ Well	Formation	Profile	Mean screen elevation	Distance from upgradient point	Hydraulic head	pH	T° (pH)	Conductivity	Eh (ENH)	pe	O_2	Alcalinity
			(m.a.s.l.)	*(m)*	*(m.a.s.l.)*	*(field)*	*(°C)*	*(µS/cm)*	*(mV)*		*(mg/L)*	*(mmol/L)*
1-98-1	Alluvial	AB	106.1	41	111.28	5.4	11.7	61	198	3	2.40	0.142
1-98-2	Alluvial	AB	96.0	41	111.28	6.2	11.6	101	156	3	2.10	1.109
1-98-3	Alluvial	AB	84.7	41	111.28	6.5	11	120	104	2	1.91	1.555
6-99	Aeolian	CD	110.3	0	111.38	4.3	14.2	33	328	6	0.67	0.001
1-06-1	Aeolian	CD	111.1	21	111.14	5.2	14.4	22	386	7	2.35	0.092
1-06-2	Aeolian	CD	109.6	21	111.16	4.9	14.2	28	457	8	1.28	0.056
1-00	Aeolian	CD	110.5	26	111.33	4.3	13.7	19	419	7	2.35	0.001
12-02-1	Aeolian	CD	111.4	33	111.31	4.8	14.7	65	496	8	8.71	0.002
12-02-2	Interface Aeolian/Alluvial	CD	109.9	33	111.32	4.6	12.8	50	446	8	9.13	0.009
4-02-1	Aeolian	CD	111.2	37	111.32	5.6	11.5	100	471	8	7.09	0.159
4-02-2	Interface Aeolian/Alluvial	CD	109.8	37	111.33	4.7	11.8	69	495	8	2.93	0.060
10-02-1	Aeolian	CD	111.3	43	111.31	5.8	14.7	66	379	6	4.60	0.144
10-02-2	Interface Aeolian/Alluvial	CD	109.8	43	111.31	4.7	14.6	74	480	8	5.75	0.061
4-00	Interface Aeolian/Alluvial	CD	110.3	49	111.31	4.6	13.6	62	455	8	7.87	0.011

№ Well	Formation	Profile	Mean screen elevation	Distance from upgradient point	Hydraulic head	pH	T° (pH)	Conductivity	Eh (ENH)	pe	O_2	Alcalinity
			(m.a.s.l.)	*(m)*	*(m.a.s.l.)*	*(field)*	*(°C)*	*(µS/cm)*	*(mV)*		*(mg/L)*	*(mmol/L)*
2-06-1	Alluvial	CD	108.3	21	111.15	5.2	13.2	38	283	5	0.58	0.061
2-06-2	Alluvial	CD	106.8	21	111.11	5.5	12	46	490	8	-	0.029
11-02-1	Alluvial	CD	108.4	33	111.24	5.0	11.9	37	226	4	0.73	0.051
11-02-2	Alluvial	CD	106.9	33	111.24	6.0	11.9	68	171	3	0.96	0.460
3-02-1	Alluvial	CD	108.2	38	111.28	5.2	12	39	393	7	0.80	0.127
3-02-2	Alluvial	CD	106.7	38	111.25	5.7	11.7	69	286	5	1.31	0.156
9-02-1	Alluvial	CD	108.4	43	111.25	5.7	12.8	16	188	3	0.78	0.155
9-02-2	Alluvial	CD	107.1	43	111.24	5.8	13	65	200	3	1.52	0.152

October 2008 chemical concentrations in Chernobyl groundwater (ionic chromatography - LAME -Chernobyl database)

№ Well	$[Cl^-]$		$[NO_3^-]$		$[SO_4^{2-}]$		$[Ca^{2+}]$		$[K^+]$		$[Mg^{2+}]$		$[Na^+]$		Electrical balance
	(mM)		*(mM)*		*(mM)*		*(mM)*		*(mM)*		*(mM)*		*(mM)*		
LD			0.001												
5-99	0.0186		<0.001		0.080		0.049		0.026		0.011		0.029		-3
6-02-1	0.0214	±0.0002	0.020	±0.0002	0.061	±0.001	0.067	±0.003	0.030	±0.004	0.010	±0.004	0.018	±0.003	-8
6-02-2	0.0208	±0.0001	0.004	±0.0002	0.110	±0.001	0.096	±0.002	0.031	±0.008	0.018	±0.004	0.044	±0.002	-2
8-02-1	0.0169	±0.0002	0.016	±0.0002	0.062	±0.001	0.062	±0.003	0.032	±0.010	0.010	±0.001	0.019	±0.001	-6
8-02-2	0.0366	±0.0002	0.010	±0.0018	0.067	±0.001	0.061	±0.004	0.036	±0.003	0.012	±0.001	0.030	±0.004	-3
8-01-1	0.0274	±0.0001	0.005	±0.0003	0.076	±0.000	0.135	±0.002	0.027	±0.000	0.017	±0.002	0.020	±0.004	-4
8-01-2	0.0165	±0.0008	0.014	±0.0017	0.081	±0.001	0.089	±0.004	0.025	±0.006	0.012	±0.004	0.019	±0.001	-4
19-00-1	0.0302	±0.0004	0.009	±0.0002	0.102	±0.001	0.111	±0.004	0.027	±0.000	0.005	±0.001	0.021	±0.002	0
19-00-2	0.0191	±0.0002	0.030	±0.0004	0.086	±0.001	0.094	±0.004	0.035	±0.005	0.008	±0.003	0.020	±0.000	-3
6-01-1	0.0271	±0.0001	0.004	±0.0001	0.201	±0.001	0.158	±0.005	0.030	±0.007	0.023	±0.004	0.030	±0.004	-4
6-01-2	0.0227	±0.0006	0.034	±0.0008	0.145	±0.005	0.148	±0.004	0.050	±0.004	0.016	±0.003	0.033	±0.007	1
2-02-1	0.0165	±0.0001	0.005	±0.0010	0.041	±0.001	0.099	±0.004	0.023	±0.005	0.022	±0.005	0.015	±0.001	-8
2-02-2	0.0207	±0.0012	0.009	±0.0007	0.246	±0.002	0.211	±0.005	0.051	±0.004	0.030	±0.002	0.041	±0.002	-2
7-00	0.0150	±0.0000	0.006	±0.0007	0.110	±0.001	0.067	±0.006	0.067	±0.009	0.015	±0.006	0.035	±0.004	-6
5-02-1	0.0250	±0.0004	<0.001		0.227	±0.002	0.174	±0.006	0.029	±0.006	0.065	±0.005	0.097	±0.002	-3
5-02-2	0.0272	±0.0000	0.004	±0.0002	0.189	±0.001	0.200	±0.008	0.042	±0.006	0.086	±0.002	0.132	±0.002	-24
7-02-1	0.0244	±0.0003	0.008	±0.0007	0.164	±0.002	0.129	±0.001	0.025	±0.004	0.045	±0.009	0.081	±0.003	-5
7-02-2	0.0446	±0.0004	0.004	±0.0006	0.217	±0.002	0.161	±0.004	0.033	±0.004	0.066	±0.002	0.166	±0.008	-34
7-01-1	0.0199	±0.0001	0.006	±0.0010	0.122	±0.001	0.114	±0.006	0.021	±0.002	0.029	±0.003	0.047	±0.002	-3
7-01-2	0.0278	±0.0001	<0.001		0.223	±0.002	0.132	±0.007	0.036	±0.004	0.053	±0.003	0.122	±0.004	-1
18-00-1	0.0213	±0.0001	0.010	±0.0008	0.138	±0.002	0.107	±0.004	0.024	±0.003	0.033	±0.004	0.049	±0.002	-4

№ Well	[Cl^-]		[NO_3^-]		[SO_4^{2-}]		[Ca^{2+}]		[K^+]		[Mg^{2+}]		[Na^+]		Electrical balance
	(mM)		*(mM)*		*(mM)*		*(mM)*		*(mM)*		*(mM)*		*(mM)*		
18-00-2	0.0297	±0.0002	<0.001		0.229	±0.002	0.166	±0.003	0.030	±0.004	0.062	±0.006	0.122	±0.000	-29
5-01-1	0.0200	±0.0002	0.018	±0.0004	0.152	±0.000	0.140	±0.005	0.030	±0.003	0.021	±0.002	0.038	±0.000	-2
5-01-2	0.0263	±0.0001	0.011	±0.0012	0.169	±0.001	0.104	±0.002	0.030	±0.007	0.046	±0.005	0.076	±0.003	-1
1-02-1	0.0222	±0.0003	0.037	±0.0001	0.269	±0.004	0.227	±0.003	0.027	±0.000	0.069	±0.002	0.052	±0.003	-4
1-98-1	0.0250	±0.0015	0.004	±0.0002	0.154	±0.003	0.136	±0.006	0.025	±0.005	0.038	±0.005	0.072	±0.002	-4
1-98-2	0.0567	±0.0002	0.005	±0.0005	0.139	±0.001	0.271	±0.009	0.030	±0.006	0.083	±0.004	0.134	±0.004	-25
1-98-3	0.0254	±0.0001	0.003	±0.0002	0.119	±0.001	0.369	±0.004	0.018	±0.001	0.106	±0.003	0.123	±0.001	-25
6-99	0.0221	±0.0002	0.004	±0.0001	0.086	±0.001	0.040	±0.005	0.043	±0.005	0.012	±0.002	0.024	±0.003	-8
1-06-1	0.0167	±0.0005	0.012	±0.0008	0.035	±0.004	0.055	±0.004	0.016	±0.004	0.010	±0.003	0.015	±0.000	-9
1-06-2	0.0196	±0.0002	0.009	±0.0011	0.066	±0.000	0.065	±0.006	0.025	±0.002	0.009	±0.002	0.024	±0.001	-5
1-00	0.0167	±0.0007	0.002	±0.0003	0.046	±0.006	0.027	±0.002	0.019	±0.001	0.004	±0.000	0.015	±0.001	-8
12-02-1	0.0205	±0.0012	0.256	±0.0025	0.094	±0.002	0.150	±0.002	0.043	±0.004	0.034	±0.005	0.043	±0.002	-1
12-02-2	0.0164	±0.0003	0.204	±0.0021	0.041	±0.001	0.103	±0.005	0.030	±0.005	0.017	±0.002	0.019	±0.002	-4
4-02-1	0.0341	±0.0001	0.291	±0.0021	0.170	±0.002	0.243	±0.006	0.085	±0.008	0.022	±0.005	0.051	±0.002	-11
4-02-2	0.0210	±0.0001	0.096	±0.0004	0.183	±0.001	0.190	±0.004	0.068	±0.001	0.020	±0.001	0.035	±0.000	-2
10-02-1	0.0606	±0.0006	0.170	±0.0016	0.128	±0.001	0.233	±0.003	0.067	±0.003	0.033	±0.002	0.059	±0.001	2
10-02-2	0.0351	±0.0001	0.095	±0.0003	0.203	±0.002	0.195	±0.002	0.037	±0.001	0.052	±0.004	0.047	±0.002	-2
4-00	0.0300	±0.0003	0.142	±0.0027	0.137	±0.003	0.158	±0.004	0.055	±0.001	0.030	±0.001	0.037	±0.002	1
2-06-1	0.0163	±0.0002	<0.001		0.067	±0.001	0.077	±0.005	0.052	±0.003	0.014	±0.004	0.026	±0.005	10
2-06-2	0.0235	±0.0009	0.004	±0.0013	0.120	±0.010	0.079	±0.003	0.027	±0.004	0.033	±0.003	0.054	±0.004	1
11-02-1	0.0179	±0.0001	0.005	±0.0004	0.076	±0.001	0.062	±0.007	0.022	±0.004	0.015	±0.003	0.028	±0.002	-5
11-02-2	0.0185	±0.0001	0.002	±0.0004	0.071	±0.000	0.096	±0.002	0.024	±0.003	0.039	±0.001	0.068	±0.003	-26
3-02-1	0.0183	±0.0003	0.005	±0.0004	0.076	±0.001	0.100	±0.003	0.021	±0.001	0.023	±0.002	0.029	±0.002	-3

№ Well	$[Cl^-]$		$[NO_3^-]$		$[SO_4^{2-}]$		$[Ca^{2+}]$		$[K^+]$		$[Mg^{2+}]$		$[Na^+]$		Electrical balance
	(mM)		*(mM)*		*(mM)*		*(mM)*		*(mM)*		*(mM)*		*(mM)*		
3-02-2	0.0214	±0.0002	0.005	±0.0003	0.148	±0.001	0.115	±0.003	0.025	±0.004	0.052	±0.004	0.114	±0.001	-2
9-02-1	0.0179	±0.0002	0.015	±0.0021	0.076	±0.001	0.101	±0.008	0.021	±0.002	0.022	±0.003	0.030	±0.001	-7
9-02-2	0.0216	±0.0001	<0.001		0.137	±0.002	0.101	±0.006	0.028	±0.006	0.047	±0.002	0.113	±0.003	-1

October 2008 - Additional chemical data

	[^{55}Mn]		[^{56}Fe]		[^{88}Sr]		Si		$\delta^{18}O$	$\delta^{2}H$
	(mol.l^{-1})		(mol.l^{-1})		(mol.l^{-1})		(mmol.l^{-1})		‰ *vs* SMOW	‰ *vs* SMOW
№ Well	MC ICP-MS		MC ICP-MS		MC ICP-MS		UV spectrometer		Laser spectrometer	Laser spectrometer
5-99	1.10×10^{-6}	$\pm3\times10^{-9}$	3.52×10^{-7}	$\pm4\times10^{-8}$	2.13×10^{-7}	$\pm7\times10^{-10}$	0.117	±0.001		
6-02-1	1.61×10^{-6}	$\pm1\times10^{-8}$	7.66×10^{-6}	$\pm5\times10^{-7}$	2.29×10^{-7}	$\pm5\times10^{-9}$	0.116	±0.002		
6-02-2	2.05×10^{-6}	$\pm4\times10^{-8}$	9.55×10^{-5}	$\pm8\times10^{-6}$	2.29×10^{-7}	$\pm4\times10^{-9}$	0.112	±0.004	-11.7	-85.0
8-02-1	1.81×10^{-6}	$\pm2\times10^{-8}$	4.53×10^{-5}	$\pm2\times10^{-6}$	1.39×10^{-7}	$\pm1\times10^{-9}$	0.097	±0.002		
8-02-2	7.36×10^{-7}	$\pm6\times10^{-9}$	5.22×10^{-7}	$\pm3\times10^{-8}$	1.78×10^{-7}	$\pm2\times10^{-9}$	0.105	±0.004	-11.2	-82.1
8-01-1	2.05×10^{-6}	$\pm2\times10^{-8}$	1.59×10^{-6}	$\pm7\times10^{-8}$	2.90×10^{-7}	$\pm3\times10^{-9}$	0.111	±0.001		
8-01-2	1.07×10^{-6}	$\pm2\times10^{-8}$	8.67×10^{-7}	$\pm4\times10^{-8}$	4.43×10^{-7}	$\pm1\times10^{-8}$	0.102	±0.001		
19-00-1	3.47×10^{-7}	$\pm2\times10^{-9}$	7.60×10^{-6}	$\pm1\times10^{-7}$	8.78×10^{-7}	$\pm1\times10^{-8}$	0.135	±0.002		
19-00-2	3.22×10^{-7}	$\pm3\times10^{-9}$	1.04×10^{-6}	$\pm1\times10^{-8}$	7.57×10^{-7}	$\pm7\times10^{-10}$	0.107	±0.003		
6-01-1	1.05×10^{-6}	$\pm1\times10^{-8}$	5.90×10^{-5}	$\pm1\times10^{-6}$	4.17×10^{-7}	$\pm4\times10^{-9}$	0.142	±0.003		
6-01-2	1.45×10^{-6}	$\pm8\times10^{-9}$	3.30×10^{-6}	$\pm3\times10^{-8}$	7.93×10^{-7}	$\pm3\times10^{-9}$	0.125	±0.000		
2-02-1	6.24×10^{-6}	$\pm2.10^{-7}$	3.01×10^{-5}	$\pm3\times10^{-6}$	1.92×10^{-7}	$\pm2\times10^{-9}$	0.120	±0.001		
2-02-2	1.28×10^{-6}	$\pm1\times10^{-8}$	2.38×10^{-6}	$\pm7\times10^{-9}$	7.65×10^{-7}	$\pm1\times10^{-8}$	0.122	±0.002		
7-00	8.48×10^{-7}	$\pm4\times10^{-9}$	$3.15.10^{-7}$	$\pm6\times10^{-8}$	2.43×10^{-7}	$\pm1\times10^{-9}$	0.120	±0.001		
5-02-1	3.26×10^{-6}	$\pm2\times10^{-8}$	6.91×10^{-5}	$\pm1\times10^{-5}$	6.21×10^{-7}	$\pm8\times10^{-9}$	0.168	±0.000		

	$[^{55}Mn^{2+}]$		$[^{56}Fe^{2+}]$		$[^{88}Sr]$		Si		$\delta^{18}O$	$\delta^{2}H$
	($mol.l^{-1}$)		($mol.l^{-1}$)		($mol.l^{-1}$)		($mmol.l^{-1}$)		‰ *vs* SMOW	‰ *vs* SMOW
№ Well	MC ICP-MS		MC ICP-MS		MC ICP-MS		UV spectrometer		Laser spectrometer	Laser spectrometer
5-02-2	5.82×10^{-6}	$\pm3\times10^{-8}$	8.41×10^{-5}	$\pm6\times10^{-6}$	7.12×10^{-7}	$\pm8\times10^{-9}$	0.188	±0.002	-10.9	-80.1
7-02-1	2.50×10^{-6}	$\pm1\times10^{-8}$	7.15×10^{-5}	$\pm6\times10^{-6}$	3.73×10^{-7}	$\pm5\times10^{-9}$	0.162	±0.004		
7-02-2	4.10×10^{-6}	$\pm3\times10^{-8}$	6.12×10^{-5}	$\pm5\times10^{-6}$	4.58×10^{-7}	$\pm9\times10^{-9}$	0.221	±0.002	-10.5	-75.6
7-01-1	1.16×10^{-6}	$\pm1\times10^{-8}$	1.66×10^{-6}	$\pm2\times10^{-8}$	4.20×10^{-7}	$\pm3\times10^{-9}$	0.142	±0.004		
7-01-2	2.19×10^{-6}	$\pm5\times10^{-8}$	2.68×10^{-5}	$\pm8\times10^{-8}$	4.14×10^{-7}	$\pm9\times10^{-9}$	0.231	±0.010	-10.7	-77.2
18-00-1	$1.13.10^{-6}$	$\pm1.3.10^{-8}$	$8.55.10^{-7}$	$\pm1.4.10^{-8}$	4.09×10^{-7}	$\pm8.2\times10^{-9}$	0.153	±0.001		
18-00-2	$2.79.10^{-6}$	$\pm2.6.10^{-8}$	$5.07.10^{-5}$	$\pm3.1.10^{-6}$	4.92×10^{-7}	$\pm1.0\times10^{-8}$	0.249	±0.010		
5-01-1	2.55×10^{-6}	$\pm3\times10^{-8}$	5.54×10^{-7}	$\pm3\times10^{-9}$	4.92×10^{-7}	$\pm9.0\times10^{-9}$	0.140	±0.002		
5-01-2	1.03×10^{-6}	$\pm7\times10^{-9}$	8.89×10^{-7}	$\pm6\times10^{-8}$	4.40×10^{-7}	$\pm2.2\times10^{-9}$	0.199	±0.002	-10.9	-80.5
1-02-1	1.99×10^{-6}	$\pm6\times10^{-9}$	6.06×10^{-7}	$\pm5\times10^{-8}$	6.85×10^{-7}	$\pm1.6\times10^{-8}$	0.168	±0.001	-11.5	-85.3
1-98-1	1.36×10^{-6}	$\pm1\times10^{-8}$	4.51×10^{-5}	$\pm2\times10^{-6}$	3.87×10^{-7}	$\pm3.3\times10^{-9}$	0.207	±0.000	-11.2	-82.0
1-98-2	1.63×10^{-6}	$\pm2\times10^{-8}$	4.85×10^{-5}	$\pm3\times10^{-7}$	3.94×10^{-7}	$\pm4.5\times10^{-9}$	0.276	±0.002	-10.9	-76.8
1-98-3	3.29×10^{-8}	$\pm4\times10^{-9}$	3.08×10^{-6}	$\pm3\times10^{-8}$	3.57×10^{-7}	$\pm1.3\times10^{-8}$	0.297	±0.001	-10.8	-79.8
6-99	9.41×10^{-7}	$\pm4\times10^{-9}$	8.77×10^{-7}	$\pm3\times10^{-8}$	2.29×10^{-7}	$\pm3.3\times10^{-9}$	0.126	±0.001		
1-06-1	3.25×10^{-7}	$\pm6\times10^{-9}$	7.89×10^{-6}	$\pm1\times10^{-7}$	1.50×10^{-7}	$\pm2.1\times10^{-9}$	0.108	±0.001		
1-06-2	3.39×10^{-7}	$\pm5\times10^{-9}$	1.94×10^{-6}	$\pm1\times10^{-7}$	1.45×10^{-7}	$\pm9.9\times10^{-10}$	0.115	±0.001		

	$[^{55}Mn^{2+}]$		$[^{56}Fe^{2+}]$		$[^{88}Sr]$		Si		$\delta^{18}O$	$\delta^{2}H$
	(mol.l^{-1})		(mol.l^{-1})		(mol.l^{-1})		(mmol.l^{-1})		‰ *vs* SMOW	‰ *vs* SMOW
№ Well	MC ICP-MS		MC ICP-MS		MC ICP-MS		UV spectrometer		Laser spectrometer	Laser spectrometer
1-00	7.89×10^{-7}	$\pm3\times10^{-9}$	2.29×10^{-7}	$\pm4\times10^{-8}$	1.17×10^{-7}	$\pm7.2\times10^{-10}$	0.123	±0.000		
12-02-1	2.25×10^{-5}	$\pm2\times10^{-7}$	9.25×10^{-7}	$\pm5\times10^{-8}$	4.56×10^{-7}	$\pm7.4\times10^{-9}$	0.247	±0.000		
12-02-2	2.15×10^{-6}	$\pm2\times10^{-8}$	1.58×10^{-6}	$\pm3\times10^{-8}$	2.96×10^{-7}	$\pm6.0\times10^{-10}$	0.120	±0.001		
4-02-1	9.55×10^{-7}	$\pm8\times10^{-9}$	1.28×10^{-7}	$\pm3\times10^{-9}$	5.93×10^{-7}	$\pm2.9\times10^{-9}$	0.136	±0.002		
4-02-2	4.56×10^{-6}	$\pm5\times10^{-8}$	4.14×10^{-7}	$\pm2\times10^{-8}$	4.29×10^{-7}	$\pm3.5\times10^{-9}$	0.160	±0.001		
10-02-1	1.17×10^{-6}	$\pm4\times10^{-8}$	1.24×10^{-6}	$\pm5\times10^{-8}$	9.01×10^{-7}	$\pm3.0\times10^{-8}$	0.120	±0.002		
10-02-2	6.01×10^{-7}	$\pm5\times10^{-9}$	1.66×10^{-6}	$\pm5\times10^{-8}$	7.48×10^{-7}	$\pm6.2\times10^{-9}$	0.129	±0.001		
4-00	5.47×10^{-7}	$\pm5\times10^{-9}$	2.19×10^{-7}	$\pm2\times10^{-8}$	4.34×10^{-7}	$\pm6.2\times10^{-9}$	0.096	±0.001		
2-06-1	1.09×10^{-6}	$\pm1\times10^{-8}$	2.38×10^{-5}	$\pm3\times10^{-7}$	1.65×10^{-7}	$\pm1.4\times10^{-9}$	0.123	±0.001		
2-06-2	7.22×10^{-7}	$\pm4\times10^{-8}$	6.85×10^{-5}	$\pm6\times10^{-6}$	2.14×10^{-7}	$\pm4.5\times10^{-9}$	0.196	±0.001	-11.0	-81.5
11-02-1	2.72×10^{-7}	$\pm4\times10^{-9}$	1.93×10^{-5}	$\pm2\times10^{-7}$	1.91×10^{-7}	$\pm1.5\times10^{-9}$	0.114	±0.004		
11-02-2	1.13×10^{-6}	$\pm1\times10^{-8}$	1.39×10^{4}	$\pm1\times10^{-6}$	2.88×10^{-7}	$\pm2.5\times10^{-9}$	0.149	±0.007		
3-02-1	1.93×10^{-6}	$\pm1\times10^{-8}$	2.16×10^{-5}	$\pm2\times10^{-6}$	2.19×10^{-7}	$\pm1.3\times10^{-9}$	0.121	±0.002		
3-02-2	2.02×10^{-6}	$\pm2\times10^{-8}$	7.81×10^{-5}	$\pm7\times10^{-6}$	3.96×10^{-7}	$\pm3.4\times10^{-9}$	0.251	±0.004	-10.8	-79.4
9-02-1	3.26×10^{-6}	$\pm1\times10^{-8}$	1.1×10^{4}	$\pm1\times10^{-5}$	2.36×10^{-7}	$\pm7.6\times10^{-10}$	0.116	±0.002		
9-02-2	3.68×10^{-6}	$\pm3\times10^{-8}$	8.4×10^{-5}	$\pm6\times10^{-6}$	4.08×10^{-7}	$\pm2.2\times10^{-9}$	0.211	±0.000		

October 2008 saturation indices simulated with PHREEQC code (Inll.dat)

N° Well	Quartz	Albite	K-Feldspar	Gibbsite	Montmor-Ca	Montmor-K	Montmor-Na	Montmor-Mg	Kaolinite
5-99	0.34	-7.29	-4.12	-0.73	-3.94	-4.30	-4.66	-3.95	-0.17
6-02-1	0.27	-6.58	-3.18	-0.71	-3.06	-3.44	-3.88	-3.10	-0.24
6-02-2	0.33	-3.72	-0.64	1.47	1.03	0.65	0.33	1.01	4.21
8-02-1	0.27	-5.17	-1.71	0.75	-0.72	-1.06	-1.51	-0.76	2.65
8-02-2	0.31	-6.93	-3.61	-0.64	-3.53	-3.86	-4.26	-3.56	-0.06
8-01-1	0.33	-7.58	-4.21	-1.61	-4.53	-4.95	-5.37	-4.59	-1.95
8-01-2	0.30	-7.69	-4.33	-1.45	-4.63	-5.03	-5.45	-4.69	-1.69
19-00-1	0.41	-5.33	-1.98	0.63	-0.89	-1.30	-1.71	-1.01	2.71
19-00-2	0.32	-6.52	-3.03	-0.22	-2.69	-3.05	-3.51	-2.78	0.81
6-01-1	0.43	-6.49	-3.26	-0.92	-3.00	-3.42	-3.80	-3.05	-0.36
6-01-2	0.40	-5.55	-2.11	0.28	-1.39	-1.73	-2.17	-1.46	1.95
2-02-1	0.36	-4.48	-1.07	0.61	0.21	-0.22	-0.65	0.19	2.56
2-02-2	0.40	-3.98	-0.63	1.28	0.85	0.50	0.09	0.80	3.96
7-00	0.34	-6.50	-2.99	-0.44	-2.95	-3.20	-3.67	-2.96	0.43
5-02-1	0.50	-4.16	-1.46	-0.01	-0.36	-0.80	-1.00	-0.34	1.58
5-02-2	0.46	-3.54	-0.87	-0.02	0.16	-0.26	-0.46	0.20	1.52
7-02-1	0.51	-4.27	-1.52	-0.08	-0.50	-0.92	-1.14	-0.49	1.46
7-02-2	0.53	-2.39	0.07	0.60	1.64	1.21	1.07	1.68	2.91
7-01-2	0.66	-3.11	-0.40	0.91	1.32	0.94	0.74	1.34	3.75
18-00-1	0.50	-5.42	-2.46	-0.14	-1.54	-1.95	-2.23	-1.53	1.31
18-00-2	0.72	-2.74	-0.07	0.73	1.65	1.25	1.06	1.67	3.48
5-01-1	0.45	-5.67	-2.52	-0.04	-1.70	-2.11	-2.45	-1.75	1.41
5-01-2	0.61	-5.19	-2.33	-0.30	-1.46	-1.83	-2.08	-1.42	1.21

N° Well	Quartz	Albite	K-Feldspar	Gibbsite	Montmor-Ca	Montmor-K	Montmor-Na	Montmor-Mg	Kaolinite
1-02-1	0.52	-1000.00	-1000.00	-1000.00	-1000.00	-1000.00	-1000.00	-1000.00	-1000.00
1-98-1	0.63	-3.81	-1.00	0.42	0.44	0.02	-0.21	0.44	2.70
1-98-2	0.76	-1.58	1.04	1.29	3.26	2.82	2.65	3.27	4.70
1-98-3	0.80	-0.65	1.81	1.83	4.69	4.16	4.05	4.69	5.87
6-99	0.36	-7.28	-3.80	-0.67	-3.77	-4.05	-4.51	-3.76	0.00
1-06-1	0.29	-5.34	-2.11	0.73	-0.78	-1.23	-1.61	-0.81	2.66
1-06-2	0.32	-5.75	-2.51	0.32	-1.62	-2.01	-2.39	-1.67	1.90
1-00	0.36	-7.91	-4.56	-1.10	-4.64	-5.00	-5.41	-4.67	-0.86
12-02-1	0.64	-3.83	-0.62	1.13	1.15	0.78	0.41	1.14	4.16
12-02-2	0.37	-7.15	-3.71	-0.76	-3.49	-3.88	-4.32	-3.53	-0.19
4-02-1	0.45	-3.39	0.10	1.34	1.41	1.13	0.67	1.33	4.19
4-02-2	0.52	-5.78	-2.23	-0.15	-1.78	-2.08	-2.56	-1.85	1.33
10-02-1	0.33	-3.68	-0.42	1.10	0.84	0.50	0.11	0.80	3.47
10-02-2	0.36	-6.28	-3.18	-0.38	-2.56	-2.97	-3.31	-2.56	0.58
2-06-1	0.37	-4.74	-1.21	0.87	-0.18	-0.46	-0.94	-0.21	3.10
2-06-2	0.60	-3.29	-0.33	1.07	1.43	1.06	0.77	1.46	3.94
11-02-1	0.37	-6.15	-2.99	-0.24	-2.37	-2.76	-3.11	-2.38	0.85
11-02-2	0.48	-3.32	-0.50	0.81	1.05	0.65	0.41	1.08	3.18
3-02-1	0.39	-6.67	-3.54	-1.10	-3.36	-3.79	-4.13	-3.37	-0.82
3-02-2	0.72	-3.26	-0.66	0.29	0.82	0.41	0.25	0.86	2.61
9-02-1	0.35	-4.54	-1.45	0.62	-0.14	-0.58	-0.90	-0.16	2.56
9-02-2	0.61	-2.74	-0.10	1.01	1.71	1.32	1.14	1.75	3.85

October 2009 field data – (from Chernobyl database)

№ Well	Formation	Profile	Mean screen elevation	Distance from upgradient point	Hydraulic head	pH	T° (pH)	Cond	Eh (ENH)	pe	O_2	Alcalinity
			(m.a.s.l.)	*(m)*	*(m.a.s.l.)*	*(field)*	*(°C)*	*(µS/cm)*	*(mV)*		*(mg/L)*	*(mmol/L)*
5-99	Aeolian	AB	110.4	0	111.07	5.9	12.5	28.3	457	8	1.93	0.052
6-02-2	Interface Aeolian/Alluvial	AB	109.7	17	111.05	5.6	12.4	48.3	311	5	1.07	0.230
8-02-2	Interface Aeolian/Alluvial	AB	109.9	23	111.04	5.6	12	26	385	7	1.31	0.048
8-01-2	Interface Aeolian/Alluvial	AB	109.8	29	111.03	5.1	12.8	29.4			2.72	
19-00-2	Interface Aeolian/Alluvial	AB	109.9	33	109.65	5.4	12	32.8	515	9	1.67	0.056
6-01-2	Interface Aeolian/Alluvial	AB	110.0	37	111.04	6.0	12.9	45.8	493	8	2.63	0.054
7-00	Interface Aeolian/Alluvial	AB	110.2	58	110.99	5.3	13	35.5	238	4	3.72	0.210
5-02-1	Alluvial	AB	108.4	17	110.99	6.3	11.6	78.8	318	5	1.13	0.340
5-02-2	Alluvial	AB	106.9	17	110.99	6.1	11	105	238	4	1.04	0.290
7-02-1	Alluvial	AB	108.4	24	111.00	6.5	11	61.4	315	5	0.50	0.260
7-02-2	Alluvial	AB	106.8	24	111.01	6.3	12.2	114.2	231	4	4.83	0.210
7-01-1	Alluvial	AB	108.3	29	110.99	5.2	11.2	42	493	8	0.50	0.090
7-01-2	Alluvial	AB	106.8	29	110.99	5.6	11.2	66.1	420	7	3.20	0.088
18-00-1	Alluvial	AB	108.1	33	111.00	5.7	11.3	44.6	400	7	0.75	0.072
18-00-2	Alluvial	AB	107.0	33	110.99	5.7	11.1	76.5	309	5	1.35	0.220
5-01-1	Alluvial	AB	108.3	37	111.00	6.3	11.3	48.5	427	7	0.63	0.046

№ Well	Formation	Profile	Mean screen elevation	Distance from upgradient point	Hydraulic head	pH	T° (pH)	Cond	Eh (ENH)	pe	O2	Alcalinity
			(m.a.s.l.)	*(m)*	*(m.a.s.l.)*	*(field)*	*(°C)*	*(µS/cm)*	*(mV)*		*(mg/L)*	*(mmol/L)*
5-01-2	Alluvial	AB	107.2	37	110.98	5.1	11	50.6	426	7	9.05	0.050
1-02-1	Alluvial	AB	108.3	41	110.98	5.3	11.7	67.6	430	7	0.80	
1-98-1	Alluvial	AB	106.1	41	111.0	5.9	11.2	71.5	200	3	2.25	0.350
1-98-2	Alluvial	AB	96.0	41	111.0	5.8	11.3	91	252	4	2.70	0.510
1-98-3	Alluvial	AB	84.7	41	111.0	6.1	11.4	108	289	5	1.70	0.810
1-00	Aeolian	CD	110.5	26	111.03	5.2	12.6	20.6	508	9	6.90	0.034
4-00	Interface Aeolian/Alluvial	CD	110.3	49	110.98	5.1	12.4	59.3	526	9	7.24	0.030
2-06-1	Alluvial	CD	108.3	21	110.84	6.0	12.7	35.1	318	5	2.34	0.150
2-06-2	Alluvial	CD	106.8	21	110.84	6.1	12.6	52.7	296	5	1.86	
11-02-1	Alluvial	CD	108.4	33	110.97	6.7	11.7	29.4	374	6	2.12	0.070
11-02-2	Alluvial	CD	106.9	33	110.97	6.1	11.5	56.7	227	4	0.68	0.280
3-02-1	Alluvial	CD	108.2	38	110.98	5.9	11.7	35.9	350	6	0.45	0.140
3-02-2	Alluvial	CD	106.7	38	110.97	6.3	11.8	67.4	271	5	1.74	0.230
9-02-1	Alluvial	CD	108.4	43	110.96	6.9	11.6	49	266	5	1.36	0.240
						5.7	12.2	49.4	292	5	5.70	
9-02-2	Alluvial	CD	107.1	43	110.96	6.5	11.4	74	262	4	1.05	0.290

October 2009 chemical concentrations in Chernobyl groundwater (ionic chromatography - LAME -Chernobyl database)

№ Well	$[Cl^-]$		$[NO_3^-]$		$[SO_4^{2-}]$		$[Ca^{2+}]$		$[K^+]$		$[Mg^{2+}]$		$[Na^+]$		Electrical balance
	(mM)		*(mM)*		*(mM)*		*(mM)*		*(mM)*		*(mM)*		*(mM)*		
LD			**0.0008**												
5-99	0.015	±0.002	0.007	±0.000	0.089	±0.008	0.052	±0.005	0.033	±0.004	0.008	±0.001	0.033	±0.002	-15
6-02-2	0.015	±0.0018	0.002	±0.0007	0.110	±0.0117	0.107	±0.0078	0.041	±0.0044	0.020	±0.0024	0.046	±0.0060	-17
8-02-2	0.013	±0.0009	0.009	±0.0007	0.078	±0.0131	0.060	±0.0042	0.040	±0.0038	0.011	±0.0005	0.033	±0.0013	-3
8-01-2	0.019	±0.0002	0.008	±0.0001	0.074	±0.0049	0.086	±0.0025	0.031	±0.0013	0.012	±0.0048	0.023	±0.0016	15
19-00-2	0.013	±0.0011	0.035	±0.0018	0.076	±0.0051	0.101	±0.0016	0.039	±0.0021	0.005	±0.0010	0.023	±0.0010	4
6-01-2	0.012	±0.0012	0.027	±0.0011	0.139	±0.0143	0.143	±0.0101	0.052	±0.0027	0.013	±0.0044	0.032	±0.0030	4
2-02-1	0.009	±0.0009			0.058	±0.0004	0.107	±0.0026	0.030	±0.0011	0.009	±0.0006	0.017	±0.0016	38
2-02-2	0.017	±0.0010			0.196	±0.0125	0.176	±0.0034	0.049	±0.0024	0.019	±0.0014	0.032	±0.0012	7
7-00	0.009	±0.0030	0.026	±0.0067	0.100	±0.0072	0.097	±0.0108	0.076	±0.0054	0.020	±0.0035	0.055	±0.0026	-10
5-02-1	0.019	±0.002	0.009	±0.002	0.210	±0.020	0.192	±0.012	0.034	±0.004	0.074	±0.004	0.107	±0.009	-9
5-02-2	0.017	±0.011		/	0.174	±0.018	0.194	±0.016	0.042	±0.004	0.086	±0.008	0.164	±0.013	6
7-02-1	0.017	±0.006	0.005	±0.002	0.168	±0.011	0.135	±0.010	0.028	±0.004	0.052	±0.004	0.092	±0.007	-12
7-02-2	0.045	±0.012		/	0.243	±0.008	0.175	±0.012	0.046	±0.004	0.072	±0.001	0.184	±0.014	-1
7-01-1	0.017	±0.006	0.005	±0.002	0.168	±0.011	0.135	±0.010	0.028	±0.004	0.052	±0.004	0.092	±0.007	4
7-01-2	0.021	±0.006		/	0.226	±0.010	0.136	±0.009	0.043	±0.005	0.061	±0.003	0.137	±0.011	0
18-00-1	0.015	±0.000		/	0.140	±0.003	0.114	±0.004	0.029	±0.001	0.031	±0.003	0.063	±0.001	2
18-00-2	0.022	±0.002		/	0.203	±0.011	0.170	±0.001	0.035	±0.001	0.065	±0.002	0.146	±0.001	0
5-01-1	0.012	±0.000	0.021	±0.001	0.145	±0.001	0.139	±0.003	0.036	±0.001	0.017	±0.001	0.045	±0.001	3
5-01-2	0.019	±0.003	0.006	±0.001	0.179	±0.026	0.111	±0.009	0.034	±0.001	0.055	±0.004	0.090	±0.005	3

№ Well	[Cl^-]		[NO_3^-]		[SO_4^{2-}]		[Ca^{2+}]		[K^+]		[Mg^{2+}]		[Na^+]		Electrical balance
	(mM)		*(mM)*		*(mM)*		*(mM)*		*(mM)*		*(mM)*		*(mM)*		
1-02-1	0.015	±0.000	0.029	±0.001	0.252	±0.019	0.229	±0.003	0.033	±0.003	0.069	±0.001	0.060	±0.001	10
1-98-1	0.018	±0.002		/	0.134	±0.005	0.196	±0.005	0.030	±0.001	0.054	±0.002	0.083	±0.001	-2
1-98-2	0.060	±0.004		/	0.142	±0.005	0.290	±0.003	0.038	±0.001	0.087	±0.003	0.161	±0.001	5
1-98-3	0.021	±0.002		/	0.107	±0.010	0.417	±0.005	0.021	±0.001	0.114	±0.001	0.143	±0.003	8
6-99	0.023	±0.007	0.002	±0.001	0.106	±0.005	0.045	±0.008	0.043	±0.007	0.015	±0.005	0.028	±0.005	-11
1-06-1	0.013	±0.001	0.006	±0.000	0.055	±0.006	0.198	±0.006	0.028	±0.003	0.050	±0.003	0.020	±0.001	60
1-06-2	0.015	±0.000	0.006	±0.001	0.075	±0.001	0.063	±0.003	0.027	±0.002	0.009	±0.001	0.026	±0.002	-6
1-00	0.010	±0.000		/	0.054	±0.001	0.031	±0.001	0.020	±0.002	<0.004	/	0.023	±0.001	-19
12-02-2	0.008	±0.001		/	0.065	±0.005	0.064	±0.003	0.026	±0.001	0.007	±0.000	0.018	±0.002	15
10-02-2	0.030	±0.001	0.073	±0.005	0.176	±0.007	0.192	±0.003	0.049	±0.002	0.038	±0.003	0.057	±0.001	11
4-00	0.038	±0.004	0.128	±0.013	0.137	±0.013	0.153	±0.004	0.060	±0.002	0.024	±0.001	0.047	±0.001	-1
2-06-1	0.011	±0.000		/	0.063	±0.005	0.076	±0.003	0.059	±0.001	0.012	±0.000	0.026	±0.002	-5
2-06-2	0.014	±0.001		/	0.113	±0.012	0.071	±0.002	0.031	±0.002	0.026	±0.002	0.054	±0.002	8
11-02-1	0.010	±0.001		/	0.080	±0.002	0.065	±0.001	0.024	±0.001	0.012	±0.001	0.032	±0.001	-7
11-02-2	0.011	±0.000		/	0.098	±0.002	0.077	±0.003	0.028	±0.002	0.029	±0.003	0.072	±0.001	-22
3-02-1	0.010	±0.001		/	0.082	±0.001	0.086	±0.004	0.020	±0.002	0.018	±0.001	0.035	±0.001	-10
3-02-2	0.013	±0.001		/	0.134	±0.006	0.107	±0.004	0.029	±0.002	0.046	±0.001	0.126	±0.001	-6
9-02-1	0.012	±0.000	0.025	±0.000	0.091	±0.004	0.097	±0.009	0.028	±0.020	0.018	±0.005	0.044	±0.031	-21
9-02-2	**0.015**	**±0.002**	**/**		**0.142**	**±0.037**	**0.105**	**±0.009**	**0.031**	**±0.003**	**0.054**	**±0.003**	**0.128**	**±0.010**	**-10**

October 2009 - additional chemical data

	$[^{55}Mn^{2+}]$		$[^{56}Fe^{2+}]$		$[^{88}Sr]$		Si		$\delta^{18}O$	$\delta^{2}H$
	($mol.l^{-1}$)		($mol.l^{-1}$)		($mol.l^{-1}$)		($mmol.l^{-1}$)		‰ *vs* SMOW	‰ *vs* SMOW
Piezometer sampled	MC ICP-MS		MC ICP-MS		MC ICP-MS		UV spectrometer		Laser spectrometer	Laser spectrometer
5-99	1.21×10^{-6}	$\pm4\times10^{-9}$	1.90×10^{-6}	$\pm5\times10^{-8}$	1.89×10^{-7}	$\pm2.4\times10^{-9}$	0.114	±0.001		
6-02-2	1.45×10^{-6}	$\pm8\times10^{-9}$	1.00×10^{-4}	$\pm7\times10^{-7}$	2.25×10^{-7}	$\pm1.7\times10^{-9}$	0.117	±0.002	-11.4	-83.2
8-02-2	1.03×10^{-6}	$\pm5\times10^{-8}$	9.70×10^{-7}	$\pm7\times10^{-8}$	3.74×10^{-7}	$\pm2.2\times10^{-8}$	0.100	±0.004	-10.6	-77.1
8-01-2	8.92×10^{-7}	$\pm2\times10^{-8}$	7.84×10^{-7}	$\pm5\times10^{-8}$	3.24×10^{-7}	$\pm1.1\times10^{-9}$	0.100	±0.003	-	-
19-00-2	3.03×10^{-7}	$\pm3\times10^{-8}$	3.74×10^{-7}	$\pm4\times10^{-9}$	7.47×10^{-7}	$\pm1.8\times10^{-8}$	0.108	±0.001		
6-01-2	1.22×10^{-6}	$\pm3\times10^{-9}$	2.11×10^{-6}	$\pm9\times10^{-8}$	6.76×10^{-7}	$\pm2.7\times10^{-9}$	0.112	±0.002		
2-02-1	6.12×10^{-6}	$\pm3\times10^{-7}$	4.74×10^{-6}	$\pm1\times10^{-7}$	1.92×10^{-7}	$\pm1.4\times10^{-8}$	0.141	±0.000		
2-02-2	1.03×10^{-6}	$\pm7\times10^{-8}$	1.25×10^{-6}	$\pm1\times10^{-7}$	6.04×10^{-7}	$\pm2.7\times10^{-8}$	0.119	±0.003		
7-00	1.14×10^{-6}	$\pm7\times10^{-9}$	6.39×10^{-5}	$\pm8\times10^{-7}$	2.69×10^{-7}	$\pm1.7\times10^{-9}$	0.201	±0.002	-10.7	-77.1
5-02-1	2.83×10^{-6}	$\pm3\times10^{-8}$	1.19×10^{-4}	$\pm1\times10^{-6}$	5.87×10^{-7}	$\pm5.3\times10^{-9}$	0.123	±0.002	-	-
5-02-2	3.53×10^{-6}	$\pm3\times10^{-8}$	7.55×10^{-5}	$\pm3\times10^{-6}$	5.74×10^{-7}	$\pm1.5\times10^{-9}$	0.140	±0.004	-11.5	-81.6
7-02-1	1.96×10^{-6}	$\pm2\times10^{-8}$	2.54×10^{-5}	$\pm2\times10^{-7}$	3.74×10^{-7}	$\pm1.1\times10^{-9}$	0.165	±0.001	-	-
7-02-2	2.28×10^{-6}	$\pm1\times10^{-8}$	9.54×10^{-5}	$\pm1\times10^{-6}$	3.52×10^{-7}	$\pm4.0\times10^{-8}$	0.212	±0.082	-10.9	-75.2
7-01-1	1.05×10^{-6}	$\pm6\times10^{-9}$	2.73×10^{-6}	$\pm9\times10^{-8}$	3.66×10^{-7}	$\pm3.3\times10^{-9}$	0.142	±0.001	-	-
7-01-2	1.97×10^{-6}	$\pm1\times10^{-8}$	2.52×10^{-5}	$\pm4\times10^{-8}$	3.76×10^{-7}	$\pm4.5\times10^{-9}$	0.237	±0.002	-11.1	-80.8

	$[^{55}Mn^{2+}]$		$[^{56}Fe^{2+}]$		$[^{88}Sr]$		Si		$\delta^{18}O$	$\delta^{2}H$
	($mol.l^{-1}$)		($mol.l^{-1}$)		($mol.l^{-1}$)		($mmol.l^{-1}$)		‰ *vs* SMOW	‰ *vs* SMOW
Piezometer sampled	MC ICP-MS		MC ICP-MS		MC ICP-MS		UV spectrometer		Laser spectrometer	Laser spectrometer
18-00-1	9.67×10^{-7}	$\pm6\times10^{-8}$	1.26×10^{-6}	$\pm6\times10^{-8}$	3.49×10^{-7}	$\pm1.4\times10^{-8}$	0.154	±0.002	-11.4	-83.5
18-00-2	$2.20.10^{-6}$	$\pm1\times10^{-7}$	4.21×10^{-5}	$\pm2\times10^{-6}$	4.05×10^{-7}	$\pm2.6\times10^{-8}$	0.257	±0.003	-11.08	-81.3
5-01-1	2.03×10^{-6}	$\pm1\times10^{-7}$	1.46×10^{-6}	$\pm1\times10^{-7}$	4.32×10^{-7}	$\pm3.2\times10^{-8}$	0.141	±0.003		
5-01-2	9.15×10^{-7}	$\pm1\times10^{-8}$	4.08×10^{-6}	$\pm2\times10^{-7}$	3.50×10^{-7}	$\pm2.1\times10^{-9}$	0.115	±0.001	-11.81	-83.21
1-02-1	2.14×10^{-6}	$\pm2\times10^{-7}$	8.71×10^{-7}	$\pm\times10^{-8}$	6.82×10^{-7}	$\pm2.4\times10^{-8}$	0.168	±0.003		
1-98-1	1.73×10^{-6}	$\pm2\times10^{-8}$	3.97×10^{-5}	$\pm2\times10^{-6}$	4.93×10^{-7}	$\pm6.4\times10^{-9}$	0.202	±0.003	-11.4	-84.1
1-98-2	1.51×10^{-6}	$\pm4\times10^{-8}$	3.87×10^{-5}	$\pm3\times10^{-6}$	3.35×10^{-7}	$\pm4.1\times10^{-9}$	0.283	±0.002	-10.91	-79.71
1-98-3	4.22×10^{-8}	$\pm3\times10^{-9}$	9.17×10^{-6}	$\pm5\times10^{-7}$	3.46×10^{-7}	$\pm2.7\times10^{-8}$	0.296	±0.004	-11.2	-80.8
6-99	9.67×10^{-7}	$\pm7\times10^{-9}$	9.61×10^{-7}	$\pm5\times10^{-8}$	2.31×10^{-7}	$\pm4.0\times10^{-9}$	0.164	±0.004		
1-06-1	1.70×10^{-6}	$\pm1\times10^{-7}$	3.45×10^{-8}	$\pm2\times10^{-9}$	3.86×10^{-7}	$\pm2.3\times10^{-8}$	0.114	±0.002		
1-06-2	3.62×10^{-7}	$\pm1\times10^{-8}$	3.81×10^{-6}	$\pm1\times10^{-7}$	1.65×10^{-7}	$\pm7.4\times10^{-9}$	0.115	±0.002		
1-00	7.03×10^{-7}	$\pm5\times10^{-8}$	2.34×10^{-7}	$\pm2\times10^{-8}$	1.29×10^{-7}	$\pm9.7\times10^{-9}$	0.119	±0.002		
12-02-2	9.92×10^{-7}	$\pm1\times10^{-7}$	7.64×10^{-7}	$\pm4\times10^{-8}$	1.37×10^{-7}	$\pm6.2\times10^{-9}$	0.121	±0.002		
10-02-2	1.06×10^{-6}	$\pm2\times10^{-8}$	1.45×10^{-4}	$\pm7\times10^{-6}$	6.16×10^{-7}	$\pm1.1\times10^{-8}$	0.107	±0.002		
4-00	4.59×10^{-7}	$\pm4\times10^{-8}$	1.51×10^{-7}	$\pm3\times10^{-9}$	3.20×10^{-7}	$\pm2.5\times10^{-8}$	0.093	±0.003		
2-06-1	1.09×10^{-6}	$\pm5\times10^{-8}$	1.92×10^{-5}	$\pm1\times10^{-9}$	1.38×10^{-7}	$\pm7.4\times10^{-9}$	0.122	±0.000		

	$[^{55}Mn^{2+}]$		$[^{56}Fe^{2+}]$		$[^{88}Sr]$		Si		$\delta^{18}O$	$\delta^{2}H$
	($mol.l^{-1}$)		($mol.l^{-1}$)		($mol.l^{-1}$)		($mmol.l^{-1}$)		‰ *vs* SMOW	‰ *vs* SMOW
Piezometer sampled	MC ICP-MS		MC ICP-MS		MC ICP-MS		UV spectrometer		Laser spectrometer	Laser spectrometer
2-06-2	5.42×10^{-7}	$\pm1\times10^{-8}$	4.74×10^{-5}	$\pm2\times10^{-6}$	1.69×10^{-7}	$\pm5.3\times10^{-9}$	0.189	±0.004		
11-02-1	2.04×10^{-7}	$\pm1\times10^{-8}$	8.37×10^{-6}	$\pm1\times10^{-7}$	1.51×10^{-7}	$\pm1.3\times10^{-8}$	0.116	±0.001		
11-02-2	1.04×10^{-6}	$\pm1\times10^{-8}$	9.27×10^{-5}	$\pm7\times10^{-6}$	1.88×10^{-7}	$\pm7.9\times10^{-9}$	0.163	±0.002		
3-02-1	1.40×10^{-6}	$\pm6\times10^{-8}$	1.91×10^{-5}	$\pm2\times10^{-6}$	1.58×10^{-7}	$\pm1.2\times10^{-8}$	0.120	±0.002		
3-02-2	1.47×10^{-6}	$\pm9\times10^{-8}$	5.97×10^{-5}	$\pm2\times10^{-6}$	2.91×10^{-7}	$\pm1.9\times10^{-8}$	0.252	±0.006		
9-02-1	6.88×10^{-7}	$\pm2\times10^{-9}$	3.88×10^{-6}	$\pm3\times10^{-7}$	1.52×10^{-7}	$\pm3.5\times10^{-10}$	0.117	±0.002		
9-02-2	1.68×10^{-6}	$\pm2\times10^{-8}$	1.23×10^{-4}	$\pm1\times10^{-6}$	1.85×10^{-7}	$\pm1.7\times10^{-9}$	0.200	±0.009		

October 2009 saturation indices simulated with PHREEQC code (lnll.dat)

N° Well	Quartz	Albite	K-Feldspar	Gibbsite	Montmor-Ca	Montmor-K	Montmor-Na	Montmor-Mg	Kaolinite
5-99	0.35	-3.18	0.06	1.72	1.72	1.40	1.02	1.68	4.75
6-02-2	0.37	-4.92	-1.71	0.07	-1.08	-1.41	-1.78	-1.10	1.48
8-02-2	0.31	-4.01	-0.67	1.38	0.66	0.36	-0.05	0.63	3.97
8-01-2	0.29	-6.59	-3.22	-0.58	-3.04	-3.41	-3.83	-3.09	0.02
19-00-2	0.34	-4.53	-1.03	1.09	0.08	-0.26	-0.72	-0.04	3.47
6-01-2	0.34	-3.07	0.39	1.77	2.00	1.67	1.22	1.92	4.82
2-02-2	0.10	-1.77	1.46	2.44	3.67	3.23	2.83	3.62	5.79
7-00	0.59	-4.14	-0.76	0.45	0.11	-0.14	-0.57	0.09	2.69
5-02-1	0.41	-2.51	0.26	1.32	2.06	1.66	1.44	2.08	4.06
5-02-2	0.48	-4.09	-1.40	-0.39	-0.76	-1.13	-1.32	-0.73	0.77
7-02-1	0.55	-1.66	1.10	1.64	3.25	2.85	2.63	3.27	4.97
7-02-2	0.63	-1000.00	-1000.00	-1000.00	-1000.00	-1000.00	-1000.00	-1000.00	-1000.00
7-01-1	0.48	-5.71	-2.96	-0.91	-2.57	-2.97	-3.18	-2.54	-0.26
7-01-2	0.70	-3.78	-1.00	-0.22	-0.10	-0.44	-0.66	-0.07	1.56
18-00-1	0.51	-2.97	-0.03	1.41	1.83	1.44	1.17	1.82	4.43
18-00-2	0.74	-3.03	-0.36	0.35	1.07	0.68	0.50	1.09	2.77
5-01-1	0.47	-2.30	0.86	1.77	2.77	2.40	2.05	2.71	5.08
5-01-2	0.39	-4.85	-2.00	0.36	-0.94	-1.30	-1.54	-0.90	2.10
1-02-1	0.54	-4.92	-1.91	-0.20	-0.97	-1.39	-1.69	-0.97	1.27
1-98-1	0.63	-1000.00	-1000.00	-1000.00	-1000.00	-1000.00	-1000.00	-1000.00	-1000.00
1-98-2	0.78	-2.15	0.51	1.00	2.45	2.04	1.86	2.46	4.14
1-98-3	0.79	-0.36	2.09	1.54	4.72	4.20	4.09	4.72	5.26
6-99	0.49	-3.51	-0.09	1.53	1.56	1.28	0.84	1.57	4.65

N° Well	Quartz	Albite	K-Feldspar	Gibbsite	Montmor-Ca	Montmor-K	Montmor-Na	Montmor-Mg	Kaolinite
1-06-2	0.34	-3.90	-0.64	1.49	0.98	0.61	0.23	0.93	4.28
1-00	0.37	-4.42	-1.23	1.29	-1000.00	-1000.00	-1000.00	-1000.00	3.92
4-00	0.27	-5.13	-1.78	0.70	-0.92	-1.23	-1.64	-0.96	2.53
2-06-1	0.38	-3.15	0.45	1.68	1.94	1.67	1.18	1.90	4.72
2-06-2	0.57	-2.46	0.54	1.38	2.40	2.05	1.75	2.42	4.50
11-02-1	0.38	-2.06	1.08	2.00	3.12	2.75	2.41	3.10	5.36
11-02-2	0.53	-1000.00	-1000.00	-1000.00	-1000.00	-1000.00	-1000.00	-1000.00	-1000.00
3-02-1	0.39	-3.94	-0.90	0.83	0.53	0.11	-0.19	0.51	3.05
3-02-2	0.71	-1.92	0.70	0.96	2.54	2.15	1.98	2.57	3.95
9-02-1	0.38	-1.61	1.47	2.10	3.59	3.21	2.89	3.57	5.56
9-02-2	0.62	-1.21	1.45	1.73	3.68	3.31	3.13	3.72	5.30

10. PHREEQC input file for calcite dissolution simulation

```
DATABASE C:\Program Files\Phreeqc\Databases\llnl.dat
SELECTED_OUTPUT
-file Dissol_calcite3.xls
-reset true
-pH
-totals Ca C(4)
-molalities HCO3-
-saturation_indices calcite
SOLUTION 1 #rainwater from Bugai et al., 2012a
pH  5.6
temp  10
units              mg/L
pe       10 #Appelo and Postma, 2005
Cl      0.74
S       6.6
Ca      2.1
K       0.4
Mg      0.5
Na      0.4
N(-3)   1.1
C(4)      7.3 as HCO3
EQUILIBRIUM_PHASES 1
CO2(g) -2 10 #log pCO2 = -2
SAVE SOLUTION 1
REACTION 1
Calcite 1
0.025 0.05 0.075 0.1 0.15 0.2 0.3 0.4 0.5 mmol
INCREMENTAL_REACTIONS true
END
```

11. PHREEQC input file for dolomite dissolution simulation

```
DATABASE C:\Program Files\Phreeqc\Databases\llnl.dat
SELECTED_OUTPUT
-file Dissol_dolomite.xls
-reset true
-pH
-totals Ca Mg C(4)
-molalities HCO3-
-saturation_indices dolomite calcite
SOLUTION 1 #rainwater from Bugai et al., 2012a
pH  5.6
temp  10
units              mg/L
pe       10 #Appelo and Postma, 2005
Cl      0.74
S       6.6
Ca      2.1
K       0.4
Mg      0.5
Na      0.4
N(-3)   1.1
C(4)      7.3 as HCO3
EQUILIBRIUM_PHASES 1
CO2(g) -2 10 #log pCO2 = -2
SAVE SOLUTION 1
REACTION 1
Dolomite 1
0.025 0.05 0.075 0.1 0.15 0.2 0.3 0.4 0.5 mmol
INCREMENTAL_REACTIONS true
END
```

12. PHREEQC input file for O2 equilibrium and decrease in rainwater

```
DATABASE C:\Program Files\Phreeqc\Databases\llnl.dat
SELECTED_OUTPUT
-file pe_O2.xls
-pe
-molalities O2
-solution true
INCREMENTAL_REACTIONS false
SOLUTION 1  #rainwater from Bugai et al., 2012a
pH  5.6
temp  10
units              mg/L
Cl   0.74
K       0.4
Mg      0.5
S       6.6
Ca      2.1
Na     0.4
N(+5)   1.1
C             7.3
EQUILIBRIUM_PHASES
O2(g) -0.678
SAVE solution 1
End
Solution 2
use solution 1
REACTION 1
O2 -1
3.55e-4   3.595e-4   3.5985e-4   3.59875e-4   3.59879e-4   3.598795e-4   3.5987953e-4   3.59879532e-4
3.598795328e-4        3.5987953289e-4        3.598795328958459e-4        3.5987953289584592789e-4
3.5987953289584592789e-4 #3.598795328958459279e-4
save solution 2
END
```

13. PHREEQC input file for pyrite dissolution simulation

```
Database C:\Program Files\Phreeqc\Databases\llnl.dat
SOLUTION 1 #rainwater from Bugai 2012
pH  5.6
temp  10
units              mg/L
Cl   0.74
K       0.4
Mg      0.5
S       6.6
Ca      2.1
Na     0.4
N(+5)   1.1
C             7.3
Fe      0.00193    # data min : 1-06-1 oct09
EQUILIBRIUM_PHASES
O2(g) -0.678
SAVE solution 1
End
use solution 1
INCREMENTAL_REACTIONS true
REACTION 1
Pyrite 1
0.0001 0.0005 0.001 0.005 0.0075 0.01 0.025  0.05 0.06 0.075 mmol
END
```

14. PHREEQC input file for cation exchange simulation in the Aeolian layer, according to Skenknect (2003)

```
Database C:\Program Files\Phreeqc\Databases\llnl_modCR.dat (Only Na, Mg, Ca, K and Sr exchanges are possible)
SELECTED_OUTPUT
-file   E_eol_Skenknect.xls
-totals Ca  K   Mg  Na  Sr

SOLUTION 1 # Synthetic water in equilibrium with aeolian sand
units   mol/L
pH      6.4
Ca      1.35e-4
K       1.05e-4
Mg      1.9e-5
Na      6.5e-5
Sr      3e-7
Cl      3e-5 charge
EXCHANGE 1 # Equilibrate exchanger
X   0.049 # CEC = 1 meq/100g ; porosity = 0.35
 -equilibrate with solution 1
SAVE exchange   1
END

Solution 2  #     1-06-1     aeolian gw
pH                5.2
temp              14.4
units             mmol/L
pe                6.54237288135593
O(0)              0.0734834271419637
Alkalinity              0.092    as HCO3
Cl                0.016720553864196
N(-3)             0.0122726070623788     as NH4
S                 0.0348895776694236
Ca                0.0550281736983893
K                 0.0158617274380938
Mg                0.0095138759494321
Na                0.0154009837233173
```

```
Al              0.000797968132530864
Mn              0.000325126273030303
Fe              0.00788690501428571
Sr              0.000150449815420455

#Exchange sol 1 + exch 1
USE Solution 2
Use Exchange 1
Save Solution 2
End

SOLUTION 3 # 12-02-2            theoretical result
pH              4.6
temp            12.8
units           mmol/L
pe              7.5593220338983
O(0)            0.285490931832395
Alkalinity              0.009   as HCO3
Cl              0.0163656910542107
N(-3)           0.203511544607075       as NH4
S               0.0409844499486538
Ca              0.102591365621966
K               0.0302960353932495
Mg              0.0173979688984094
Na              0.0191937607250204
Si              0.119810341041937
U               0.0000000420168067226891
Al              0.00131687247012346
Mn              0.00214787878787879
Fe              0.00158035714285714
Sr              0.00029553346905303
End
```

15. PHREEQC input file for cation exchange simulation in the Aeolian layer

```
Database C:\Program Files\Phreeqc\Databases\llnl.dat
SELECTED_OUTPUT
-file   E_eol.xls
-totals Ca  K   Mg  Na  Sr  Al Mn Fe

SOLUTION 1 # T8         1-06-2
pH              4.93
temp            14.2
units           mmol/L
pe              7.73898305084746
O(0)            0.0400250156347717
Alkalinity              0.056   as HCO3
Cl              0.0195879617173396
N(-3)           0.00859871211426016   as NH4
S               0.0658780192056943
Ca              0.064866119683887
K               0.0246065361020059
Mg              0.00891393684037798
Na              0.0236482489346536
Si              0.114844552052364
U               0.00000237394957983193
Al              0.00161252577176543
Mn              0.000338510111842424
Fe              0.00193855412949405
Sr              0.000144807454128788
EXCHANGE 1 # Equilibrate exchanger
X   0.049 # CEC = 1 meq/100g ; porosity = 0.35
 -equilibrate with solution 1
SAVE exchange   1
END

Solution 2  #   1-06-1    aeolian gw
pH              5.2
temp            14.4
units           mmol/L
pe              6.54237288135593
O(0)            0.0734834271419637
```

```
Alkalinity              0.092    as HCO3
Cl              0.016720553864196
N(-3)           0.0122726070623788     as NH4
S               0.0348895776694236
Ca              0.0550281736983893
K               0.0158617274380938
Mg              0.0095138759494321
Na              0.0154009837233173
Al              0.000797968132530864
Mn              0.000325126273030303
Fe              0.00788690501428571
Sr              0.000150449815420455

#Exchange sol 1 + exch 1
USE Solution 2
Use Exchange 1
Save Solution 2
End

SOLUTION 3 # 12-02-2    gw at the interface alluvial/aeolian
pH              4.6
temp            12.8
units           mmol/L
pe              7.5593220338983
O(0)            0.285490931832395
Alkalinity              0.009    as HCO3
Cl              0.0163656910542107
N(-3)           0.203511544607075      as NH4
S               0.0409844499486538
Ca              0.102591365621966
K               0.0302960353932495
Mg              0.0173979688984094
Na              0.0191937607250204
Si              0.119810341041937
U               0.0000000420168067226891
Al              0.00131687247012346
Mn              0.00214787878787879
Fe              0.00158035714285714
```

Sr 0.00029553346905303

End

16. PHREEQC input file for cation exchange simulation in the Alluvial layer

```
Database C:\Program Files\Phreeqc\Databases\llnl.dat

SELECTED_OUTPUT
-file   E_allu_2.xls
-totals Ca  K   Mg  Na  Al  Mn  Fe  Sr

SOLUTION 1      #       T8 2-06-2     deep alluvial groundwater   CD profile
pH              5.5
temp            12
units           mmol/L
pe              8.30508474576271
Alkalinity              0.029    as HCO3
Cl              0.0235106501234558
N(-3)           0.00409624021223755   as NH4
S               0.120234863076681
Ca              0.0786835960124737
K               0.0271058361954416
Mg              0.0330114173695631
Na              0.0544367753723771
Si              0.19635992475358
U               0.000000105042016806723
Al              0.000472479438987654
Mn              0.000722411639278788
Fe              0.0684761904761905
Sr              0.000214409729083333

EXCHANGE       1 #Exchanger 1
  X    0.246   #CEC= 5 meq/L; porosity = 0.35
  -equilibrate with solution 1
SAVE exchange   1
End

SOLUTION 2      #       T8 12-02-2        shallow groundwater      CD profile
pH              4.6
temp            12.8
units           mmol/L
pe              7.5593220338983
```

```
O(0)            0.285490931832395
Alkalinity              0.009    as HCO3
Cl              0.0163656910542107
N(-3)           0.203511544607075      as NH4
S               0.0409844499486538
Ca              0.102591365621966
K               0.0302960353932495
Mg              0.0173979688984094
Na              0.0191937607250204
Si              0.119810341041937
U               0.0000000420168067226891
Al              0.00131687247012346
Mn              0.00214787878787879
Fe              0.00158035714285714
Sr              0.00029553346905303

USE EXCHANGE    1
save solution 2
END

SOLUTION 3      #       11-02-2
pH              6
temp            11.9
units           mmol/L
pe              2.89830508474576
O(0)            0.0300187617260788
Alkalinity              0.46     as HCO3
Cl              0.0185448977529073
N(-3)           0.00236530309563779   as NH4
S               0.0711669159840631
Ca              0.0963231667600982
K               0.0244946762470123
Mg              0.0394272731916659
Na              0.067568468757874
Si              0.149094728596607
U               0.0000003781512605042
Al              0.0000332047335728395
Mn              0.00113377528880606
```

Fe	0.138571428571429
Sr	0.00028772096880303
End	

17. PHREEQC input file for cation exchange simulation for the total flow line

```
Database C:\Program Files\Phreeqc\Databases\llnl.dat
SELECTED_OUTPUT
-file   E_total.xls
-totals Ca  K   Mg  Na  Sr  Al Mn Fe

SOLUTION 1 # T8         1-06-2  supposed to be in equilibrium with exchanger 1
pH              4.93
temp            14.2
units           mmol/L
pe              7.73898305084746
O(0)            0.0400250156347717
Alkalinity              0.056    as HCO3
Cl              0.0195879617173396
N(-3)           0.00859871211426016   as NH4
S               0.0658780192056943
Ca              0.064866119683887
K               0.0246065361020059
Mg              0.00891393684037798
Na              0.0236482489346536
Si              0.114844552052364
U               0.00000237394957983193
Al              0.00161252577176543
Mn              0.000338510111842424
Fe              0.00193855412949405
Sr              0.000144807454128788

EXCHANGE 1 # Equilibrate exchanger
X   0.049 # CEC = 1 meq/100g ; porosity = 0.35
 -equilibrate with solution 1
SAVE exchange   1

END

Solution 2  #     1-06-1   start solution for simulation
pH              5.2
temp            14.4
units           mmol/L
```

```
pe              6.54237288135593
O(0)            0.0734834271419637
Alkalinity              0.092    as HCO3
Cl              0.016720553864196
N(-3)           0.0122726070623788     as NH4
S               0.0348895776694236
Ca              0.0550281736983893
K               0.0158617274380938
Mg              0.0095138759494321
Na              0.0154009837233173
Al              0.000797968132530864
Mn              0.000325126273030303
Fe              0.00788690501428571
Sr              0.000150449815420455

USE Solution 2
Use Exchange 1
Save Solution 2
End

SOLUTION 3 # 12-02-2    theoretical result of exchange 1
pH              4.6
temp            12.8
units           mmol/L
pe              7.5593220338983
O(0)            0.285490931832395
Alkalinity              0.009    as HCO3
Cl              0.0163656910542107
N(-3)           0.203511544607075      as NH4
S               0.0409844499486538
Ca              0.102591365621966
K               0.0302960353932495
Mg              0.0173979688984094
Na              0.0191937607250204
Si              0.119810341041937
U               0.0000000420168067226891
Al              0.00131687247012346
Mn              0.00214787878787879
```

```
Fe              0.00158035714285714
Sr              0.00029553346905303
End

SOLUTION 4 #    T8 2-06-2 supposed to be in equilibrium with exchanger 2
pH              5.5
temp            12
units           mmol/L
pe              8.30508474576271
Alkalinity              0.029    as HCO3
Cl              0.0235106501234558
N(-3)           0.00409624021223755   as NH4
S               0.120234863076681
Ca              0.0786835960124737
K               0.0271058361954416
Mg              0.0330114173695631
Na              0.0544367753723771
Si              0.19635992475358
U               0.000000105042016806723
Al              0.000472479438987654
Mn              0.000722411639278788
Fe              0.0684761904761905
Sr              0.000214409729083333

EXCHANGE      2 #Exchanger 1
  X    0.246   #CEC= 5 meq/L; porosity = 0.35
  -equilibrate with solution 4
SAVE exchange   2
End

USE SOLUTION 2
USE EXCHANGE    2
save solution   2
END

SOLUTION 5      #       11-02-2  theoretical result of exchange 2
pH              6
temp            11.9
```

units	mmol/L
pe	2.89830508474576
O(0)	0.0300187617260788
Alkalinity	0.46 as HCO3
Cl	0.0185448977529073
N(-3)	0.00236530309563779 as NH4
S	0.0711669159840631
Ca	0.0963231667600982
K	0.0244946762470123
Mg	0.0394272731916659
Na	0.067568468757874
Si	0.149094728596607
U	0.0000003781512605042 02
Al	0.0000332047335728395
Mn	0.00113377528880606
Fe	0.138571428571429
Sr	0.00028772096880303
End	

18. PHREEQC input file for simulation of albite hydrolysis in the Alluvial layer

```
Database C:\Program Files\Phreeqc\Databases\llnl.dat
SELECTED_OUTPUT
-file   H_allu.xls
-Alkalinity
-totals Ca  K   Mg  Na  Sr  Al Mn Fe  Cl N(-3) S Si
-Saturation_indices Albite   Kaolinite

SOLUTION 1 # 12-02-2    start solution
pH              4.6
temp            12.8
units           mmol/L
pe              7.5593220338983
O(0)            0.285490931832395
Alkalinity              0.009    as HCO3
Cl              0.0163656910542107
N(-3)           0.203511544607075      as NH4
S               0.0409844499486538
Ca              0.102591365621966
K               0.0302960353932495
Mg              0.0173979688984094
Na              0.0191937607250204
Si              0.119810341041937
U               0.0000000420168067226891
Al              0.00131687247012346
Mn              0.00214787878787879
Fe              0.00158035714285714
Sr              0.00029553346905303

EQUILIBRIUM_PHASES 1
  Albite   -4   0.00015
End

SOLUTION 5      #       11-02-2  theoretical result
pH              6
temp            11.9
units           mmol/L
pe              2.89830508474576
```

O(0)	0.0300187617260788	
Alkalinity	0.46	as HCO3
Cl	0.0185448977529073	
N(-3)	0.00236530309563779	as NH4
S	0.0711669159840631	
Ca	0.0963231667600982	
K	0.0244946762470123	
Mg	0.0394272731916659	
Na	0.067568468757874	
Si	0.149094728596607	
U	0.0000000378151260504202	
Al	0.0000332047335728395	
Mn	0.00113377528880606	
Fe	0.138571428571429	
Sr	0.00028772096880303	

End

19. Uranium standard analyses

Uranium standard	Position wheel	Deposit (ng)	Analysis date	^{235}U (V)	^{238}U (V)	$^{238}U/^{235}U$	
U010	21	28	24/10/2011				
U010	20	28	24/10/2011	0.10	9.18	96.47	
U010	19	28	24/10/2011	0.05	5.31	97.33	
U010	18	28	24/10/2011	2.07	202.23	97.75	
U010	17	28	24/10/2011	0.34	32.79	97.88	
U010	2	28	21/11/2011	0.00	0.00	1.93	No signal Material problem
U010	3	28	21/11/2011	0.00	0.00	0.96	No signal Material problem
U010	4	28	21/11/2011	0.00	0.00	0.97	No signal Material problem
U010	1	28	21/11/2011	0.00	0.00	4.00	No signal Material problem
U010	5	28	21/11/2011				No signal Material problem
U010	7	28	22/11/2011	1.12	107.58	96.26	
U010	8	28	22/11/2011	0.86	83.58	96.77	
U010	9	28	22/11/2011	2.74	263.25	96.21	
Unat	11	30	22/11/2011	0.36	49.65	137.84	
Unat	12	30	22/11/2011	1.80	247.24	137.60	
Unat	13	30	22/11/2011	1.85	254.34	137.56	
Unat	14	30	22/11/2011	0.37	50.23	137.58	
U010	2	28	23/11/2011				
U010	3	28	23/11/2011	0.68	67.37	98.60	
U010	4	28	23/11/2011	0.77	75.67	98.29	
U010	5	28	23/11/2011	1.56	153.36	98.60	
U010	7	28	23/11/2011	0.00	0.00	51.02	
U010	8	28	23/11/2011	0.25	24.85	98.62	
U010	9	28	23/11/2011	0.00	0.00	4.49	

Uranium standard	Position wheel	Deposit (ng)	Analysis date	^{235}U (V)	^{238}U (V)	$^{238}U/^{235}U$	
U010	10	28	23/11/2011	1.64	162.16	98.77	
U010	11	28	23/11/2011	2.59	256.02	98.80	
U010	12	28	24/11/2011	2.29	227.21	99.02	
U010	13	28	24/11/2011	0.13	12.57	100.13	
Unat	15	30	24/11/2011	0.52	72.48	138.34	
Unat	16	30	24/11/2011	2.31	319.02	137.93	
Unat	17	30	24/11/2011	0.74	102.45	138.42	
Unat	18	30	24/11/2011	1.61	221.58	137.74	
U010	9		25/11/2011	0.32	31.84	99.08	
Unat	19	30	25/11/2011	1.30	178.39	137.68	
Unat	20	30	25/11/2011	0.00	0.21	113.84	
Unat	21	30	25/11/2011	2.38	327.63	137.45	

20. Sample data for uranium behavior study

	October 2008				October 2009			
	Eh (ENH)	pe	^{238}U		Eh (ENH)	pe	^{238}U	
N° Well	(mV)		($mol.l^{-1}$)		(mV)		($mol.l^{-1}$)	
5-99	460	7.8	5.2×10^{-11}	$\pm5\times10^{-12}$	457	7.7	5.6×10^{-11}	$\pm5\times10^{-12}$
6-02-1	388	6.6	2.3×10^{-10}	$\pm8\times10^{-12}$				
6-02-2	232	3.9	1.8×10^{-10}	$\pm5\times10^{-26}$	311	5.3	1.4×10^{-10}	$\pm1\times10^{-11}$
8-02-1	223	3.8	8.4×10^{-11}	$\pm1\times10^{-26}$				
8-02-2	306	5.2	6.3×10^{-11}	±0	385	6.5	4.9×10^{-10}	$\pm1\times10^{-11}$
8-01-1	438	7.4	2.1×10^{-9}	$\pm1\times10^{-11}$				
8-01-2	492	8.3	8.2×10^{-10}	$\pm1\times10^{-11}$			5.0×10^{-10}	$\pm5\times10^{-12}$
19-00-1	438	7.4	3.7×10^{-9}	$\pm9\times10^{-11}$				
19-00-2	392	6.6	2.6×10^{-9}	$\pm7\times10^{-11}$	515	8.7	1.8×10^{-9}	$\pm1\times10^{-10}$
6-01-1	235	4.0	1.7×10^{-9}	$\pm7\times10^{-11}$				
6-01-2	478	8.1	7.5×10^{-10}	$\pm3\times10^{-11}$	493	8.4	5.4×10^{-10}	$\pm1\times10^{-11}$
2-02-1	202	3.4	9.2×10^{-10}	$\pm1\times10^{-11}$			9.9×10^{-11}	$\pm8\times10^{-12}$
2-02-2	450	7.6	4.7×10^{-10}	$\pm8\times10^{-12}$			2.7×10^{-10}	$\pm2\times10^{-11}$
7-00	418	7.1	1.4×10^{-10}	$\pm2\times10^{-10}$	238	4.0	5.2×10^{-11}	$\pm5\times10^{-12}$
5-02-1	227	3.8	1.7×10^{-10}	$\pm1\times10^{-11}$	318	5.4	1.4×10^{-10}	$\pm5\times10^{-12}$
5-02-2	194	3.3	1.4×10^{-10}	$\pm5\times10^{-12}$	238	4.0	9.8×10^{-11}	$\pm5\times10^{-12}$
7-02-1	199	3.4	1.2×10^{-10}	$\pm1\times10^{-26}$	315	5.3	2.8×10^{-10}	$\pm5\times10^{-12}$
7-02-2	188	3.2	7.1×10^{-11}	±0	231	3.9	1.2×10^{-10}	$\pm6\times10^{-12}$
7-01-1	378	6.4	1.1×10^{-9}	$\pm3\times10^{-11}$	493	8.4	7.0×10^{-10}	$\pm1\times10^{-11}$
7-01-2	308	5.2	3.6×10^{-10}	$\pm5\times10^{-12}$	420	7.1	2.9×10^{-10}	±0E+00
18-00-1	307	5.2	1.4×10^{-9}	$\pm3\times10^{-11}$	400	6.8	1.0×10^{-9}	$\pm6\times10^{-11}$
18-00-2	179	3.0	1.2×10^{-10}	$\pm1\times10^{-26}$	309	5.2	8.7×10^{-11}	$\pm4\times10^{-12}$
5-01-1	416	7.1	1.9×10^{-10}	$\pm8\times10^{-12}$	427	7.2	1.5×10^{-10}	$\pm4\times10^{-12}$
5-01-2	476	8.1	3.5×10^{-10}	$\pm5\times10^{-12}$	426	7.2	3.1×10^{-10}	±0
1-02-1	457	7.7	4.0×10^{-10}	$\pm1\times10^{-11}$	430	7.3	3.0×10^{-10}	$\pm2\times10^{-11}$
1-02-2	259	4.4						
1-98-1	198	3.4	3.4×10^{-11}	±0	200	3.4	6.5×10^{-11}	$\pm3\times10^{-12}$
1-98-2	156	2.6	2.5×10^{-11}	$\pm6\times10^{-27}$	252	4.3	2.7×10^{-11}	$\pm9\times10^{-13}$
1-98-3	104	1.8	1.7×10^{-11}	±0	289	4.9	2.6×10^{-11}	$\pm7\times10^{-13}$

21. Uranium analyses on thermal ionization mass spectrometer

Sample (year well)	Date	Position wheel	Filament	Graphite	^{234}U	^{235}U	^{236}U	^{238}U	$^{238}U/^{235}U$	Theoretical standard deviation
T9 5-01-2	25/11/2011	3	Hand-made	4 µL	3.75×10^{-3}	0.05	4.29×10^{-3}	6.59	135.56	Too high
T9 7-01-1	25/11/2011	2	Hand-made	4 µL	4.38×10^{-3}	0.17	4.19×10^{-3}	23.93	137.40	± 2.2
T9 18-00-1	25/11/2011	1	Hand-made	4 µL	3.28×10^{-3}	0.23	2.83×10^{-3}	31.25	138.54	± 2.2
T9 18-00-1	07/01/2012	8	Hand-made	4 µL	8.71×10^{-3}	0.45	7.35×10^{-3}	61.97	137.14	± 2.2
T9 7-01-1	07/01/2012	8	Hand-made	4 µL	1.26×10^{-2}	1.28	7.91×10^{-3}	176.54	137.70	± 2.2
T9 18-00-1	07/01/2012	5	Hand-made	4 µL	2.67×10^{-3}	0.07	2.18×10^{-3}	9.39	136.24	Too high
T9 18-00-1	07/01/2012	3	Hand-made	3 µL	1.53×10^{-3}	0.02	1.28×10^{-3}	2.91	133.49	Too high
T9 7-00	19/01/2012	13	Hand-made	4 µL	3.58×10^{-3}	0.05	1.68×10^{-3}	7.46	140.56	Too high
T9 7-00	19/01/2012	12	Hand-made	4 µL	8.44×10^{-3}	0.76	1.09×10^{-2}	104.54	137.11	± 2.2
T9 7-01-1	19/01/2012	11	Hand-made	4 µL	3.66×10^{-3}	0.01	1.51×10^{-3}	1.87	152.31	Too high
T9 7-01-1	19/01/2012	10	Hand-made	4 µL	4.24×10^{-3}	0.14	2.24×10^{-3}	19.84	139.83	± 2.2
T9 7-01-2	19/01/2012	9	Hand-made	4 µL	8.32×10^{-3}	0.48	5.98×10^{-3}	66.39	139.59	± 2.2
T9 18-00-1		13	Hand-made	4 µL	1.64×10^{-4}	0.00	7.97×10^{-5}	0.04	40.02	Too high
T9 18-00-1		13	Hand-made	4 µL	2.99×10^{-5}	0.00	8.13×10^{-5}	0.03	113.13	Too high
T9 7-01-2		14	Hand-made	4 µL	5.26×10^{-3}	0.10	6.06×10^{-3}	13.64	138.73	Too high
T9 5-01-2		15	Hand-made	4 µL	2.75×10^{-3}	0.07	3.54×10^{-3}	9.89	137.47	Too high
T8 1-98-1	21/01/2012	17	Hand-made	4 µL	6.20×10^{-3}	0.31	5.74×10^{-3}	42.74	138.47	± 2.2
T8 1-98-1	21/01/2012	18	Hand-made	4 µL	9.29×10^{-3}	0.21	1.19×10^{-2}	29.99	139.57	± 2.2
T8 1-98-2	21/01/2012	19	Hand-made	4 µL	4.57×10^{-5}	0.00	5.96×10^{-5}	0.02	266.66	Too high

Sample (year. well)	Date	Position wheel	Filament	Graphite	^{234}U	^{235}U	^{236}U	^{238}U	$^{238}U/^{235}U$	Theoretical standard deviation
T8 1-98-3	21/01/2012	20	Hand-made	4 µL	1.09×10^{-4}	0.00	1.10×10^{-4}	0.00	0.60	Too high
T9 5-01-2	21/01/2012	16	Hand-made	4 µL	3.21×10^{-3}	0.12	3.81×10^{-3}	17.19	139.92	± 2.2
T9 18 00 1	12/06/2012	9	Hand-made	4 µL	4.05×10^{-3}	0.18	5.00×10^{-3}	24.58	138.39	± 2.2
T8 8 01 1	12/06/2012	11	Hand-made	4 µL	2.96×10^{-3}	0.12	2.16×10^{-3}	16.09	137.35	± 2.2
T9 19 00 2	12/06/2012	13	Hand-made	4 µL	2.08×10^{-3}	0.09	1.82×10^{-3}	12.08	138.55	Too high
T9 19 00 2	12/06/2012	14	Hand-made	4 µL	1.50×10^{-3}	0.22	1.32×10^{-3}	29.70	137.28	± 2.2
T8 2 02 2	13/06/2012	15	Hand-made	4 µL	2.28×10^{-3}	0.00	2.04×10^{-3}	0.48	137.45	Too high
T8 2 02 2	13/06/2012	16	Hand-made	4 µL	6.69×10^{-4}	0.02	8.65×10^{-4}	3.21	136.80	Too high
T8 19 00 2	13/06/2012	17	Hand-made	4 µL	1.03×10^{-3}	0.10	1.04×10^{-3}	13.62	138.26	Too high
T8 19 00 2	13/06/2012	18	Hand-made	4 µL	2.72×10^{-3}	0.04	2.47×10^{-3}	5.84	136.66	Too high
T9 18 00 1	13/06/2012	10	Hand-made	4 µL	1.08×10^{-3}	0.24	1.47×10^{-3}	33.33	136.29	± 2.2
T8 8 01 1	13/06/2012	12	Hand-made	4 µL	4.08×10^{-3}	0.27	1.82×10^{-3}	38.43	139.99	± 2.2
T8 6 01 2	14/06/2012	9	Hand-made	4 µL	7.36×10^{-3}	0.05	7.28×10^{-3}	6.82	135.61	Too high
T8 6 01 2	14/06/2012	10	Hand-made	4 µL	1.55×10^{-3}	0.17	1.23×10^{-3}	23.87	137.29	± 2.2
T8 8 01 2	14/06/2012	11	Hand-made	4 µL	2.31×10^{-3}	1.05	1.84×10^{-3}	144.67	137.15	± 2.2

22. NIST SRM987 analyses on double rhenium filaments

Quantity (ng)	*Tantal*	*Evaporation Filament heating (reached value in mA/rate)*	*Ionization Filament heating (reached value in mA/rate)*	*EVA max value (mA)*	*Cycles*	^{85}Rb *(V)*	^{86}Sr *(V)*	^{87}Sr *(V)*	^{87}Sr *corr Rb (V)*	^{88}Sr *(V)*	$^{86}Sr/^{88}Sr$	$^{87}Sr/^{86}Sr$	*Note*
50		400/100	3000/450->3200/100		151	-2×10^{-3}	121.39	86.19	86.19	1015.98	0.11948	0.70999	
50		400/100	3000/450->3300/100		146	1×10^{-3}	25.02	17.77	17.77	209.63	0.11934	0.71041	
50		400/100	3000/450->3300/100		126	1×10^{-2}	145.59	103.39	103.38	1008.88	0.14430	0.71012	
50		400/100	3000/450->3300/100			1×10^{-2}	93.97	66.72	66.71	786.34	0.11950	0.70990	
50		400/100	2900/450		142	1×10^{-4}	92.17	65.44	65.44	771.39	0.11948	0.71000	
50		400/100	2800/100->3000/450		68	-2×10^{-4}	58.27	41.38	41.38	487.82	0.11945	0.71008	
50		400/100	3000/450->3500/100			8×10^{-3}	129.33	91.91	91.91	1084.47	0.11925	0.71068	

Quantity (ng)	*Tantal*	*Evaporation Filament heating (reached value in mA/rate)*	*Ionization Filament heating (reached value in mA/rate)*	*EVA max value (mA)*	*Cycles*	*^{85}Rb (V)*	*^{86}Sr (V)*	*^{87}Sr (V)*	*^{87}Sr corr Rb (V)*	*^{88}Sr (V)*	*$^{86}Sr/^{88}Sr$*	*$^{87}Sr/^{86}Sr$*	*Note*
50		*400/100*	*3000/450->3300/100*			*1×10^{-4}*	*7.57*	*5.38*	*5.38*	*63.46*	*0.11933*	*0.71036*	*x2*
50		400/100	3000/450->3300/100			3×10^{-3}	0.00	0.00	0.00	0.02	0.12589	0.18378	
50		400/100	3000/450->3300/100			3×10^{-3}	42.36	30.08	30.08	354.63	0.11945	0.71008	
50		400/100	3000/450->3400/100			4×10^{-3}	0.00	0.00	0.00	0.03	0.12507	0.66855	
50		400/100	3000/450		157	6×10^{-4}	126.09	89.53	89.53	1055.37	0.11947	0.71003	
50		400/100	3000/450->3376/10		82	1×10^{-3}	49.98	35.49	35.49	418.33	0.11948	0.70997	
50		400/100	3000/450		132	2×10^{-4}	102.10	72.50	72.50	854.64	0.11946	0.71006	
50		400/100	3000/450->3300/100	8000	103	5×10^{-4}	92.06	65.36	65.36	770.43	0.11949	0.70998	
50		400/100	3000/450	7000	389	4×10^{-5}	239.36	170.05	170.05	1967.21	0.12168	0.71042	

Quantity (ng)	*Tantal*	*Evaporation Filament heating (reached value in mA/rate)*	*Ionization Filament heating (reached value in mA/rate)*	*EVA max value (mA)*	*Cycles*	*^{85}Rb (V)*	*^{86}Sr (V)*	*^{87}Sr (V)*	*^{87}Sr corr Rb (V)*	*^{88}Sr (V)*	*$^{86}Sr/^{88}Sr$*	*$^{87}Sr/^{86}Sr$*	*Note*
50		400/100	2800/450->3200/100	8000	305	5×10^{-2}	154.45	109.72	109.70	1293.75	0.11938	0.71028	
50		400/100	2800/450->3200/100	8000	71	2×10^{-3}	41.21	29.27	29.27	345.06	0.11945	0.71027	
50		400/100	2800/450->3200/100	8000	67	6×10^{-4}	49.14	34.90	34.90	404.68	0.12142	0.71017	
50		400/100	2800/450->2900/100						0.00				heatslope 10
50		400/100	2800/450->3100/100	8000	299	2×10^{-3}	225.85	160.35	160.35	1890.37	0.11948	0.70999	heatslope 10
50		400/100	2800/450->3200/100	8000	454	2×10^{-3}	129.42	91.95	91.95	1084.68	0.11932	0.71047	heatslope 10
50		400/100	2800/450->3200/100	8000	354	3×10^{-3}	23.30	16.56	16.56	195.42	0.11921	0.71080	heatslope 10

12.5		*400/40*	*2800/250->3100/25*						*0.00*		*0.11743*	*#DIV/0!*	
25		400/40	2800/250->3200/25	25000		7×10^{-3}	32.04	22.76	22.76	268.48	0.11932	0.71042	Heating problems
25		400/40->1000/40	2800/250->2900/25	8000		1×10^{-3}	43.37	30.74	30.74	363.03	0.11946	0.70888	heatslope 10
12.5	Ta	1000/100	3500/450->4000/100		293	6×10^{-3}	24.03	17.06	17.06	201.12	0.11947	0.70999	
12.5	Ta	1000/100	3500/450->4000/100		314	33×10^{-3}	94.67	67.29	67.29	794.22	0.11920	0.71081	
12.5	Ta	1000/100	3000/450->4000/100		282	8×10^{-3}	4.73	3.35	3.35	39.45	0.11992	0.70835	
25	Ta	500/100->600/100->1000/100	3300/50->3600/200->4000/200		193	1×10^{-4}	64.24	45.65	45.65	538.61	0.11926	0.71068	
25	*Ta*	*400/100->500/10->0->500/100->600/25->0->700/100*	*2800/250->3300/50->0->3300/500->3400/50->0->3500/100*		*328*	*5×10^{-3}*	*43.21*	*30.69*	*30.69*	*361.96*	*0.11938*	*0.71024*	*Heating problems*
25	Ta	800/200->1200/100	2800/450->3800/100		358	1×10^{-2}	131.24	93.16	93.16	1098.13	0.11951	0.70983	

23. NIST SRM987 analyses on single rhenium filaments

Ta	*Heating (reached value in mA/rate)*	*Deposit (ng)*	*Cycles*	^{84}Sr *(V)*	^{85}Rb *(V)*	^{86}Sr *(V)*	^{87}Sr *(V)*	^{87}Sr *corr Rb (V)*	^{88}Sr *(V)*	$^{86}Sr/^{88}Sr$	$^{87}Sr/^{86}Sr$ *corr Rb (V)*	$^{84}Sr/^{86}Sr$	*Note*
sandwich	manual 2400/150 - max pilot = 8000 - heatslope 20	50	446		0.0088	216.27	153.93	153.92	1818.74	0.11891	0.71172		
sandwich	manual 2400/150 - max pilot = 8000 - heatslope 20	50	624		0.1289	272.89	194.17	194.12	2292.47	0.11904	0.71132		Stopped
sandwich	manual 2400/150 - max pilot = 8000 - heatslope 20	50	208		0.0029	120.79	86.00	86.00	1015.56	0.11894	0.71191		
sandwich	manual 2400/150	50	624		-	503.71	358.37	358.37	4233.14	0.11892	0.71147		Analyze= 3h

sandwich	manual 2400/150 - max pilot = 15000 - heatslope 40	50	444		-	653.91	464.55	464.55	5479.32	0.11934	0.71043		instable
sandwich	manual 2400/150 - max pilot = 12000 - heatslope 35	50	325		0.0052	346.76	246.67	246.67	2913.28	0.11903	0.71135		
sandwich	manual 2400/150 - max pilot = 12000 - heatslope 30	50	504		-	380.92	271.27	271.27	3207.10	0.11877	0.71214		instable
sandwich	manual 2400/150 - max pilot = 10000 - heatslope 30	50	596		-	585.74	416.51	416.51	4917.32	0.11912	0.71109		
sandwich	manual 2400/150 - max pilot = 10000 - heatslope 30	50	537		0.0045	540.86	384.40	384.40	4535.89	0.11924	0.71071		

sandwich	manual 2400/150 - max pilot = 15000 - heatslope 30	50	413		0.0086	583.44	414.83	414.82	4896.71	0.11915	0.71099		
sandwich	manual 2400/150 - max pilot = 15000 - heatslope 10	50	626		0.0114	528.43	375.64	375.64	4433.24	0.11920	0.71086		
sandwich	manual 2400/150 - max pilot = 15000 - heatslope 20	50	825		0.0120	1335.34	949.82	949.81	11179.45	0.11945	0.71129		
sandwich	manual 2400/150 - max pilot = 17500 - heatslope 20	50	572		-	910.90	647.60	647.60	7643.80	0.11917	0.71095		
sandwich	manual 2400/150 - max pilot = 15000 - heatslope 20	50			0.0000	387.01	274.96	274.96	3243.24	0.11933	0.71047		

sandwich	manual 2400/150 - max pilot = 15000 - heatslope 20	12,5	303		0.0025	220.01	156.22	156.21	1841.61	0.11947	0.71003		
sandwich	*manual 2400/150 - max pilot = 15000 - heatslope 20*	*12,5*	*767*		*-*	*281.48*	*200.69*	*200.69*	*2375.38*	*0.11850*	*0.71298*		*stopped*
sandwich	*manual 2400/150 - max pilot = 15000 - heatslope 20*	*12,5*	*518*		*0.0042*	*193.97*	*138.19*	*138.19*	*1634.56*	*0.11867*	*0.71243*		*stopped*
sandwich	manual 2400/150 - max pilot = 15000 - heatslope 20	12,5	427		-	108.78	77.32	77.32	912.58	0.11920	0.71086		
sandwich	manual 2400/150 - max pilot = 15000 - heatslope 20	12,5	725		0.0020	289.04	205.70	205.70	2430.04	0.11895	0.71165		

sandwich	*manual 2400/150 - max pilot = 15000 - heatslope 20*	*12,5*	*1419*		*0.0323*	*643.71*	*457.95*	*457.94*	*5408.83*	*0.11901*	*0.71140*		*stopped*
sandwich	*manual 2400/150 - max pilot = 15000 - heatslope 20*	*12,5*	*682*		*0.0024*	*0.00*	*0.00*	*0.00*	*2051.46*	*0.11912*	*#DIV/0!*		*Stopped Temperature room up 28°C*
flashed	manual 2400/150 - max pilot = 15000 - heatslope 20	12,5	230		0.0004	45.78	32.55	32.55	384.40	0.11909	0.71115		
flashed	manual 2400/150 - max pilot = 8000 - heatslope 20	12,5	335		0.0036	161.49	114.81	114.80	1355.08	0.11918	0.71089		
flashed	manual 2400/150 - max pilot = 8000 - heatslope 20	12,5	348		0.0009	144.60	102.84	102.84	1214.34	0.11907	0.71122		

flashed	manual 2400/150 - max pilot = 8000 - heatslope 20	12,5	293		0.0026	113.26	80.51	80.50	950.12	0.11921	0.71077		
Ta	*Heating (reached value in mA/rate)*	*Deposit (ng)*	*Cycles*	^{84}Sr *(V)*	^{85}Rb *(V)*	^{86}Sr *(V)*	^{87}Sr *(V)*	^{87}Sr *corr Rb (V)*	^{88}Sr *(V)*	$^{86}Sr/^{88}Sr$	$^{87}Sr/^{86}Sr$ *corr Rb (V)*	$^{84}Sr/^{86}Sr$	*Note*
flashed	manual 2400/150 - max pilot = 8000 - heatslope 20	12,5	382		0.0041	222.77	158.39	158.39	1869.70	0.11915	0.71098		
flashed	2400/150(->2800/100->3400/50)	25	247	7.36	0.0013	130.76	93.03	93.03	1098.95	0.11899	0.71147	0.05629	
flashed	2400/150(->2800/100->3400/50)	25	244	1.17	0.0008	20.86	14.89	14.89	176.43	0.11824	0.71377	0.05595	
flashed	2400/150(->2800/100->3400/50)	25	238	0.77	0.0013	13.70	9.76	9.76	115.27	0.11885	0.71211	0.05618	

flashed	2400/150(->2800/100->3400/50)	25	258	10.28	0.0037	182.68	130.02	130.02	1536.36	0.11890	0.71173	0.05625	
flashed	2400/150(->2800/100->3400/50)	25	248	0.46	0.0006	8.17	5.83	5.83	69.06	0.11833	0.71356	0.05602	
flashed	2400/150(->2800/100->3400/50)		329	1.24	0.0019	21.98	15.65	15.64	1848.72	0.11890	0.71169	0.05625	
flashed flashé	2400/150(->2800/100->3400/50)			4.12	0.0003	73.14	52.04	52.04	614.76	0.11898	0.71150	0.05627	
flashed	2400/150(->2800/100->3400/50)		229	0.43	0.0061	7.57	5.39	5.38	63.59	0.11899	0.71170	0.05629	
flashed	2400/150(->2800/100->3400/50)		228	2.29	0.0088	40.65	28.91	28.91	341.26	0.11911	0.71110	0.05635	
flashed	automatic	25	664	28.75	0.0001	510.47	363.18	363.18	4289.74	0.11900	0.71145	0.05631	
flashed	automatic	25	149	5.05	0.0007	89.74	63.86	63.86	754.36	0.11897	0.71154	0.05627	

flashed	automatic	25	632	29.98	-	532.54	378.90	378.90	4475.91	0.11898	0.71150	0.05630	
flashed	automatic	25	306	12.01	0.0047	212.94	151.39	151.39	1787.10	0.11915	0.71096	0.05639	
flashed	automatic	25	868	40.76	-	725.09	516.19	516.19	6100.85	0.11885	0.71190	0.05621	
flashed	automatic	25	700	33.06	0.0022	587.89	418.43	418.43	4944.43	0.11890	0.71176	0.05624	
Industrial Flashed	automatic	25	1132	54.99	0.0108	976.13	694.27	694.26	8198.26	0.11907	0.71124	0.05633	
Industrial Flashed	automatic	25	1624	79.11	0.0183	1406.22	1000.86	1000.85	11826.97	0.11890	0.71173	0.05626	
Industrial Flashed	automatic	12,5	1308	63.47	0.0325	1127.28	801.96	801.95	9472.13	0.11901	0.71140	0.05630	
Industrial Flashed	automatic	12,5	344	32.27	0.0075	572.98	407.55	407.54	4812.86	0.11905	0.71127	0.05632	
Industrial Flashed	automatic	25	1560	78.60	0.0256	1397.23	994.35	994.34	11748.93	0.11892	0.71165	0.05626	
Industrial Flashed	automatic	12,5		55.06	0.0151	978.50	696.31	696.30	8226.51	0.11895	0.71160	0.05627	

Industrial Flashed	automatic	12,5	727	33.37		594.01	423.07	423.07	5000.25	0.11874	0.71223	0.05617	
Industrial Flashed	automatic	12,5	185	5.14	0.0037	91.39	65.04	65.04	768.52	0.11891	0.71172	0.05628	
Industrial Flashed	automatic	12,5	303	11.97	0.0001	212.66	151.30	151.29	1787.16	0.11899	0.71145	0.05629	
Industrial Flashed	automatic	12,5	518	22.92	0.0003	407.67	290.21	290.21	3430.05	0.11885	0.71189	0.05623	
Industrial Flashed	automatic	12,5	346	14.13	0.0027	251.10	178.64	178.64	2110.09	0.11900	0.71143	0.05628	
Industrial Flashed	automatic	25		8.39	0.0046	179.64	127.98	127.98	1510.50	0.11893	0.71242	0.04669	
Industrial Flashed	automatic	12,5		11.11	0.0068	219.94	156.69	156.69	1848.61	0.11897	0.71244	0.05051	
Industrial Flashed	automatic			6.73	0.0091	160.63	114.49	114.49	1351.03	0.11890	0.71273	0.04192	

Industrial Flashed	NBSchimie_140612auto_7			4.77	0.0027	93.28	66.49	66.49	784.89	0.11884	0.71277	0.05114	

24. [^{88}Sr] concentrations and ^{90}Sr volumetric activities on AB profile in October 2008

№ Well	^{88}Sr		Activity ^{90}Sr	
	(mol.l^{-1})		(Bq.l^{-1})	
5-99	2.13×10^{-7}	$\pm7.6\times10^{-10}$	158	±10
6-02-1	2.29×10^{-7}	$\pm5.1\times10^{-9}$	193	±13
6-02-2	2.29×10^{-7}	$\pm4.1\times10^{-9}$	3	±1
8-02-1	1.39×10^{-7}	$\pm1.2\times10^{-9}$	76	±5
8-02-2	1.78×10^{-7}	$\pm1.8\times10^{-9}$	14	±2
8-01-1	2.90×10^{-7}	$\pm3.4\times10^{-9}$	443	±28
8-01-2	4.43×10^{-7}	$\pm9.6\times10^{-9}$	410	±26
19-00-1	8.78×10^{-7}	$\pm1.1\times10^{-8}$	1380	±90
19-00-2	7.57×10^{-7}	$\pm6.6\times10^{-10}$	511	±32
6-01-1	4.17×10^{-7}	$\pm4.3\times10^{-9}$	442	±28
6-01-2	7.93×10^{-7}	$\pm3.0\times10^{-9}$	643	±41
2-02-1	1.92×10^{-7}	$\pm2.1\times10^{-9}$	146	±10
2-02-2	7.65×10^{-7}	$\pm1.2\times10^{-8}$	616	±39
7-00	2.43×10^{-7}	$\pm1.4\times10^{-9}$	24	±2
5-02-1	6.21×10^{-7}	$\pm8.0\times10^{-9}$	1	
5-02-2	7.12×10^{-7}	$\pm7.6\times10^{-9}$	3	±1
7-02-1	3.73×10^{-7}	$\pm4.7\times10^{-9}$	1	
7-02-2	4.58×10^{-7}	$\pm8.8\times10^{-9}$	3	±1
7-01-1	4.20×10^{-7}	$\pm3.1\times10^{-9}$	69	±5
7-01-2	4.14×10^{-7}	$\pm9.0\times10^{-9}$	3	±1
18-00-1	4.09×10^{-7}	$\pm8.2\times10^{-9}$	68	±5
18-00-2	4.92×10^{-7}	$\pm1.0\times10^{-8}$	1	
5-01-1	4.92×10^{-7}	$\pm9.0\times10^{-9}$	264	±17
5-01-2	4.40×10^{-7}	$\pm2.2\times10^{-9}$	1	
1-02-1	6.85×10^{-7}	$\pm1.6\times10^{-8}$	21	±2
1-98-1	3.87×10^{-7}	$\pm3.3\times10^{-9}$	2	±1
1-98-2	3.94×10^{-7}	$\pm4.5\times10^{-9}$	1	
1-98-3	3.57×10^{-7}	$\pm1.3\times10^{-8}$	5	±1

25. $^{86}Sr/^{88}Sr$, $^{86}Sr/^{88}Sr$ corrected, $^{87}Sr/^{86}Sr$, $^{87}Sr/^{86}Sr$ corrected, [^{88}Sr] concentrations and ^{90}Sr volumetric activities of groundwater collected for isotopic analyses.

Piezometer sampled	Analysis date	$^{84}Sr/^{86}Sr$ measured	$^{86}Sr/^{88}Sr$ measured	$^{87}Sr/^{86}Sr$ measured	**$^{86}Sr/^{88}Sr$ corrected**	**$^{87}Sr/^{86}Sr$ corrected**
6-02-2	09-2011	0.05634	0.11912	0.71533	**0.11938**	**0.71455**
	01-2012	0.05717	0.11817	0.71088	**0.11678**	**0.71514**
5-02-2	09-2011	0.05659	0.11925	0.71328	**0.11900**	**0.71404**
8-02-2	09-2011	0.05630	0.11937	0.71348	**0.11972**	**0.71244**
	01-2012	0.05616	0.11907	0.71367	**0.11970**	**0.71178**
7-02-2	*09-2011*	*0.06476*	*0.11846*	*0.711305*	***0.10542***	***0.75565***
	01-2012	0.05638	0.11896	0.71254	**0.11915**	**0.71199**
7-01-2	*09-2011*	*0.05655*	*0.11863*	*0.71514*	***0.11848***	***0.71560***
	01-2012	0.05632	0.11908	0.71357	**0.11938**	**0.71267**
18-00-2	*09-2011*	*0.05573*	*0.11879*	*0.71416*	***0.12033***	***0.70955***
	01-2012	0.05620	0.11881	0.71384	**0.11936**	**0.71218**
5-01-2	09-2011	0.05633	0.11900	0.71410	**0.11929**	**0.71325**
	01-2012	0.05638	0.11892	0.71420	**0.11910**	**0.71366**
1-02-1	09-2011	*0.05631*	*0.11902*	*0.71564*	***0.11934***	***0.71467***
	01-2012	0.05628	0.11881	0.71601	**0.11920**	**0.71486**
1-98-1	09-2011	0.05619	0.11886	0.71414	**0.11944**	**0.71238**
	01-2012	0.05617	0.11878	0.71395	**0.11940**	**0.71209**
1-98-2	09-2011	0.05644	0.11863	0.71254	**0.11870**	**0.71233**
	01-2012	0.05616	0.11864	0.71256	**0.11927**	**0.71067**
1-98-3	01-2012	0.05613	0.11882	0.71101	**0.11953**	**0.70891**

Italic values are the discarded values.

26. Samples analyses on single rhenium filaments with flashed Ta at the CEA-Marcoule

	Analyses						Correction				
Sample	^{84}Sr	$^{84}Sr/^{86}Sr$	$^{84}Sr/^{87}Sr$	$^{84}Sr/^{88}Sr$	**$^{86}Sr/^{88}Sr$**	**$^{87}Sr/^{86}Sr$**	r1/S1	S2	S2'	$^{86}Sr/^{88}Sr$	$^{87}Sr/^{86}Sr$
T8 1-02-1	0.15	0.05110	0.07139	0.006083	**0.11905**	**0.71579**	0.90486	0.00748	0.08315	0.13250	0.67913
T8 2-02-2	0.12	0.04516	0.06329	0.005384	**0.11921**	**0.71355**	0.79970	0.00888	0.09013	0.15725	0.62651
T8 5-02-2	*0.08*	*0.04394*	*0.06164*	*0.005233*	***0.11911***	***0.71279***	*0.77805*	*0.00928*	*0.09201*	*0.16440*	*0.61376*
T8 5-99	0.28	0.04485	0.06297	0.005349	**0.11927**	**0.71218**	0.79422	0.00898	0.09074	0.15907	0.62232
T8 6-01-2	2.66	0.03474	0.04878	0.004130	**0.11888**	**0.71223**	0.61527	0.01695	0.11400	0.30010	0.49533
T8 7-00	0.05	0.04602	0.06438	0.005447	**0.11835**	**0.71479**	0.81494	0.00856	0.08883	0.15159	0.63574
T8 8-01-1	0.60	0.04710	0.06624	0.005604	**0.11897**	**0.71116**	0.83415	0.00831	0.08792	0.14724	0.64230
T8 8-02-2	0.83	0.03914	0.05492	0.004652	**0.11885**	**0.71274**	0.69319	0.01172	0.10100	0.20758	0.55910
T8 18-00-2	11.93	0.04618	0.06490	0.005505	**0.11922**	**0.71158**	0.81775	0.00858	0.08902	0.15192	0.63435
T8 18-00-2	0.00	0.20418	-1.68060	0.240813	**1.17942**	**-0.12149**	3.61572	0.03921	-0.34371	0.69434	-0.16430
T8 5-01-2	0.12	0.04610	0.06452	0.005491	**0.11909**	**0.71459**	0.81640	0.00859	0.08874	0.15213	0.63632
T9 7-01-2	0.31	0.04701	0.06582	0.005598	**0.11908**	**0.71422**	0.83243	0.00835	0.08766	0.14781	0.64420